frontiers | Research Topics

Differences between emmetropic and myopic eyes: implications for myopia development, its progression, and ocular health

Edited by
Pablo De Gracia, Pablo Pérez-Merino, Alexandra Benavente-Perez and Fuensanta Vera-Diaz

Published in
Frontiers in Medicine

ISSN 1664-8714
ISBN 978-2-8325-6638-1
DOI 10.3389/978-2-8325-6638-1

Generative AI statement
Any alternative text (Alt text) provided alongside figures in the articles in this ebook has been generated by Frontiers with the support of artificial intelligence and reasonable efforts have been made to ensure accuracy, including review by the authors wherever possible. If you identify any issues, please contact us.

About Frontiers

Frontiers is more than just an open access publisher of scholarly articles: it is a pioneering approach to the world of academia, radically improving the way scholarly research is managed. The grand vision of Frontiers is a world where all people have an equal opportunity to seek, share and generate knowledge. Frontiers provides immediate and permanent online open access to all its publications, but this alone is not enough to realize our grand goals.

Frontiers journal series

The Frontiers journal series is a multi-tier and interdisciplinary set of open-access, online journals, promising a paradigm shift from the current review, selection and dissemination processes in academic publishing. All Frontiers journals are driven by researchers for researchers; therefore, they constitute a service to the scholarly community. At the same time, the *Frontiers journal series* operates on a revolutionary invention, the tiered publishing system, initially addressing specific communities of scholars, and gradually climbing up to broader public understanding, thus serving the interests of the lay society, too.

Dedication to quality

Each Frontiers article is a landmark of the highest quality, thanks to genuinely collaborative interactions between authors and review editors, who include some of the world's best academicians. Research must be certified by peers before entering a stream of knowledge that may eventually reach the public - and shape society; therefore, Frontiers only applies the most rigorous and unbiased reviews. Frontiers revolutionizes research publishing by freely delivering the most outstanding research, evaluated with no bias from both the academic and social point of view. By applying the most advanced information technologies, Frontiers is catapulting scholarly publishing into a new generation.

What are Frontiers Research Topics?

Frontiers Research Topics are very popular trademarks of the *Frontiers journals series*: they are collections of at least ten articles, all centered on a particular subject. With their unique mix of varied contributions from Original Research to Review Articles, Frontiers Research Topics unify the most influential researchers, the latest key findings and historical advances in a hot research area.

Find out more on how to host your own Frontiers Research Topic or contribute to one as an author by contacting the Frontiers editorial office: frontiersin.org/about/contact

Differences between emmetropic and myopic eyes: implications for myopia development, its progression, and ocular health

Topic editors

Pablo De Gracia — University of Detroit Mercy, United States

Pablo Pérez-Merino — Daza de Valdés Institute of Optics, Spanish National Research Council (CSIC), Spain

Alexandra Benavente-Perez — State University of New York, United States

Fuensanta Vera-Diaz — New England College of Optometry, United States

Citation

De Gracia, P., Pérez-Merino, P., Benavente-Perez, A., Vera-Diaz, F., eds. (2025). *Differences between emmetropic and myopic eyes: implications for myopia development, its progression, and ocular health*. Lausanne: Frontiers Media SA. doi: 10.3389/978-2-8325-6638-1

Table of contents

frontiers | Frontiers in Medicine

TYPE Editorial
PUBLISHED 10 July 2025
DOI 10.3389/fmed.2025.1644062

OPEN ACCESS

EDITED AND REVIEWED BY
Jodhbir Mehta,
Singapore National Eye Center, Singapore

*CORRESPONDENCE
Pablo De Gracia
degracpa@udmercy.edu

RECEIVED 09 June 2025
ACCEPTED 16 June 2025
PUBLISHED 10 July 2025

CITATION
De Gracia P, Vera-Diaz FA, Benavente-Pérez A and Pérez-Merino P (2025) Editorial: Differences between emmetropic and myopic eyes: implications for myopia development, its progression, and ocular health.
Front. Med. 12:1644062.
doi: 10.3389/fmed.2025.1644062

Editorial: Differences between emmetropic and myopic eyes: implications for myopia development, its progression, and ocular health

Pablo De Gracia[1]*, Fuensanta A. Vera-Diaz[2], Alexandra Benavente-Pérez[3] and Pablo Pérez-Merino[4]

[1]University of Detroit Mercy School of Optometry, Novi, MI, United States, [2]New England College of Optometry, Boston, MA, United States, [3]SUNY College of Optometry, New York, NY, United States, [4]Instituto de Óptica, Consejo Superior de Investigaciones Científicas, Madrid, Spain

KEYWORDS

myopia development, axial elongation, environmental risk factors, scleral remodeling, retinal signaling pathways, peripheral blur anisotropy, retinal pigment epithelium (RPE), visual experience and myopia modulation

Editorial on the Research Topic
Differences between emmetropic and myopic eyes: implications for myopia development, its progression, and ocular health

Myopia has emerged as a pressing public health concern worldwide of increasing prevalence that represents a growing burden due to the myopia-associated visual impairment. This, coupled with our expanding understanding of its complex etiology, underscores the urgent need for multidisciplinary research in myopia. This Research Topic of *Frontiers in Medicine* brings together nine original studies that traverse the full spectrum of myopia science—from large-scale epidemiological insights to innovative investigations of optical and molecular mechanisms. Together, they offer an integrated perspective on how we define, detect, and potentially intervene in the development and progression of myopia.

Global and environmental perspectives on myopia

This Research Topic frames the global impact of myopia with three large-scale epidemiological studies. Mu et al. investigated changes in myopia prevalence among nearly 850,000 school-age children in Shenzhen, China, before, during, and after the COVID-19 pandemic. Their findings highlight the accelerating impact of behavioral shifts—specifically decreased outdoor activity and increased near work—on myopia. Complementing this, Li et al. presented a prospective study of nearly 38,000 children in Xuzhou, China, revealing semester-level myopia progression and emphasizing the vulnerability of early primary school students. Adding an environmental dimension, Liu T. et al. conducted a cross-sectional study linking satellite-derived measurements of outdoor artificial light at night (ALAN) to increased myopia prevalence in over 33,000 adolescents, identifying it as a modifiable environmental risk factor with implications for urban lighting policy.

Structural and functional changes in the myopic eye

Three studies in this Research Topic explored structural and functional manifestations of myopia. Huang et al. compared macular characteristics in eyes with myopic choroidal neovascularization and their contralateral eyes, and propose that reduced perforating scleral vessels and choroidal thinning may be potential diagnostic markers for advanced myopia disease. Bueno et al. used second harmonic generation microscopy to study collagen remodeling in the posterior sclera of chicks with form-deprivation myopia, revealing increased collagen alignment without changes in thickness. Their use of objective Radon Transform-based quantification suggests that collagen architecture beyond overall scleral dimensions may play a key role in the biomechanical behavior of the myopic eye. Importantly, the study challenges prior assumptions that scleral thinning is a hallmark of axial elongation, instead emphasizing the importance of fiber orientation in ocular growth. These findings offer a new window into the role of the sclera in myopia and support the use of advanced imaging techniques to monitor tissue-level remodeling *in vivo*. Kendrick et al. introduced a Radial Asymmetry Metric to quantify peripheral blur anisotropy in myopia. Their study provides compelling evidence that blur asymmetry is not only more pronounced at greater retinal eccentricities but also differs in orientation in myopic eyes, with larger vertically oriented blur in the temporal retina. This framework represents an advance over traditional Modulation Transfer Function analyses by capturing both the direction and magnitude of blur that are otherwise missed. Their results point to the importance of peripheral image quality and its anisotropic properties in shaping ocular growth.

Molecular and cellular mechanisms underpinning eye growth

Transitioning from macroscale to molecular insights, two studies in this topic aimed to elucidate the signaling pathways that govern myopia development. Palumaa et al. presented a meta-analysis of retinal transcriptome data from animal models, identifying both conserved and species-specific gene expression patterns—several of which overlap with human data. They unify data across multiple datasets from mice and chicks with experimental myopia, revealing consistent molecular responses not evident in individual studies. Among the conserved pathways, Transforming Growth Factor-beta signaling and circadian entrainment emerged as central regulators, while species-specific patterns highlighted dopamine signaling in mice and glucagon in chicks. The convergence between animal model data and human genetic findings adds translational weight to the molecular targets identified. The authors also underscored the value of meta-analytic strategies in enhancing reproducibility and discovering novel gene targets for future investigation. Sanchez et al. offered novel insights into the role of exosomes derived from the retinal pigment epithelium in tree shrews, revealing proteomic differences in myopic eyes through an innovative *ex vivo* model. Their profiling identified over 500 proteins, with dozens uniquely expressed in each group and 286 significantly differentially regulated. In myopic eyes, upregulated proteins were primarily associated with cytoskeletal remodeling, oxidative stress response, and extracellular matrix dynamics—aligned with active tissue remodeling. Conversely, non-myopic eyes showed enrichment of proteins involved in phototransduction and mitochondrial homeostasis. These findings support the hypothesis that RPE-derived exosomes modulate emmetropization through cell signaling and metabolic regulation, and suggest potential applications in biomarker discovery and future pharmacological interventions for myopia.

Visual experience and experimental modulation

The last study of this Research Topic described how visual experience can be manipulated to influence ocular growth at a mechanistic level. Liu H. et al. investigated the effects of dynamic checkerboard visual stimuli—with different spatial and temporal frequencies—on ocular physiology and molecular signaling in chicks. Through a controlled experimental design with short-, medium-, and long-term exposure durations, the authors measured changes in choroidal thickness, ocular biometry, dopamine metabolite concentrations, and the expression of key genes linked to eye growth. Their findings reveal that exposure to 10 Hz flickering stimuli, particularly with ON-type patterns leads to greater elongation and myopia, and also correlates with increased levels of retinal dopamine metabolites. Additionally, gene expression analyses suggested an integrated visual, neurochemical, and genetic response. While choroidal thinning was an early feature in myopia, its predictive value for long-term growth was limited, indicating that multiple signaling pathways operate in concert. This study offers important evidence that the visual scene—its flicker rate, contrast polarity, and spatial granularity—can influence biological responses relevant to myopia, supporting the development of novel interventions to slow its progression.

Conclusion

Taken together, the nine contributions to this Research Topic present a compelling, multifaceted picture of myopia. Large-scale epidemiological studies reveal alarming trends in prevalence and progression, along with environmental risk factors such as artificial light exposure. Structural and functional analyses underscore differences in scleral and choroidal architecture as well as peripheral blur asymmetry in myopic eyes. Molecular and proteomic investigations expose conserved signaling pathways across species and the role of exosomes in intraocular communication. Finally, experimental manipulation of visual stimuli demonstrates how image dynamics can directly influence refractive error development.

Together, these articles converge on a shared insight: myopia is a complex, multi-system condition best understood through integrated perspectives. We hope this Research Topic serves as both a scientific resource and a catalyst for future interdisciplinary

advances in understanding myopia. We hope this Research Topic will serve as a valuable resource for researchers, clinicians, and policymakers working toward the shared goal of reducing the global burden of myopia.

Author contributions

PD: Writing – review & editing, Writing – original draft. FV-D: Writing – review & editing, Writing – original draft. AB-P: Writing – review & editing, Writing – original draft. PP-M: Writing – review & editing, Writing – original draft.

Conflict of interest

The authors declare that the research was conducted in the absence of any commercial or financial relationships that could be construed as a potential conflict of interest.

Generative AI statement

The author(s) declare that no Generative AI was used in the creation of this manuscript.

Publisher's note

All claims expressed in this article are solely those of the authors and do not necessarily represent those of their affiliated organizations, or those of the publisher, the editors and the reviewers. Any product that may be evaluated in this article, or claim that may be made by its manufacturer, is not guaranteed or endorsed by the publisher.

frontiers | Frontiers in Medicine

TYPE Original Research
PUBLISHED 10 July 2024
DOI 10.3389/fmed.2024.1391269

OPEN ACCESS

EDITED BY
Pablo De Gracia,
University of Detroit Mercy, United States

REVIEWED BY
Neeraj K. Singh,
Indiana University Bloomington, United States
Siti Nurliyana Abdullah,
University of Brunei Darussalam, Brunei

*CORRESPONDENCE
Xiaojuan Wang
✉ wangruye8008@163.com

†These authors have contributed equally to this work and share first authorship

RECEIVED 27 February 2024
ACCEPTED 01 July 2024
PUBLISHED 10 July 2024

CITATION
Li L, Liao Y, Wang Q, Wang M, Zhang W and Wang X (2024) Trends in myopia development among Chinese children and adolescents in Xuzhou during one academic year. *Front. Med.* 11:1391269. doi: 10.3389/fmed.2024.1391269

Trends in myopia development among Chinese children and adolescents in Xuzhou during one academic year

Lin Li[1†], Ya Liao[2†], Qian Wang[2], Mei Wang[2], Wenxuan Zhang[2] and Xiaojuan Wang[2*]

[1]School of Medical Technology, Xuzhou Medical University, Xuzhou, China, [2]Department of Ophthalmology, The First People's Hospital of Xuzhou, The Affiliated Xuzhou Municipal Hospital of Xuzhou Medical University, Xuzhou, China

Purpose: This study investigates the prevalence and progression of myopia among primary and secondary school students in Xuzhou City, China, during one academic year.

Methods: The study employed a prospective research design and utilized a whole-group sampling method to conduct non-cycloplegic spot photo screenings on 37,938 students from 44 primary and secondary schools in Xuzhou City, China. A one-year study was conducted to gather spherical equivalent refraction (SER), and subsequent analysis was carried out to explore the disparities in myopia prevalence among primary and secondary school students within the same academic year, as well as the progression of myopia.

Results: During the 2022 academic year, the overall prevalence of myopia in the first and second semesters was 62.6 and 64.2% respectively, indicating an increasing trend. Particularly in primary school (Grades 1–6), the prevalence of myopia increased with higher grade levels, and significant variations in myopia prevalence were observed mainly in grades 1–3 and 7 ($p < 0.05$). The incidence rate of myopia in middle school remained stable, while in primary school, there was a positive correlation between myopia incidence and the grade level, with the highest rate of 20.1% in grade 6. Among the myopic population, the median value of spherical equivalent refraction slightly decreased between the two semesters. The proportion of high myopia increased among students in grades 5–8.

Conclusion: Our study revealed that within one academic year, the prevalence of myopia and the severity of myopia have significantly increased in Xuzhou City, China, accompanied by an increase in the proportion of high myopia. For different grade levels, we should adopt personalized prevention and control measures, with a particular focus on lower grade levels and students who have just entered a new grade.

KEYWORDS

myopia, development, children, adolescents, prevalence

Introduction

Myopia is a common condition that causes visual impairment and is a major public health problem, especially among children and adolescents (1). In the absence of effective preventive and control measures, it is projected that the global myopia population will approach approximately 5 billion by the year 2050, with high myopia affecting approximately 10% of the global population. East Asia and Southeast Asia are identified as regions with the highest prevalence of myopia, where the occurrence among young adults ranges from 80 to 90%. Furthermore, the prevalence of high myopia among this demographic in these regions is relatively elevated, ranging from 10 to 20%. High myopia substantially increases the risk of ocular complications, encompassing myopic maculopathy, retinal detachment, glaucoma, cataracts, and a range of other pathologies. These conditions have the potential to cause enduring and irreversible visual impairment (2, 3). The global cost of myopia interventions is also rising (4).

Based on research surveys (5–10), there has been a consistent rise in the prevalence of myopia among children and adolescents in China, indicating a severe situation regarding myopic incidence. However, current longitudinal studies on this topic, both in China and other countries (5–8, 10), typically have a minimal time interval of 1 year. Nonetheless, several findings have found a significant prevalence in the incidence and progression of myopia within a single academic year (two semesters) among students, particularly in higher grades burdened with heavier academic loads. Consequently, we undertook a 1-year study, meticulously examining the myopia status of primary and secondary school students in Xuzhou City throughout two semesters. The primary objective was to assess the incidence and developmental trends of myopia among these students within the same academic year. Gaining insights into the patterns of myopia incidence and development among children and adolescents is imperative for refining and adapting local measures aimed at preventing and controlling myopia.

Methods

Study population

In accordance with the requirements of the "Comprehensive Control of Myopia in Children and Adolescents" program (11), Xuzhou City has implemented comprehensive vision screening for primary and secondary school students since the beginning of 2019. The screening took place twice a year, within 1 month after the commencement of each semester (6 months). This study employed a whole-group sampling method to select 44 schools from five districts in Xuzhou City randomly. The survey data collected from the same cohort of students during both the first and second semesters of the 2022 academic year were analyzed. A total of 38,041 students participated in the research, with individuals wearing contact lenses or affected by other conditions that could potentially impact ocular data collection being excluded from the study. Ultimately, 37,938 students were included in the final analysis. This study followed the principles of the Helsinki Declaration and was approved by the Ethics Committee of Xuzhou Medical University Xuzhou Municipal Hospital, China (No. Xyll[2019]022).

Data collection

A week before the initiation of the screening process, thorough communication was conducted with the schools to acquire comprehensive demographic information about the students, encompassing their names, genders, ages, and other pertinent particulars. It was explicitly communicated that participants were strictly prohibited from wearing contact lenses on the examination day. Furthermore, a comprehensive briefing was provided to all participants and their respective guardians, elucidating the study's purpose, extent, and significance. Before the examination, explicit verbal consent was obtained from the guardians to ensure their understanding and agreement with the research protocol.

Subjects were screened for refractive error using the Spot photo screener (Welch Allyn, VS100) for non-cycloplegic photorefraction. The screening was performed by experienced ophthalmic staff, including one ophthalmologist and five optometrists. Before the refractive screening, subjects underwent a slit lamp examination and were asked about their ocular history to exclude those with cataracts or other conditions that may affect refraction, as well as those who had undergone refractive surgery or wore contact lenses. Subjects with a history of ortho-k lenses within the last month were also recorded. The examiner used the Spot photo screener to collect data from the subjects in a relative darkroom at a distance of approximately 1 m in the uncorrected state. The data was automatically generated and uploaded to the terminal for recording. If significant refractive errors, strabismus, or anisometropia were detected, feedback was provided to the school and parents with a recommendation for further examination at a medical clinic.

Definition

The spherical equivalent refraction (SER) is calculated by adding the sum of the sphere power with half of the cylinder power. If the result exceeds the ±7.50 D range of the Spot screener, it is recorded as ±8.00D. If the SER of either eye is less than or equal to −0.50 D, the student is classified as myopic. Individuals who wear ortho-k lenses are also considered myopic (12). The degree of myopia is classified into mild myopia ($-3.00\ D < SER \leq -0.50\ D$), moderate myopia ($-6.00\ D < SER \leq -3.00\ D$), and high myopia ($SER \leq -6.00\ D$).

Statistical analyses

The statistical analysis was conducted using SPSS 27.0 (IBMSPSS, Armonk, NY, United States), Microsoft Excel 2010, and the figures were prepared using OriginPro 2021. The statistical tests were two-sided, and a p-value < 0.05 was considered statistically significant. The skewed distribution of continuous variables was represented by the median (interquartile range, IQR), while count data was presented as frequency (rate). The Mann–Whitney U test was used to compare differences between the two groups, and the chi-square test was used to compare the prevalence and incidence of myopia among different grade levels. Spearman rank correlation test was used to assess the correlation between the spherical equivalent refraction (SER) of the left and right eyes. Due to the high correlation between the SER of

both eyes (Spearman's rank correlation = 0.932, $p < 0.01$), we used the SER of the right eye to evaluate the progression of myopia in students.

Results

General characteristics

The study encompassed a cohort of 38,041 students enrolled in 44 schools. A total of 104 participants were excluded from the analysis due to specific criteria, including the use of contact lenses, recent ortho-k lens wear, prior eye surgeries, or the presence of other ocular conditions that could potentially influence the refractive status. Consequently, the final dataset comprised 37,938 eligible records meeting the inclusion criteria. Among these records, 20,799 (54.8%) corresponded to male students, while 17,139 (45.2%) represented female students. The distribution of the sample size, grade levels, and gender can be found in Figure 1.

Myopia prevalence and incidence

Table 1 presents the changes in the prevalence of myopia among students in grades 1–9 during the first and second semesters of the 2022 academic year, including both male and female students. The overall myopia prevalence for the 2022 academic year was 62.6 and 64.2%, showing an increasing trend. Within the same semester, there was a linear relationship between myopia prevalence and grade, with an increase in myopia prevalence as the grade level advanced during the primary school stage. The variation in myopic prevalence among different grades is mainly concentrated in grades 1–3 and 7 ($p < 0.05$). Among them, the largest increase in myopia prevalence is observed in grade 3 (2.8%), followed by grade 2 (2.6%), grade 1 (2.2%), and grade 7 (1.4%). The myopia prevalence in both males and females increases from the beginning and end of the same academic year, with females having a higher myopia prevalence than males.

The incidence rate of myopia during the academic year of 2022 exhibited notable variations primarily among primary school students, while the incidence rate remained relatively stable among middle school students. Within the primary school stage, there was a positive correlation between the incidence of myopia and grade level, with the highest incidence rate of 20.1% observed in the 6th grade. Moreover, there was no statistically significant difference in myopia incidence between males and females (Table 2).

Refractive error

Table 3 shows the spherical equivalent refraction (SER) of primary and secondary school students throughout the 2022 academic year, encompassing the first and second semesters. Within the myopic population (identified as myopic during the initial semester screening), the median SER values exhibited a slight decline during both halves of the year. Nonetheless, the extent of this change was relatively modest. Figure 2 illustrates the distribution of spherical equivalent refraction (SER) for children and adolescents in grades 1–9 during the 2022 academic year.

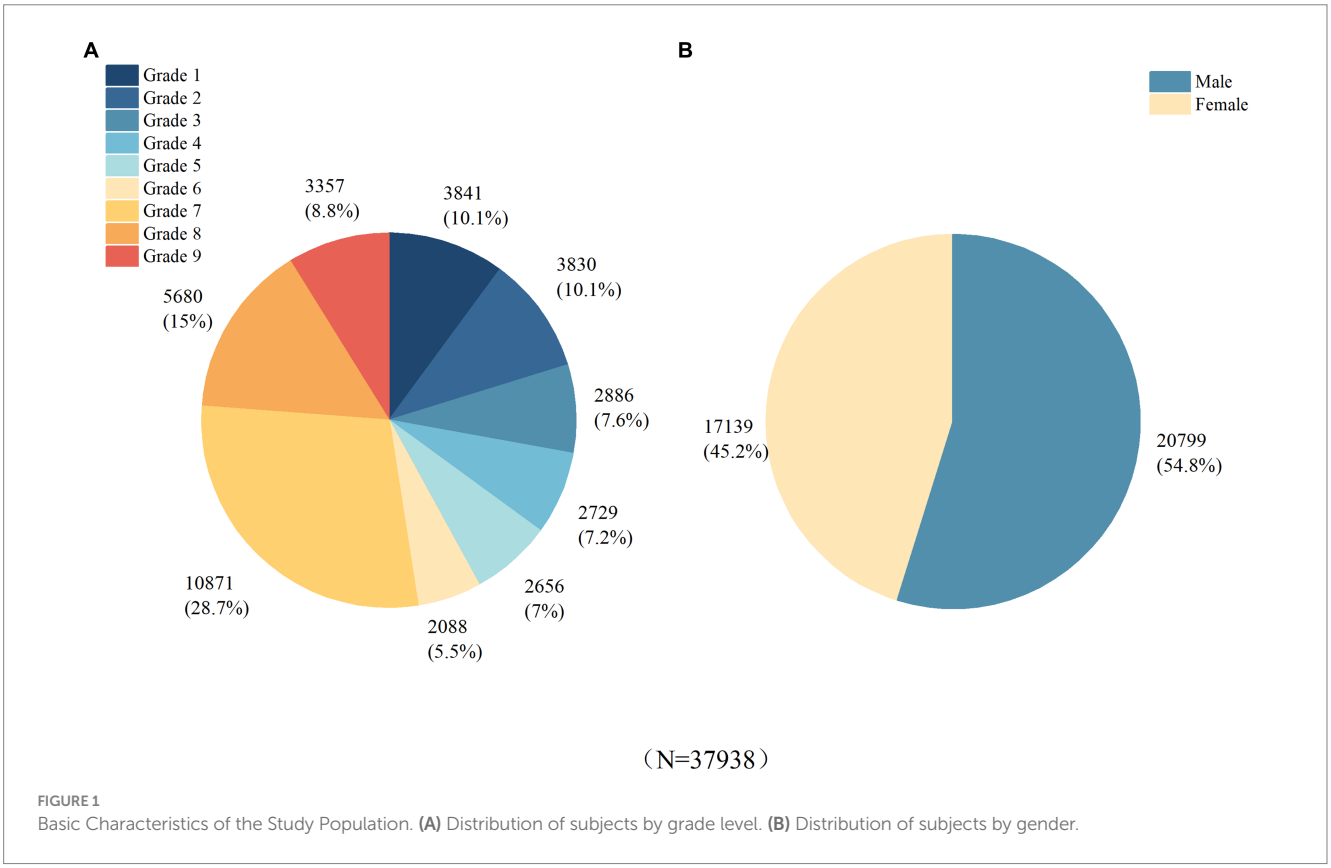

FIGURE 1
Basic Characteristics of the Study Population. **(A)** Distribution of subjects by grade level. **(B)** Distribution of subjects by gender.

TABLE 1 Myopia prevalence by grade and gender (%).

	First semester	Second semester	*p*
Grades			
1	37.7%	39.9%	**0.044***
2	50.4%	53.0%	**0.028***
3	49.2%	52.0%	**0.033***
4	58.6%	60.9%	0.087
5	68.0%	68.7%	0.555
6	76.7%	77.7%	0.417
7	68.6%	70.0%	**0.024***
8	73.6%	74.4%	0.325
9	68.3%	70.1%	0.119
p	**<0.001***	**<0.001***	
Gender			
Male	59.7%	61.3%	**<0.001***
Female	66.1%	67.7%	**0.002***
p	**<0.001***	**<0.001***	
Total	62.6%	64.2%	**<0.001***

This table presents the prevalence of myopia, stratified by both grade level and gender.
*Significance was set at $p < 0.05$.

TABLE 2 The incidence rate of myopia in the 2022 academic year (%).

	Myopia incidence	*p*
Grades		
1	8.4%	**<0.001****
2	10.6%	
3	13.3%	
4	14.8%	
5	13.5%	
6	20.1%	
1–6	11.9%	
7	15.1%	0.617[b]
8	16.1%	
9	15.7%	
7–9	15.4%	
Gender		0.345
Male	15.1%	
Female	16.0%	
Total		**<0.001***

*Significance was set at $p < 0.05$.
a, b represent *p*-values for comparisons between myopia incidence in primary and junior high school grades, respectively.

Fluctuations in the severity of myopia

Further analysis showed that the proportion of mild myopia in grades 6–8 decreased from semester 1 to 2 (46.0, 36.9, 39.3% vs. 42.9, 35.4, 37.4%), while the proportion of moderate myopia increased in grades 4–9 (11.3, 17.4, 23.4, 23.7, 25.5, 23.2% vs. 14.6, 20.5, 26.6, 26.2, 28.3, 25.8%). In addition, there was an increase in the proportion of high myopia in grades 5–8 (0.4, 1.1, 1.6, 1.9% vs1.0, 1.9, 2.2, 2.6%) (Table 4; Figure 3).

Discussion

Our research has unveiled that within the educational landscape in China, the prevalence and incidence of myopia among primary and secondary school students are far from desirable, and the situation is exacerbated with higher grade levels. Employing a longitudinal approach, we monitored the myopia trajectory of students spanning grades 1–9 in Xuzhou, China, throughout a single academic year encompassing both the initial and subsequent semesters. Unlike the majority of studies that typically have a one-year interval between examinations, our research findings revealed a significant progression and increase in the incidence, prevalence, and severity of myopia among children and adolescents within a single semester (6 months).

Our research investigation revealed that the prevalence of myopia among primary and secondary school students in Xuzhou City during the first and second semesters of the 2022 academic year was 62.6 and 64.2%, respectively. Notably, there was a significant increase in myopia prevalence during the second semester compared to the first semester. Furthermore, consistent with findings from both domestic and international surveys, the myopia rate among females was higher than that among males (13–15). This trend may be attributed to the relatively lower amount of time females spend engaging in outdoor activities compared to males, and longer periods of close-eye use (16, 17). Research on the prevalence of myopia, both nationally and internationally, was mostly based on cross-sectional studies with a minimum time interval of 1 year. There is a paucity of longitudinal studies focusing on short-term changes in myopia. According to a meta-analysis of myopia prevalence among children and adolescents in China from 1998 to 2016, the overall myopia prevalence rate among children aged 3–19 years was 37.7%. The study also found a close association between myopia prevalence and gender, and the analysis showed an increasing trend in myopia prevalence as the study years progressed (18). According to the data from the Chinese Ministry of Education for the 2019–2020 academic year, the prevalence of myopia among primary school students was 36.49%. Looking at other provinces and cities in China, the prevalence of myopia among primary school students is 37.7% in Hong Kong, and 33.6% in Chongqing (19, 20). In northern India, the prevalence of myopia among primary school children was reported to be 21.1%, in South Korea, the prevalence of myopia among children and adolescents aged 5–18 years reached as high as 65.4%. Another study conducted in Singapore revealed a myopia prevalence rate of 31.6% among primary school children. Interestingly, in Japan, a similar survey reported a significantly higher prevalence of myopia, with Japanese elementary school students reaching 76.5% (21–24). The prevalence of myopia is generally high in East Asia. Therefore, it is of the utmost importance to implement effective strategies for the early detection of myopia and the implementation of myopia prevention and control measures.

The findings of this study demonstrate a clear linear relationship between grade level and the prevalence of myopia, particularly in primary school grades where the prevalence of myopia escalates with

TABLE 3 SER values for different grade levels in the 2022 academic year (D).

	No myopia			Myopia		
	First semester	Second semester	*p*	First semester	Second semester	*p*
Grades						
1	+0.25 (0.00,+0.50)	+0.25 (0.00,+0.50)	**0.001***	−2.75 (−4.25, −1.00)	−2.75 (−4.25, −1.25)	**<0.001***
2	+0.25 (0.00,+0.50)	+0.25 (0.00,+0.50)	**<0.001***	−2.50 (−4.25, −1.00)	−2.75 (−4.50, −1.25)	**<0.001***
3	+0.25 (0.00, +0.25)	+0.25 (0.00, +0.50)	**<0.001***	−1.50 (−2.75, −0.75)	−1.75 (−3.00, −1.00)	**<0.001***
4	0.00 (0.00, +0.25)	0.00 (−0.25, +0.50)	**<0.001***	−1.75 (−3.00, −1.00)	−2.25 (−3.25, −1.25)	**<0.001***
5	0.00 (0.00, +0.25)	0.00 (−0.25, +0.25)	**<0.001***	−2.00 (−3.25, −1.00)	−2.25 (−3.75, −1.25)	**<0.001***
6	0.00 (−0.25, +0.25)	0.00 (−0.25, +0.25)	**<0.001***	−2.25 (−3.75, −1.25)	−2.50 (−4.00, −1.25)	**<0.001***
7	+0.25 (0.00, +0.50)	+0.25 (−0.25, +0.50)	**<0.001***	−2.50 (−4.00, −1.25)	−3.00 (−4.25, −1.50)	**<0.001***
8	+0.25 (0.00 + 0.50)	+0.00 (−0.25 + 0.50)	**<0.001***	−2.75 (−4.00, −1.25)	−3.00 (−4.25, −1.50)	**<0.001***
9	+0.25 (0.00 + 0.50)	+0.25 (−0.25 + 0.50)	**<0.001***	−2.50 (−4.00, −1.25)	−2.75 (−4.25, −1.25)	**<0.001***
Total	+0.25 (0.00 + 0.50)	+0.25 (0.00 + 0.50)	**<0.001***	−2.50 (−3.75, −1.25)	−2.75 (−4.00, −1.25)	**<0.001***
p	**<0.001***	**<0.001***		**<0.001***	**<0.001***	

*Significance was set at $p < 0.05$.

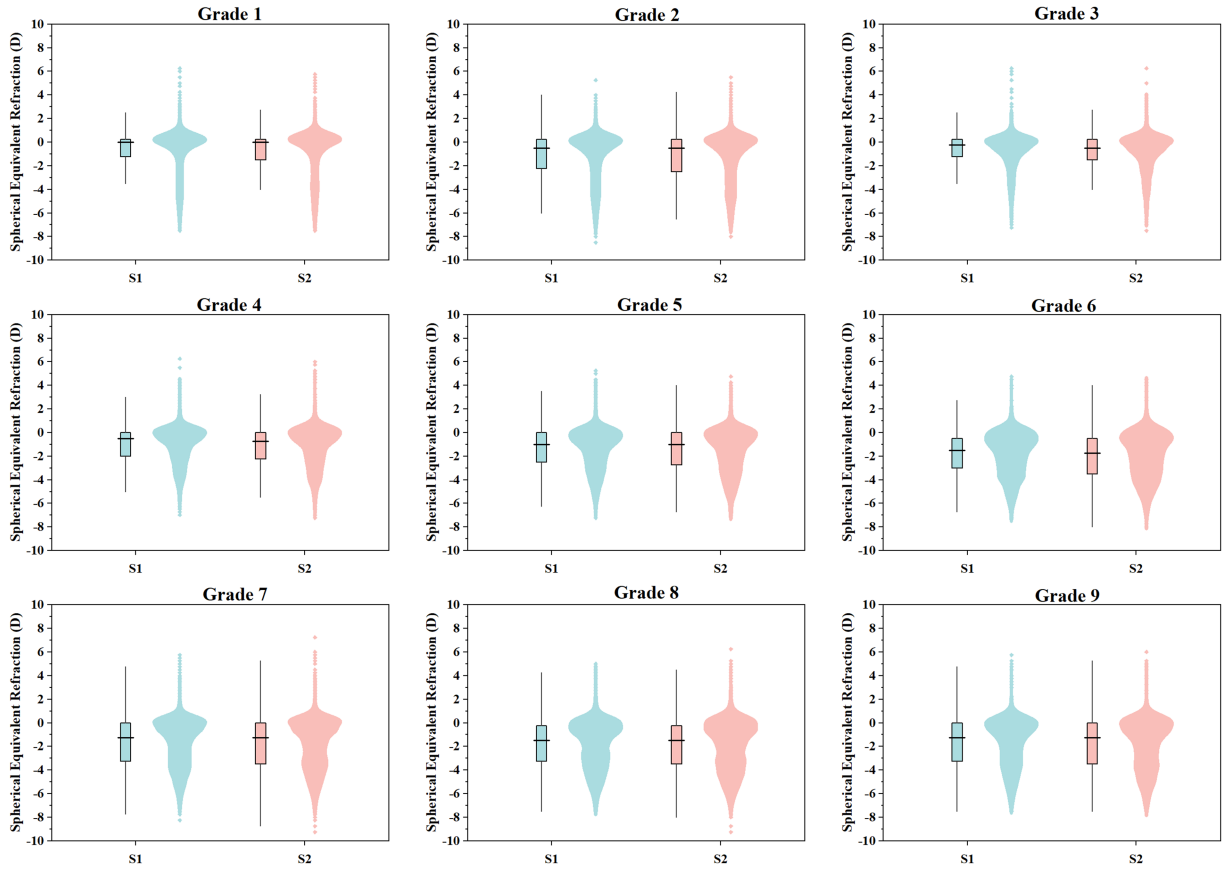

FIGURE 2
Distribution of spherical equivalent refraction in subjects from Grade 1 to Grade 9 during the 2022 academic year. S1 denotes First Semester, S2 denotes Second Semester.

higher grade levels. Numerous studies have consistently established a strong association between myopia prevalence and grade levels (25–28), which can be attributed to heightened academic pressures, prolonged close-eye use, diminished engagement in outdoor activities, and sleep decrease as students progress to higher grades. The changes in ocular parameters that contribute to refractive error predominantly

TABLE 4 Changes in the degree of myopia in the 2022 academic year (%).

Grades	2022 S1				2022 S2				*p*
	No myopia	Mild myopia	Moderate myopia	High myopia	No myopia	Mild myopia	Moderate myopia	High myopia	
1	66.1%[a]	19.1%[a]	13.5%[a]	1.3%[a]	64.3%[a]	19.9%[a]	14.3%[a]	1.6%[a]	0.329
2	55.2%[a]	26.3%[a]	16.2%[a]	2.2%[a]	52.9%[b]	27.0%[a]	17.6%[a]	2.5%[a]	0.186
3	57.3%[a]	33.5%[a]	8.8%[a]	0.3%[a]	54.5%[b]	35.0%[a]	10.0%[a]	0.5%[a]	0.113
4	49.2%[a]	39.3%[a]	11.3%[a]	0.1%[a]	45.9%[b]	39.1%[a]	14.6%[b]	0.4%[a]	**<0.001***
5	40.2%[a]	42.0%[a]	17.4%[a]	0.4%[a]	38.9%[a]	39.6%[a]	20.5%[b]	1.0%[b]	**0.002***
6	29.5%[a]	46.0%[a]	23.4%[a]	1.1%[a]	28.6%[a]	42.9%[b]	26.6%[b]	1.9%[b]	**0.007***
7	37.8%[a]	36.9%[a]	23.7%[a]	1.6%[a]	36.2%[b]	35.4%[b]	26.2%[b]	2.2%[b]	**<0.001***
8	33.2%[a]	39.3%[a]	25.5%[a]	1.9%[a]	31.7%[a]	37.4%[b]	28.3%[b]	2.6%[b]	**<0.001***
9	37.9%[a]	36.9%[a]	23.2%[a]	2.0%[a]	36.6%[a]	35.1%[a]	25.8%[b]	2.4%[a]	**0.040***
Total	43.8%[a]	35.2%[a]	19.7%[a]	1.4%[a]	42.0%[b]	34.2%[b]	22.0%[b]	1.9%[b]	**<0.001***

*Significance was set at $p < 0.05$.
First Semester (S1); Second Semester (S2).
In the population with the same level of myopia within the same grade, different superscript letters indicate.
Significant differences between semesters ($p < 0.05$).

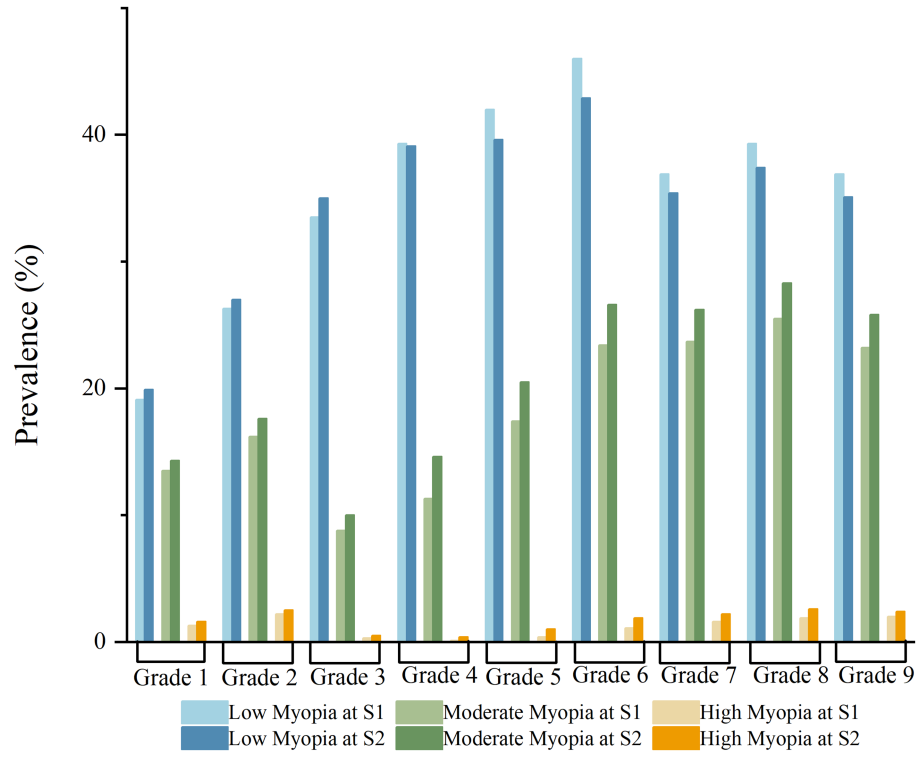

FIGURE 3
Distribution of myopia rates across different grade levels in primary and secondary schools during the 2022 academic year. Comparison of myopia rates between the first semester (S1) and the second semester (S2).

occur during childhood (29–31). In addition, the impact of COVID-19 on education and lifestyle has led to an increase in near-work activities and screen time, accompanied by a decrease in outdoor activities. This has made regular eye examinations even more important in preparing for myopia management (32). The current research findings indicate a significant increase in the prevalence of myopia during the second semester of the academic year, with a particular emphasis on students in grades 1–3 and 7. Consequently, it is imperative to prioritize targeted interventions aimed at controlling and preventing myopia in these specific cohorts, namely lower-grade students and those who

have recently transitioned to a higher-grade level. Such focused interventions hold significant potential for effectively curbing the escalating prevalence of myopia and its associated risks among school-aged children.

In Guangzhou, the annual incidence of myopia was between 20 and 30% in 2018 (33). Furthermore, in Anyang City, the yearly incidence of myopia increased from 7.8% in grades 1 and 2 to 25.3% in grades 5 and 6 (7). In our study, the overall incidence rate of myopia among primary and secondary school students within 6 months was 13.4%. Among primary school students, it was 11.9%, and among secondary school students, it was 15.4%. However, further analysis revealed that the incidence of myopia showed a linear increase with grade level in primary schools, while it tended to stabilize in different grades of secondary schools. This observation may be related to the education system in China and the developmental characteristics of children and adolescents themselves. The academic workload and visual stress for primary school students tend to increase as they progress to higher grades, accompanied by rapid changes in axial length. On the other hand, secondary school students generally have a heavier academic workload, but the changes in visual stress may be relatively smaller compared to primary school, and eye growth and development are more stable than in childhood. However, overall, the incidence of myopia in secondary school is still higher than that in primary school, which is consistent with the findings of the Mojiang Myopia Progression Study. This study reported that the annual incidence of myopia among first-grade primary school students was 33.6%, while it increased to 54% by the first grade of secondary school (5). These findings highlight the continued importance of implementing early myopia prevention strategies, with specific attention to the primary school stage, emphasizing the crucial need for sustained awareness and intervention measures during this critical period to tackle the risk factors linked to myopia development.

In our study, we analyzed the changes in refractive diopters over one semester in eyes with myopia and eyes without myopia. We have found that eyes with myopia exhibit a greater progression of myopia compared to eyes without myopia. This finding is consistent with the earlier viewpoint proposed by Mäntyjärvi (34), and can be expressed as follows: There exists a well-controlled controlled eye growth, but once the eyes cross the zero point and become myopic, the change in refractive error increases throughout the same period. As early as the late 1990s, highly competitive Hong Kong also observed this phenomenon. They reported that in a small sample of myopic eyes, the myopic progression over two and a half years in 6-year-old children was −1.92D, while non-myopic eyes showed only a −0.41D shift in refractive error during the same period (35). Our research findings indicate that among primary school students from Grade 2 to junior high school students in Grade 9, myopic eyes showed a myopic progression of −0.25D to −0.50D over one semester, while non-myopic eyes had no myopic shift (0D) during the same period. The results show a similar trend to the previously mentioned study conducted in Hong Kong. This further confirms the above viewpoint that once the eye alters into myopia, crossing over zero-point, its growth is no longer perfectly controlled and the axial length increase is getting out of control. Furthermore, we also investigated the changes in the degree of myopia among children who were already myopic. We found that, overall, there was a decrease in the prevalence of low myopia and an increase in the prevalence of moderate to high myopia in the second semester compared to the first semester among primary and secondary school students. When examining the data by grade level, this trend was observed from the fourth grade to the ninth grade. Another study that investigated the trends of myopia among primary and junior school students in the post-COVID-19 epidemic period over 3 years also reported the changes in the prevalence of different myopia degrees (36). From the data, it can be observed that the trend of the increasing prevalence of moderate to high myopia started in the fourth grade, which is consistent with the findings of our study. Nonetheless, our study, which investigated the changes over one semester, yielded the same outcomes. These findings emphasize the importance of timely implementing measures to control myopia, regulate its progression, and prevent a rapid worsening in its severity upon manifestation. Under the same educational background, it is important to adopt different myopia prevention measures for students in different grades of primary school, taking into account the school, family, and individual aspects. Moreover, Shanghai myopia research has found that well-implemented school myopia management can effectively reduce the risk of myopia among students. These measures mainly include encouraging outdoor activities during recess or physical education class providing adequate instruction in reading and writing postures, and good writing on blackboards, desks, and chairs with suitable heights (37).

Limitations

This study differs from the majority of cross-sectional myopia screening studies as it adopts a prospective longitudinal design. Additionally, compared to the commonly used one-year observation period, our study has a more intensive and frequent observation period, and we have a sufficiently large sample size. However, there are certain limitations to this study. We employed non-cycloplegic refraction for myopia screening, as the use of cycloplegic agents in schools requires parental consent and may not be operationally feasible in large samples or school environments. This may have an impact on the detection of myopia. Nevertheless, the large sample size compensates for this limitation.

Conclusion

In summary, our research indicates a high incidence of myopia among primary and secondary school students in Xuzhou, China, within one academic year. There is a significant increase in myopia prevalence within a single semester, accompanied by notable progression and a rise in high myopia rates. These issues worsen with higher grade levels. To effectively prevent and control myopia in children and adolescents, it is crucial to conduct two refractive examinations per year for early detection and intervention. Personalized prevention and control measures tailored to different grade levels are essential for effective management.

Data availability statement

The original contributions presented in the study are included in the article/supplementary material, further inquiries can be directed to the corresponding author.

Ethics statement

The studies involving humans were approved by Ethics Committee of Xuzhou Medical University Xuzhou Municipal Hospital, China. The studies were conducted in accordance with the local legislation and institutional requirements. Written informed consent for participation was not required from the participants or the participants' legal guardians/next of kin because This is an observational study, and before conducting visual screening each semester, we inform parents and teachers about the screening's purpose, methods, and the necessary precautions to take before the exam. We have obtained verbal consent from the parents, which was approved by the Ethics Committee of Xuzhou Municipal Hospital.

Author contributions

LL: Conceptualization, Formal analysis, Investigation, Methodology, Project administration, Visualization, Writing – original draft, Writing – review & editing. YL: Conceptualization, Formal analysis, Methodology, Supervision, Writing – original draft, Writing – review & editing. QW: Methodology, Supervision, Writing – original draft, Writing – review & editing. MW: Methodology, Supervision, Writing – original draft, Writing – review & editing. WZ: Conceptualization, Methodology, Software, Supervision, Visualization, Writing – original draft, Writing – review & editing. XW: Conceptualization, Methodology, Software, Supervision, Writing – original draft, Writing – review & editing.

Funding

The author(s) declare that financial support was received for the research, authorship, and/or publication of this article. This work was supported by grants from the Xuzhou Medical Leading Talent Training Project (Grant No. XWRCHT20210022).

Acknowledgments

The authors would like to thank all participants who voluntarily contributed to this study. This article has been published as a preprint under the doi number https://doi.org/10.21203/rs.3.rs-3828222/v1.

Conflict of interest

The authors declare that the research was conducted in the absence of any commercial or financial relationships that could be construed as a potential conflict of interest.

Publisher's note

References

1. Chen YX, Liao CM, Tan Z, He MG. Who needs myopia control? *Int J Ophthalmol*. (2021) 14:1297–301. doi: 10.18240/ijo.2021.09.01

2. Holden BA, Fricke TR, Wilson DA, Jong M, Naidoo KS, Sankaridurg P, et al. Global prevalence of myopia and high myopia and temporal trends from 2000 through 2050. *Ophthalmology*. (2016) 123:1036–42. doi: 10.1016/j.ophtha.2016.01.006

3. Haarman AEG, Enthoven CA, Tideman JWL, Tedja MS, Verhoeven VJ, Klaver C. The complications of myopia: a review and meta-analysis. *Invest Ophthalmol Vis Sci*. (2020) 61:49. doi: 10.1167/iovs.61.4.49

4. Foo LL, Lanca C, Wong CW, Ting D, Lamoureux E, Saw SM, et al. Cost of myopia correction: a systematic review. *Front Med*. (2021) 8:718724. doi: 10.3389/fmed.2021.718724

5. Li L, Zhong H, Li J, Li CR, Pan CW. Incidence of myopia and biometric characteristics of premyopic eyes among Chinese children and adolescents. *BMC Ophthalmol*. (2018) 18:178. doi: 10.1186/s12886-018-0836-9

6. Fan DSP, Lam DSC, Lam RF, Lau JT, Chong KS, Cheung EY, et al. Prevalence, incidence, and progression of myopia of school children in Hong Kong. *Invest Ophthalmol Vis Sci*. (2004) 45:1071–5. doi: 10.1167/iovs.03-1151

7. Li SM, Wei S, Atchison DA, Kang MT, Liu L, Li H, et al. Annual incidences and progressions of myopia and high myopia in Chinese schoolchildren based on a 5-year cohort study. *Invest Ophthalmol Vis Sci*. (2022) 63:8. doi: 10.1167/iovs.63.1.8

8. Bro T, Löfgren S. Relatively stable prevalence of myopia among Swedish children aged 4 to 7 years between 2015 and 2020. *Optom Vis Sci*. (2023) 100:91–5. doi: 10.1097/OPX.0000000000001972

9. Zhou WJ, Zhang YY, Li H, Wu YF, Xu J, Lv S, et al. Five-year progression of refractive errors and incidence of myopia in school-aged children in Western China. *J Epidemiol*. (2016) 26:386–95. doi: 10.2188/jea.JE20140258

10. Saw SM, Tong L, Chua WH, Chia KS, Koh D, Tan DT, et al. Incidence and progression of myopia in Singaporean school children. *Invest Ophthalmol Vis Sci*. (2005) 46:51–7. doi: 10.1167/iovs.04-0565

11. Jiangsu Provincial Department of Education, D.o.P.E., Health and Arts Education. Opinions on comprehensive prevention and control of Myopiaamong children and adolescents in Jiangsu Province (Su education, sports, health and arts: No. 7); (2019).

12. National Health Commission of the People's republic of China. Specification for screening of refractive error in primary and secondary school students (WS/T 663–2020). Beijing: National Health Commission of the People's Republic of China (2020).

13. Jing S, Yi X, Lei Y, Hu L, Cheng W, Wen T, et al. Prevalence and risk factors for myopia and high myopia: a cross-sectional study among Han and Uyghur students in Xinjiang, China. *Ophthalmic Physiol Opt*. (2022) 42:28–35. doi: 10.1111/opo.12907

14. Jiang D, Zhang D, Zhang Y, Shi B, Gao H, Guo Y, et al. The trend of myopia rate in 61 350 children and adolescents: a cross-sectional research in Ningbo. *Zhejiang Acta Ophthalmol*. (2020) 98:e525–6. doi: 10.1111/aos.14343

15. Morgan A, Young R, Narankhand B, Chen S, Cottriall C, Hosking S. Prevalence rate of myopia in schoolchildren in rural Mongolia. *Optom Vis Sci*. (2006) 83:53–6. doi: 10.1097/01.opx.0000195567.88641.af

16. Ip JM, Saw SM, Rose KA, Morgan IG, Kifley A, Wang JJ, et al. Role of near work in myopia: findings in a sample of Australian school children. *Invest Ophthalmol Vis Sci*. (2008) 49:2903–10. doi: 10.1167/iovs.07-0804

17. Wu LJ, You QS, Duan JL, Luo YX, Liu LJ, Li X, et al. Prevalence and associated factors of myopia in high-school students in Beijing. *PLoS One*. (2015) 10:e0120764. doi: 10.1371/journal.pone.0120764

18. Dong L, Kang YK, Li Y, Wei WB, Jonas JB. Prevalence and time trends of myopia in children and adolescents in China: a systemic review and meta-analysis. *Retina*. (2020) 40:399–411. doi: 10.1097/IAE.0000000000002590

19. Yue Y, Liu X, Yi S, Liu B, Yi H, Li H. High prevalence of myopia and low hyperopia reserve in 4411 Chinese primary school students and associated risk factors. *BMC Ophthalmol*. (2022) 22:212. doi: 10.1186/s12886-022-02436-5

20. Choy BNK, You Q, Zhu MM, Lai JSM, Ng ALK, Wong IYH. Prevalence and associations of myopia in Hong Kong primary school students. *Jpn J Ophthalmol*. (2020) 64:437–49. doi: 10.1007/s10384-020-00733-4

21. Singh NK, James RM, Yadav A, Kumar R, Asthana S, Labani S. Prevalence of myopia and associated risk factors in schoolchildren in North India. *Optom Vis Sci*. (2019) 96:200–5. doi: 10.1097/OPX.0000000000001344

22. Kim H, Seo JS, Yoo WS, Kim GN, Kim RB, Chae JE, et al. Factors associated with myopia in Korean children: Korea National Health and nutrition examination survey 2016–2017 (KNHANES VII). *BMC Ophthalmol*. (2020) 20:31–7. doi: 10.1186/s12886-020-1316-6

23. Karuppiah V, Wong L, Tay V, Ge X, Kang LL. School-based programme to address childhood myopia in Singapore. *Singapore Med J*. (2021) 62:63–8. doi: 10.11622/smedj.2019144

24. Yotsukura E, Torii H, Inokuchi M, Tokumura M, Uchino M, Nakamura K, et al. Current prevalence of myopia and association of myopia with environmental factors among schoolchildren in Japan. *JAMA Ophthalmol*. (2019) 137:1233–9. doi: 10.1001/jamaophthalmol.2019.3103

25. Leng L, Zhang J, Xie S, Ding W, Ji R, Tian Y, et al. Effect of sunshine duration on myopia in primary school students from northern and southern China. *Int J Gen Med*. (2021) 14:4913–22. doi: 10.2147/IJGM.S328281

26. Hung HD, Chinh DD, Tan PV, Duong NV, Anh NQ, Le NH, et al. The prevalence of myopia and factors associated with it among secondary school children in rural Vietnam. *Clin Ophthalmol*. (2020) 14:1079–90. doi: 10.2147/OPTH.S251218

27. Peng W, Zhang Z, Wang F, Sun S, Sun Y. Association of educational environment with the prevalence of myopia: a cross-sectional study in Central China. *Front Public Health*. (2023) 11:1188198. doi: 10.3389/fpubh.2023.1188198

28. Xu SJ, Wan YH, Xu ZH, Zhang H, Xu L, Wang B, et al. Association between time spent on physical exercise, sleep, homework and suspected myopia among students. *Zhonghua Liu Xing Bing Xue Za Zhi*. (2016) 37:183–6. doi: 10.3760/cma.j.issn.0254-6450.2016.02.006

29. Yii FSL. Emmetropic eye growth in east Asians and non-east Asians. *Ophthalmic Physiol Opt*. (2023) 43:1412–8. doi: 10.1111/opo.13195

30. Rozema J, Dankert S, Iribarren R, Lanca C, Saw SM. Axial growth and lens power loss at myopia onset in Singaporean children. *Invest Ophthalmol Vis Sci*. (2019) 60:3091–9. doi: 10.1167/iovs.18-26247

31. Zadnik K, Mutti DO, Mitchell GL, Jones LA, Burr D, Moeschberger ML. Normal eye growth in emmetropic schoolchildren. *Optom Vis Sci*. (2004) 81:819–28. doi: 10.1097/01.opx.0000145028.53923.67

32. Singh NK. Myopia epidemic post–coronavirus disease 2019. *Optom Vis Sci*. (2020) 97:911–2. doi: 10.1097/OPX.0000000000001591

33. Wang SK, Guo Y, Liao C, Chen Y, Su G, Zhang G, et al. Incidence of and factors associated with myopia and high myopia in Chinese children, based on refraction without cycloplegia. *JAMA Ophthalmol*. (2018) 136:1017–24. doi: 10.1001/jamaophthalmol.2018.2658

34. Mäntyjärvi MI. Changes of refraction in schoolchildren. *Arch Ophthalmol*. (1985) 103:790–2. doi: 10.1001/archopht.1985.01050060050022

35. Goldschmidt E, Lam CSY, Opper S. The development of myopia in Hong Kong children. *Acta Ophthalmol Scand*. (2001) 79:228–32. doi: 10.1034/j.1600-0420.2001.790303.x

36. Zhou W, Li Q, Chen H, Liao Y, Wang W, Pei Y, et al. Trends of myopia development among primary and junior school students in the post-COVID-19 epidemic period. *Front Public Health*. (2022) 10:970751. doi: 10.3389/fpubh.2022.970751

37. Shi JJ, Wang YJ, Lyu PP, Hu JW, Wen XS, Shi HJ. Effects of school myopia management measures on myopia onset and progression among Chinese primary school students. *BMC Public Health*. (2023) 23:1819. doi: 10.1186/s12889-023-16719-z

frontiers | Frontiers in Medicine

TYPE Original Research
PUBLISHED 22 July 2024
DOI 10.3389/fmed.2024.1344968

OPEN ACCESS

EDITED BY
Pablo De Gracia,
University of Detroit Mercy, United States

REVIEWED BY
Javier Rojas-Viñuela,
Natural Optics Balaguer, Spain
Pathik Amin,
University of Chicago Medicine, United States

*CORRESPONDENCE
Zongduan Zhang
✉ zzduan@yeah.net
Lijun Shen
✉ slj@mail.eye.ac.cn

†These authors have contributed equally to this work

RECEIVED 27 November 2023
ACCEPTED 09 July 2024
PUBLISHED 22 July 2024

CITATION
Huang G, She X, Zhang Y, Zhang Z and Shen L (2024) Comparative analysis of macular characteristics in mCNV and contralateral eyes.
Front. Med. 11:1344968.
doi: 10.3389/fmed.2024.1344968

Comparative analysis of macular characteristics in mCNV and contralateral eyes

Gongyu Huang[1†], Xiangjun She[1†], Yun Zhang[1], Zongduan Zhang[1*] and Lijun Shen[2*]

[1]National Clinical Research Center for Ocular Diseases, Eye Hospital, Wenzhou Medical University, Wenzhou, China, [2]Zhejiang Provincial People's Hospital (Affiliated People's Hospital, Hangzhou Medical College), Hangzhou, China

Purpose: To illustrate the characteristics of perforating scleral vessels in macular regions between mCNV eyes and contralateral eyes in unilateral mCNV patients.

Methods: This was a retrospective study that included patients with unilateral naive mCNV. The study aimed to identify and analyze the distribution of perforating scleral vessels (PSVs) in the macular region of mCNV eyes and contralateral eyes. The central macular choroidal thicknesses (mChT) were measured using optical coherence tomography angiography (OCTA). The grades of myopic atrophic maculopathy (MAM) and macular myopic diffuse chorioretinal atrophy (DCA) were evaluated within groups. The number of PSVs and mChT were compared between contralateral and mCNV eyes based on the grade of DCA. The ROC curves were utilized to explore the diagnostic indexes for mCNV.

Results: A total of 102 eyes from 51 patients with unilateral mCNV were included. There was no significance in the severity of MAM or the grade of DCA between mCNV eyes and contralateral eyes ($p = 0.074$, $p = 0.054$, respectively). The mean number of PSVs in mCNV eyes was fewer than the contralateral eyes [1.00 (1.00–2.00) vs. 2.00 (0.75–3.00), $p = 0.030$]. The mChT in mCNV eyes was thinner than the contralateral eyes [36.00 (25.00–53.75) μm vs. 46.00 (31.00–75.25) μm, $p = 0.001$]. The mean grade of DCA in mCNV eyes was higher than that in contralateral eyes [3.00 (3.00–3.00) vs. 3.00 (2.00–3.00), $p = 0.004$]. When DCA involved the macular region, there were more PSVs in contralateral eyes than in mCNV eyes [1.50 (1.00–2.00) vs. 2.00 (1.00–3.00), $p = 0.042$]. Similarly, when DCA involved the foveal region, there were more PSVs in contralateral eyes than in mCNV eyes [1.50 (1.00–2.00) vs. 3.00 (2.00–4.00), $p = 0.004$]. The grade of DCA and mChT were valuable factors for predicting mCNV eyes ($AUC = 0.6566$, $p = 0.021$; $AUC = 0.6304$, $p = 0.029$; respectively). When the extent of DCA exceeded the foveal region, the count of PSVs was a good diagnostic factor for predicting mCNV ($AUC = 0.7430$, $p = 0.003$).

Conclusion: The mean amount of PSVs was significantly lower in the mCNV eyes compared to the contralateral eyes. When the extent of DCA exceeded the foveal region, the count of PSVs was a good diagnostic factor for predicting mCNV. Myopic eyes with a higher grade of DCA and a thinner mChT were more likely to develop mCNV.

KEYWORDS

pathological myopia, choroidal neovasclurization, perforating scleral vessels, myopic macular maculopathies, diffuse choroid atrophy

Introduction

Pathologic myopia is defined as myopia accompanied by typical degenerative lesions, including myopic maculopathies that are equal to or more severe than diffuse chorioretinal atrophy (DCA). DCA is a grade 2 lesion in the META-analysis classification system for pathologic myopia (1). The appearance of a posterior staphyloma is also considered a typical degenerative lesion in pathologic myopia (2). Pathologic myopia is a significant cause of visual impairment and blindness in East Asia, with an estimated prevalence of 1 to 3% in the population. The accompanying degenerative changes in the posterior segment of the eye and the macula can lead to vision loss, and pathologic myopia is one of the main causes of blindness in East Asia (3).

Myopic choroidal neovascularization (mCNV) has been estimated to develop in 5 to 10% of eyes with pathological myopia, and it is the most common cause of vision loss among all myopic-related macular complications (4, 5). The prognosis of mCNV without clinical treatment is poor (6–8). A decade-long study showed that vision decreased significantly to 20/200 or less in untreated mCNV patients followed for 10 years (7).

Cohen SY et al. investigated the population with mCNV and showed that about 14% of patients were diagnosed with bilateral naive mCNV, which means that most patients suffered from unilateral mCNV (9). About 15% of patients diagnosed with naive mCNV in unilateral eyes developed mCNV in the contralateral eyes within 8 years of follow-up (5, 6).

Lacquer cracks and patchy atrophies have been hypothesized to play a role in the pathogenesis of mCNV in patients with pathological myopia, and the apparent thinning of the choroid and loss of choroidal vessels in pathologic myopia may lead to the progression of myopic macular atrophy (10, 11). Monitoring for signs of mCNV in patients with pathological myopia, and early diagnosis and treatment of mCNV, can help preserve vision and prevent further vision loss.

However, Querques et al. reported that perforating scleral vessels (PSVs) were usually detected in lacquer cracks (12). Ruiz-Medrano et al. reported that PSVs were detected in more than 90% of mCNV eyes (13). They speculated that PSV might contribute to the formation of myopic maculopathy. In our previous study, we found that the eyes with PSVs adjacent to mCNV had worse efficacy of anti-VEGF treatment (14).

Whether the structure of PSV was an important sign for mCNV was not known. This study aimed to analyze the characteristics of PSVs in the macular region between mCNV eyes and contralateral eyes in patients with unilateral mCNV. Additionally, we aimed to identify risk factors for mCNV within the macular region.

Methods

Ethics approval for this retrospective observational study was obtained from the Research Ethics Committee of the Affiliated Eye Hospital of Wenzhou Medical University, China. The ethics acceptance number is H2023-012-K-09, and the registration number of this clinical trial is ChiCTR2300070120. All procedures for this study were conducted in accordance with the Declaration of Helsinki. We reviewed the medical records of patients who visited the Affiliated Eye Hospital of Wenzhou Medical University from November 2017 to September 2022.

The inclusion criteria for this study were as follows: (1) Patients with bilateral eyes met the following diagnostic criteria for high myopia: spherical refraction ≤ -6.00D or axial length longer than 26 mm, with typically degenerative changes in the retina, choroid, and sclera; (2) presence of naive mCNV: ① appeared as a flat, small, greyish subretinal lesion beneath or in close proximity to the fovea with or without hemorrhage on fundus photography; ② assessed on en face images generated by the automatically segmented outer retina slabs and choriocapillaris slabs, mCNV appeared as a large hyperintense vascular anastomotic network on OCT and OCTA devices; ③ B-scan images on OCT/OCTA appeared as highly reflective dome-shaped elevations above the retinal pigment epithelial band (because most mCNVs were type 2 CNVs), ④ FA findings in mCNV usually comprise well-defined hyper fluorescence in the early phase with leakage in the late phase in a classic CNV pattern of leakage (15, 16). The exclusion criteria were as follows: (1) CNV was secondary to other diseases, such as multifocal choroiditis, panuveitis, idiopathic CNV, and neovascular AMD; (2) the imaging quality of OCTA and fundus images was poor, or OCTA images showed poor correspondence in the macular area; (3) coexisting or history of any other severe ocular or systemic disease, or undergone other intraocular surgeries in addition to cataract or refractive surgery.

The age, gender, best corrected visual acuity (BCVA) measured with a Landolt C chart, and spherical equivalent (SE) were collected from the medical records. The grade of myopic chorioretinal atrophy (MAM) was determined by color fundus photography (TRC-50DX, Topcon Corporation, Tokyo, Japan) and confocal scanning laser ophthalmoscopy (cSLO; Optos Daytona, Optos, England). SD-OCT (Spectralis SD-OCT; Heidelberg Engineering, Germany) was used to measure the central macular choroidal thickness (mChT). Horizontal and vertical B-scans, as well as en-face images, mainly included outer retina slabs, choriocapillaris slabs, and choroid slabs automatically generated within the 3×3 mm, 6×6 mm, and 9×9 mm by OCTA (Angio OCT; Optovue, Fremont, CA, United States) and swept-source OCTA (SS-OCTA) (VG200D; SVision Imaging, Ltd., Luoyang, China) were used to assess the number and distribution of PSVs. Fluorescein angiography was performed when necessary.

Acquisition and analysis of PSVs' distribution

The criteria for defining PSVs were as follows: (1) linear or wavy morphology in OCTA images; (2) low reflectance appearance; (3) extension from the sclera through the choroid toward the retina (12, 17). The position of PSVs was determined by where they joined the choroid based on en-face images manually adjusted the thickness of contiguous slabs of choroid and sclera on OCTA combined with horizontal and vertical B-scans. When necessary, fluorescein angiography results were also used to confirm the position of PSVs (Figure 1).

The ETDRS grid, which was automatically generated on the OCTA device, was used to determine the relative position between the PSVs and the fovea within the macular region (3×3 mm area with the fovea as the center). The innermost ring of the ETDRS grid was 1 mm in diameter, and the middle ring was 3 mm in diameter. The ETDRS

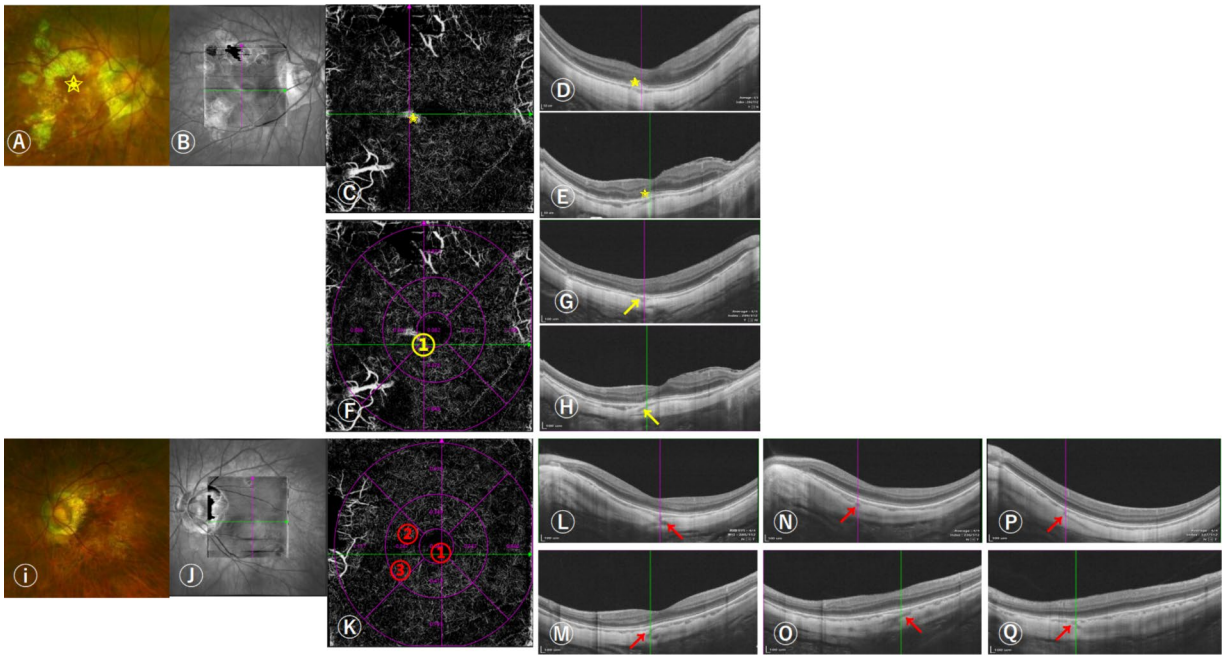

FIGURE 1
Images of the distributions of perforating scleral vessels (PSVs) in the macular region using swept-source OCT (SS-OCT). **(A)** 57-year-old woman was diagnosed with unilateral naive myopic choroidal neovascularization (mCNV) in her right eye; her equivalent refractive error of OD was −11.75 D and OS was −10.38 D. She had one PSV in her right eye and three in her left eye. The scanning laser ophthalmoscopy and OCT images indicated that OD was graded as A3T0N2s, OS was graded as A2T0N0, and the grade of DCA was D3. The boxes **(B,J)** indicated the scan area on SS-OCT. **(A–H)** The right fundus shows a grayish mCNV (yellow star in **A,C–E**) and **(D,E)** the corresponding horizontal and vertical B-scan images of mCNV. **(F)** The cross lines indicate the location of the PSV and are marked with a yellow number (yellow arrows in **G,H**) indicating horizontal and vertical B-scan images corresponding to the location of the PSV in figure **(F)**. **(I–Q)** Left fundus without mCNV, **(K)** the cross lines indicated the location of the first PSV, and the locations of the three PSVs entering the choroid are marked with red numbers. **(L,M)** indicated horizontal and vertical B-scan images corresponding to the location of the first PSV, **(N,O)** the location of the second PSV, and **(P,Q)** the location of the third PSV.

grid was positioned manually to correspond best to the position of the center of the fovea. Meanwhile, 6 × 6 mm and 9 × 9 mm scans on OCTA were used to check the accuracy of the distribution of PSVs at the edge of the 3 × 3 mm scan area. The total number of PSVs was recorded by counting all PSVs within the macular region. In addition, we divided the position of PSVs into five types: (1) PSVs in the foveal area; (2) in the superior area of the fovea; (3) in the inferior area of the fovea; (4) in the nasal area of the fovea; (5) in the temporal area of the fovea. (Figure 1) Two experienced retinal doctors repeated the measurements three times to confirm the presence of PSVs, the disagreement was decided by a senior expert. The distributions and counts of PSVs in both eyes were compared in patients with unilateral as well as bilateral mCNV.

Definition and grading of myopic maculopathy (MM)

Fundus photographs combined with B-scan images on OCTA were analyzed, and the macular microvasculature was also assessed. According to a recent international classification system (ATN), myopic maculopathies are divided into three types: myopic atrophic maculopathy (MAM), myopic tractional maculopathy (MTM), and myopic neovascularization (MNM) (1). The MAM is further classified into 5 grades: A0 (normal macula without any myopic retinal lesions), A1 (tessellated fundus only), A2 (diffuse chorioretinal atrophy), A3 (patchy chorioretinal atrophy), and A4 (complete macular atrophy). Diffuse chorioretinal atrophy (DCA) is a common pathological change in highly myopic eyes.

DCA appears as a faint yellowish lesion in color fundus photography and usually starts from the temporal side of the peripapillary region and gradually involves the entire posterior pole (18). The central macular choroidal thickness in eyes with diffuse chorioretinal atrophy (usually less than 100 μm) is thinner than that in eyes with a tessellated fundus, and the choroidal capillary density is significantly reduced. This disproportionate thinning of the choroid may be a key factor in diffuse atrophy and pathologic myopia (19). The distance from the fovea to the temporal edge of the optic disc was denoted as 3 mm, half of which was equal to the radius of the middle circle of the Early Treatment Diabetic Retinopathy Study (ETDRS) grid and one-sixth of which was equal to the radius of the inner circle of the grid. In these eyes with a diagnosis of DCA, we subclassified diffuse chorioretinal atrophy (DCA) according to the extent of atrophic changes on fundus photographs into 4 grades: without DCA or with DCA but without involvement of a radius of 3 mm around the fovea (D0); involvement to a radius of 1.5 to 3 mm around the fovea (D1); involvement of the parafovea (D2); and involvement of the fovea (D3) (20). MTM were classified into 6 grades: T0 (no macular schisis), T1 (inner or outer foveoschisis), T2 (inner and outer foveoschisis), T3 (foveal retinal detachment), T4 (full-thickness macular hole), and T5 (T4 + retinal detachment). The central macular choroidal thickness (mChT) was measured three times on B-scan images using SD-OCT.

Statistical analysis

The Kolmogorov–Smirnov test was used to check the normality of numerical variables. Normally distributed variables were presented as mean ± SD, non-normally distributed variables were presented as median (the first quartile to the third quartile), and $P < 0.05$ was considered statistically significant and shown in bold in the tables. The independent t-test, or Mann–Whitney *U* test, was used to compare continuous variables. Non-continuous variables were compared based on the Mann–Whitney *U* test. The Wilcoxon signed-rank test was used to compare the count of PSVs between bilateral eyes. Receiver operating characteristic (ROC) curves were plotted to assess the ability of PSVs and mChT to distinguish a subject with mCNV. The area under the ROC curve (AUC) was used to determine the diagnostic accuracy of the indexes mentioned above. The closer the value of the AUC was to 1.0, the more perfect the discrimination was (21). All data were analyzed using the commercial analytical software program SPSS 26.0.0 (SPSS Inc., Chicago, IL). GraphPad Prism 8.3.0 (GraphPad Prism Inc., San Diego, California, United States) was used to calculate relevant metrics and plot the ROC curves.

Results

Demographics and fundus characteristics of participants

102 eyes of 51 patients (11 males and 40 females) diagnosed with unilateral naive mCNV at their initial visit were enrolled. (Table 1) In patients with unilateral mCNV, the mean age was 53.51 ± 14.01 years old, the mean spherical equivalent (SE) was −13.03 ± 3.12D, the mean SE of contralateral eyes was −12.43 ± 4.71D ($p = 0.074$). The mean BCVA of mCNV eyes was 0.40 (0.22–0.85), and that of contralateral eyes was 0.22 (0.05–0.40) ($p = 0.000$).

There was no significant difference in the grade of MAM and MTM between mCNV eyes and contralateral eyes ($p = 0.054$, $p = 0.171$, respectively). In the MAM classification analysis, the proportion of eyes with DCA was highest in both mCNV eyes (66%) and contralateral eyes (82%). In mCNV eyes, 0 (0%) eyes were categorized as D0, 1 (3%) eye as D1, 4 (12%) eyes as D2, and 28 (85%) eyes as D3. In contralateral eyes, 1 (2%) eye was categorized as D0, 6 (14%) eyes as D1, 12 (29%) eyes as D2, and 23 (55%) eyes as D3. The mean grade of DCA in mCNV eyes was higher than in contralateral eyes (3.00 (3.00–3.00) vs. 3.00 (2.00–3.00), $p = 0.004$).

The average central macular choroidal thickness (mChT) of mCNV eyes was thinner than that of contralateral eyes: 36.00 (25.00–53.75) μm vs. 46.00 (31.00–75.25) μm ($p = 0.029$). Regarding the count and distribution of PSVs within the macular region, there were more PSVs in contralateral eyes than in mCNV eyes ($p = 0.030$), especially in the parafoveal and inferior foveal regions ($p = 0.028$) ($p = 0.011$).

TABLE 1 Demographic profiles and fundus characteristics of participants with unilateral mCNV.

	CNV eye ($n = 51$)	Contralateral eye ($n = 51$)	*p* value
Age, *y*	53.51 ± 14.01		
Male, *n* (%)	11 (22%)		
SE,D	−13.03 ± 3.12	−12.43 ± 4.71	0.074*
BCVA, logMAR	0.40 (0.22–0.85)	0.22 (0.05–0.40)	0.000†
MAM			
Grade, *n* (%)	2.00 (2.00–3.00)	2.00 (2.00–2.00)	0.054‡
0	0	0	
1	1 (2%)	2 (4%)	
2	33 (65%)	42 (82%)	
3	13 (25%)	2 (4%)	
4	4 (8%)	5 (10%)	
DCA			
Number (%)	33 (66%)	42 (82%)	
Grade, *n* (%)	3.00 (3.00–3.00)	3.00 (2.00–3.00)	0.004†
0	0	1 (2%)	
1	1 (3%)	6 (14%)	
2	4 (12%)	12 (29%)	
3	28 (85%)	23 (55%)	
MTM	0.00 (0.00–1.00)	0.00 (0.00–0.00)	0.171†
mChT, μm	36.00 (25.00–53.75)	46.00 (31.00–75.25)	0.001‡
PSV count			
Total	1.00 (1.00–2.00)	2.00 (0.75–3.00)	0.030‡
Foveal	0.00 (0.00–0.25)	0.00 (0.00–0.00)	0.971†
Parafovea	1.00 (0.00–2.00)	2.00 (0.00–3.00)	0.028‡
Superior	0.00 (0.00–1.00)	0.00 (0.00–1.00)	0.183†
Inferior	0.00 (0.00–0.00)	0.00 (0.00–1.00)	0.011‡
Nasal	0.00 (0.00–1.00)	0.00 (0.00–1.00)	0.618†
Temporal	0.00 (0.00–0.00)	0.00 (0.00–1.00)	0.479†

BCVA, best corrected visual acuity; MAM, myopic macular atrophy.
DCA, diffuse chorioretinal atrophy; MTM, myopic macular traction.
mChT, central macular choroidal thickness; PSV, perforating scleral vessels.
*Student's *t*-test. †Mann–whitney *U* test. ‡Wilcoxon signed-rank test.

Binocular features of PSVs in eyes with the same grade of DCA

The structures of PSVs were compared in mCNV eyes and contralateral eyes based on the same grade of DCA. When DCA involved the macular region (grade of DCA equal to D2 and D3), the mean BCVA of mCNV eyes was worse than that of the contralateral eyes ($p = 0.000$), and the count of PSVs in the macular region of mCNV eyes was less than that in the contralateral eyes [1.50 (1.00–2.00) vs. 2.00 (1.00–3.00); $p = 0.042$]. Similarly, when DCA involved the fovea (grade of DCA equal to D3), the mean BCVA of mCNV eyes was worse than that of contralateral eyes ($p = 0.000$), and the count of PSVs in the macular region of mCNV eyes was less than that in the contralateral eyes [1.50 (1.00–2.00) vs. 3.00 (2.00–4.00); $p = 0.004$]. However, the number of PSVs in the foveal region of bilateral eyes was not significantly different,

TABLE 2 The features of PSVs in patients with unilateral mCNV according to the degree of DCA.

	Macula involved (D2 + D3)			Fovea involved (D3)		
	mCNV eye	Contralateral eye		mCNV eye	Contralateral eye	
	(n = 32)	(n = 35)	P value	(n = 28)	(n = 23)	P value
Age,y	53.06 ± 13.49	52.11 ± 14.74	0.605*	53.61 ± 12.71	52.96 ± 15.68	0.310*
SE,D	−12.51 ± 3.11	−11.82 ± 3.44	0.681*	−12.71 ± 3.27	−12.20 ± 3.80	0.399*
BCVA,logMAR	0.46 (0.24–0.96)	0.10 (0.05–0.22)	0.000†	0.46 (0.30–0.82)	0.10 (0.05–0.22)	0.000†
mChT,μm	38.00 (25.00–54.00)	45.00 (30.75–62.00)	0.158†	36.00 (24.25–51.75)	38.00 (25.00–53.00)	0.472†
PSV count						
Total	1.50 (1.00–2.00)	2.00 (1.00–3.00)	0.042†	1.50 (1.00–2.00)	3.00 (2.00–4.00)	0.004†
Foveal	0.00 (0.00–0.75)	0.00 (0.00–1.00)	0.947†	0.00 (0.00–0.75)	0.00 (0.00–1.00)	0.453†

BCVA, best corrected visual acuity; mChT, central macular choroidal thickness; PSV, perforating scleral vessels. *Student's t-test. †Mann–whitney U test.

regardless of the grade of DCA ($p = 0.947$ for D2 + D3; $p = 0.453$ for D3) (Table 2).

The diagnostic value of PSVs for mCNV

Receiver operating characteristic (ROC) curves were used to analyze the diagnosis value for mCNV. The results in Figure 2 depict that the grade of DCA showed an Area Under the Curve (AUC) of 0.6566 and a cut-off value of 2.50, producing an 84.9% specificity and 45.2% sensitivity with a p-value of 0.021. The mChT produced an AUC of 0.6304 and a cut-off value of 30.50 μm with a 44.7% specificity and 76.6% sensitivity with a p-value of 0.029. Most of the eyes in our study showed a grade of DCA equal to D3. To exclude the effects of chorioretinal atrophy, the ROC curve analysis of the number of PSVs in the macular region when the grade of DCA was equal to D3 showed an AUC of 0.7430 and the cut-off value of 2.50, producing an 82.1% specificity and 52.2% sensitivity with a p-value of 0.003. Therefore, the grade of DCA, mChT, and the number of PSVs of eyes diagnosed with D3 were all potentially useful diagnostic factors for mCNV. However, further studies are required to confirm the diagnostic value of these factors for mCNV.

The number of PSVs in the macula or foveal region was not a perfect diagnostic factor, with AUC values of 0.6011 (p = 0.078) and 0.5165 (p = 0.733), respectively. Also, the number of PSVs in the foveal region was not a perfect diagnostic factor when the DCA grade was equal to D3, with an AUC value of 0.5489 and a p-value of 0.551 (Table 3).

Discussion

This study investigated the differences in the mChT and the number of PSVs in the macular region in patients with unilateral mCNV. The results showed that mChT was thinner and there were fewer PSVs in the macular region in mCNV eyes compared to the contralateral eyes. When the extents of DCA were closer to the fovea, there were more PSVs in the macular region in the contralateral eyes than in the mCNV eyes. When DCA approached the fovea, the number of PSVs in the macular region might be a potentially useful diagnostic factor for mCNV.

Previous research suggests that mCNV may be correlated with myopic atrophic maculopathy (MAM) (22–24). Some researchers reported that there was no significant correlation between mCNV and myopic tractional maculopathy (MTM) (25). One study by Flores-Moreno I et al. showed that in myopic eyes, the thickness of the choroid decreased (26). In our study, we did not find any significant difference in SE, grade of MAM, or MTM between the bilateral eyes of either unilateral or bilateral mCNV patients. However, our results suggest that the mChT was thinner in the mCNV eyes than in the contralateral eyes. This finding supports the theory that mCNV may be associated with choroidal thinning, which could be a potential risk factor for mCNV. Further studies are necessary to confirm this association and investigate the underlying mechanisms involved.

Ishida T et al. reported a connection between mCNV and intrascleral vessels. They found that 75% of PSVs were detected below or around the mCNV, and indocyanine green angiography showed that these PSVs were intrascleral arteries originating from the short posterior ciliary arteries (SPCAs). Swept-source OCT showed that some of the mCNVs had continuous connections with scleral vessels, mainly the SPCA (27). PSVs are commonly observed in highly myopic eyes. Some studies also suggest that PSVs may originate from the posterior ciliary artery (PCA) and SPCA (28, 29). This suggests that PSVs merge into the choroid and provide blood flow and oxygen diffusion to the choroid.

Asakuma et al. (30) reported a high prevalence of DCA (91.6%) in patients with myopic retinopathy. However, Liu et al. (20) reported a lower prevalence of DCA (20.6%) in the high myopic group. Our study showed that a large proportion of both mCNV eyes and contralateral eyes had DCA, with proportions of 66 and 82%, respectively. The average grade of DCA in mCNV eyes was also higher than in contralateral eyes, suggesting that the extent of DCA was closer to the fovea in mCNV eyes.

In our study, we observed more PSVs in contralateral eyes than mCNV eyes in the macular region, especially in the parafovea area of the retina and the inferior quadrant of the fovea. Also, when the DCA involved the macula, we found more PSVs in the contralateral eyes than in the mCNV eyes. This finding is interesting because it suggests that in highly myopic eyes where the choroid is almost non-existent, in eyes with slightly more PSV counts, the probability of mCNV being detected may be smaller. There may be a negative correlation between PSV and mCNV, but the role of PSV in the generation of mCNV and the mechanism of this are not yet clear. We speculate that in highly myopic eyes with an almost absent choroid, when the blood flow from

TABLE 3 Results of important parameters from ROC curve.

Variables	AUC	95% confidence interval	*P* value	Youden's J statistic	Cut-off value
DCA grade	0.6566	0.54–0.78	0.021	0.3009	2.50
mChT, μm	0.6304	0.52–0.74	0.029	0.2128	30.50
Macular PSV count	0.6011	0.49–0.71	0.078		
Foveal PSV count	0.5165	0.40–0.63	0.773		
DCA = 3, macular PSV count	0.7430	0.61–0.88	0.003	0.3431	2.50
DCA = 3, foveal PSV count	0.5489	0.39–0.71	0.551		

DCA, diffuse chorioretinal atrophy; mChT, central macular choroidal thickness; PSV, perforating scleral vessels; AUC, Area under the curve.

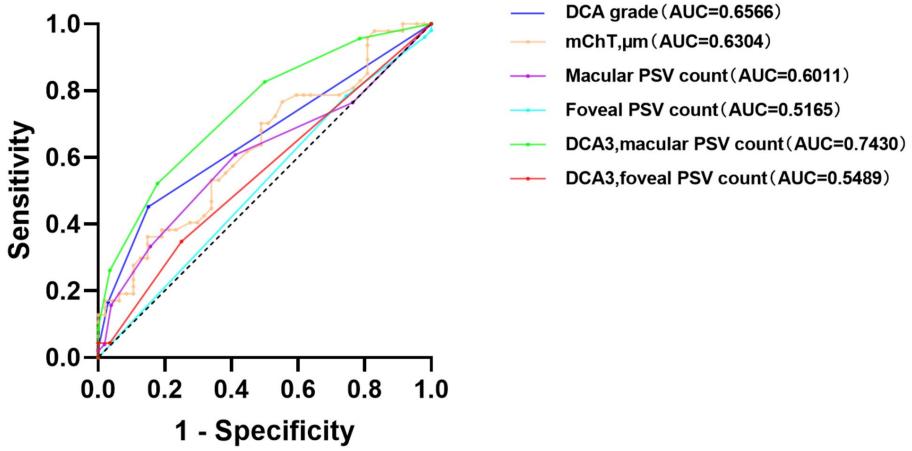

FIGURE 2
Receiver operating characteristic (ROC) curves of parameters for mCNV.

PSVs is weakened, mCNVs are more likely to appear in the macular area. These findings suggest that in highly myopic eyes, the choroidal blood flow may be insufficient to nourish the retinal tissue, leading to the development of mCNV.

By analyzing AUC values under ROC curves, we found that the grade of DCA >2.5 and the mChT <30.5 μm were the diagnostic factors for mCNV. When the grade of DCA was D3, the number of PSVs in the macular region was less than 2.5, which was also an effective diagnostic factor for mCNV. These results suggest that in highly myopic eyes accompanied by atrophied choroids, PSVs may play an important role in the blood flow supply for choroids. When there are fewer PSVs in the macular region, this phenomenon may be weakened, and the probability of the development of mCNV may increase.

We acknowledge that our study had several limitations. First, the sample size was relatively small, and a larger sample size experiment is needed in the future to verify our current research results. Second, this was a retrospective cross-sectional clinical study that had limited research capacity on the role of PSVs in the pathogenesis of mCNV and required appropriate animal model experiments for verification. Third, histopathological analysis was needed to verify the connection between mCNV and intrascleral vessels, and more relevant studies are needed to explore the pathological mechanism in the future.

Data availability statement

The raw data supporting the conclusions of this article will be made available by the authors, without undue reservation.

Ethics statement

The studies involving humans were approved by the Research Ethics Committee of the Affiliated Eye Hospital of Wenzhou Medical University. The studies were conducted in accordance with the local legislation and institutional requirements. Written informed consent for participation was not required from the participants or the participants' legal guardians/next of kin in accordance with the national legislation and institutional requirements.

Author contributions

GH: Data curation, Investigation, Writing – original draft. XS: Data curation, Funding acquisition, Methodology, Writing – review & editing. YZ: Project administration, Supervision,

Writing – review & editing. ZZ: Conceptualization, Supervision, Validation, Visualization, Writing – review & editing. LS: Conceptualization, Supervision, Validation, Visualization, Writing – review & editing.

Funding

The author(s) declare that financial support was received for the research, authorship, and/or publication of this article. This study was supported by the Zhejiang Provincial Natural Science Foundation of China (LQ20H120004) and the National Natural Science Foundation of China (82101158).

Conflict of interest

The authors declare that the research was conducted in the absence of any commercial or financial relationships that could be construed as a potential conflict of interest.

Publisher's note

References

1. Ohno-Matsui K, Kawasaki R, Jonas JB, Cheung CMG, Saw SM, Verhoeven VJM, et al. International photographic classification and grading system for myopic maculopathy. *Am J Ophthalmol*. (2015) 159:877–883.e7. doi: 10.1016/j.ajo.2015.01.022

2. Ohno-Matsui K, Lai TY, Lai CC, Cheung CM. Updates of pathologic myopia. *Prog Retin Eye Res*. (2016) 52:156–87. doi: 10.1016/j.preteyeres.2015.12.001

3. Iwase A, Araie M, Tomidokoro A, Yamamoto T, Shimizu H, Kitazawa Y. Prevalence and causes of low vision and blindness in a Japanese adult population: the Tajimi study. *Ophthalmology*. (2006) 113:1354–1362.e1. doi: 10.1016/j.ophtha.2006.04.022

4. Cheung CMG, Arnold JJ, Holz FG, Park KH, Lai TYY, Larsen M, et al. Myopic choroidal neovascularization: review, guidance, and consensus statement on management. *Ophthalmology*. (2017) 124:1690–711. doi: 10.1016/j.ophtha.2017.04.028

5. Grossniklaus HE, Green WR. Pathologic findings in pathologic myopia. *Retina*. (1992) 12:127–33. doi: 10.1097/00006982-199212020-00009

6. Avila MP, Weiter JJ, Jalkh AE, Trempe CL, Pruett RC, Schepens CL. Natural history of choroidal neovascularization in degenerative myopia. *Ophthalmology*. (1984) 91:1573–81. doi: 10.1016/S0161-6420(84)34116-1

7. Yoshida T, Ohno-Matsui K, Yasuzumi K, Kojima A, Shimada N, Futagami S, et al. Myopic choroidal neovascularization: a 10-year follow-up. *Ophthalmology*. (2003) 110:1297–305. doi: 10.1016/S0161-6420(03)00461-5

8. Kojima A, Ohno-Matsui K, Teramukai S, Ishihara Y, Shimada N, Yoshida T, et al. Estimation of visual outcome without treatment in patients with subfoveal choroidal neovascularization in pathologic myopia. *Graefes Arch Clin Exp Ophthalmol*. (2006) 244:1474–9. doi: 10.1007/s00417-006-0324-4

9. Cohen SY, Laroche A, Leguen Y, Soubrane G, Coscas GJ. Etiology of choroidal neovascularization in young patients. *Ophthalmology*. (1996) 103:1241–4. doi: 10.1016/S0161-6420(96)30515-0

10. Wong CW, Teo YCK, Tsai STA, Ting SWD, Yeo YSI, Wong WKD, et al. Characterization of the choroidal vasculature in myopic maculopathy with optical coherence tomographic angiography. *Retina*. (2019) 39:1742–50. doi: 10.1097/IAE.0000000000002233

11. Wong CW, Phua V, Lee SY, Wong TY, Cheung CM. Is choroidal or scleral thickness related to myopic macular degeneration? *Invest Ophthalmol Vis Sci*. (2017) 58:907–13. doi: 10.1167/iovs.16-20742

12. Querques G, Corvi F, Balaratnasingam C, Casalino G, Parodi MB, Introini U, et al. Lacquer cracks and perforating scleral vessels in pathologic myopia: a possible causal relationship. *Am J Ophthalmol*. (2015) 160:759–766.e2. doi: 10.1016/j.ajo.2015.07.017

13. Ruiz-Medrano J, Almazan-Alonso E, Flores-Moreno I, Puertas M, García-Zamora M, Ruiz-Moreno JM. Relationship between myopic choroidal neovascularization activity and perforating scleral vessels in high myopia. *Retina*. (2022) 42:204–9. doi: 10.1097/IAE.0000000000003290

14. Yao W, Xu J, She X, Yu J, Liang Z, Ye X, et al. Perforating scleral vessels adjacent to myopic choroidal neovascularization achieved a poor outcome after intravitreal anti-VEGF therapy. *Front Med*. (2022) 9:1065397. doi: 10.3389/fmed.2022.1065397

15. Arya M, Rebhun CB, Cole ED, Sabrosa AS, Arcos-Villegas G, Louzada RN, et al. Visualization of choroidal neovascularization using two commercially available spectral domain optical coherence tomography angiography devices. *Retina*. (2019) 39:1682–92. doi: 10.1097/IAE.0000000000002241

16. Lai TY, Cheung CM. MYOPIC CHOROIDAL NEOVASCULARIZATION: diagnosis and treatment. *Retina*. (2016) 36:1614–21. doi: 10.1097/IAE.0000000000001227

17. Giuffrè C, Querques L, Carnevali A, De Vitis LA, Bandello F, Querques G. Choroidal neovascularization and coincident perforating scleral vessels in pathologic myopia. *Eur J Ophthalmol*. (2017) 27:e39–45. doi: 10.5301/ejo.5000875

18. Tokoro T. Explanatory factors of Chorioretinal atrophy In: Atlas of posterior fundus changes in pathologic myopia. Tokyo: Springer Japan (1998). 23–50.

19. Fang Y, Du R, Nagaoka N, Yokoi T, Shinohara K, Xu X, et al. OCT-based diagnostic criteria for different stages of myopic maculopathy. *Ophthalmology*. (2019) 126:1018–32. doi: 10.1016/j.ophtha.2019.01.012

20. Liu R, Guo X, Xiao O, Li Z, Zhang J, Lee JTL, et al. Diffuse Chorioretinal Atrophy In Chinese High Myopia: the ZOC-BHVI high myopia cohort study. *Retina*. (2020) 40:241–8. doi: 10.1097/IAE.0000000000002397

21. Medeiros FA, Zangwill LM, Bowd C, Vessani RM, Susanna R Jr, Weinreb RN. Evaluation of retinal nerve fiber layer, optic nerve head, and macular thickness measurements for glaucoma detection using optical coherence tomography. *Am J Ophthalmol*. (2005) 139:44–55. doi: 10.1016/j.ajo.2004.08.069

22. Kurt RA, Sarıgül Sezenöz A, Akkoyun I, Yılmaz G. The correlation of atrophy, traction and neovascularization in myopic choroidal neovascularization according to a novel myopic maculopathy classification system (atrophy (a), traction (T), neovascularization (N): ATN). *Int Ophthalmol*. (2022) 42:2925–32. doi: 10.1007/s10792-022-02423-1

23. Cheung CM, Loh BK, Li X, Mathur R, Wong E, Lee SY, et al. Choroidal thickness and risk characteristics of eyes with myopic choroidal neovascularization. *Acta Ophthalmol*. (2013) 91:e580–1. doi: 10.1111/aos.12117

24. Ikuno Y, Jo Y, Hamasaki T, Tano Y. Ocular risk factors for choroidal neovascularization in pathologic myopia. *Invest Ophthalmol Vis Sci*. (2010) 51:3721–5. doi: 10.1167/iovs.09-3493

25. Chen Q, He J, Hu G, Xu X, Lv H, Yin Y, et al. Morphological characteristics and risk factors of myopic maculopathy in an older high myopia population-based on the new classification system (ATN). *Am J Ophthalmol*. (2019) 208:356–66. doi: 10.1016/j.ajo.2019.07.010

26. Flores-Moreno I, Lugo F, Duker JS, Ruiz-Moreno JM. The relationship between axial length and choroidal thickness in eyes with high myopia. *Am J Ophthalmol*. (2013) 155:314–319.e1. doi: 10.1016/j.ajo.2012.07.015

27. Ishida T, Watanabe T, Yokoi T, Shinohara K, Ohno-Matsui K. Possible connection of short posterior ciliary arteries to choroidal neovascularisations in eyes with pathologic myopia. *Br J Ophthalmol*. (2019) 103:457–62. doi: 10.1136/bjophthalmol-2018-312015

28. Ohno-Matsui K, Akiba M, Ishibashi T, Moriyama M. Observations of vascular structures within and posterior to sclera in eyes with pathologic myopia by swept-source optical coherence tomography. *Invest Ophthalmol Vis Sci*. (2012) 53:7290–8. doi: 10.1167/iovs.12-10371

29. Pedinielli A, Souied EH, Perrenoud F, Leveziel N, Caillaux V, Querques G. In vivo visualization of perforating vessels and focal scleral ectasia in pathological myopia. *Invest Ophthalmol Vis Sci*. (2013) 54:7637–43. doi: 10.1167/iovs.13-12981

30. Asakuma T, Yasuda M, Ninomiya T, Noda Y, Arakawa S, Hashimoto S, et al. Prevalence and risk factors for myopic retinopathy in a Japanese population: the Hisayama study. *Ophthalmology*. (2012) 119:1760–5. doi: 10.1016/j.ophtha.2012.02.034

frontiers | Frontiers in Medicine

TYPE Original Research
PUBLISHED 30 August 2024
DOI 10.3389/fmed.2024.1368219

OPEN ACCESS

EDITED BY
Pablo Pérez-Merino,
Ghent University, Belgium

REVIEWED BY
Mijie Li,
National University of Singapore, Singapore
Janos Nemeth,
Semmelweis University, Hungary

*CORRESPONDENCE
Weihua Yang
benben0606@139.com

†These authors have contributed equally to this work

RECEIVED 17 January 2024
ACCEPTED 21 August 2024
PUBLISHED 30 August 2024

CITATION
Mu J, Zhong H, Jiang M and Yang W (2024) Epidemiological characteristics of myopia among school-age children before, during, and after the COVID-19 pandemic: a cohort study in Shenzhen, China.
Front. Med. 11:1368219.
10.3389/fmed.2024.1368219

Epidemiological characteristics of myopia among school-age children before, during, and after the COVID-19 pandemic: a cohort study in Shenzhen, China

Jingfeng Mu†, Haoxi Zhong†, Mingjie Jiang and Weihua Yang*

Shenzhen Eye Hospital, Jinan University, Shenzhen Eye Institute, Shenzhen, China

Objectives: To evaluate the epidemiological characteristics of myopia among school-aged children before, during, and after the coronavirus disease (COVID-19) pandemic.

Methods: A total of 848,697 students aged 6–15 years from 786 primary and secondary schools in Shenzhen, China, were randomly selected as research subjects. We conducted annual myopia screenings from 2019 to 2022. 2019 was considered before the COVID-19 pandemic, 2020 as during the pandemic, and 2021 and 2022 as after the pandemic. Demographic characteristics, visual acuity, and spherical equivalent refraction (SE) were collected.

Results: During the 4-year follow-up period, the uncorrected visual acuity (UCVA) of the study subjects progressed following a trend of -0.18 ± 0.30D (-0.17 ± 0.29D for boys, -0.21 ± 0.32Dfor girls) ($p < 0.001$). Those students who were in grade 4 aged 9–10 years at the baseline examination showed the greatest decline in visual acuity (0.23). The SE of the study subjects progressed following a trend of -1.00 ± 1.27D (-0.96 ± 1.25D for boys, -1.05 ± 1.31D for girls) ($p < 0.001$). The students who were in grade 5 aged 10–11 years at the baseline examination showed the greatest decline in SE ($1.15\text{D} \pm 1.22$, $p < 0.001$). The prevalence of myopia (UCVA<5.0 and SE < −0.50D of any eye) increased by 28.2% (27.0% for boys and 29.8% for girls). Those students who were in grade 2 aged 7–8 years at the baseline examination showed the greatest increase in myopia prevalence (37.6%, $p < 0.001$). During the COVID-19 pandemic, the subjects' visual acuity and SE measurements decreased by -0.05 ± 0.19 ($p < 0.001$) and -0.36 ± 0.89D ($p < 0.001$) respectively, and the prevalence of myopia increased by 11.3% (10.6% for boys and 12.2% for girls) ($p < 0.001$). The 3-year cumulative incidence of myopia for non-myopic grade 1 aged 6–7 years students with baseline SE of ≥1.00D, ≥ 0.50D and < 1.00D, ≥0D and < 0.50D, and ≥ −0.50D and < 0D were 6.8, 24.8, 39.0, and 48.1%, respectively.

Conclusion: During the COVID-19 pandemic, the SE of school-aged children showed myopic drift and decreased visual acuity. Myopia progressed faster among girls than among boys in the same grades. The risk of myopia among school-aged children persisted even after the home quarantine of the COVID-19 pandemic was lifted.

KEYWORDS

myopia, epidemiology, school-aged children, COVID-19, cohort study

Introduction

Myopia is a global public health issue and represents one of the main causes of vision loss. Studies predict that by 2050, half of the world's population will suffer from myopia and the prevalence of severe myopia will reach 9.8% (1). Myopia has long been an epidemic in Asian populations (2), particularly in China, where its prevalence remains high and is rapidly increasing (3). Myopia, particularly severe myopia, can increase the risk of eye diseases such as retinal detachment, macular degeneration, and glaucoma (4, 5), as well as irreversible visual impairment and blindness (6). Visual impairment poses a huge economic burden across the globe (7), with an annual economic loss of approximately $244 billion worldwide (8).

Since the outbreak of coronavirus disease-19 (COVID-19) in China at the end of 2019, most countries worldwide have controlled its spread by maintaining social distancing, home quarantines, and through other methods (9). China lifted its at-home quarantine program in May 2020. During the COVID-19 pandemic, approximately 278 million primary and secondary school students in China received online education at home (10). One survey found that home quarantine, particularly online learning, led to a reduction in children's outdoor activities, increased use of electronic devices, and irregular sleep and dietary habits (11, 12). During the COVID-19 pandemic, children spent more time watching electronic screens and less time outdoors (13). Reduced outdoor activity, increased use of electronic devices, and insufficient sleep are known risk factors for the occurrence and progression of myopia (14, 15). Several studies have assessed the development of myopia in children and adolescents before and after the COVID-19 pandemic. The prevalence of myopia among children and adolescents in China's Chongqing province, for example, increased from 45.3 to 55.4% (16). Similarly, the spherical equivalent refractions (SE) of primary and secondary school students in Wenzhou province progressed from −0.23 D to −0.34 D (17).

Cross-sectional studies have been used to assess the occurrence and development of myopia during the COVID-19 pandemic; however, it has been difficult to assess the impact of the pandemic on myopia. In several cohort studies, the observation time was too short to draw sound conclusions. Cohort studies have important scientific value for revealing the causes of various diseases. When based on large samples and long-term follow-up observations, they can effectively control for various biases, explore the causal relationship between exposure and effects, and provide strong etiological evidence. This study used a large-scale population cohort study to observe a cohort of research subjects for four consecutive years to evaluate the epidemiological characteristics and developmental trends of myopia among school-aged children.

Methods

Study design and population

This study selected primary and secondary school students aged 6–15 yeas in Shenzhen to conduct a myopia follow-up cohort study, and longitudinally observed the development trend of myopia in the participants from 2019 to 2022. Using the cluster random sampling method, students from 786 primary and secondary schools in Shenzhen were selected as study participants. Shenzhen has no countryside and is the third most populous city in China. The students recruited for the study were all from urban areas. Students in grades 1–6 aged 6–11 years attending primary schools and students in grades 7–9 aged 12–15 years attending secondary schools were recruited. The included students needed to be able to complete all examinations set for the study, cooperate to complete a 4-year follow-up, and both them and their guardians needed to agree to participate in the study. Students who could not complete the myopia screenings were excluded.

We conducted myopia screenings of the research participants from September to November of every year from 2019–2022. We define the periods as follows: 2019 was considered before the COVID-19 pandemic, 2020 as during the pandemic, and 2021 and 2022 as after the pandemic. A total of 851,891 students participated in myopia screenings for the first time during this study, and 848,697 completed the 4-year follow-up, with a loss-to-follow-up rate of 0.37%. The follow-up results are presented in Table 1. In total, 848,697 primary and secondary school students, including 460,983 boys and 387,714 girls, were enrolled in this study.

This study's procedure met the requirements of the Declaration of Helsinki and was approved by the Ethics Committee of the Shenzhen Eye Hospital (2023KYYJ047-02). Before participating in the study, the students and their parents/guardians were informed of the research objectives and examination procedures, and informed consent forms were signed by all of the participants' parents or guardians.

Data collection

Myopia screening

Basic information of participants in the present study including sex, date of birth, school name, and grade were collected. The included research participants were screened for myopia by trained optometrists or ophthalmologists. The screening items included uncorrected visual acuity and refraction tests, and all processes were strictly performed in accordance with the specifications for screening refractive error in primary and secondary school students (WS/T 663–2020). A

TABLE 1 Follow-up of the study participants.

	2019	2022	Rate of loss to follow-up (%)
Grade			
Grade 1	156,024	155,462	0.36
Grade 2	151,172	150,846	0.22
Grade 3	129,281	129,019	0.20
Grade 4	108,089	107,871	0.20
Grade 5	94,930	94,704	0.24
Grade 6	83,947	83,642	0.36
Grade 7	63,300	62,713	0.93
Grade 8	41,638	41,236	0.97
Grade 9	23,510	23,204	1.30
Sex			
Male	462,851	460,983	0.40
Female	389,040	387,714	0.34

logarithmic visual acuity chart (Eye Vision 1,603–01) was used to examine uncorrected visual acuity in both eyes. An autorefractor (NIDEK AR-1) was used to check for non-cycloplegic SE. This study relied on the Shenzhen Children and Adolescents Myopia Monitoring Big Data Platform. All screening data was uploaded in real time to the platform for storage and summary.

Definition of myopia

Myopia was defined as the uncorrected visual acuity of any eye of the participants <5.0, as well as a non-cycloplegic SE of < −0.50 diopter (D) (18). Myopic students were classified according to the SE values of their right eyes. Mild myopia was defined as −3.00 D ≤ SE < −0.50 D, moderate myopia was defined as −6.00 D ≤ SE < −3.00 D, and severe myopia was defined as SE < −6.00 D.

Statistical analysis

Statistical analyses were performed using R (version 4.1.0), and the significance level was set at $\alpha = 0.05$. As the binocular visual acuity ($r = 0.833$, $p < 0.05$) and SE ($r = 0.879$, $p < 0.05$) of the participants in this study were highly correlated, only the right eye was included in the analysis. Continuous variables are described using $\bar{x} \pm s$,and analysis of variance was used to compare differences between different groups. Categorical data were compared using the χ^2 test, and $p < 0.05$ was considered statistically significant.

Results

A total of 848,697 students from primary and secondary schools in Shenzhen participated in this study. The prevalence rates of myopia in grade 1–9 students in 2019 were 13.6, 19.0, 28.7, 41.0, 52.5, 62.5, 70.9, 77.5, and 81.7%, respectively (Table 2).

From 2019 to 2022, visual acuity measurements across all grades followed a downward trend. Over the observation period, the participants showed a decrease of 0.18 ± 0.30 ($p < 0.001$) in uncorrected visual acuity, with boys and girls experiencing a decrease of 0.17 ± 0.29 ($p < 0.001$) and 0.21 ± 0.32 ($p < 0.001$), respectively. Students who were in grade 4 at baseline showed the greatest decline in visual acuity (0.23 ± 0.31, $p < 0.001$), followed by those who were in grades 3 (0.22 ± 0.31, $p < 0.001$) and 5 (0.22 ± 0.31, $p < 0.001$) at baseline. Except for those students who were in grades 7–9 at baseline, boys in the other grades showed lower uncorrected visual acuity decreases than girls. Among the girls, those who were in grade 4 at baseline showed the greatest decrease in visual acuity (0.26 ± 0.33, $p < 0.001$), while among the boys, those who were in grades 4–6 at baseline showed the greatest decrease in visual acuity (0.20 ± 0.29, $p < 0.001$). During the COVID-19 pandemic, the participants' visual acuity levels decreased by 0.05 ± 0.19 ($p < 0.001$), of which those who were in grades 4–6 at baseline experienced the greatest decline (0.07, $p < 0.001$). A more detailed overview of the results is provided in Table 3 and Figures 1A, 2C.

From 2019 to 2022, the SE of the participants showed a myopic drift, decreasing by 1.00 ± 1.27 D ($p < 0.001$). Boys and girls dropped by 0.96 ± 1.25 D ($p < 0.001$) and 1.05 ± 1.31 D ($p < 0.001$), respectively. The students who were in grade 5 at baseline showed the highest decrease in SE (1.15 D ± 1.22, $p < 0.001$), followed by those who were in grades 4 (1.13 D ± 1.30, $p < 0.001$) and 3 (1.09 D ± 1.35, $p < 0.001$) at baseline. Except for those who were in grades 6–9 at baseline, the SE decreases of the boys in the other grades were lower than those of the girls. Among the girls, those who were in grade 4 at baseline showed the greatest decrease in SE (1.20 D ± 1.33, $p < 0.001$). Among the boys, those who were in grade 5 at baseline showed the greatest decrease in SE (1.12 D ± 1.22, $p < 0.001$). During the COVID-19 pandemic, the participants' SE decreased by 0.36 D ± 0.89 ($p < 0.001$), among which the students who were in grade 7 at baseline had the highest decrease (0.45 D ± 0.78, $p < 0.001$). A more detailed overview of the results is provided in Table 4 and Figures 1B, 2D.

During the observation period, the prevalence of myopia among the participants of all grades showed an increasing trend. It increased by 28.2% overall, by 27.0 and 29.8% in boys and girls ($p < 0.001$), respectively, showing a statistically significant difference. The students who were in grade 2 at baseline had the highest increase (37.6%, $p < 0.001$), followed by those who were in grades 3 (36.6%, $p < 0.001$) and 1 (32.4%, $p < 0.001$) at baseline. During the COVID-19 pandemic, the prevalence of myopia among the participants increased by 11.3% (10.6% for boys and 12.2% for girls), with the highest increase (15.7%) seen in those who were in grade 3 at baseline. Detailed results are shown in Table 5 and Figure 2B. Further analysis showed that as the grade increased the proportion of mild myopia increased first, followed by a decrease—both of which were statistically significant ($p < 0.05$). With increasing grades, the proportion of severe and moderate myopia also increased, showing a statistically significant difference ($p < 0.05$) (Table 6 and Figure 2A).

We selected students in grade 1 who were not myopic at baseline for follow-up and found that the 3-year cumulative incidence of myopia of students with baseline SE of ≥1.00 D, ≥ 0.50 D and < 1.00 D, ≥ 0 D and < 0.50 D, and ≥ −0.50 D and < 0 D were 6.8, 24.8, 39.0, and 48.1%, respectively. Detailed results are presented in Table 7.

Discussion

This four-year cohort study focused on uncorrected visual acuity, SE, and the incidence and prevalence of myopia among school-aged children in Shenzhen, China. During the observation period, it was found that the uncorrected visual acuity and SE measurements of the study participants decreased by 0.18 and 1.00 D, respectively, and that the prevalence of myopia increased by 28.2%. The students who were in grade 4 at baseline showed the greatest decrease in visual acuity (0.23), those who were in grade 5 at baseline showed the greatest decrease in SE (1.15 D), and the prevalence of myopia increased the most among the students who were in grade 2 at baseline (37.6%). Girls showed a greater decrease in visual acuity and SE, and a greater increase in the prevalence of myopia compared to boys of the same grades. For non-myopic students in grade 1 at baseline, the cumulative incidences of myopia in the first, second, and third years of follow-up were 13.5, 22.6, and 36.2%, respectively.

In 2020, many countries around the world—including China—adopted home quarantine policies to prevent and control the COVID-19 pandemic (9). At-home quarantining proved to be an effective way to control the COVID-19 pandemic (19). China suspended schools nationwide from February to May of 2020, with students studying at home or undergoing online learning (10). Specifically, schools were suspended between February and May 2020

TABLE 2 Baseline data of participants in this study in 2019.

Grade at baseline	*N*	Visual acuity	Spherical equivalentrefractions (D)	Prevalence of myopia (%)
Grade 1	155,462	4.93 ± 0.14	−0.12 ± 0.95	13.6
Male	84,119	4.93 ± 0.14	−0.10 ± 0.93	13.1
Female	71,343	4.92 ± 0.14	−0.13 ± 0.96	14.1
Grade 2	150,846	4.92 ± 0.16	−0.32 ± 1.02	19.0
Male	81,357	4.92 ± 0.16	−0.29 ± 1.01	18.2
Female	69,489	4.92 ± 0.16	−0.36 ± 1.02	19.8
Grade 3	129,019	4.89 ± 0.21	−0.58 ± 1.14	28.7
Male	70,040	4.89 ± 0.21	−0.54 ± 1.14	27.0
Female	58,979	4.88 ± 0.22	−0.64 ± 1.13	30.8
Grade 4	107,871	4.83 ± 0.27	−0.90 ± 1.29	41.0
Male	59,055	4.84 ± 0.26	−0.83 ± 1.30	37.8
Female	48,816	4.81 ± 0.28	−0.99 ± 1.28	44.9
Grade 5	94,704	4.76 ± 0.31	−1.26 ± 1.47	52.5
Male	51,898	4.78 ± 0.30	−1.15 ± 1.47	47.8
Female	42,806	4.72 ± 0.32	−1.39 ± 1.45	58.2
Grade 6	83,642	4.68 ± 0.35	−1.65 ± 1.64	62.5
Male	45,958	4.72 ± 0.33	−1.52 ± 1.64	57.2
Female	37,684	4.64 ± 0.35	−1.80 ± 1.62	69.0
Grade 7	62,713	4.60 ± 0.38	−2.05 ± 1.80	70.9
Male	33,821	4.64 ± 0.37	−1.92 ± 1.81	65.9
Female	28,892	4.54 ± 0.38	−2.19 ± 1.77	76.7
Grade 8	41,236	4.52 ± 0.39	−2.47 ± 1.91	77.5
Male	22,254	4.57 ± 0.38	−2.35 ± 1.93	73.1
Female	18,982	4.47 ± 0.39	−2.62 ± 1.88	82.6
Grade 9	23,204	4.47 ± 0.38	−2.80 ± 2.01	81.7
Male	12,481	4.52 ± 0.37	−2.70 ± 2.03	78.3
Female	10,723	4.42 ± 0.38	−2.93 ± 1.98	85.6

10.3389/fmed.2024.1368219

TABLE 3 Visual acuity progression among school-aged children from 2019–2022.

Grade at baseline	Change from 2019–2022	Annual change			*F*	*P**
		2019–2020	2020–2021	2021–2022		
Grade 1	−0.12 ± 0.28	−0.01 ± 0.16	−0.04 ± 0.17	−0.07 ± 0.19	4,632.97	< 0.001
Male	−0.11 ± 0.27	−0.01 ± 0.16	−0.03 ± 0.16	−0.06 ± 0.18	1,911.80	< 0.001
Female	−0.14 ± 0.29	−0.01 ± 0.16	−0.04 ± 0.17	−0.08 ± 0.20	2,793.32	< 0.001
Grade 2	−0.19 ± 0.29	−0.05 ± 0.17	−0.06 ± 0.19	−0.08 ± 0.20	1,036.41	< 0.001
Male	−0.16 ± 0.28	−0.04 ± 0.16	−0.05 ± 0.18	−0.07 ± 0.19	259.37	< 0.001
Female	−0.22 ± 0.31	−0.05 ± 0.17	−0.07 ± 0.20	−0.09 ± 0.22	729.85	< 0.001
Grade 3	−0.22 ± 0.31	−0.06 ± 0.19	−0.07 ± 0.20	−0.08 ± 0.21	322.01	< 0.001
Male	−0.19 ± 0.29	−0.05 ± 0.18	−0.06 ± 0.19	−0.07 ± 0.20	193.66	< 0.001
Female	−0.25 ± 0.32	−0.08 ± 0.20	−0.09 ± 0.21	−0.09 ± 0.23	46.01	< 0.001
Grade 4	−0.23 ± 0.31	−0.07 ± 0.20	−0.07 ± 0.21	−0.08 ± 0.22	84.01	< 0.001
Male	−0.20 ± 0.29	−0.06 ± 0.19	−0.06 ± 0.19	−0.08 ± 0.21	203.11	< 0.001
Female	−0.26 ± 0.33	−0.09 ± 0.22	−0.09 ± 0.22	−0.08 ± 0.23	32.61	< 0.001
Grade 5	−0.22 ± 0.31	−0.07 ± 0.21	−0.08 ± 0.22	−0.08 ± 0.22	67.21	< 0.001
Male	−0.20 ± 0.29	−0.06 ± 0.20	−0.07 ± 0.20	−0.08 ± 0.21	125.46	< 0.001
Female	−0.25 ± 0.33	−0.09 ± 0.22	−0.08 ± 0.23	−0.08 ± 0.23	27.76	< 0.001
Grade 6	−0.21 ± 0.30	−0.07 ± 0.22	−0.07 ± 0.22	−0.07 ± 0.22	0.00	> 0.05
Male	−0.20 ± 0.29	−0.06 ± 0.21	−0.07 ± 0.21	−0.07 ± 0.21	28.96	< 0.001
Female	−0.22 ± 0.32	−0.08 ± 0.23	−0.07 ± 0.23	−0.07 ± 0.23	23.75	< 0.001
Grade 7	−0.17 ± 0.31	−0.06 ± 0.23	−0.07 ± 0.22	−0.05 ± 0.23	122.01	< 0.001
Male	−0.17 ± 0.29	−0.05 ± 0.22	−0.07 ± 0.21	−0.05 ± 0.22	96.01	< 0.001
Female	−0.17 ± 0.32	−0.06 ± 0.24	−0.07 ± 0.23	−0.04 ± 0.25	116.90	< 0.001
Grade 8	−0.12 ± 0.29	−0.05 ± 0.23	−0.05 ± 0.23	−0.02 ± 0.23	233.85	< 0.001
Male	−0.13 ± 0.28	−0.05 ± 0.22	−0.05 ± 0.21	−0.03 ± 0.22	61.31	< 0.001
Female	−0.11 ± 0.30	−0.05 ± 0.24	−0.05 ± 0.24	−0.02 ± 0.24	98.86	< 0.001
Grade 9	−0.10 ± 0.27	−0.05 ± 0.23	−0.03 ± 0.22	−0.03 ± 0.23	62.00	< 0.001
Male	−0.11 ± 0.26	−0.05 ± 0.21	−0.03 ± 0.21	−0.03 ± 0.22	37.74	< 0.001
Female	−0.09 ± 0.28	−0.04 ± 0.24	−0.02 ± 0.23	−0.03 ± 0.24	19.14	< 0.001
Total	−0.18 ± 0.30	−0.05 ± 0.19	−0.06 ± 0.20	−0.07 ± 0.21	2,118.21	< 0.001
Male	−0.17 ± 0.29	−0.05 ± 0.18	−0.06 ± 0.19	−0.07 ± 0.20	1,274.61	< 0.001
Female	−0.21 ± 0.32	−0.06 ± 0.21	−0.07 ± 0.21	−0.08 ± 0.23	824.34	< 0.001

The *p*-values refer to overall comparisons.

as part of the initial response to the COVID-19 outbreak. In addition to the school closures, Shenzhen experienced several other public health measures aimed at controlling the spread of the virus. These included: Before COVID-19 (2019): Regular schooling and activities were uninterrupted, with no special public health measures related to COVID-19. During COVID-19 (2020): Significant disruptions occurred due to the strict lockdown and school closures, with a shift to remote learning and limited physical interactions. After COVID-19 (2021–2022): A gradual return to normalcy was observed, but some public health measures persisted to prevent new outbreaks.

COVID-19 has had a negative impact on health-related behaviors in children (20–22). The time children spent watching electronic screens reached a peak, while the time spent outdoors declined significantly. Screen time in school-aged children increased by approximately 30 h/week during the COVID-19 pandemic (23). Chinese children used smartphones for long periods to play video games and browse the internet during the COVID-19 pandemic (24). Students in grades 4–6 often use smartphones for online learning and social media (24). After the COVID-19 outbreak, it became particularly critical to monitor myopia in a timely manner and explore the characteristics of myopia onset, which is helpful for formulating targeted myopia prevention and control strategies in school-aged children. This study spanned the pre-, mid-, and post-pandemic periods, and analyzed the epidemiological characteristics of myopia among school-aged children in China, with a goal of providing a scientific basis for formulating targeted myopia prevention and control strategies in this vulnerable demographic.

We found that the visual acuity measurements of our study participants decreased by 0.18 over four years, and by 0.05, 0.06, and 0.07 over 2019–2020, 2020–2021, and 2021–2022, respectively. The SE

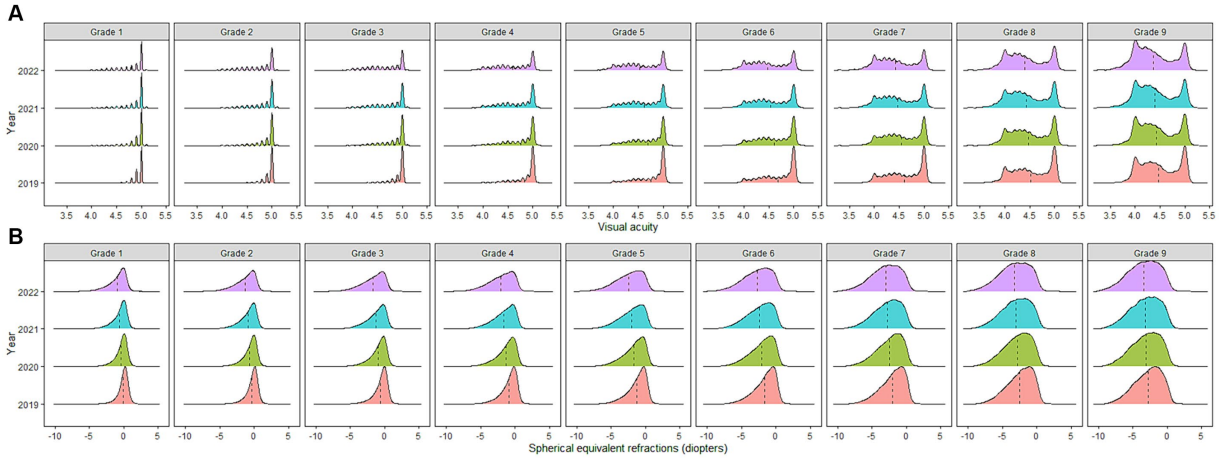

FIGURE 1
(A) Distribution of visual acuity among school-aged children in China from 2019–2022. **(B)** Distribution of spherical equivalent refractions among school-aged children in China from 2019–2022. *The dashed line represents the mean value.

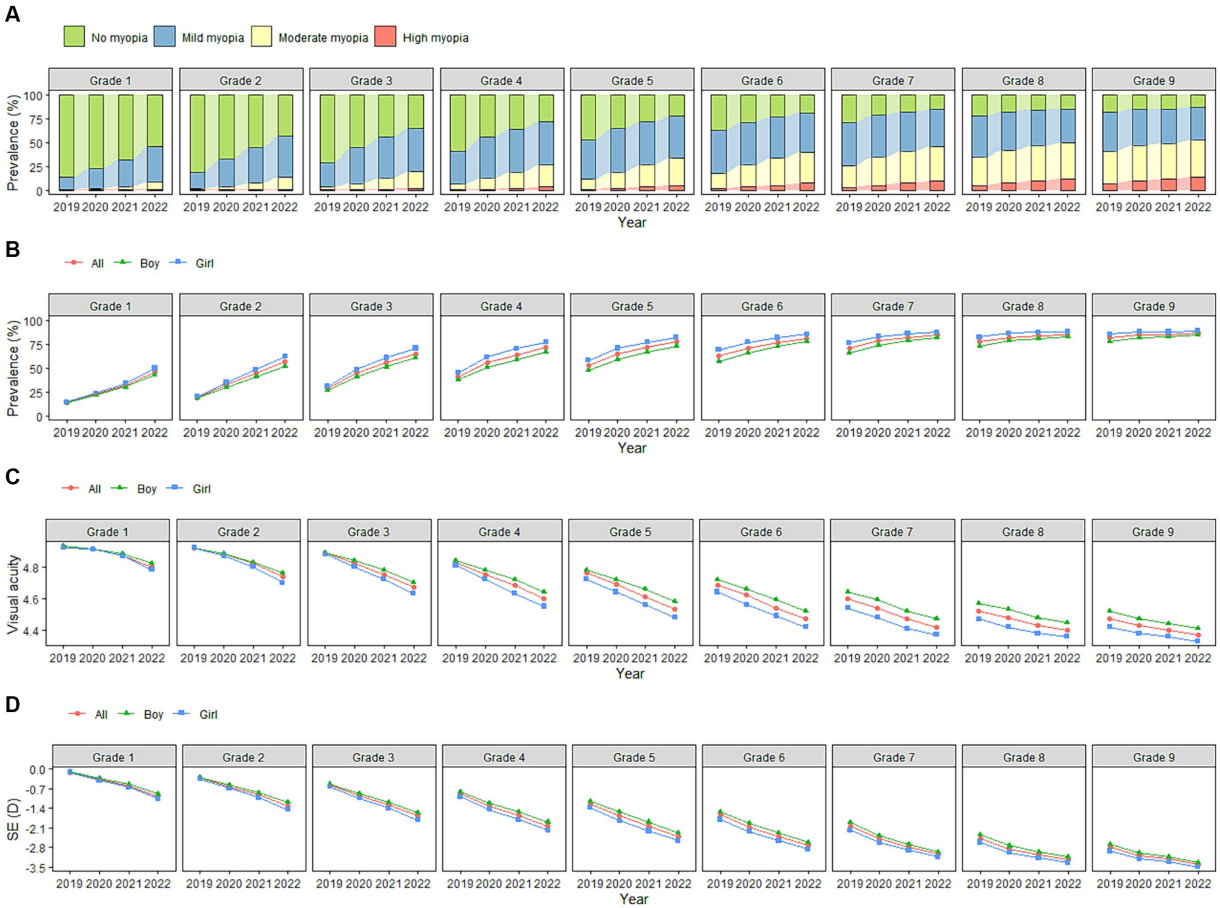

FIGURE 2
(A) Changes in constituent ratio of myopia among school-aged children in China from 2019–2022. **(B)** Changes in myopia prevalence among school-aged children in China from 2019–2022. **(C)** Changes in visual acuity among school-aged children in China from 2019–2022. **(D)** Changes in spherical equivalent refractions among school-aged children in China from 2019–2022.

decreased by 1.00 D over four years, and by 0.36 D, 0.30 D, and 0.35 D over 2019–2020, 2020–2021, and 2021–2022, respectively. Consistent with the results of other studies (17, 25), the risk of myopia among school-aged children remained high in 2021 and 2022, after the home-quarantine order was lifted. This may be related to failures to change unhealthy lifestyles and habits of eye use that many children developed during the pandemic. Study found that, although children were more involved in health-related behaviors after the pandemic

TABLE 4 Spherical equivalent refraction progression among school-aged children from 2019–2022.

Grade at baseline	Change from 2019–2022 (D)	Annual change (D)			*F*	*P**
		2019–2020	2020 2021	2021–2022		
Grade 1	−0.86 ± 1.33	−0.26 ± 0.96	−0.23 ± 0.88	−0.36 ± 0.85	893.50	< 0.001
Male	−0.80 ± 1.30	−0.24 ± 0.94	−0.22 ± 0.85	−0.34 ± 0.81	461.09	< 0.001
Female	−0.93 ± 1.36	−0.28 ± 0.98	−0.25 ± 0.91	−0.40 ± 0.88	526.12	< 0.001
Grade 2	−0.99 ± 1.35	−0.31 ± 0.94	−0.30 ± 0.87	−0.38 ± 0.81	374.39	< 0.001
Male	−0.91 ± 1.31	−0.29 ± 0.92	−0.27 ± 0.84	−0.35 ± 0.77	197.24	< 0.001
Female	−1.09 ± 1.40	−0.33 ± 0.97	−0.33 ± 0.90	−0.43 ± 0.84	268.57	< 0.001
Grade 3	−1.09 ± 1.35	−0.37 ± 0.91	−0.33 ± 0.83	−0.39 ± 0.78	169.97	< 0.001
Male	−1.01 ± 1.30	−0.35 ± 0.88	−0.30 ± 0.80	−0.37 ± 0.75	138.17	< 0.001
Female	−1.19 ± 1.39	−0.40 ± 0.94	−0.37 ± 0.86	−0.42 ± 0.81	49.16	< 0.001
Grade 4	−1.13 ± 1.30	−0.41 ± 0.88	−0.34 ± 0.79	−0.37 ± 0.75	203.53	< 0.001
Male	−1.06 ± 1.27	−0.38 ± 0.84	−0.31 ± 0.77	−0.37 ± 0.74	137.55	< 0.001
Female	−1.20 ± 1.33	−0.46 ± 0.92	−0.37 ± 0.82	−0.37 ± 0.77	180.45	< 0.001
Grade 5	−1.15 ± 1.22	−0.42 ± 0.83	−0.36 ± 0.76	−0.37 ± 0.72	164.48	< 0.001
Male	−1.12 ± 1.22	−0.39 ± 0.82	−0.35 ± 0.76	−0.38 ± 0.71	38.46	< 0.001
Female	−1.18 ± 1.22	−0.46 ± 0.83	−0.36 ± 0.77	−0.36 ± 0.72	228.34	< 0.001
Grade 6	−1.08 ± 1.14	−0.42 ± 0.81	−0.35 ± 0.76	−0.31 ± 0.69	458.62	< 0.001
Male	−1.08 ± 1.14	−0.40 ± 0.81	−0.36 ± 0.76	−0.32 ± 0.68	130.06	< 0.001
Female	−1.07 ± 1.13	−0.43 ± 0.81	−0.33 ± 0.76	−0.31 ± 0.69	273.30	< 0.001
Grade 7	−0.99 ± 1.11	−0.45 ± 0.78	−0.30 ± 0.71	−0.25 ± 0.72	1249.72	< 0.001
Male	−1.03 ± 1.09	−0.45 ± 0.78	−0.31 ± 0.69	−0.26 ± 0.67	641.84	< 0.001
Female	−0.95 ± 1.13	−0.44 ± 0.77	−0.28 ± 0.73	−0.23 ± 0.77	606.85	< 0.001
Grade 8	−0.76 ± 1.05	−0.38 ± 0.76	−0.20 ± 0.72	−0.18 ± 0.71	938.06	< 0.001
Male	−0.80 ± 1.02	−0.39 ± 0.75	−0.21 ± 0.68	−0.19 ± 0.66	554.64	< 0.001
Female	−0.72 ± 1.09	−0.36 ± 0.76	−0.19 ± 0.76	−0.17 ± 0.75	361.36	< 0.001
Grade 9	−0.60 ± 1.05	−0.30 ± 0.81	−0.10 ± 0.70	−0.21 ± 0.71	423.25	< 0.001
Male	−0.64 ± 1.01	−0.32 ± 0.81	−0.11 ± 0.65	−0.22 ± 0.64	277.60	< 0.001
Female	−0.56 ± 1.09	−0.28 ± 0.81	−0.08 ± 0.76	−0.20 ± 0.79	175.47	< 0.001
Total	−1.00 ± 1.27	−0.36 ± 0.89	−0.30 ± 0.81	−0.35 ± 0.77	1288.99	< 0.001
Male	−0.96 ± 1.25	−0.34 ± 0.87	−0.29 ± 0.79	−0.34 ± 0.74	539.06	< 0.001
Female	−1.05 ± 1.31	−0.38 ± 0.91	−0.31 ± 0.84	−0.36 ± 0.80	695.63	< 0.001

The *p*-values refer to overall comparisons.

subsided, their participation levels were lower than they were in the pre-COVID-19 period (13). In this study, the SE of the participants during the COVID-19 pandemic decreased by 0.36 D, which was similar to that in Shantou and Guangdong (−0.35 D) (26), and lower than that in Chongqing (−0.43 D) (27), Anyang (−0.46 D) (28), and Wenzhou (−0.44 D) (29).

One survey found that the prevalence of myopia among children and adolescents in nine Chinese provinces increased by 11.7% during the COVID-19 pandemic (30). Similarly, the prevalence of myopia among the students in this study increased by 11.3% during the COVID-19 pandemic. With increasing age, the prevalence of severe myopia gradually increased, and there was no severe myopia observed among preschool children. The prevalence of severe myopia has been reported to increase slowly during primary school, then rapidly during secondary school and high school (31). The prevalence of severe myopia among the participants in this study gradually increased in 2019, 2020, 2021, and 2022, to 0.9, 1.7, 2.6, and 3.8%, respectively. The prevalence of severe myopia is predicted to increase significantly globally, with 9.8% of the global population predicted to suffer from severe myopia by 2050 (1). In this study, the prevalence of severe myopia among the study participants in 2022 was 3.8%, which was higher than that in Shandong (2.0%) (32) and Anyang (1.2%) (33), but lower than that in Beijing (8.6%) (31) and Zhejiang (9.4%) (34). These differences may be caused by multiple factors, including lifestyle, environment, and genetics.

When humans are born, the eyeball is in a hyperopic state, with its SE ranging from +2.50 ~ +3.00 D. Over time, this SE gradually tends toward mild hyperopia or emmetropia. This process is often called "emmetropization" (35), and the degree of hyperopia present in the process is called "hyperopia reserve" (28). Hyperopia reserves in

TABLE 5 Prevalence of myopia among school-aged children from 2019–2022.

Grade at baseline	Change of prevalence from 2019–2022 (%)	Prevalence (%)				χ^2	P*
		2019	2020	2021	2022		
Grade 1	32.4	13.6	22.5	31.8	46.0	43,901.76	< 0.001
Male	29.8	13.1	21.8	30.2	42.9	20,626.44	< 0.001
Female	35.6	14.1	23.4	33.8	49.7	23,623.25	< 0.001
Grade 2	37.6	19.0	32.2	44.6	56.6	50,153.44	< 0.001
Male	33.9	18.2	30.1	41.2	52.1	22,642.81	< 0.001
Female	42.2	19.8	34.7	48.5	62.0	28,276.03	< 0.001
Grade 3	36.6	28.7	44.4	55.6	65.3	38,301.51	< 0.001
Male	33.6	27.0	40.9	51.3	60.6	17,657.91	< 0.001
Female	40.0	30.8	48.5	60.8	70.8	21,070.14	< 0.001
Grade 4	30.7	41.0	55.7	64.2	71.7	23,064.20	< 0.001
Male	29.4	37.8	51.0	59.1	67.2	11,201.33	< 0.001
Female	32.3	44.9	61.4	70.4	77.2	12,331.63	< 0.001
Grade 5	24.9	52.5	64.3	71.4	77.4	14,586.11	< 0.001
Male	25.5	47.8	58.9	66.5	73.3	7,870.26	< 0.001
Female	24.1	58.2	70.9	77.2	82.3	6,916.91	< 0.001
Grade 6	18.8	62.5	71.2	76.8	81.3	8,342.17	< 0.001
Male	20.4	57.2	66.1	72.7	77.6	4,972.49	< 0.001
Female	16.7	69.0	77.4	81.9	85.7	3,457.71	< 0.001
Grade 7	13.6	70.9	78.5	82.3	84.5	4,051.49	< 0.001
Male	16.0	65.9	74.4	78.8	81.9	2,632.59	< 0.001
Female	11.0	76.7	83.3	86.3	87.7	1,504.84	< 0.001
Grade 8	7.9	77.5	82.3	84.2	85.4	1,028.43	< 0.001
Male	9.8	73.1	78.6	81.2	82.9	736.62	< 0.001
Female	5.8	82.6	86.7	87.7	88.4	325.47	< 0.001
Grade 9	5.1	81.7	85.1	85.3	86.8	249.71	< 0.001
Male	6.6	78.3	82.3	83.1	84.9	198.40	< 0.001
Female	3.5	85.6	88.3	88.0	89.1	67.93	< 0.001
Total	28.2	38.7	50.0	58.4	66.9	148352.68	< 0.001
Male	27.0	36.1	46.7	54.8	63.1	73505.10	< 0.001
Female	29.8	41.7	53.9	62.7	71.5	77024.24	< 0.001

The *p*-values refer to overall comparisons.

children and adolescents gradually decrease over time. With a decrease in the hyperopia reserve, the cumulative incidence of myopia in primary school students gradually increases over 1–3 years. If students have not yet developed myopia in the first grade of primary school, but are already in the emmetropic state (−0.50 to 0 D), their 3-year cumulative incidence of myopia can be as high as >48%. When the hyperopia reserve reaches above +1.00 D, the 3-year cumulative incidence of myopia is likely to be <7%. Pre-myopia is a key intermediate stage in refractive development, and the pre-myopia stage is a high-risk stage of myopia (36). Therefore, early screening myopia is an effective means to prevent myopia. Children and adolescents use their eyes at close ranges too early and too often, which leads to excessive consumption of hyperopia reserves and increases the likelihood of developing myopia. Therefore, scientific and timely monitoring of hyperopia reserves in children and early detection of children at high risk of developing myopia are important for its prevention and control.

There are some significant advantages to this study. First, its sample size was large, with over 840,000 children and adolescents participating. Second, participant compliance was good, with a loss-to-follow-up rate of only 0.37%. Third, the study population included students of all grades in primary and secondary schools, and the results comprehensively reflected the epidemiological characteristics of myopia in students of all ages. Fourth, this study relied on the Shenzhen Children and Adolescents Myopia Monitoring Big Data Platform, and all data were uploaded to the platform in real time at the screening site, which saved time and effort and provided data-based support for the study. Fifth, based on the baseline, the study participants were followed up continuously for 3 years, which was a long enough period to reveal changes in myopia over time. However,

10.3389/fmed.2024.1368219

TABLE 6 Proportion of varying degrees of myopia among school-aged children from 2019–2022.

Grade at baseline	2019 (%)				2020 (%)				2021 (%)				2022 (%)				χ^2	P
	No myopia	Mild myopia	Moderate myopia	Severe myopia	No myopia	Mild myopia	Moderate myopia	Severe myopia	No myopia	Mild myopia	Moderate myopia	Severe myopia	No myopia	Mild myopia	Moderate myopia	Severe myopia		
Grade 1	86.4	12.7	0.7	0.1	77.5	20.9	1.5	0.1	68.2	28.0	3.6	0.2	54.0	37.9	7.6	0.5	123,252.56	≤0.001
Grade 2	81.0	17.6	1.2	0.1	67.8	28.6	3.4	0.2	55.4	37.4	6.7	0.4	43.4	43.6	12.1	1.0		
Grade 3	71.3	25.7	2.9	0.1	55.6	37.4	6.6	0.4	44.4	43.2	11.6	0.9	34.7	45.6	17.8	1.8		
Grade 4	59.0	34.8	6.0	0.3	44.3	43.5	11.3	0.9	35.8	45.4	17.1	1.7	28.3	45.3	23.3	3.1		
Grade 5	47.5	41.2	10.7	0.6	35.7	45.6	17.1	1.6	28.6	45.1	23.2	3.0	22.6	43.6	28.8	4.9		
Grade 6	37.5	44.5	16.6	1.4	28.8	44.8	23.3	3.1	23.2	43.3	28.6	4.9	18.7	41.4	32.8	7.1		
Grade 7	29.1	45.0	23.1	2.9	21.5	43.9	29.5	5.0	17.7	41.5	33.7	7.1	15.5	38.4	36.8	9.3		
Grade 8	22.5	43.2	29.6	4.7	17.7	40.5	34.4	7.4	15.8	37.9	36.9	9.4	14.6	35.8	38.1	11.6		
Grade 9	18.3	40.7	34.0	7.0	14.9	38.1	37.4	9.7	14.7	36.4	37.8	11.2	13.2	34.4	39.0	13.5		
x^2	220,546.22				198,161.70				165,680.18									
P*	≤0.001				≤0.001				≤0.001									

The p-values refer to overall comparisons.

TABLE 7 Cumulative incidence of myopia among students in Grade 1 with different baseline spherical equivalent refraction.

Baseline SE (D)	1-year follow-up (%)	2-year follow-up (%)	3-year follow-up (%)
−0.5 ≤ Baseline SE < 0 (n = 34,327)	24.6	34.3	48.1
0 ≤ Baseline SE < 0.5 (n = 51,926)	12.9	23.9	39.0
0.5 ≤ Baseline SE < 1 (n = 28,391)	4.5	11.6	24.8
Baseline SE ≥ 1 (n = 7,901)	1.6	2.4	6.8
χ^2	6,565.52	6,586.15	6,836.07
P	< 0.001	< 0.001	< 0.001

there are some key shortcomings to this study that are worth noting as well. First, although non-cycloplegic refractive examination has been proven to have high sensitivity and specificity for large-scale myopia screening (37), it may overestimate the prevalence of myopia to some extent. Second, some biological parameters of the eyeball that are closely related to refraction, such as the corneal radius (CR) and axial length (AL), were not included as screening indicators. One study found that AL and the AL/CR ratio are closely related to refractive status (38). Third, the age of the subjects in this study was not recorded during follow-up, so age-specific SE changes of the subjects could not be analyzed.

This study revealed changing trends in visual acuity and refractive status during and after the COVID-19 pandemic among school-aged children in China. Over a follow-up period of 4 years, the participants' visual acuity measurements progressed to −0.18 ± 0.30 D (−0.17 ± 0.29 D for boys, −0.21 ± 0.32 D for girls), their SE progressed to −1.00 ± 1.27 D (−0.96 ± 1.25 D for boys, −1.05 ± 1.31 D for girls), and the prevalence of myopia and severe myopia increased by 28.2 and 2.9%, respectively. During the COVID-19 pandemic, the participants' visual acuity and SE measurements decreased by 0.05 and 0.36 D, respectively, and the prevalence of myopia increased by 11.3%. As the risk of myopia did not decrease after the at-home quarantine order was lifted, we recommend timely monitoring and early intervention for myopia in school-aged children.

Data availability statement

The original contributions presented in the study are included in the article/supplementary materials, further inquiries can be directed to the corresponding author.

Ethics statement

The studies involving humans were approved by the Ethics Committee of the Shenzhen Eye Hospital. The studies were conducted in accordance with the local legislation and institutional requirements. Written informed consent for participation in this study was provided by the participants' legal guardians/next of kin.

Author contributions

JM: Formal analysis, Software, Writing – original draft. HZ: Writing – original draft. MJ: Data curation, Investigation, Writing – review & editing. WY: Supervision, Validation, Writing – review & editing.

Funding

The author(s) declare that financial support was received for the research, authorship, and/or publication of this article. This work was supported by Shenzhen Science and Technology Program (JCYJ20230807114608016).

Conflict of interest

The authors declare that the research was conducted in the absence of any commercial or financial relationships that could be construed as a potential conflict of interest.

Publisher's note

References

1. Holden BA, Fricke TR, Wilson DA, Jong M, Naidoo KS, Sankaridurg P, et al. Global prevalence of myopia and high myopia and temporal trends from 2000 through 2050. *Ophthalmology*. (2016) 123:1036–42. doi: 10.1016/j.ophtha.2016.01.006

2. Jan C, Li L, Keay L, Stafford RS, Congdon N, Morgan I. Prevention of myopia, China. *Bull World Health Organ*. (2020) 98:435–7. doi: 10.2471/BLT.19.240903

3. Sankaridurg P, Tahhan N, Kandel H, Naduvilath T, Zou H, Frick KD, et al. Impact of myopia. *Invest Ophthalmol Vis Sci*. (2021) 62:2. doi: 10.1167/iovs.62.5.2

4. Dong L, Kang YK, Li Y, Wei WB, Jonas JB. Prevalence and time trends of myopia in children and adolescents in China: a systemic review and meta-analysis. *Retina*. (2020) 40:399–411. doi: 10.1097/IAE.0000000000002590

5. Bullimore MA, Ritchey ER, Shah S, Leveziel N, Bourne RRA, Flitcroft DI. The risks and benefits of myopia control. *Ophthalmology*. (2021) 128:1561–79. doi: 10.1016/j.ophtha.2021.04.032

6. Wong TY, Ferreira A, Hughes R, Carter G, Paul MP. Epidemiology and disease burden of pathologic myopia and myopic choroidal neovascularization: an evidence-based systematic review. *Am J Ophthalmol*. (2014) 157:9–25.e12. doi: 10.1016/j.ajo.2013.08.010

7. Eckert KA, Carter MJ, Lansingh VC, Wilson DA, Furtado JM, Frick KD, et al. A simple method for estimating the economic cost of productivity loss due to blindness and moderate to severe visual impairment. *Ophthalmic Epidemiol*. (2015) 22:349–55. doi: 10.3109/09286586.2015.1066394

8. Naidoo KS, Fricke TR, Frick KD, Jong M, Naduvilath TJ, Resnikoff S, et al. Potential lost productivity resulting from the global burden of myopia: systematic review, meta-analysis, and modeling. *Ophthalmology*. (2019) 126:338–46. doi: 10.1016/j.ophtha.2018.10.029

9. Li Q, Guan X, Wu P, Wang X, Zhou L, Tong Y, et al. Early transmission dynamics in Wuhan, China, of novel coronavirus-infected pneumonia. *N Engl J Med*. (2020) 382:1199–207. doi: 10.1056/NEJMoa2001316

10. Brooks SK, Webster RK, Smith LE, Woodland L, Wessely S, Greenberg N, et al. The psychological impact of quarantine and how to reduce it: rapid review of the evidence. *Lancet*. (2020) 395:912–20. doi: 10.1016/S0140-6736(20)30460-8

11. Wang G, Zhang Y, Zhao J, Zhang J, Jiang F. Mitigate the effects of home confinement on children during the COVID-19 outbreak. *Lancet*. (2020) 395:945–7. doi: 10.1016/S0140-6736(20)30547-X

12. Markovic A, Mühlematter C, Beaugrand M, Camos V, Kurth S. Severe effects of the COVID-19 confinement on young children's sleep: a longitudinal study identifying risk and protective factors. *J Sleep Res*. (2021) 30:e13314. doi: 10.1111/jsr.13314

13. De Bruijn AGM, Te Wierike SCM, Mombarg R. Trends in and relations between children's health-related behaviors pre-, mid-and post-Covid. *Eur J Pub Health*. (2023) 33:196–201. doi: 10.1093/eurpub/ckad007

14. Rose KA, Morgan IG, Ip J, Kifley A, Huynh S, Smith W, et al. Outdoor activity reduces the prevalence of myopia in children. *Ophthalmology*. (2008) 115:1279–85. doi: 10.1016/j.ophtha.2007.12.019

15. Wei SF, Li SM, Liu L, Li H, Kang MT, Sun YY, et al. Sleep duration, bedtime, and myopia progression in a 4-year follow-up of Chinese children: the Anyang childhood eye study. *Invest Ophthalmol Vis Sci*. (2020) 61:37. doi: 10.1167/iovs.61.3.37

16. Wang W, Zhu L, Zheng S, Ji Y, Xiang Y, Lv B, et al. Survey on the progression of myopia in children and adolescents in Chongqing during COVID-19 pandemic. *Front Public Health*. (2021) 9:646770. doi: 10.3389/fpubh.2021.646770

17. Chang P, Zhang B, Lin L, Chen R, Chen S, Zhao Y, et al. Comparison of myopic progression before, during, and after COVID-19 lockdown. *Ophthalmology*. (2021) 128:1655–7. doi: 10.1016/j.ophtha.2021.03.029

18. Wang J, Xie H, Morgan I, Chen J, Yao C, Zhu J, et al. How to conduct school myopia screening: comparison among myopia screening tests and determination of associated cutoffs. *Asia Pac J Ophthalmol*. (2022) 11:12–8. doi: 10.1097/APO.0000000000000487

19. Pellegrini M, Bernabei F, Scorcia V, Giannaccare G. May home confinement during the COVID-19 outbreak worsen the global burden of myopia? *Graefes Arch Clin Exp Ophthalmol*. (2020) 258:2069–70. doi: 10.1007/s00417-020-04728-2

20. Kharel M, Sakamoto JL, Carandang RR, Ulambayar S, Shibanuma A, Yarotskaya E, et al. Impact of COVID-19 pandemic lockdown on movement behaviours of children and adolescents: a systematic review. *BMJ Glob Health*. (2022) 7:e007190. doi: 10.1136/bmjgh-2021-007190

21. Paterson DC, Ramage K, Moore SA, Riazi N, Tremblay MS, Faulkner G. Exploring the impact of COVID-19 on the movement behaviors of children and youth: a scoping review of evidence after the first year. *J Sport Health Sci*. (2021) 10:675–89. doi: 10.1016/j.jshs.2021.07.001

22. Ten Velde G, Lubrecht J, Arayess L, van Loo C, Hesselink M, Reijnders D, et al. Physical activity behaviour and screen time in Dutch children during the COVID-19 pandemic: pre-, during-and post-school closures. *Pediatr Obes*. (2021) 16:e12779. doi: 10.1111/ijpo.12779

23. Montag C, Elhai JD. Discussing digital technology overuse in children and adolescents during the COVID-19 pandemic and beyond: on the importance of considering affective neuroscience theory. *Addict Behav Rep*. (2020) 12:100313. doi: 10.1016/j.abrep.2020.100313

24. Sun Y, Li Y, Bao Y, Meng S, Sun Y, Schumann G, et al. Brief report: increased addictive internet and substance use behavior during the COVID-19 pandemic in China. *Am J Addict*. (2020) 29:268–70. doi: 10.1111/ajad.13066

25. Wang W, Peng S, Zhang F, Zhu B, Zhang L, Tan X. Progression of vision in Chinese school-aged children before and after COVID-19. *Int J Public Health*. (2022) 67:1605028. doi: 10.3389/ijph.2022.1605028

26. Guo C, Li Y, Luo L, Lin J, Qiu K, Zhang M. Progression and incidence of myopia among schoolchildren in the post-COVID-19 pandemic period: a prospective cohort study in Shantou, China. *BMJ Open*. (2023) 13:e074548. doi: 10.1136/bmjopen-2023-074548

27. Zhou WJ, Zhang YY, Li H, Wu YF, Xu J, Lv S, et al. Five-year progression of refractive errors and incidence of myopia in school-aged children in Western China. *J Epidemiol*. (2016) 26:386–95. doi: 10.2188/jea.JE20140258

28. Li SM, Wei S, Atchison DA, Kang MT, Liu L, Li H, et al. Annual incidences and progressions of myopia and high myopia in Chinese schoolchildren based on a 5-year cohort study. *Invest Ophthalmol Vis Sci*. (2022) 63:8. doi: 10.1167/iovs.63.1.8

29. Wong YL, Yuan Y, Su B, Tufail S, Ding Y, Ye Y, et al. Prediction of myopia onset with refractive error measured using non-cycloplegic subjective refraction: the WEPrOM study. *BMJ Open Ophthalmol*. (2021) 6:e000628. doi: 10.1136/bmjophth-2020-000628

30. Hu Y, Ding X, Guo X, Chen Y, Zhang J, He M. Association of age at myopia onset with risk of high myopia in adulthood in a 12-year follow-up of a Chinese cohort. *JAMA Ophthalmol*. (2020) 138:1129–34. doi: 10.1001/jamaophthalmol.2020.3451

31. Guo Y, Duan JL, Liu LJ, Sun Y, Tang P, Lv YY, et al. High myopia in greater Beijing school children in 2016. *PLoS One*. (2017) 12:e0187396. doi: 10.1371/journal.pone.0187396

32. Wu JF, Bi HS, Wang SM, Hu YY, Wu H, Sun W, et al. Refractive error, visual acuity and causes of vision loss in children in Shandong, China. The Shandong children eye study. *PLoS One*. (2013) 8:e82763. doi: 10.1371/journal.pone.0082763

33. Li SM, Liu LR, Li SY, Ji YZ, Fu J, Wang Y, et al. Anyang childhood eye study group. Design, methodology and baseline data of a school-based cohort study in Central China: the Anyang childhood eye study. *Ophthalmic Epidemiol*. (2013) 20:348–59. doi: 10.3109/09286586.2013.842596

34. Wang J, Ying GS, Fu X, Zhang R, Meng J, Gu F, et al. Prevalence of myopia and vision impairment in school students in eastern China. *BMC Ophthalmol*. (2020) 20:2. doi: 10.1186/s12886-019-1281-0

35. Medina A. The cause of myopia development and progression: theory, evidence, and treatment. *Surv Ophthalmol*. (2022) 67:488–509. doi: 10.1016/j.survophthal.2021.06.005

36. Flitcroft DI, He M, Jonas JB, Jong M, Naidoo K, Ohno-Matsui K, et al. IMI – defining and classifying myopia: a proposed set of standards for clinical and epidemiologic studies. *Invest Ophthalmol Vis Sci*. (2019) 60:M20–30. doi: 10.1167/iovs.18-25957

37. Lin S, Ma Y, He X, Zhu J, Zou H. Using decision curve analysis to evaluate common strategies for myopia screening in school aged children. *Ophthalmic Epidemiol*. (2019) 26:286–94. doi: 10.1080/09286586.2019.1616774

38. Mu J, Zeng D, Fan J, Liu M, Zhong H, Shuai X, et al. The accuracy of the axial length and axial length/corneal radius ratio for myopia assessment among Chinese children. *Front Pediatr*. (2022) 10:859944. doi: 10.3389/fped.2022.859944

frontiers | Frontiers in Medicine

TYPE Original Research
PUBLISHED 27 September 2024
DOI 10.3389/fmed.2024.1469422

OPEN ACCESS

EDITED BY
Brian Vohnsen,
University College Dublin, Ireland

REVIEWED BY
Rafa Iribarren,
Drs. Iribarren Eye Consultants, Argentina
Fuensanta Vera-Diaz,
New England College of Optometry, United States
Síofra Harrington,
Technological University Dublin, Ireland

*CORRESPONDENCE
Zhihong Liu
✉ lzh_2580@sina.com

†These authors have contributed equally to this work

RECEIVED 01 August 2024
ACCEPTED 18 September 2024
PUBLISHED 27 September 2024

CITATION
Liu T, Tan W, Fu Y, Cheng B, Tian H, Liu C, Wang Z, Zhang Y, Guan S and Liu Z (2024) Association of outdoor artificial light at night with myopia among Chinese adolescents: a representative cross-sectional study. *Front. Med.* 11:1469422. doi: 10.3389/fmed.2024.1469422

Association of outdoor artificial light at night with myopia among Chinese adolescents: a representative cross-sectional study

Ting Liu[1,2,3†], Weixing Tan[4†], Youjuan Fu[5†], Beijing Cheng[6†], Hua Tian[4], Can Liu[1,3], Zhixiang Wang[2], Yanting Zhang[4], Suzhen Guan[1,3] and Zhihong Liu[1,3*]

[1]School of Public Health, Ningxia Medical University, Yinchuan, China, [2]Hospital Infection Management Department, People's Hospital of Ningxia Hui Autonomous Region, Ningxia Medical University, Yinchuan, China, [3]Key Laboratory of Environmental Factors and Chronic Disease Control, Yinchuan, China, [4]School Health Section, Ningxia Center for Disease Control and Prevention, Yinchuan, China, [5]School of Inspection, Ningxia Medical University, Yinchuan, China, [6]Key Laboratory of Environmental Medicine Engineering, Ministry of Education, School of Public Health, Southeast University, Nanjing, China

Background: The association between the rapid increase in myopia among adolescents and the amount of outdoor artificial light at night (ALAN) remains unclear. The aim of this study was to investigate the association between outdoor ALAN and myopia in adolescents.

Methods: Stratified cluster random sampling was used to obtain a sample of 33,160 students (age range: 9–18 years; mean: 13.51 years) with complete data from 120 primary and secondary schools across the Ningxia region in China in 2021. Myopia was defined as a spherical equivalent (SE) ≤−0.5 diopters (D) in at least one eye, determined by automated refractometers without cycloplegia. Outdoor ALAN data were obtained from satellite data and the two-year average outdoor ALAN exposure for each participant was determined by matching it to their school address (home addresses were not available). The association between ALAN and myopia was assessed using multiple logistic regression models and restricted cubic spline (RCS) regression. Stratified analyses were performed by age, sex, residence, school level, and outdoor exercise time.

Results: The myopia group had higher outdoor ALAN levels than the non-myopia group [median (interquartile spacing): 14.44 (3.88–26.56) vs. 6.95 (1.21–21.74) nanoWatts/cm^2/sr]. After adjusting for covariates identified through stepwise regression, it was observed that the prevalence of myopia increased by 4% for every 10-unit change [95% confidence interval (CI): 1.02–1.07]. Compared to the first quantile (Q1) of outdoor ALAN exposure, the odds ratio (OR) of myopia was 1.20 (95% CI: 1.08–1.34) in the fourth quantile. RCS further showed a positive nonlinear relationship between outdoor ALAN exposure and myopia (p for nonlinear <0.001). Stronger effects were not found in subgroup analyses.

Conclusion: Outdoor ALAN exposure is positively and nonlinearly associated with the prevalence of myopia in adolescents. Controlling outdoor light pollution may constitute a potential strategy to reduce the incidence of myopia in adolescents.

KEYWORDS

ALAN, artificial light at night, myopia, representative cross-sectional study, Chinese adolescents

1 Introduction

Myopia is a refractive error in eye health, leading to blurred vision when observing distant objects (1–3). According to Holden et al. (4), the global prevalence of myopia in 2000 was 22.9% (1.406 billion people). Projections indicated that by 2050, myopia will affect 49.8% (4.758 billion) of the global population (4). Myopia occurs primarily in childhood through early adulthood, making adolescents a key group of concern (5, 6). Myopia poses a high risk for irreversible visual impairment caused by diseases such as glaucoma, retinal detachment, or myopic maculopathy. The increasing prevalence and associated risks not only escalate healthcare costs but also diminish the quality of life, posing a substantial burden on the global healthcare and economy (7–9). Consequently, a comprehensive understanding of the influencing factors of myopia becomes imperative.

Factors influencing myopia development include genetics, environment, and their interplay (10–12). Among these, inadequate sunlight exposure or limited time spent outdoors during daylight is usually suggested as an important driver of myopia prevalence (13, 14). However, outdoor artificial light at night (ALAN) differs from natural light during the day, potentially yielding distinct effects (14, 15). ALAN, with its high intensity, unnatural wavelengths, and abrupt switches, poses potential health risks (16, 17). Furthermore, in contemporary times, ALAN is growing at an annual rate of 5–20% (18), thus warranting our attention.

A review also highlighted the non-coincidental correlation between the widespread use of light-emitting diodes (LEDs) and the accelerating spike in the prevalence of myopia (14). Several studies have provided some plausible explanations for the above phenomenon (14, 19–22). Chronic exposure to ALAN may lead to severe circadian rhythm disturbances that alter the circadian rhythm of the retina (23, 24). Recent reviews have elucidated how retinal circadian rhythm disruption affects the onset and progression of myopia (14, 20, 21, 25). Additionally, ALAN suppressed melatonin production and deprived people of sleep, both of which were also important factors in the development of myopia (19, 22). Numerous epidemiological studies have investigated the association between ALAN and various outcomes, including obesity, fasting blood glucose, blood pressure, and sleep (18, 26–29). However, the association with myopia is notably limited.

A few epidemiologic studies have attempted to explore the relationship between nighttime light exposure and myopia development, but the results have been inconsistent (30–33). Quinn et al. (33) found that the development of myopia in children was strongly associated with their exposure to nighttime lighting in the first 2 years of life. However, subsequent research by Gwiazda et al. (32) found no significant relationship between myopia prevalence and exposure to nighttime lighting during the first 2 years or later. Similarly, Czepita et al. (30) reported that light from fluorescent lamps was associated with a higher incidence of astigmatism, but Czepita et al. (31) later found no association between nighttime light usage and myopia in Polish children without a family history of myopia. Additionally, to our knowledge, no available studies have explored the associations of ALAN with myopia among Chinese adolescents. To address the knowledge gap, we conducted a large representative cross-sectional study in 2021 among school adolescents in 22 districts/counties/cities in Ningxia, China. The study aimed to quantify the association between ALAN and myopia, and to examine the modifying effects of certain individual characteristics.

2 Methods

2.1 Study design and population

The survey samples were obtained from the monitoring program of students' myopia and health influencing factors conducted from September to December 2021 by the Ningxia Center for Disease Control and Prevention. Ningxia is located in the northwest of China, with 9 districts, 11 counties and 2 cities under its jurisdiction, covering a total area of 66,400 square kilometers.[1] Ningxia is also an autonomous region of China known as the Ningxia Hui Autonomous Region. We used stratified cluster random sampling to select schools for monitoring, and a total of 120 schools were selected. The detailed spatial distribution of surveyed schools in each district or county is shown in Figure 1. About two classes per school per grade were taken as the basic unit of investigation. Given responsiveness, our study only focused on in-school adolescents (fourth grade through high school). A total of 34,777 adolescents participated in the survey, with each participant receiving a physical examination and a structured questionnaire. The questionnaires were paper-based and completed by the adolescents themselves, with completion taking approximately 10 to 30 min. After excluding 1,617 (4.65%) participants with missing covariates, a total of 33,160 adolescents were included in the final analysis. The study was approved by the Ethics Committee of the People's Hospital of Ningxia Hui Autonomous Region ([2022]-NZR-093) and was conducted in accordance with the guidelines of the Declaration of Helsinki.

2.2 Myopia determination

In this study, myopia was diagnosed following the national standard "Technical Specifications for Student Health Examination" (GB/T 26343) and the health industry standard "Specification for Myopia Screening in Primary and Secondary School Students" (WS/T 663-2020). Briefly, ophthalmologists or trained investigators used automated refractometers to perform eye examinations without

1 http://nxdata.com.cn/

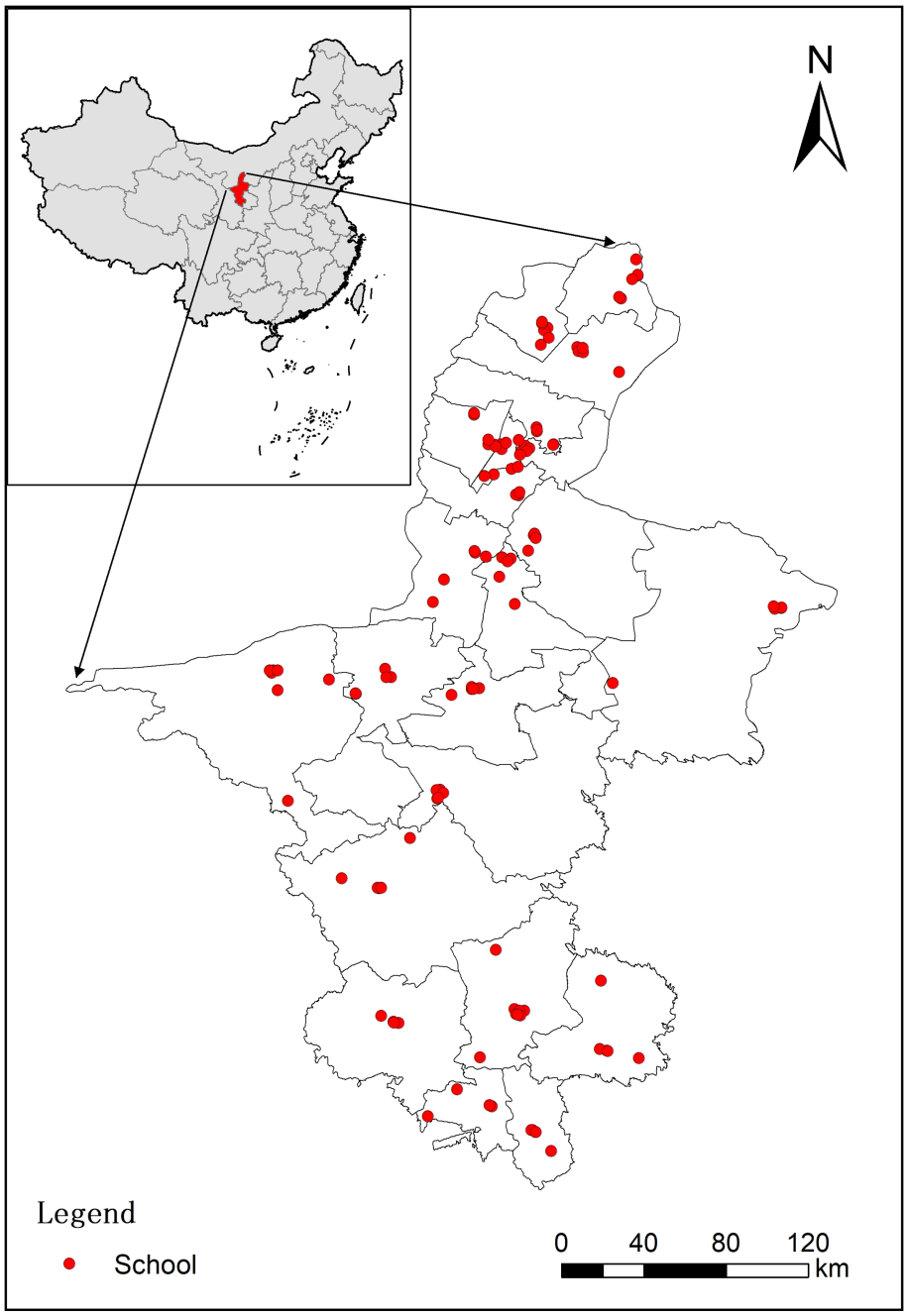

FIGURE 1
Spatial distribution of schools of the study subjects in Ningxia province, China. Red dots represent the schools ($n = 120$) of the study subjects; the gray lines represent administrative boundaries of 22 districts/counties/cities in Ningxia province, China.

cycloplegia. All refractometers were compliant with the ISO 10342:2010 standard for ophthalmic instruments. Three measurements were taken in each eye and averaged. If the spherical equivalent (SE) of any two measurements differed by ≥0.50 diopters (D), the eye was re-measured and a new mean value was calculated. SE was calculated by the following formula: SE = sphericity degree + 0.5 × cylindrical degree. SE was used to assess refractive error in this study, consistent with previous epidemiologic surveys of children (34, 35). Based on previous literature and industry standards (WS/T 663-2020), myopia was defined as a SE of ≤−0.5 D in at least one eye (36, 37). In addition, students with suspected eye abnormalities were referred to a specialist for further evaluation.

2.3 Environmental data

During the survey, the residential address of each participant's school was collected and subsequently the longitude and latitude of each participant's school were extracted. Outdoor ALAN data were sourced from NASA/NOAA's Visible Infrared Imaging Radiometer

Suite (VIIRS) Day/Night Band (DNB) low-light imaging data, which provides high-quality nighttime light products[2] (18, 38). The intensity of outdoor ALAN was quantified in raster units, ranging from 0 to 472.86 nanoWatts/cm^2/sr, with a spatial resolution of 500 m. Taking Supplementary Figure S1 as an example, we presented the annual average outdoor ALAN exposure for 2020 in Ningxia province. Considering our population data collection occurred in 2021, we downloaded outdoor ALAN data for the years 2018–2020. Then, using ArcGIS version 10.2 software, we extracted the annual mean values of outdoor ALAN for each school buffer (1 km, 3 km, and 5 km) for the years 2018–2020. Considering that the majority of the included schools follow a three-year curriculum, for the main analysis, we used the 1 km buffer and 2-year average of outdoor ALAN exposure as the main exposure variable. Also, the effects of multiple definitions of outdoor ALAN were explored.

The assessment of the schools' green space was conducted using the normalized difference vegetation index (NDVI). NDVI values range from −1 to 1 (3). Higher NDVI values indicate higher levels of green space around the school. NDVI data were sourced from Moderate Resolution Imaging Spectroradiometer (MODIS) surface reflectance data.[3] Considering the seasonality of vegetation, we extracted the summer three-month average (June to August) from the MODIS VI product (MOD13Q1) as the primary exposure, with a spatial resolution of 250 m. Taking Supplementary Figure S2 as an example, we also presented the annual average NDVI exposure for 2020 in Ningxia province. For the main analysis, we also used the 1 km buffer and 2-year average of NDVI exposure as the main exposure variable.

The daily data of particulate matter ≤2.5 mm ($PM_{2.5}$) at a 1 km spatial resolution were obtained from ChinaHighAirPollutants database[4] (39). $PM_{2.5}$ was ultimately selected as the primary exposure variable given the generally high correlation of air pollution indicators. Additionally, using ArcGIS version 10.2 software, the 1 km data were resampled to 500 m for subsequent matching purposes. For the main analysis, the 1 km buffer and 2-year average of $PM_{2.5}$ exposure was used as the main exposure variable.

2.4 Covariates

Based on previous studies (3, 40, 41), covariates were selected as follows: demographic characteristics [age, sex, residence, nationality, school level, exposure time, body mass index (BMI), and parental myopia]; behavioral and lifestyle factors (nighttime sleep, outdoor exercise time per day, frequency of sugar per week, frequency of oil per week, frequency of fruit per week, frequency of vegetable per week, computers and TVs spend time per day, after-school homework time per day, after-school tutoring time per day, eye exercises per day, and annual frequency of visual inspections); and regional macro-indicators [gross domestic product (GDP) *per capita*, population density, and health technical personnel].

Among these factors, exposure time represented time exposed to the school environment: grade 4 to 6, indicating >3 year of exposure time; grade 7 and grade 10, indicating 1 year of exposure time; grade 8 and grade 11, indicating 2 year of exposure time; grade 9 and grade 12, indicating 3 year of exposure time, respectively. BMI was calculated by dividing the weight (kg) of each participant by the square of height (m). Data on demographic and behavioral/lifestyle factors were collected using a structured questionnaire. Behavioral/lifestyle factors were primarily assessed through questions about the past week. For example, participants were asked: "How much time is spent on outdoor exercise per day over the past week?" with response options including: less than 1 h, 1–2 h, and 2 h or more. Data on regional macro-indicators were obtained from Ningxia Statistical Yearbook of 2020.[5]

2.5 Statistical analysis

Continuous variables that were normal or approximately normal were described by the mean [standard deviation (SD)], while those that were not normally distributed were expressed as the median [interquartile spacing (IQR)]. Descriptive statistics for categorical variables were expressed as numbers (percentages, %). Depending on the distribution of the variables, student's *t*-tests, Mann–Whitney *U*-tests, or chi-square tests were used to compare differences in individual characteristics between non-myopic and myopic participants.

Multiple logistic regression was used to estimate the associations between outdoor ALAN (per 10 units or per quartile increase) exposure and the prevalence of myopia. We constructed three models. Model 1 was not adjusted for any covariates. Based on univariate analysis ($p < 0.1$), Model 2 adjusted for age, sex, residence, nationality, school level, exposure time, body mass index, parental myopia, nighttime sleep, outdoor exercise time, fruit, vegetable, computers and TVs spend time, after-school homework time, after-school tutoring time, eye exercises, annual frequency of visual inspections, health technical personnel, NDVI, and $PM_{2.5}$. A stepwise selection approach was used to build a parsimonious model. Thus, Model 3 (main model) adjusted for age, sex, residence, nationality, school level, exposure time, body mass index, parental myopia, fruit, vegetable, after-school homework time, eye exercises, annual frequency of visual inspections, and $PM_{2.5}$.

In examining the relationship between outdoor ALAN exposure and the prevalence of myopia, we further investigated the shape of the exposure-response curve using restricted cubic spline (RCS) regression. For the RCS, the knots were set to the 5th, 25th, 50th, 75th and 95th percentiles, and the reference value was 0. The nonlinear *p*-value of the RCS was calculated by the Wald test.

Based on prior literature and our database, we selected five individual characteristics to explore the modifying effects, which were associated with myopia with moderate to high strength of evidence (3, 40). These characteristics were: (1) age (≤10 years and >10 years), (2) sex (male and female), (3) residence (rural areas and urban areas), (4) school level (primary, junior, and senior), and (5) outdoor exercise time (<1 h, 1–2 h, and ≥2 h). We used *Z*-tests to examine whether the differences between the subgroup effect estimates were significant or

2 https://eogdata.mines.edu/products/vnl/

3 https://ladsweb.modaps.eosdis.nasa.gov/

4 https://weijing-rs.github.io/product.html

5 http://nxdata.com.cn/files_nx_pub/html/tjnj/2020/indexfiles/indexch.htm

not. In addition, multiple comparisons existed for school level and outdoor exercise time. Thus, the Benjamini–Hochberg FDR method was calculated to correct for multiple comparisons.

We also performed a series of sensitivity analyses. First, we redefined four ALAN levels based on a variety of buffers (e.g., 3 km and 5 km) and annual averages (e.g., 1-year and 3-year average). Second, we excluded exposures with a duration of ≤1 year. Third, considering potential data clustering in schools, we used a generalized linear mixed model to test main results. All analyses were completed using SPSS for Windows (version 23.0) and R software (version 4.1.3). A two-tailed *p*-value of less than 0.05 was considered statistically significant.

3 Results

3.1 Descriptive statistics

Supplementary Table S1 shows the characteristics of 33,160 Chinese adolescents. The age of the students participating in the study ranged from 9 to 18 years (mean ± SD: 13.51 ± 2.55 years). Supplementary Table S1 also shows that the overall prevalence of myopia among students was 61.4% (20,325 out of 33,160). Table 1 further illustrates the variations in myopia prevalence across different groups. For example, a higher prevalence of myopia was observed among older adolescents, females, individuals from urban areas, and those of Han Chinese ethnicity, as well as among individuals with higher levels of education. Briefly, with the exception of five variables (outdoor exercise time, frequency of sugar, frequency of oil, GDP *per capita*, population density), all other variables showed differences between the two groups ($p < 0.05$).

The radiance of LAN exposure exhibited significant variation across Ningxia Province, as illustrated in Supplementary Figure S1. In general, most areas experienced lower-intensity outdoor ALAN, while higher-intensity outdoor ALAN was notably concentrated in northern cities. The distribution of outdoor ALAN among the 120 study sites (schools) displayed a leftward skew, and the median (IQR) ALAN exposure for all study sites was 12.90 (2.10, 25.04) nanoWatts/cm^2/sr, as depicted in Supplementary Figure S3.

3.2 Associations of outdoor ALAN with myopia

Significant differences in outdoor ALAN levels were observed between the non-myopia group and the myopia group ($p < 0.001$; see Figure 2). Outdoor ALAN levels were higher in the myopia group [median (IQR): 14.44 nanoWatts/cm^2/sr (3.88–26.56)] than in the non-myopia group [median (IQR): 6.95 nanoWatts/cm^2/sr (1.21–21.74)].

Table 2 presents the ORs and 95% CIs for the associations between outdoor ALAN exposure and the prevalence of myopia. In Model 1, without adjusting for any covariates, there was an 18% increase in myopia prevalence for every 10-unit change in outdoor ALAN. In Model 2, after adjusting for covariates identified through univariate analysis ($p < 0.1$), a 4% increase in myopia prevalence was observed for every 10-unit change in outdoor ALAN. Similar results were obtained using stepwise regression approaches in Model 3.

To preliminarily explore non-linear relationships, we categorized outdoor ALAN into quartiles (Q1, Q2, Q3, and Q4). As shown in Table 2, association estimates were calculated for the top three quartiles compared to the lowest outdoor ALAN quartile. In Model 1, statistically significant positive associations were observed between outdoor ALAN and myopia prevalence ($OR_{Q4\ vs.\ Q1}$: 2.08, 95% CI: 1.95–2.22). Model 2 and Model 3 found similar association estimates ($OR_{Q4\ vs.\ Q1}$: 1.21, 95% CI: 1.08–1.35; $OR_{Q4\ vs.\ Q1}$: 1.20, 95% CI: 1.08–1.34, respectively). Considering the simplicity of the model, we use Model 3 as the main model for subsequent analysis.

We further investigated the shape of the exposure-response curve in examining the relationship between outdoor ALAN exposure and myopia prevalence (Figure 3). The relationship between outdoor LAN exposure (reference concentration: 0 nanoWatts/cm^2/sr) and the prevalence of myopia exhibited a nonlinear exposure-response curve (p for nonlinear <0.001). The effect steeply increased at low outdoor ALAN levels, remained stable at medium levels, and gradually increased at high levels. Overall, the RCS analysis indicated a nonlinear positive dose-response association between long-term outdoor ALAN exposure and myopia in adolescents.

3.3 Subgroup and sensitivity analysis

Table 3 shows the associations of outdoor ALAN with myopia prevalence modified by age, sex, residence, parental myopia, school level, and outdoor exercise time. Compared to the outdoor ALAN in Q1, the outdoor ALAN in Q4 was significantly associated with increased odds of myopia in adolescents older than 10 years of age, with no myopic parents, attending junior school, and spending more time outdoors. Both males and females showed a significant increase in the prevalence of myopia when exposed to outdoor ALAN in Q4 compared to Q1. Compared to the outdoor ALAN in Q1, the outdoor ALAN in Q2 was significantly associated with increased odds of myopia in rural areas. It is worth noting that we only found statistically significant differences between urban and rural areas ($p = 0.029$).

In sensitivity analyses, the associations between outdoor ALAN and myopia prevalence remained stable (see Supplementary Tables S2, S3). First, defining four ALAN levels was based on a variety of buffers (e.g., 3 km and 5 km) and annual averages (e.g., 1-year and 3-year average). The associations varied to some extent in different definitions, but the direction remained stable. Second, excluding exposure time ≤1 year, we observed a slight decrease in the effects ($OR_{Q4\ vs.\ Q1}$: 1.16, 95% CI: 1.02–1.31). Third, considering potential data clustering in schools, we used a generalized linear mixed model and observed the increased effects. For instance, a 8% increase in myopia prevalence was observed for every 10-unit change in outdoor ALAN. Compared to the outdoor ALAN in Q1, the outdoor ALAN in Q4 was significantly associated with increased odds of myopia ($OR_{Q4\ vs.\ Q1}$: 1.40, 95% CI: 1.00–1.96).

4 Discussion

4.1 Main findings

This study is the first to identify a positive nonlinear association between long-term exposure to outdoor ALAN and myopia in

TABLE 1 Description of non-myopia (n = 12,808) and myopia (n = 20,352) groups.

Variables[a]		Non-myopia [N (%)/ mean ± SD/median (IQR)]	Myopia [N (%)/ mean ± SD/median (IQR)]	$t/Z/\chi^2$	p-value
Age (years)		12.57 ± 2.31	14.10 ± 2.51	−57.08	<0.001
Sex	Male	7,270 (44.34)	9,127 (55.66)	446.50	<0.001
	Female	5,538 (33.04)	11,225 (66.96)		
Residence[b]	Rural areas	4,546 (52.39)	4,131 (47.61)	939.53	<0.001
	Urban areas	8,262 (33.75)	16,221 (66.25)		
Nationality[c]	Han nationality	5,907 (32.74)	12,134 (67.26)	577.64	<0.001
	Other nationalities	6,901 (45.64)	8,218 (54.36)		
School level[d]	Primary	6,656 (54.14)	5,637 (45.86)	2713.18	<0.001
	Junior	4,500 (37.24)	7,585 (62.76)		
	Senior	1,652 (18.81)	7,130 (81.19)		
Exposure time[e]	1 year	2,490 (35.80)	4,466 (64.20)	469.96	<0.001
	2 years	1,999 (28.85)	4,930 (71.15)		
	≥3 years	8,319 (43.16)	10,956 (56.84)		
Body mass index (kg/m^2)[f]		19.99 ± 3.70	19.74 ± 3.64	5.85	<0.001
Parental myopia[g]	No	10,349 (43.15)	13,635 (56.85)	748.54	<0.001
	Yes	2,459 (26.80)	6,717 (73.20)		
Nighttime sleep (h)		8.51 ± 1.37	7.85 ± 1.47	41.29	<0.001
Outdoor exercise time per day	<1 h	2,610 (38.02)	4,255 (61.98)	4.71	0.095
	1–2 h	5,007 (38.23)	8,090 (61.77)		
	≥2 h	5,191 (39.33)	8,007 (60.67)		
Frequency of sugar per week	Never or sometimes	12,117 (38.63)	19,253 (61.37)	0.00	0.985
	Everyday	691 (38.60)	1,099 (61.40)		
Frequency of oil per week	Never or sometimes	12,317 (38.56)	19,627 (61.44)	1.64	0.201
	Everyday	491 (40.38)	725 (59.62)		
Frequency of fruit per week	Never or sometimes	4,214 (37.46)	7,036 (62.54)	9.78	0.002
	Everyday	8,594 (39.22)	13,316 (60.78)		
Frequency of vegetable per week	Never or sometimes	1,960 (42.57)	2,644 (57.43)	35.13	<0.001
	Everyday	10,848 (37.99)	17,708 (62.01)		
Computers and TVs spend time per day	<1 h	6,247 (40.36)	9,232 (59.64)	62.75	<0.001
	1–2 h	3,826 (38.77)	6,043 (61.23)		
	≥2 h	2,735 (35.01)	5,077 (64.99)		
After-school homework time per day	<1 h	6,234 (49.56)	6,345 (50.44)	1226.58	<0.001
	1–2 h	4,347 (36.02)	7,722 (63.98)		
	≥2 h	2,227 (26.16)	6,285 (73.84)		
After-school tutoring time per day	<1 h	10,608 (39.19)	16,457 (60.81)	54.91	<0.001
	1–2 h	1,372 (39.27)	2,122 (60.73)		
	≥2 h	828 (31.83)	1,773 (68.17)		
Eye exercises per day	No	418 (33.07)	846 (66.93)	29.56	<0.001
	1–2 times	11,164 (38.54)	17,804 (61.46)		
	>2 times	1,226 (41.87)	1,702 (58.13)		
Annual frequency of visual inspections	No	1,652 (43.23)	2,169 (56.77)	153.70	<0.001
	1–2 times	8,293 (36.39)	14,496 (63.61)		
	>2 times	2,863 (43.71)	3,687 (56.29)		

(Continued)

TABLE 1 (Continued)

Variables[a]		Non-myopia [*N* (%)/ mean ± SD/median (IQR)]	Myopia [*N* (%)/ mean ± SD/median (IQR)]	$t/Z/\chi^2$	*p*-value
GDP *per capita* (Yuan)		43,675 (32,145, 54,575)	43,675 (31,649, 65,407)	−1.49	0.135
Population density (population/km^2)		100.85 (68.73, 195.30)	113.80 (67.49, 212.61)	−0.89	0.371
Health technical personnel (per 1,000 population)		6.64 (5.20, 8.19)	6.64 (5.23, 8.19)	−4.24	<0.001
NDVI		0.46 ± 0.12	0.45 ± 0.12	8.34	<0.001
$PM_{2.5}$ (μg/m^3)		32.82 ± 3.82	32.49 ± 4.05	7.35	<0.001
Outdoor ALAN (nanoWatts/cm^2/sr)		6.95 (1.21, 21.74)	14.44 (3.88, 26.56)	−23.70	<0.001

SD, standard deviation; IQR, interquartile range; GDP, gross domestic product; NDVI, normalized difference vegetation index; $PM_{2.5}$, particulate matter ≤2.5 mm; ALAN, artificial light at night. Data on demographic and behavioral/lifestyle factors were collected using a structured questionnaire. Data on regional macro-indicators were obtained from Ningxia Statistical Yearbook of 2020.

[a]Data were complete and there was no missing data.

[b]Defined by whether the school was in a rural or urban area.

[c]Other nationalities were mainly Hui nationality (n = 14,884, 98.4%).

[d]School level included primary (grades 4 through 6), junior (grades 7 through 9), and senior (grades 10 through 12).

[e]Exposure time to the school environment: grade 4 to 6, indicating >3 year of exposure time; grade 7 and grade 10, indicating 1 year of exposure time; grade 8 and grade 11, indicating 2 year of exposure time; grade 9 and grade 12, indicating 3 year of exposure time, respectively.

[f]BMI was calculated by dividing the weight (kg) of each participant by the square of height (m).

[g]Defined as one or both parents suffering from myopia.

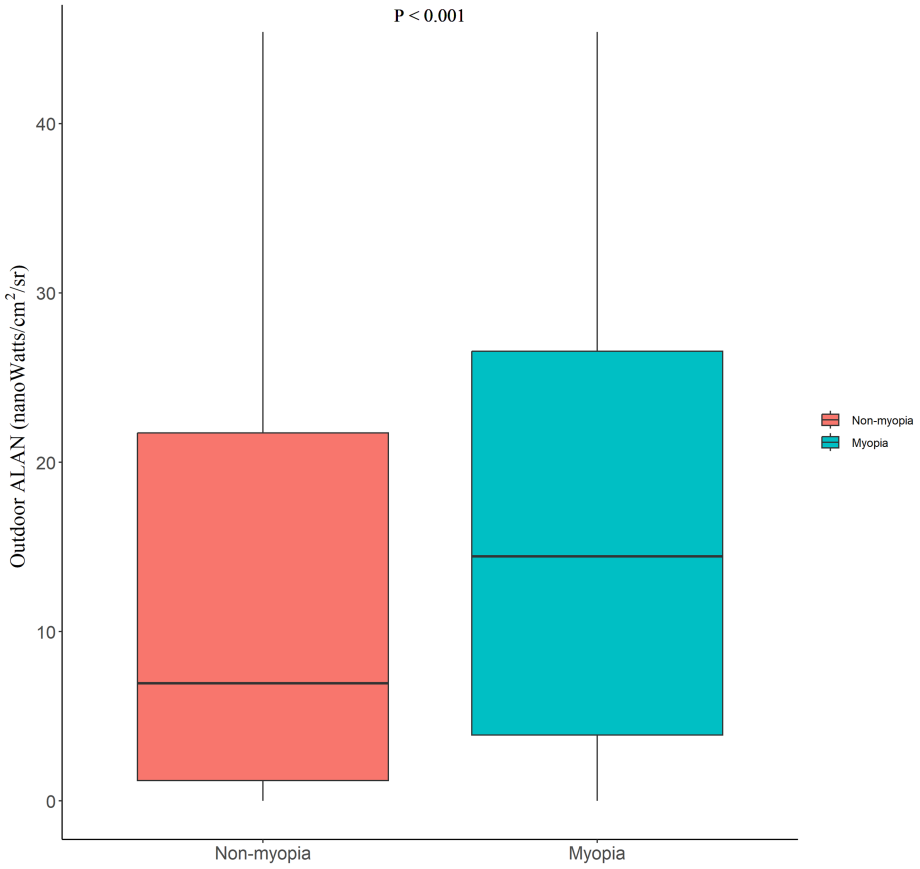

FIGURE 2
Differences in the outdoor ALAN between the non-myopia and myopia groups. "$p < 0.001$" represented a significant difference in the median by the Mann–Whitney *U*-test. ALAN, artificial light at night.

TABLE 2 Associations of outdoor ALAN with myopia in different models.

Models	OR (95% CI)	*p*-value
Model 1		
Continuous variable (per 10 units)	**1.18 (1.16, 1.20)**	**<0.001**
Quartile variable		
Q1	Reference	
Q2	**1.62 (1.52, 1.72)**	**<0.001**
Q3	**1.97 (1.85, 2.09)**	**<0.001**
Q4	**2.08 (1.95, 2.22)**	**<0.001**
Model 2		
Continuous variable (per 10 units)	**1.04 (1.01, 1.07)**	**0.002**
Quartile variable		
Q1	Reference	
Q2	1.07 (0.98, 1.18)	0.147
Q3	1.06 (0.95, 1.18)	0.309
Q4	**1.21 (1.08, 1.35)**	**0.001**
Model 3		
Continuous variable (per 10 units)	**1.04 (1.02, 1.07)**	**0.001**
Quartile variable		
Q1	Reference	
Q2	1.06 (0.97, 1.16)	0.190
Q3	1.04 (0.94, 1.16)	0.409
Q4	**1.20 (1.08, 1.34)**	**0.001**

ALAN, artificial light at night; OR, odds ratio; 95% CI, 95% confidence interval. Model 1: crude model. Model 2 (based on univariate analysis: $p < 0.1$): adjusted for age, sex, residence, nationality, school level, exposure time, body mass index, parental myopia, nighttime sleep, outdoor exercise time, fruit, vegetable, computers and TVs spend time, after-school homework time, after-school tutoring time, eye exercises, annual frequency of visual inspections, health technical personnel, NDVI, and $PM_{2.5}$. Model 3 (based on stepwise selection approaches): adjusted for age, sex, residence, nationality, school level, exposure time, body mass index, parental myopia, fruit, vegetable, after-school homework time, eye exercises, annual frequency of visual inspections, and $PM_{2.5}$. Statistical significance was indicated by bold font.

adolescents. Although a stronger correlation was not found in a specific population (e.g., sex), the findings still offer important insights. Given the rising rates of ALAN and myopia in contemporary society, the study offers crucial first-hand evidence of ALAN's potential impact on eye health.

4.2 Comparison with previous work and possible explanations

Holden et al. (4) reported a global myopia prevalence of 22.9% (1.406 billion people) in 2000, projecting a significant increase to 49.8% (4.758 billion) by 2050 (4). A comprehensive review underscored a non-coincidental correlation between the widespread adoption of LEDs and the escalating prevalence of myopia (14). While daytime LEDs used for general lighting may impact visual performance and eye strain, ALAN, characterized by exposure to artificial light during nighttime hours, may have distinct and potentially more significant effects on myopia development (14, 25). Research on the association of ALAN with myopia is very limited, as only a few epidemiologic studies conducted abroad have shown inconsistent results (30–33). Quinn et al. (33) identified a strong link between childhood myopia development and exposure to nighttime lighting during the first 2 years of life. However, a follow-up study by Gwiazda et al. (32) found no significant relationship between nighttime lighting exposure—whether in the first 2 years or later—and the prevalence of myopia. Similarly, Czepita et al. (30) observed a high incidence of astigmatism associated with fluorescent lighting. In a subsequent study, Czepita et al. (31) found no association between myopia and nighttime light use in Polish children without a family history of myopia. These inconsistent results may partly be attributed to the accuracy of exposure measurements, statistical methods, and the limitation on specific populations.

Our study extends previous work in three ways. First, unlike previous studies that used questionnaires to assess artificial light (30–33), we used relatively high-precision data of outdoor ALAN (38). By focusing on outdoor ALAN, our study introduces a new perspective on environmental influences on myopia, offering insights beyond the commonly studied indoor lighting. Second, we used a variety of methods, including logistic regression and RCS methods, to mutually validate the results. These methods demonstrated a positive nonlinear dose–response relationship between ALAN and myopia, providing a more comprehensive understanding of the association. Third, to our knowledge, this is the first and largest study examining the link between ALAN and myopia in adolescent. These three extensions further add support for a positive association between ALAN and myopia.

The exact mechanisms between ALAN and myopia are not clear. One possible mechanism is that long-term exposure to ALAN may lead to severe disruption of circadian rhythms, thereby altering the circadian rhythm of the retina. Several systematic reviews have detailed this mechanism, including Lei et al. (27), Regmi et al. (42), and Nickla (25). In addition, several other systematic reviews have noted that retinal circadian rhythm disturbances may specifically affect the onset and progression of myopia, such as Chakraborty et al. (20), Stone et al. (21), and Zhang et al. (14). Another possible mechanism is that ALAN inhibits melatonin production and deprives sleep, both of which are also important factors in the development of myopia, as supported by Chakraborty et al. (19) and Touitou et al. (22). These mechanisms form, in part, the biological basis for the link between ALAN and myopia.

4.3 Public health and clinical implications

Our study found that long-term exposure to outdoor ALAN may be positively associated with myopia. This association provides important insights for clinical practice and public health. Ophthalmologists can advise adolescents to take a series of measures, such as avoiding overexposure to strong light sources at night, which are expected to reduce the incidence of myopia. Eye care professionals can advise adolescents to avoid or minimize exposure to ALAN, which may help reduce the incidence of myopia. For high-risk groups in light-polluted environments, especially students, regular eye health checkups are especially important, and early detection and

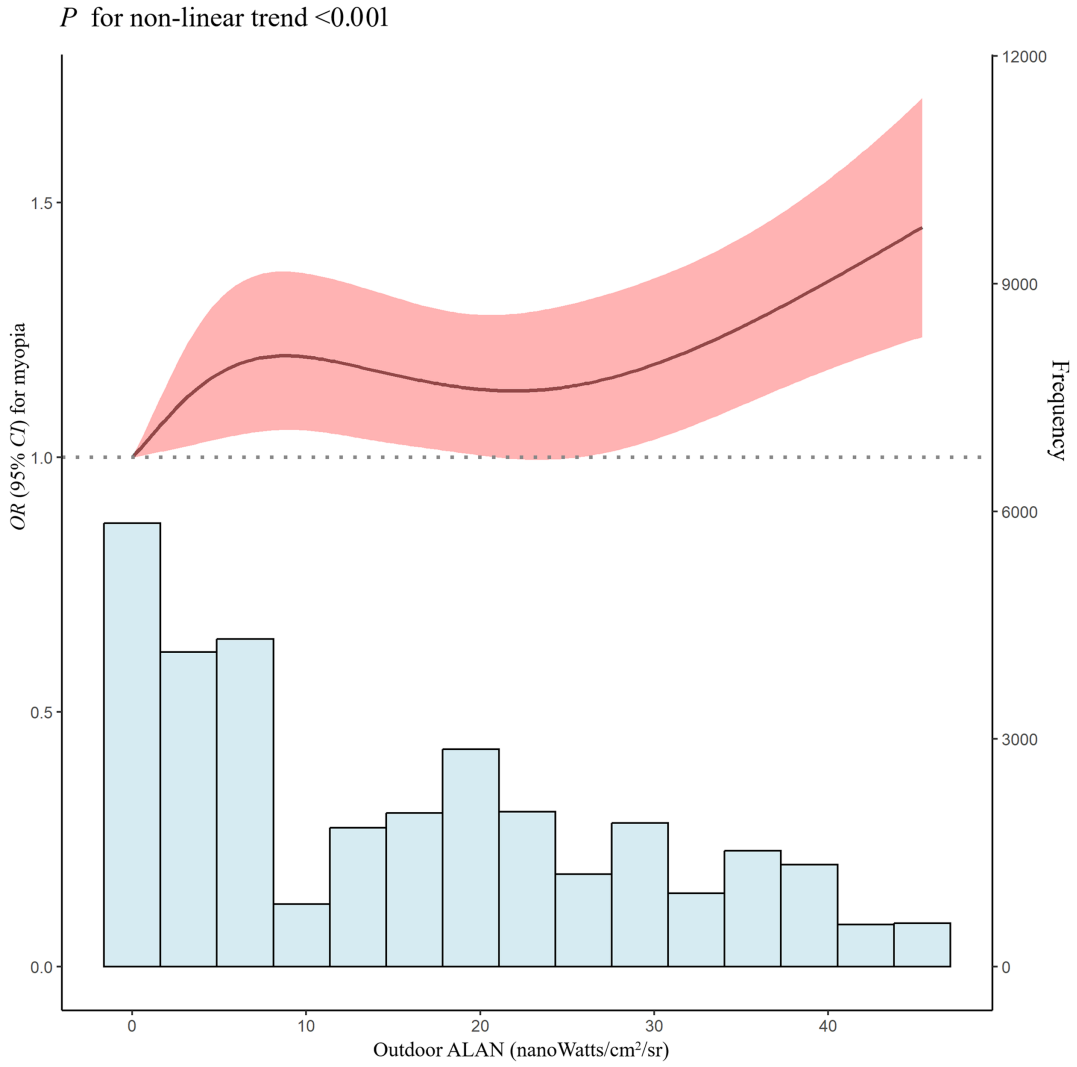

FIGURE 3
Nonlinear association of outdoor ALAN exposure with OR for myopia. ALAN, artificial light at night; OR, odds ratio; 95% CI, 95% confidence interval. Adjusted for age, sex, residence, nationality, school level, exposure time, body mass index, parental myopia, fruit, vegetable, after-school homework time, eye exercises, annual frequency of visual inspections, and $PM_{2.5}$.

intervention will improve the effectiveness of myopia prevention and control.

In addition, understanding the association between outdoor light pollution and myopia provides an important knowledge base for the public. Although no specific sensitive groups were identified, the effect did diminish after adjusting for other known risk factors such as lifestyle factors. This suggests that individuals may be able to take steps to mitigate the effects of ALAN. Educational institutions and health departments can work together to conduct publicity campaigns to raise public awareness of outdoor light pollution in order to reduce its harmful effects on eye health. It is crucial to incorporate light pollution prevention and control measures in urban planning, such as rationalizing lighting facilities and reducing glare exposure, to improve the urban environment and reduce eye health risks. Taken together, this study provides substantial guidance for the development of more effective eye health strategies that not only contribute to the eye health of individuals, but also have a positive impact at the public health level.

5 Strengths and limitations

Our study has several strengths. First, this is the first and largest research to explore the association between outdoor ALAN and adolescent myopia, using a representative sample. This makes our results more generalizable to adolescents in other parts of China, especially to populations in cities in northwestern China. Second, the study incorporated covariates of multiple dimensions (such as demographic characteristics, behavioral/lifestyle factors, and regional macro-indicators) to make the results closer to the real situation by adjusting for confounders as much as possible. Third, we conducted multiple sensitivity analyses and subgroup analyses to emphasize the robustness of our results.

Nevertheless, there are also several limitations. First, cross-sectional studies have inherent limitations and fail to provide evidence of a causal relationship between ALAN and myopia. Further cohort and experimental studies (including clinical trials and animal studies)

TABLE 3 Associations of outdoor ALAN with myopia by subgroups.

Quartile variable	Age			Quartile variable	School level[a]		
	≤10 years	>10 years	$p_{interaction}$		Primary	Junior	$p_{interaction}$
Q1	Reference	Reference		Q1	Reference	Reference	
Q2	1.06 (0.76, 1.47)	1.08 (0.98, 1.19)	0.907	Q2	1.08 (0.88, 1.32)	1.12 (0.99, 1.26)	0.918
Q3	1.38 (0.95, 2.02)	1.01 (0.90, 1.12)	0.273	Q3	1.21 (0.96, 1.52)	1.02 (0.89, 1.18)	0.690
Q4	1.37 (0.93, 2.00)	1.20 (1.07, 1.35)	0.529	Q4	1.14 (0.90, 1.44)	1.40 (1.20, 1.64)	0.801

Quartile variable	Sex			Quartile variable	School level[a]		
	Male	Female	$p_{interaction}$		Primary	Senior	$p_{interaction}$
Q1	Reference	Reference		Q1	Reference	Reference	
Q2	1.03 (0.91, 1.16)	1.10 (0.96, 1.26)	0.451	Q2	1.08 (0.88, 1.32)	0.89 (0.63, 1.26)	0.694
Q3	1.03 (0.90, 1.18)	1.06 (0.91, 1.23)	0.799	Q3	1.21 (0.96, 1.52)	0.81 (0.58, 1.13)	0.336
Q4	1.23 (1.07, 1.42)	1.18 (1.01, 1.38)	0.700	Q4	1.14 (0.90, 1.44)	1.12 (0.79, 1.58)	0.934

Quartile variable	Residence			Quartile variable	Outdoor exercise time per day[a]		
	Rural areas	Urban areas	$p_{interaction}$		<1 h	1–2 h	$p_{interaction}$
Q1	Reference	Reference		Q1	Reference	Reference	
Q2	1.13 (1.00, 1.30)	0.91 (0.79, 1.06)	**0.029**	Q2	0.92 (0.75, 1.15)	1.11 (0.97, 1.28)	0.557
Q3	1.04 (0.81, 1.35)	0.91 (0.78, 1.05)	0.945	Q3	0.86 (0.68, 1.10)	1.16 (0.99, 1.36)	0.282
Q4	—	1.05 (0.91, 1.22)	—	Q4	1.08 (0.84, 1.39)	1.28 (1.08, 1.51)	0.426

Quartile variable	Parental myopia			Quartile variable	Outdoor exercise time per day[a]		
	No	Yes	$p_{interaction}$		<1 h	≥2 h	$p_{interaction}$
Q1	Reference	Reference		Q1	Reference	Reference	
Q2	1.11 (1.00, 1.23)	0.90 (0.74, 1.10)	0.065	Q2	0.92 (0.75, 1.15)	1.07 (0.92, 1.23)	0.426
Q3	1.04 (0.92, 1.16)	1.01 (0.81, 1.26)	0.824	Q3	0.86 (0.68, 1.10)	1.02 (0.87, 1.19)	0.426
Q4	1.26 (1.12, 1.42)	1.03 (0.82, 1.29)	0.483	Q4	1.08 (0.84, 1.39)	1.20 (1.01, 1.41)	0.557

ALAN, artificial light at night; —, not analysis. Adjusted for age, sex, residence, nationality, school level, exposure time, body mass index, parental myopia, fruit, vegetable, after-school homework time, eye exercises, annual frequency of visual inspections, and $PM_{2.5}$. Statistical significance between groups was indicated by bold font.
[a]The Benjamini–Hochberg FDR method was calculated to correct for multiple comparisons.

are needed to elucidate these findings and to further our understanding of the mechanisms by which ALAN causes myopia in adolescents. Second, the outdoor ALAN data include only daily, monthly and annual data, not hourly data (see text footnote 2). Therefore, we were unable to assess the effects of ALAN exposure during the last few hours of the day on myopia. Future studies should develop and use hourly ALAN data to further validate and extend the current findings. Third, this study was only able to use ALAN data obtained from satellite remote sensing to represent ALAN exposure at participants' schools. Individual participant addresses were not obtained, which may have led to measurement bias. Given that most schools in China use the principle of proximity to school, the ALAN values near schools reflect to some extent the level of residential exposure. It is undeniable that this measurement bias may underestimate the true effect of ALAN exposure. In future studies, we will collect individual addresses to better match exposure levels and reduce the likelihood of misclassification. Fourth, indoor ALAN exposure could not be measured. Indoor ALAN exposure might significantly impact myopia and potentially confound the results related to outdoor ALAN exposure (43). Thus, we measured alternative indicators (such as after-school homework time and after-school tutoring time) and adjusted for these variables to mitigate the potential impact of indoor ALAN exposure on the study results. Future studies should include both indoor and outdoor ALAN exposure to provide a more comprehensive understanding of how different types of light exposure affect myopia. Fifth, considering that urbanization may be an important confounder (3), we initially included three regional macro-indicators (GDP *per capita*, population density, and health technical personnel) and residence for potential adjustment in our analysis. Although some factors may not be included in the final model, they were carefully considered during the analysis. Finally, unmeasured variables may cause residual confounding (44), such as outdoor time during daylight. However, our model was adjusted for a range of important/alternative covariates (e.g., outdoor exercise time) that were closely associated with the outcomes. Therefore, we believe that the effects of unmeasured residual confounding on the results are likely to be limited and are unlikely to change the direction of the main results.

6 Conclusion

In conclusion, our study reveals a positive nonlinear relationship between long-term outdoor ALAN exposure and adolescent myopia. No stronger correlations were found in specific populations. These findings deepen our understanding of environmental influences on myopia. Further cohort studies are essential to clarify the association between outdoor ALAN and myopia, as well as to understand the underlying mechanisms that contribute to adolescent myopia.

Data availability statement

The data analyzed in this study is subject to the following licenses/restrictions: the complete data used throughout the study are available from the corresponding author upon reasonable request. Requests to access these datasets should be directed to ZL, lzh_2580@sina.com.

Ethics statement

The studies involving humans were approved by the Ethics Committee of the People's Hospital of Ningxia Hui Autonomous Region ([2022]-NZR-093). The studies were conducted in accordance with the local legislation and institutional requirements. The participants provided their written informed consent to participate in this study.

Author contributions

TL: Formal analysis, Validation, Writing – original draft. WT: Formal analysis, Validation, Writing – original draft. YF: Formal analysis, Validation, Writing – original draft. BC: Formal analysis, Validation, Writing – original draft. HT: Data curation, Methodology, Writing – original draft. CL: Data curation, Methodology, Writing – original draft. ZW: Data curation, Methodology, Writing – original draft. YZ: Data curation, Methodology, Writing – original draft. SG: Data curation, Investigation, Validation, Writing – review & editing. ZL: Data curation, Investigation, Validation, Writing – review & editing.

Funding

The author(s) declare that financial support was received for the research, authorship, and/or publication of this article. This study was funded by the Natural Science Foundation of Ningxia (Grant No. 2023AAC03459), and Health Commission of Ningxia Research Project (Grant No. 2023-NWKYP-006).

Acknowledgments

The authors are grateful to the staff of Ningxia Medical University and Ningxia Center for Disease Control and Prevention for supporting this study.

Conflict of interest

The authors declare that the research was conducted in the absence of any commercial or financial relationships that could be construed as a potential conflict of interest.

Publisher's note

Supplementary material

The Supplementary material for this article can be found online at: https://www.frontiersin.org/articles/10.3389/fmed.2024.1469422/full#supplementary-material

References

1. Chi K, Li B, Huang H, Sun J, Zheng Y, Zhao L. Exploring the research landscape of high myopia: trends, contributors, and key areas of focus. *Med Sci Monit*. (2023) 29:e941670. doi: 10.12659/MSM.941670

2. Li H, Liu S, Zhang K, Zhu X, Dai J, Lu Y. Gut microbiome and plasma metabolome alterations in myopic mice. *Front Microbiol*. (2023) 14:1251243. doi: 10.3389/fmicb.2023.1251243

3. Zhang C, Wang C, Guo X, Xu H, Qin Z, Tao L. Effects of greenness on myopia risk and school-level myopia prevalence among high school-aged adolescents: cross-sectional study. *JMIR Public Health Surveill*. (2023) 9:e42694. doi: 10.2196/42694

4. Holden BA, Fricke TR, Wilson DA, Jong M, Naidoo KS, Sankaridurg P, et al. Global prevalence of myopia and high myopia and temporal trends from 2000 through 2050. *Ophthalmology*. (2016) 123:1036–42. doi: 10.1016/j.ophtha.2016.01.006

5. Li T, Yang J, Yan J, Yao X, Du B, Wu Q, et al. Interaction between parental myopia and children lifestyle on the incidence of myopia among children aged 6–18 years: a cross-sectional study in Tianjin, China. *BMJ Open*. (2024) 14:e080929. doi: 10.1136/bmjopen-2023-080929

6. Morgan IG, French AN, Ashby RS, Guo X, Ding X, He M, et al. The epidemics of myopia: aetiology and prevention. *Prog Retin Eye Res*. (2018) 62:134–49. doi: 10.1016/j.preteyeres.2017.09.004

7. Kaiti R, Shyangbo R, Sharma IP, Dahal M. Review on current concepts of myopia and its control strategies. *Int J Ophthalmol*. (2021) 14:606–15. doi: 10.18240/ijo.2021.04.19

8. Naidoo KS, Fricke TR, Frick KD, Jong M, Naduvilath TJ, Resnikoff S, et al. Potential lost productivity resulting from the global burden of myopia: systematic review, meta-analysis, and modeling. *Ophthalmology*. (2019) 126:338–46. doi: 10.1016/j.ophtha.2018.10.029

9. Zhang C, Zhao J, Zhu Z, Li Y, Li K, Wang Y, et al. Applications of artificial intelligence in myopia: current and future directions. *Front Med*. (2022) 9:840498. doi: 10.3389/fmed.2022.840498

10. Baird PN, Saw SM, Lanca C, Guggenheim JA, Smith Iii EL, Zhou X, et al. Myopia. *Nat Rev Dis Primers*. (2020) 6:99. doi: 10.1038/s41572-020-00231-4

11. Lee SS, Lingham G, Wang CA, Diaz Torres S, Pennell CE, Hysi PG, et al. Changes in refractive error during young adulthood: the effects of longitudinal screen time, ocular sun exposure, and genetic predisposition. *Invest Ophthalmol Vis Sci*. (2023) 64:28. doi: 10.1167/iovs.64.14.28

12. Martinez-Albert N, Bueno-Gimeno I, Gene-Sampedro A. Risk factors for myopia: a review. *J Clin Med*. (2023) 12:12. doi: 10.3390/jcm12186062

13. Brown DM, Mazade R, Clarkson-Townsend D, Hogan K, Datta Roy PM, Pardue MT. Candidate pathways for retina to scleral signaling in refractive eye growth. *Exp Eye Res*. (2022) 219:109071. doi: 10.1016/j.exer.2022.109071

14. Zhang C, Zhu Z, Zhao J, Li Y, Zhang Z, Zheng Y. Ubiquitous light-emitting diodes: potential threats to retinal circadian rhythms and refractive development. *Sci Total Environ*. (2023) 862:160809. doi: 10.1016/j.scitotenv.2022.160809

15. Flitcroft DI, Harb EN, Wildsoet CF. The spatial frequency content of urban and indoor environments as a potential risk factor for myopia development. *Invest Ophthalmol Vis Sci*. (2020) 61:42. doi: 10.1167/iovs.61.11.42

16. Tancredi S, Urbano T, Vinceti M, Filippini T. Artificial light at night and risk of mental disorders: a systematic review. *Sci Total Environ*. (2022) 833:155185. doi: 10.1016/j.scitotenv.2022.155185

17. Zielinska-Dabkowska KM, Schernhammer ES, Hanifin JP, Brainard GC. Reducing nighttime light exposure in the urban environment to benefit human health and society. *Science*. (2023) 380:1130–5. doi: 10.1126/science.adg5277

18. Yi W, Wang W, Xu Z, Liu L, Wei N, Pan R, et al. Association of outdoor artificial light at night with metabolic syndrome and the modifying effect of tree and grass cover. *Ecotoxicol Environ Saf*. (2023) 264:115452. doi: 10.1016/j.ecoenv.2023.115452

19. Chakraborty R, Micic G, Thorley L, Nissen TR, Lovato N, Collins MJ, et al. Myopia, or near-sightedness, is associated with delayed melatonin circadian timing and lower melatonin output in young adult humans. *Sleep*. (2021) 44:44. doi: 10.1093/sleep/zsaa208

20. Chakraborty R, Ostrin LA, Nickla DL, Iuvone PM, Pardue MT, Stone RA. Circadian rhythms, refractive development, and myopia. *Ophthalmic Physiol Opt*. (2018) 38:217–45. doi: 10.1111/opo.12453

21. Stone RA, McGlinn AM, Chakraborty R, Lee DC, Yang V, Elmasri A, et al. Altered ocular parameters from circadian clock gene disruptions. *PLoS One*. (2019) 14:e0217111. doi: 10.1371/journal.pone.0217111

22. Touitou Y, Reinberg A, Touitou D. Association between light at night, melatonin secretion, sleep deprivation, and the internal clock: health impacts and mechanisms of circadian disruption. *Life Sci*. (2017) 173:94–106. doi: 10.1016/j.lfs.2017.02.008

23. Nickla DL, Totonelly K. Brief light exposure at night disrupts the circadian rhythms in eye growth and choroidal thickness in chicks. *Exp Eye Res*. (2016) 146:189–95. doi: 10.1016/j.exer.2016.03.003

24. Touitou Y, Point S. Effects and mechanisms of action of light-emitting diodes on the human retina and internal clock. *Environ Res*. (2020) 190:109942. doi: 10.1016/j.envres.2020.109942

25. Nickla DL. Ocular diurnal rhythms and eye growth regulation: where we are 50 years after Lauber. *Exp Eye Res*. (2013) 114:25–34. doi: 10.1016/j.exer.2012.12.013

26. Koo YS, Song JY, Joo EY, Lee HJ, Lee E, Lee SK, et al. Outdoor artificial light at night, obesity, and sleep health: cross-sectional analysis in the KoGES study. *Chronobiol Int*. (2016) 33:301–14. doi: 10.3109/07420528.2016.1143480

27. Lei T, Hua H, Du H, Xia J, Xu D, Liu W, et al. Molecular mechanisms of artificial light at night affecting circadian rhythm disturbance. *Arch Toxicol*. (2024) 98:395–408. doi: 10.1007/s00204-023-03647-5

28. Shen M, Li Y, Li S, Chen X, Zou B, Lu Y. Association of exposure to artificial light at night during adolescence with blood pressure in early adulthood. *Chronobiol Int*. (2023) 40:1419–26. doi: 10.1080/07420528.2023.2266485

29. Sirhan-Atalla M, Gabinet NM, Portnov BA. Disaggregating the effects of daytime and nighttime light exposures on obesity, overweight, prostate and breast cancer morbidity worldwide. *Chronobiol Int*. (2023) 40:483–514. doi: 10.1080/07420528.2023.2187230

30. Czepita D, Gosławski W, Mojsa A. Occurrence of refractive errors among students who before the age of two grew up under the influence of light emitted by incandescent or fluorescent lamps. *Ann Acad Med Stetin*. (2005) 51:33–6.

31. Czepita D, Mojsa A, Czepita M, Lachowicz E. Myopia and night lighting. Investigations on children with negative family history. *Klin Ocz*. (2012) 114:22–5.

32. Gwiazda J, Ong E, Held R, Thorn F. Myopia and ambient night-time lighting. *Nature*. (2000) 404:144. doi: 10.1038/35004663

33. Quinn GE, Shin CH, Maguire MG, Stone RA. Myopia and ambient lighting at night. *Nature*. (1999) 399:113–4. doi: 10.1038/20094

34. Li SM, Wei S, Atchison DA, Kang MT, Liu L, Li H, et al. Annual incidences and progressions of myopia and high myopia in Chinese schoolchildren based on a 5-year cohort study. *Invest Ophthalmol Vis Sci*. (2022) 63:8. doi: 10.1167/iovs.63.1.8

35. Zhou Y, Zhang XF, Chen XJ, Wang M, Cai JR, Xiong YJ, et al. Prevalence of anisometropia and influencing factors among school-age children in Nantong, China: a cross-sectional study. *Front Public Health*. (2023) 11:1190285. doi: 10.3389/fpubh.2023.1190285

36. He M, Xiang F, Zeng Y, Mai J, Chen Q, Zhang J, et al. Effect of time spent outdoors at school on the development of myopia among children in China: a randomized clinical trial. *JAMA*. (2015) 314:1142–8. doi: 10.1001/jama.2015.10803

37. Xu Y, Cui L, Kong M, Li Q, Feng X, Feng K, et al. Repeated low-level red light therapy for myopia control in high myopia children and adolescents: a randomized clinical trial. *Ophthalmology*. (2024). doi: 10.1016/j.ophtha.2024.05.023 [Epub ahead of print].

38. Elvidge CD, Zhizhin M, Ghosh T, Hsu F-C, Taneja J. Annual time series of global VIIRS nighttime lights derived from monthly averages: 2012 to 2019. *Remote Sens*. (2021) 13:922. doi: 10.3390/rs13050922

39. Wang Y, Liu Q, Tian Z, Cheng B, Guo X, Wang H, et al. Short-term effects of ambient PM_1, $PM_{2.5}$, and PM_{10} on internal metal/metalloid profiles in older adults: a distributed lag analysis in China. *Environ Int*. (2023) 182:108341. doi: 10.1016/j.envint.2023.108341

40. Morgan IG, Wu PC, Ostrin LA, Tideman JWL, Yam JC, Lan W, et al. IMI risk factors for myopia. *Invest Ophthalmol Vis Sci*. (2021) 62:3. doi: 10.1167/iovs.62.5.3

41. Yin C, Gan Q, Xu P, Yang T, Xu J, Cao W, et al. Dietary patterns and associations with myopia in Chinese children. *Nutrients*. (2023) 15:1946. doi: 10.3390/nu15081946

42. Regmi P, Young M, Minigo G, Milic N, Gyawali P. Photoperiod and metabolic health: evidence, mechanism, and implications. *Metabolism*. (2023) 152:155770. doi: 10.1016/j.metabol.2023.155770

43. Bhandary SK, Dhakal R, Sanghavi V, Verkicharla PK. Ambient light level varies with different locations and environmental conditions: potential to impact myopia. *PLoS One*. (2021) 16:e0254027. doi: 10.1371/journal.pone.0254027

44. Cheng BJ, Wang J, Meng XL, Sun L, Hu B, Li HB, et al. The association between essential trace element mixture and cognitive function in Chinese community-dwelling older adults. *Ecotoxicol Environ Saf*. (2022) 231:113182. doi: 10.1016/j.ecoenv.2022.113182

frontiers | Frontiers in Medicine

TYPE Original Research
PUBLISHED 22 October 2024
DOI 10.3389/fmed.2024.1462024

OPEN ACCESS

EDITED BY
Pablo De Gracia,
University of Detroit Mercy, United States

REVIEWED BY
James Germann,
University of Rochester, United States
Xinyu Liu,
Singapore Eye Research Institute (SERI), Singapore

*CORRESPONDENCE
Juan M. Bueno
bueno@um.es

RECEIVED 09 July 2024
ACCEPTED 24 September 2024
PUBLISHED 22 October 2024

CITATION
Bueno JM, Martínez-Ojeda RM, Fernández EJ and Feldkaemper M (2024) Quantitative structural organization of the sclera in chicks after deprivation myopia measured with second harmonic generation microscopy.
Front. Med. 11:1462024.
doi: 10.3389/fmed.2024.1462024

Quantitative structural organization of the sclera in chicks after deprivation myopia measured with second harmonic generation microscopy

Juan M. Bueno[1]*, Rosa M. Martínez-Ojeda[1], Enrique J. Fernández[1] and Marita Feldkaemper[2]

[1]Laboratorio de Óptica, Instituto Universitario de Investigación en Óptica y Nanofísica, Universidad de Murcia, Murcia, Spain, [2]Section of Neurobiology of the Eye, Institute for Ophthalmic Research, Tuebingen, Germany

Visual deprivation causes enhanced eye growth and the development of myopia, which is associated with a change in the arrangement of collagen fibers within the sclera. A second harmonic generation (SHG) microscope has been used to image the collagen fibers of unstained scleral punches from the posterior part of chicken eyes. We aimed to analyze the fibrous scleral tissue and quantify the changes in collagen organization in relation to the extent of induced deprivation myopia. The scleral architecture was assessed with the Radon transform (RT) through the parameter called structural dispersion (SD) that provides an objective tool to quantify the level of organization of the collagen network. We found that final refraction and axial length changes were linearly correlated. However, no significant differences in scleral thickness were found for different amounts of induced myopia. In contrast, a significant correlation between SD and refraction was demonstrated, ranging from a non-organized (in the control sclerae) to a quasi-aligned distribution (with a dominant direction of the fibers, in the sclera of myopic chicks). These findings demonstrate a remodeling process of the scleral collagen associated with myopia progression that can be measured accurately combining SHG imaging microscopy and RT algorithms.

KEYWORDS

myopia, deprivation, sclera, collagen, second harmonic microscopy

1 Introduction

The sclera is the white outer shell of the eye, a tough connective tissue with a complex organization of collagen fibers. It contains approximately 50% collagen by weight (about 90% type I) (1). This dense collagenous structure provides protection against external injury. Different microscopy techniques have been used to investigate the structure of the sclera and to measure the preferred orientations of the collagen lamellae. These include bright-field, scanning electron and atomic force microscopy, among others (2–5).

Myopia is an ocular condition resulting from a mismatch between the eye's optical power and its axial length. The size and shape of the myopic eye are partly determined by the resistance of the sclera (6). Early studies of the human myopic eye detected thinner collagen fiber bundles and reduced scleral thickness at the posterior pole of the eye as compared with

the emmetropic eye (6, 7). A study in monkeys' eyes with experimentally induced myopia found that smaller fiber diameters are associated with a marked scleral thinning (8). Scleral thinning was also shown to occur during the development of axial myopia in a shrew model (9). Extensive details on the role of the sclera in the development of myopia can be seen in the work by McBrien and Gentle (10).

Chickens have been widely used as an animal model in myopia studies (11–13). The induction of visual deprivation using monocular diffusers or defocus with negative lenses has been reported to cause ocular elongation and subsequent myopia (11), which is associated with scleral growth (14) and increased creep rate of posterior and equatorial sclera (15). The chick's sclera is composed of two layers: an outer fibrous layer (similar to that of the mammals), mainly composed of collagen type I and an inner cartilaginous layer, which contains collagen types II and IV, and aggrecan as the predominant cartilage proteoglycan (16, 17).

Second harmonic generation (SHG) microscopy is a non-lineal imaging modality especially suitable for visualizing collagen-based samples without the need of chemical markers, fixation procedures or histological preparation (18–20). Due to the rich collagen content of the sclera, this ocular component has been widely studied using this technique (21–26). Several experiments have used *ex-vivo* non-stained samples from both porcine (21, 22, 25) and human eyes (23, 24, 26). More recently, SHG images of the sclera in living human eyes have also been successfully obtained (27). However, to the best of our knowledge experiments combining SHG imaging and chicken scleras have not been previously reported.

It has been shown that the spatial arrangement of collagen in the sclera is altered by various conditions such as glaucoma (28), aging (29), or myopia (9, 10) to name a few. However, some previous studies on scleral changes were not fully consistent. More recently, quantitative analyses on the scleral arrangement as a function of myopia in guinea pig eyes using SHG imaging microscopy have been reported (30, 31). In particular, this article goes a step further on this topic and we evaluate and quantify the changes suffered by the sclera of myopic chickens by combining SHG images and the Radon transform (RT).

2 Materials and methods

2.1 Animals and tissue preparation

The scleral tissue used in this study was obtained from 13 chickens (aged 7–10 days) examined as part of a study on the development of myopia. All experiments were conducted in accordance with the ARVO statement for the use of animals and approved by the University of Tübingen Commission for Animal Welfare. White Leghorn chickens were raised under an 11/13 h light/dark cycle, with the light phase starting at 8:00 a.m. Water and food were supplied *ad libitum*. Illumination was provided by light bulbs that produced an average ambient illuminance of 500 lx on the cage floor.

Deprivation myopia was induced by attaching translucent plastic diffusers (32) over one eye for 7 days. Fellow eyes had normal vision and served as contralateral controls. Refractive state was measured without cycloplegia right before diffuser treatment started and at the end of the treatment period by automated infrared photoretinoscopy (33). Ocular dimensions were determined by A-scan ultrasonography as previously described (32), also at the beginning and at the end of the treatment period. Averages of three measurements for both refraction and axial length from contralateral control and treated eyes were taken.

Animals were sacrificed by an overdose of ether. The eyes were immediately enucleated and cut with a razor blade in the equatorial plane, approximately 1 mm posterior to the ora serrata. The anterior segment of the eye was discarded and the vitreous removed. From each ocular globe, tissue punches (8-mm in diameter) were taken from an area close to the optic nerve head (Figure 1). Then, both the retinal pigment epithelium and the choroidal layers were removed. The remaining scleral tissue was fixed by 30 min of immersion in 4% paraformaldehyde (PFA) in 0.1 M phosphate buffer, washed and afterwards stored to be sent in 1% PFA solution for SHG imaging.

2.2 SHG image acquisition

SHG images of the sclera samples were obtained using a multiphoton microscopy system [see (34) for further details of the setup]. In brief, the instrument combined a commercial inverted microscope (TE2000-U; Nikon, Japan) with a 800-nm (central wavelength) Ti:sapphire laser (Mira900f; Coherent, St Clara, CA). The repetition frequency of the laser was 76 MHz, and the pulse width was ~120 fs. The beam was focused on the sample through a long working distance objective (20x, NA 0.50, Nikon, ELWD series), with an average power of 80 mW. The focusing objective collected the nonlinear signal emitted by the sample. The signal emitted in the backward direction passed through a dedicated narrow-band spectral filter (400 ± 10 nm) before reaching the detector. The detector was a photomultiplier tube (PMT; R7205-01, Hamamatsu). A DC motor coupled to the objective allowed optical sectioning across the entire specimen along the Z-direction.

Each non-stained scleral punch (see section 2.3) was placed on the microscope stage with its fibrous layer facing down on a glass bottom dish filled with phosphate buffer. The inset in Figure 1 shows one of the specimens prepared for SHG image acquisition.

Two imaging protocols were used to record the SHG signal from the scleral tissue: tomographic imaging (35) and "regular" XY-plane imaging. The latter was set to operate at 1 frame/s. SHG images were $180 \times 180\ \mu m^2$ in size (256×256 pixel^2) and corresponded to the plane with best intensity projection within the sclera. For the former, the separation across adjacent points was 2 µm and it was used to image the fibrous portion of the chicken sclera. Whereas XY images allowed the visualization of the sclera collagen fibers, tomographic images permitted the calculation of the sample's thickness (see section 2.3). No image averaging was performed. Illustrative examples of SHG images acquired with both protocols are presented in Figure 2.

2.3 Image analysis

Image processing was performed by a dedicated software developed under MatLab™ (The MathWorks, Inc., Natick, MA). Fibrous scleral thickness of the was obtained from the tomographic images as follows (Figure 3). For each X_i location (vertical axis on Figure 3a) the intensity profile along the Z axis was extracted (horizontal axis on Figures 3a,b). For each set of data forming an axial

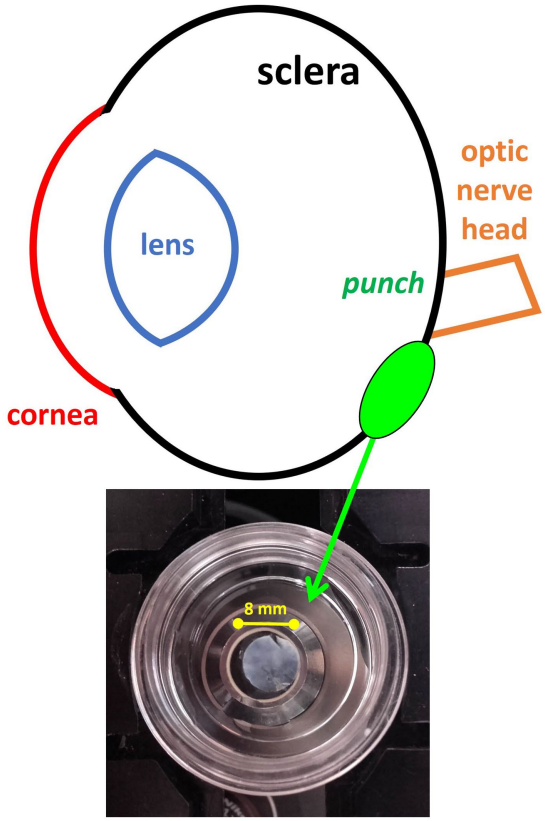

FIGURE 1
Illustrative drawing representing the location from where the chicken sclera tissue was harvested. The inset picture shows the scleral punch placed on the microscope glass bottom dish.

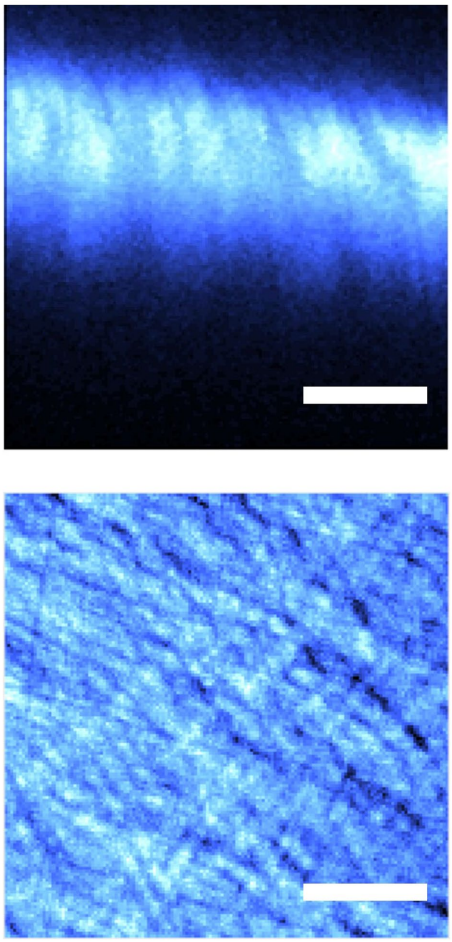

FIGURE 2
SHG images of the chicken sclera: axial tomography (top) and image across an XY plane (bottom). Scale bar: 50 μm.

profile, the corresponding derivatives were used for an accurate edge detection. Then, the distance between every pair of edge points (at both sides of the profile) was taken as the local thickness (t_i, see red arrows in Figure 3). The final thickness for each sample used herein was the mean value across all X_i locations.

To explore the organization of the scleral collagen fibers of each SHG image (Figure 4a), the RT method was applied. This is a mathematical tool that combined with the Fourier Transform (FFT) robustly quantifies the preferential (or dominant) orientation (PO) of the fibers (Figures 4b,c) and the structural dispersion (SD) value. A detailed description of this formalism and its advantages when wavy collagen fibers and crimped architecture appear in the image can be found in (36). The RT of the FFT image ensures that all peaks are close to the center of the x′ reference axis (Figure 4c). This $x' = 0$ line represents the angular information of the fibers (Figure 4d). In particular, the peak provides the PO (green arrow), and the SD is computed as standard deviation of the values of the angular distribution (37). If a PO exists, the distribution of Figure 4d can be fitted by a Gaussian function centered on the actual PO value. When $SD \leq 20°$, the sample is composed of fibers quasi-aligned along a PO. For a sample presenting a non-organized structure, SD will be larger than 40°. A partially organized distribution is considered when SD values are within the range (20°, 40°]. As a general rule, the higher the SD, the lower the level of organization of the fibers within the tissue. At this step the algorithm is not designed to compute the thickness of the fibers with the SHG image.

2.4 Statistics

Data are shown as the mean ± standard deviation. The difference between the experimental eyes and the fellow eyes were analyzed with a paired *t*-test. In Figures 5b, 6, 7, the measured parameters were expressed as changes/increment (Δ, after-before).

3 Results

3.1 Refraction and axial length

The diffuser-treated eyes developed axial myopia during the 1-week treatment period (mean final refraction: −4.70 ± 2.71 D, see Figure 8). Fellow control eyes, which were exposed to normal visual experience, remained slightly hyperopic (+2.49 ± 0.64 D). The refraction values between the two groups of eyes were statistically different (paired *t*-test, $p < 0.0001$).

Figure 5a shows the individual refraction as a function of the axial length after deprivation. It can be seen that higher degrees of myopia are closely associated with longer ocular length. This result is as expected. In the figure, the black line shows the best linear fit from the experimental data, which is significant ($R = 0.77$, $p < 0.0001$). The final

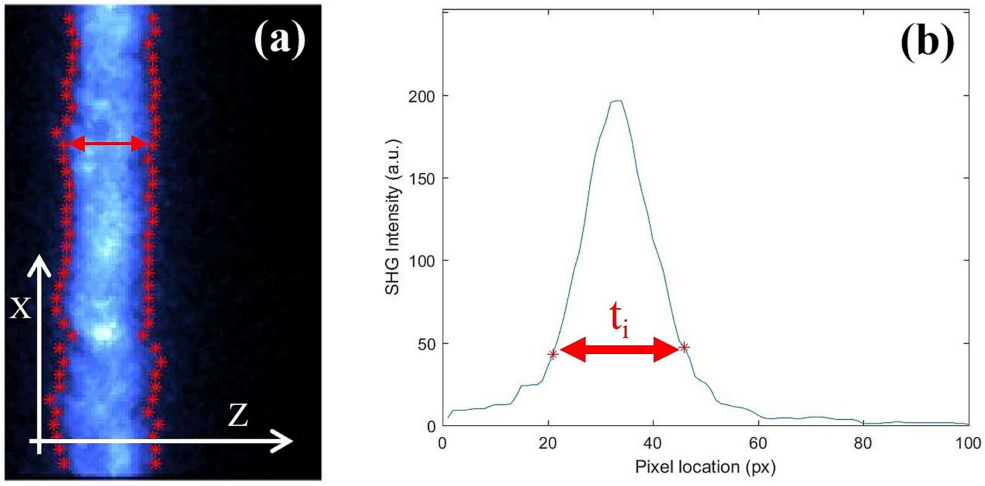

FIGURE 3
(a) Tomographic SHG images of a chicken sclera along the X direction. Red dots set the position of the edge estimated after the derivative of the curve at every point. (b) Example of an intensity profile as a function of depth for a particular X_i location.

refraction values were in the range of −10.1 D to +3.6 D. For completeness, the relationship between the change from baseline in refraction (ΔRx) and axial length (ΔAL) is shown in Figure 5b. Again, a statistically significant linear correlation was found ($R = 0.78$, $p < 0.0001$).

3.2 Fibrous scleral thickness

As an example, Figure 9 shows two randomly chosen SHG intensity profiles along the depth location (i.e., the Z-axis of the tissue as shown in Figure 3) for scleras from chicken eyes with low and high levels of myopia. Visual inspection reveals little difference between the two profiles, resulting in similar thickness values.

To confirm the apparent lack of change in the scleral thickness as a function of refraction, all samples were analyzed following the experimental procedure described above. Figure 6 shows the values of thickness of the fibrous sclera as a function of axial length change for all the samples included in the experiment. The values ranged between 50 and 70 μm (mean value: 62 ± 6 μm). Each value corresponded to the average across the entire SHG tomography. No relationship between both parameters was found here. There was no correlation between the scleral thickness and the final refraction either.

This absence of changes with myopia was confirmed in a parallel experiment using a commercial optical coherence tomography (OCT) instrument (Spectralis, Heidelberg Engineering). Measurements provided a mean fibrous scleral thickness value of 58 ± 9 μm, with no significant difference between myopic and control eyes.

3.3 Organization of the scleral collagen fibers

Figure 10 shows, as representative examples, SHG images of the sclera in eyes with low (left) and high (right) axial length changes (or alternatively, low and high changes in refraction after the deprivation treatment). Directly from the images it is difficult to detect changes in the collagen structure distribution, although the scleral fibers are visible and well delineated. The insets of Figure 10 show the corresponding SD values computed through the RT procedure explained in Methods (section 2.3). Moreover, no relationship between SHG intensity and refraction or axial length was found.

Although some motion artifacts are apparent at the edges of the images, affected areas were never included in the image processing procedure. Our algorithm was designed to automatically detect and eliminate those regions from the analysis.

To further explore and quantify possible differences in the scleral collagen arrangement as a function of myopia, the SD was calculated for all samples. SD values as a function of the axial length increment are depicted in Figure 7. A decreasing (statistically significant) linear trend was observed ($R = 0.65$, $p = 0.0004$). The correlation of SD with the final axial length, not shown in the figure, was similar ($SD = -16.07 \cdot AL_{FINAL} + 180.46$; $R = 0.67$, $p = 0.0002$).

The relationship between SD and the final ocular refraction is shown in Figure 11 for all specimens. The fitting to a linear model shows a weaker, but still significant, correlation compared to the evolution of SD as a function of axial length increment ($R = 0.48$, $p = 0.01$). It is interesting to note a broader inter-sample dispersion in the SD values in the group of eyes with refraction at +3D and closer to 0D.

Finally, Figure 12 depicts the overall impact of deprivation on the sclera organization of treated eyes, compared to fellow (non-deprived) eyes. While the average SD for the control group was 34 ± 11° (which is close to a non-organized collagen structure), this value was significantly reduced to 19 ± 7° in the deprived eyes (values within the range of the quasi-aligned distribution). Differences between the two groups were statistically significant ($p = 0.02$, paired t-test).

4 Discussion and conclusion

The sclera is not a static outer layer of the eye, but a dynamic tissue capable of altering the composition and structure of its extracellular

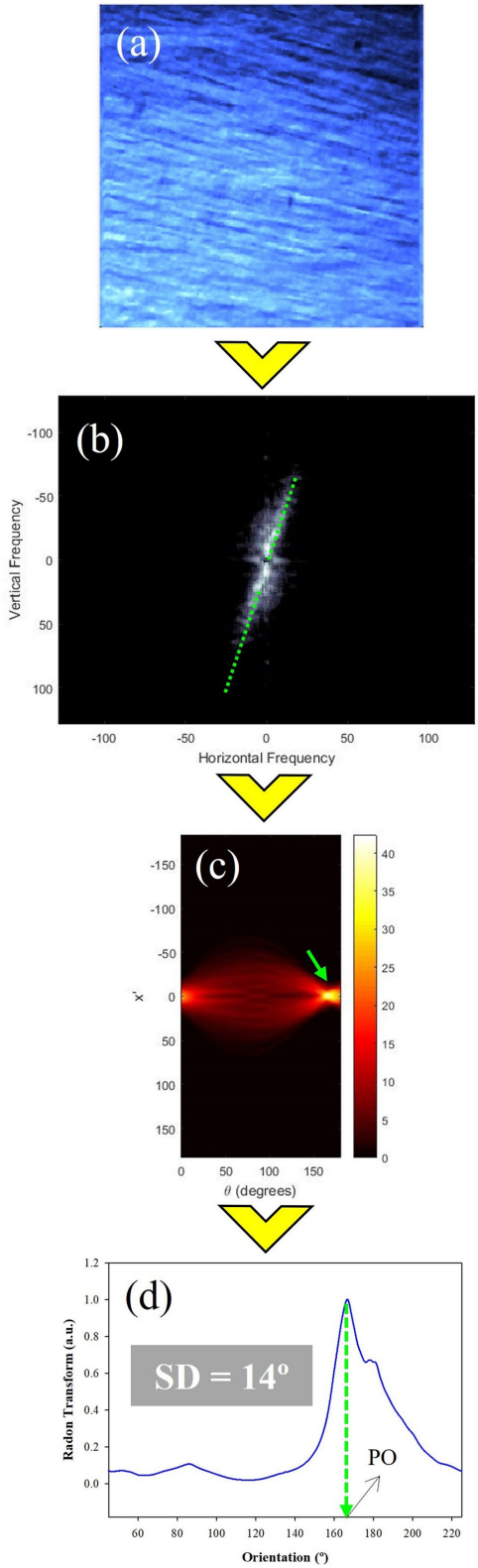

FIGURE 4
RT procedure to perform the calculation of the structural organization of the collagen fibers of the fibrous chicken sclera. (a) Original SHG image; (b) FFT image; (c) RT of the FFT image where the peak (green arrow) corresponds to the preferential orientation; (d) RT plot for x′ = 0. The insets indicate the values of SD and PO.

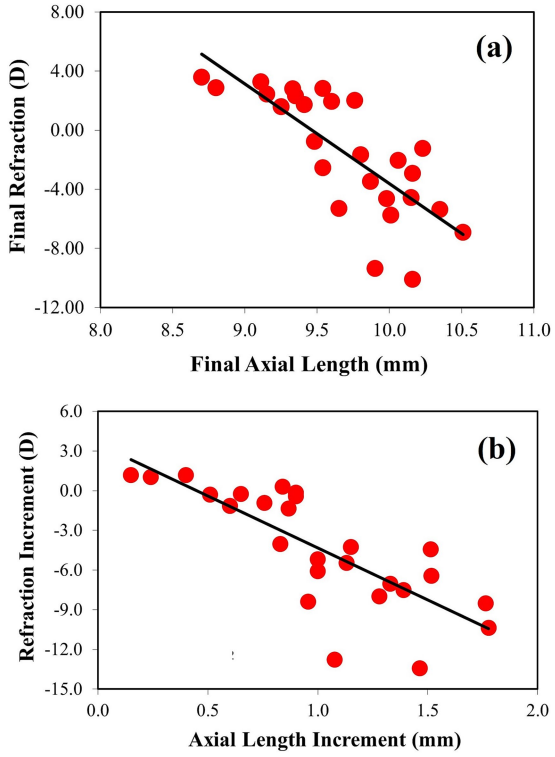

FIGURE 5
(a) Relationship between refraction (in D) and axial length (in mm) (best linear fit (solid black line): $Rx_{final} = -6.74*AL_{final} + 63.74$). (b) Change in refraction during the treatment period as a function of change in axial length (best linear fit (solid black line): $\Delta Rx_{final} = 7.86*\Delta AL_{final} + 3.52$).

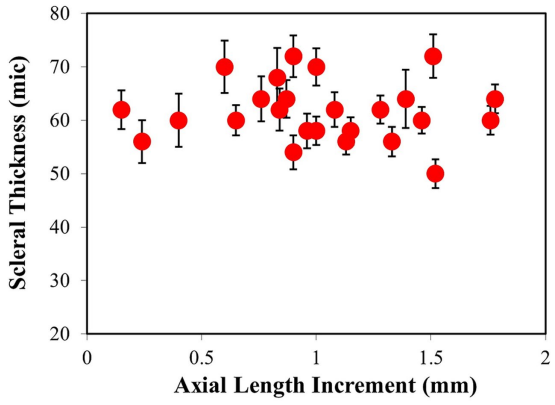

FIGURE 6
Averaged values of fibrous scleral thickness (μm) vs. the increment in axial length (mm).

matrix (i.e., collagen) in response to changes in the visual environment (38). In recent decades, there has been increasing interest in studying changes in various ocular structures due to myopia. In particular, changes in the myopic sclera as a result of axial elongation were early reported (6). As myopia progression alters the structure of this outer ocular envelope, non-invasive and quantitative analyses of the collagen

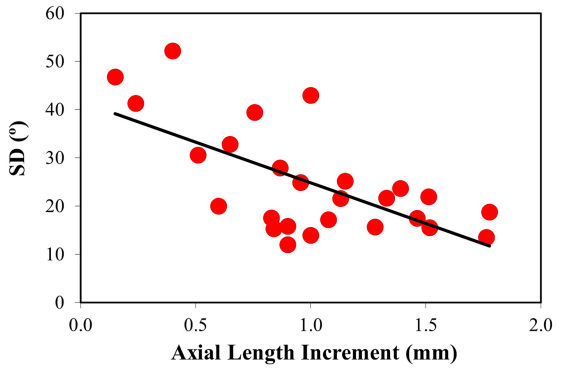

FIGURE 7
Changes in SD with axial length increment. Linear regression fitted to the data shows a statistically significant decrease. Best linear fit: SD = –16.85·ΔAL + 41.66.

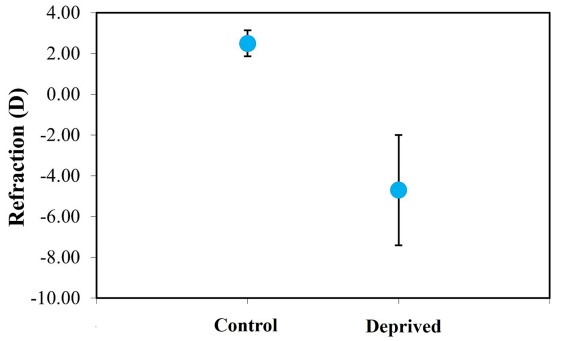

FIGURE 8
Average refraction in control and deprived chicken eyes (after 1 week of wearing a diffuser). Error bars indicate the standard deviation.

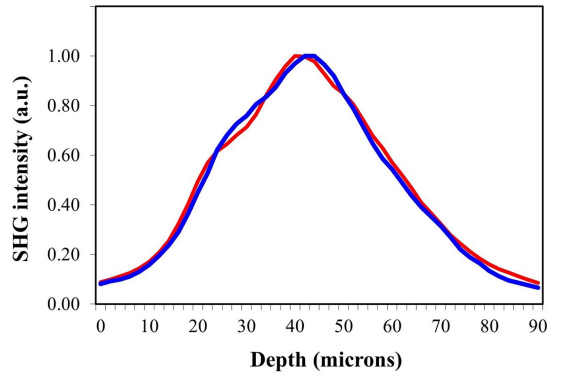

FIGURE 9
SHG intensity profiles as a function of depth for scleral punches from myopic eyes with refraction values of –1.23 D (blue) and – 9.35 D (red).

fiber distribution are of great importance. These will help to better understand how myopia development alters collagen organization within the sclera.

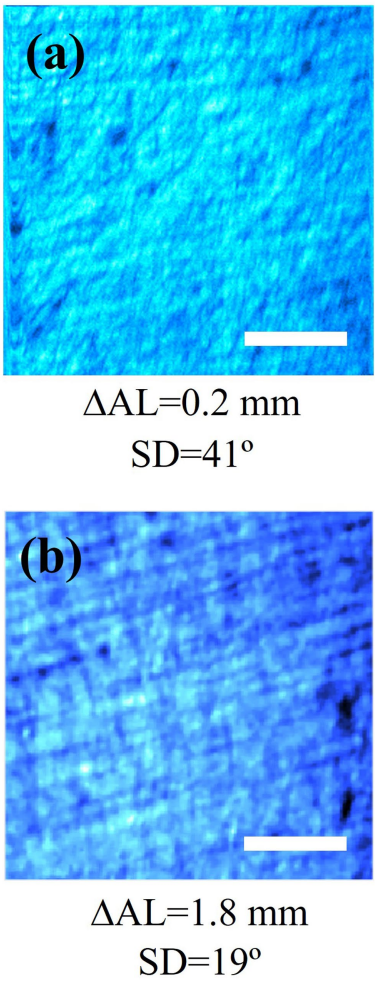

FIGURE 10
SHG images for chicken scleras with low (left) and high (right) axial length increments after deprivation. Insets indicate the change in axial length (ΔAL) and the SD values computed by the RT algorithm. Scale bar in (a,b): 50 μm.

Although morphological changes in the sclera were early recognized (2, 6), only a few studies have quantitatively characterized the extracellular matrix of the sclera and its relationship to myopia [see for instance the review by Harper and Summers (39)]. More recently, techniques such as polarization-sensitive OCT (40) and SHG microscopy (30, 31) have been used in guinea pigs for this purpose. In the former, the authors reported a positive correlation between scleral birefringence and refractive error that predicted the onset of myopia (40). On the other hand, SHG images revealed that scleral collagen fibers of form-deprivation myopic eyes were more aligned (30). Similar results were showed by Germann et al. since they found an increase in the order coefficient of the fibers when comparing the treated myopic eye and the non-myopic fellow eye (31).

In the present work we used chickens as myopia animal models. Unlike the rodent sclera (and mammals' in general) (41) where only a fibrous layer appears, the chicken sclera consists of an inner cartilaginous layer and an outer fibrous layer that resembles

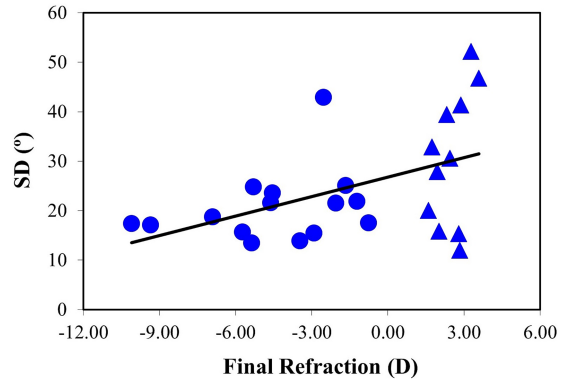

FIGURE 11
SD values as a function of the final refraction. The black line corresponds to the best linear fit (SD = 1.31·Rx_{final} + 26.80). Data for eyes with refraction values at +3D and closer to 0D are represent with a different symbol (triangles).

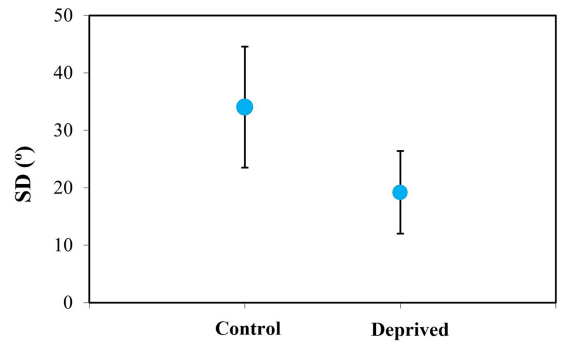

FIGURE 12
Averaged values of scleral SD in control and deprived chicken eyes (after 1 week of wearing diffuser). Error bars indicate the standard deviation.

mammalian sclera. Herein, SHG microscopy was used to image unstained scleral punches in both control and form-deprivation myopic chicken eyes. The thickness of the fibrous sclera was measured and the degree of organization of its collagen fibers was computed as a function of various myopia-related ocular parameters.

In contrast to the cartilaginous layer, the fibrous layer undergoes remodeling during excessive eye growth, a mechanism that might underlie the development of myopia (10). In particular, collagen fibers in the human sclera have been observed to become lamellar rather than interwoven with increasing degree of myopia (2, 6). A decrease in collagen concentration has also been observed in the posterior sclera of highly myopic humans (42). More recently, the use of wide-angle x-ray scattering mapping has shown statistically significant differences in posterior scleral fiber angle deviation when comparing non-myopic and highly myopic human eyes (>6 D) (43).

Our results on scleral remodeling in myopic eyes are consistent with previous studies in mammalian animal models and humans. The degree of organization of the scleral collagen was found to increase with myopia. In particular, there is a significant linear negative relationship between SD and the ocular axial length (slope: −16°/mm). On average, it decreased from ~50° (unorganized) to ~15° (quasi-organized). Moreover, as refraction and axial length are closely related, SD was also significantly (positively) correlated with final refraction (slope: 1.3°/D). This means that the more myopic the eye is, the higher organized the scleral collagen is.

It has been also reported that high myopia in both humans and monkeys is associated with severe thinning of the (fibrous) sclera, particularly at the posterior pole of the eye (6, 8). However, the significance of scleral thinning is still unclear. Although this might be related to a reduction in collagen fiber diameter (2), some authors claimed that this thinning was a consequence of passive stretching of the scleral tissue around the enlarged myopic eye (44, 45). However, a shrew model forced a reinterpretation of this hypothesis, since this significant thinning in the posterior part of the eye occurred after both short- and long-term deprivation treatments (9).

Our data show that the fibrous scleral thickness remains relatively constant. In our specimens, thickness values varied between 50 and 70 µm, but no correlation with the degree of myopia was observed. This result differs from previous findings in mammalian models or humans (2, 6–9, 37). Other studies have found that the thinning of the fibrous sclera in chicks is similar to what was observed in myopic mammals (16, 46, 47). On the opposite, a recent study in chicks did not find a significant difference in the thickness of the fibrous scleral layer between myopic and control eyes (48). Although this agrees with our results, there are large differences in terms of absolute fibrous sclera thickness between both experiments. Whereas Yan and colleagues measured a mean thickness of 110 µm (48), we obtained 62 µm using SHG tomography and 58 µm by means of OCT. This divergence may be partly explained by the fact that chicken hybrid line in Yan's study was different from ours. Moreover, their animals were also slightly older.

Additional physical parameters such as the fiber size or the tissue elasticity were out of the scope of this work. However, it is interesting to note that smaller collagen fiber diameters in the fibrous sclera of chicken myopic eyes (16, 49) and mammalian models (including humans) (2, 9, 30) have been previously described. This narrowing of the fibers may be associated with both biochemical and biomechanical changes in the scleral extracellular matrix (15, 42, 50). Scleral elasticity has been showed to increase in eyes developing myopia, mainly due to the reduced collagen content (51). Other evidence suggests that the biomechanical properties of sclera (elasticity and creep) may play a significant regulatory role in the axial elongation of myopic eyes (15, 52). Whereas elasticity is related to the immediate change in the tissue length when a force is applied (i.e., extension vs. load), creep describes the slow, time-dependent extension/compression under a constant load (i.e., extension vs. time) (15). Although biomechanical parameters have not been specifically addressed here, further analyses on these may help to clarify whether scleral collagen changes in myopia result from passive stretch or from active tissue remodeling.

In conclusion, SHG microscopy images of the chicken scleral tissue were used to objectively study the changes produced during the development of deprivation myopia. The spatially resolved distribution of scleral collagen fibers was visualized and quantified as a function of ocular refraction. The axial elongation associated with increasing amounts of myopia is closely related to the rearranging of the scleral tissue. Our experiment showed a process of remodeling of the posterior sclera during axial elongation. The collagen pattern changes from a non-organized distribution into a quasi-organize arrangement.

Data availability statement

Data underlying the results presented in this paper may be obtained from the authors upon reasonable request.

Ethics statement

The animal study was approved by the University of Tuebingen Commission for Animal Welfare and by the Ethical Committee of the University of Murcia. The entire experiment followed the guidelines of the Association for Research in Vision and Ophthalmology Statement for the Use of Animals in Ophthalmic and Vision Research.

Author contributions

JB: Conceptualization, Data curation, Formal analysis, Funding acquisition, Investigation, Methodology, Project administration, Supervision, Validation, Writing – original draft. RM-O: Formal analysis, Methodology, Software, Writing – review & editing. EF: Conceptualization, Data curation, Writing – review & editing. MF: Data curation, Methodology, Writing – review & editing.

Funding

The author(s) declare that financial support was received for the research, authorship, and/or publication of this article. This work was supported by the Agencia Estatal de Investigación, Spain (PID2020-113919RB-I00/AEI/10.13039/501100011033).

Conflict of interest

The authors declare that the research was conducted in the absence of any commercial or financial relationships that could be construed as a potential conflict of interest.

Publisher's note

References

1. Keeley F, Morin JD, Vesely S. Characterization of collagen from normal human sclera. *Exp Eye Res*. (1984) 39:533–42. doi: 10.1016/0014-4835(84)90053-8

2. Curtin BJ, Iwamoto T, Renaldo D. Normal and staphylomatous sclera of high myopia. An electron microscopic study. *Arch Ophthalmol*. (1979) 97:912–5. doi: 10.1001/archopht.1979.01020010470017

3. Komai Y, Ushiki T. The three-dimensional organization of collagen fibrils in the human cornea and sclera. *Invest Ophthalmol Vis Sci*. (1991) 32:2244–58.

4. Meek K, Fullwood NJ. Corneal and scleral collagens - a microscopist's perspective. *Micron*. (2001) 32:261–72. doi: 10.1016/s0968-4328(00)00041-x

5. Yamamoto S, Hashizume H, Hitomi J, Shigeno M, Sawaguchi S, Abe H, et al. The subfibrillar arrangement of corneal and scleral collagen fibrils as revealed by scanning electron and atomic force microscopy. *Arch Histol Cytol*. (2000) 63:127–35. doi: 10.1679/aohc.63.127

6. Curtin BJ, Teng CC. Scleral changes in pathological myopia. *Trans Am Acad Ophthalmol Otolaryngol*. (1958) 62:777–88.

7. Curtin BJ. Physiopathologic aspects of scleral stress-strain. *Trans Am Ophthalmol Soc*. (1969) 67:417–61.

8. Funata M, Tokoro T. Scleral change in experimentally myopic monkeys. *Graefes Arch Clin Exp Ophthalmol*. (1990) 228:174–9. doi: 10.1007/BF00935729

9. McBrien NA, Cornell LM, Gentle A. Structural and ultrastructural changes to the sclera in a mammalian model of high myopia. *Invest Ophthalmol Vis Sci*. (2001) 42:2179–87.

10. McBrien NA, Gentle A. Role of the sclera in the development and pathological complications of myopia. *Prog Retin Eye Res*. (2003) 22:307–38. doi: 10.1016/S1350-9462(02)00063-0

11. Schaeffel F, Glasser A, Howland HC. Accommodation, refractive error and eye growth in chickens. *Vis Res*. (1988) 28:639–57. doi: 10.1016/0042-6989(88)90113-7

12. Troilo D, Wallman J. The regulation of eye growth and refractive state: an experimental study of emmetropization. *Vis Res*. (1991) 31:1237–50. doi: 10.1016/0042-6989(91)90048-a

13. Wallman J. Retinal control of eye growth and refraction. *Prog Retinal Res*. (1993) 12:133–53. doi: 10.1016/0278-4327(93)90007-G

14. Christensen AM, Wallman J. Evidence that increased scleral growth underlies visual deprivation myopia in chicks. *Invest Ophthalmol Vis Sci*. (1991) 32:2143–50.

15. Phillips JR, Khalaj M, McBrien NA. Induced myopia associated with increased scleral creep in chick and tree shrew eyes. *Invest Ophthalmol Vis Sci*. (2000) 41:2028–34.

16. Marzani D, Wallman J. Growth of the two layers of the chick sclera is modulated reciprocally by visual conditions. *Invest Ophthalmol Vis Sci*. (1997) 38:1726–39.

17. Rada JA, Thoft RA, Hassell JR. Increased aggrecan (cartilage proteoglycan) production in the sclera of myopic chicks. *Dev Biol*. (1991) 147:303–12. doi: 10.1016/0012-1606(91)90288-e

18. Fine S, Hansen WP. Optical second harmonic generation in biological systems. *Appl Opt*. (1971) 10:2350–3. doi: 10.1364/AO.10.002350

19. Kim BM, Eichler J, Da Silva LB. Frequency doubling of ultrashort laser pulses in biological tissues. *Appl Opt*. (1999) 38:7145–50. doi: 10.1364/ao.38.007145

20. Campagnola PJ, Clark HA, Mohler WA, Lewis A, Loew LM. Second-harmonic imaging microscopy of living cells. *J Biomed Opt*. (2001) 6:277–86. doi: 10.1117/1.1383294

21. Han M, Giese G, Bille J. Second harmonic generation imaging of collagen fibrils in cornea and sclera. *Opt Express*. (2005) 13:5791–7. doi: 10.1364/opex.13.005791

22. Teng SW, Tan HY, Peng JL, Lin HH, Kim KH, Lo W, et al. Multiphoton autofluorescence and second-harmonic generation imaging of the ex vivo porcine eye. *Invest Ophthalmol Vis Sci*. (2006) 47:1216–24. doi: 10.1167/iovs.04-1520

23. Lo W, Tan HY, Lin MG, Hsueh CM, Chen WL, Lin SJ, et al. Forward and backward second harmonic generation imaging of corneal and scleral collagen In: Proceedings of SPIE 6860, Multiphoton Microscopy in the Biomedical Sciences VIII, 68600F (2008)

24. Sun H, Kurtz RM, Juhasz T. Evaluation of human sclera after femtosecond laser ablation using two photon and confocal microscopy. *J Biomed Opt*. (2012) 17:081411. doi: 10.1117/1.JBO.17.8.081411

25. Yamanari M, Nagase S, Fukuda S, Ishii K, Tanaka R, Yasui T, et al. Scleral birefringence as measured by polarization-sensitive optical coherence tomography and ocular biometric parameters of human eyes in vivo. *Biomed Opt Express*. (2014) 5:1391–402. doi: 10.1364/BOE.5.001391

26. Bueno JM, Gualda EJ, Artal P. Adaptive optics multiphoton microscopy to study *ex vivo* ocular tissues. *J Biomed Opt*. (2010) 15:066004. doi: 10.1117/1.3505018

27. Ávila FJ, Gambín A, Artal P, Bueno JM. *In vivo* two-photon microscopy of the human eye. *Sci Rep*. (2019) 9:10121. doi: 10.1038/s41598-019-46568-z

28. Pijanka JK, Coudrillier B, Ziegler K, Sorensen T, Meek KM, Nguyen TD, et al. Quantitative mapping of collagen fiber orientation in non-glaucoma and glaucoma posterior human sclerae. *Invest Ophthalmol Vis Sci*. (2012) 53:5258–70. doi: 10.1167/iovs.12-9705

29. Coudrillier B, Pijanka J, Jefferys J, Sorensen T, Quigley HA, Boote C, et al. Collagen structure and mechanical properties of the human sclera: analysis for the effects of age. *J Biomech Eng*. (2015) 137:041006. doi: 10.1115/1.4029430

30. Hoerig C, McFadden S, Hoang QV, Mamou J. Biomechanical changes in myopic sclera correlate with underlying changes in microstructure. *Exp Eye Res*. (2022) 224:109165. doi: 10.1016/j.exer.2022.109165

31. Germann JA, Villegas L, Revuelta L, Marcos S. Effects of pharmacological treatments of myopia on scleral collagen organization in myopic guinea pig models. *Invest Ophthalmol Vis Sci*. (2023) 64:2859.

32. Schaeffel F, Howland HC. Properties of the feedback loops controlling eye growth and refractive state in the chicken. *Vis Res*. (1991) 31:717–34. doi: 10.1016/0042-6989(91)90011-s

33. Seidemann A, Schaeffel F. Effects of longitudinal chromatic aberration on accommodation and emmetropization. *Vis Res*. (2002) 42:2409–17. doi: 10.1016/s0042-6989(02)00262-6

34. Skorsetz M, Artal P, Bueno JM. Performance evaluation of a sensorless adaptive optics multiphoton microscope. *J Micros*. (2016) 261:249–58. doi: 10.1111/jmi.12325

35. Bueno JM, Palacios R, Pennos A, Artal P. Second-harmonic generation microscopy of photocurable polymer intrastromal implants in *ex-vivo* corneas. *Biomed Opt Express*. (2015) 6:2211–9. doi: 10.1364/BOE.6.002211

36. Mega Y, Robitaille M, Zareian R, McLean J, Ruberti J, DiMarzio C. Quantification of lamellar orientation in corneal collagen using second harmonic generation images. *Opt Lett*. (2012) 37:3312–4. doi: 10.1364/OL.37.003312

37. Ávila FJ, Bueno JM. Analysis and quantification of collagen organization with the structure tensor in second harmonic microscopy images of ocular tissues. *Appl Opt*. (2015) 54:9848–54. doi: 10.1364/AO.54.009848

38. Rada JA, Shelton S, Norton TT. The sclera and myopia. *Exp Eye Res*. (2006) 82:185–200. doi: 10.1016/j.exer.2005.08.009

39. Harper AR, Summers JA. The dynamic sclera: extracellular matrix remodeling in normal ocular growth and myopia development. *Exp Eye Res*. (2015) 133:100–11. doi: 10.1016/j.exer.2014.07.015

40. Liu X, Jiang L, Ke M, Sigal IA, Chua J, Hoang QV, et al. Posterior scleral birefringence measured by triple-input polarization-sensitive imaging as a biomarker of myopia progression. *Nat Biomed Eng*. (2023) 7:986–1000. doi: 10.1038/s41551-023-01062-w

41. Lluch S, Ventura J, López-Fuster MJ. Eye morphology in some wild rodents. *Anat Histol Embryol*. (2008) 37:41–51. doi: 10.1111/j.1439-0264.2007.00796.x

42. Avetisov ES, Savitskaya NF, Vinetskaya MI, Iomdina EN. A study of biochemical and biomechanical qualities of normal and myopic sclera in humans of different age groups. *Metab Pediatr Syst Ophthalmol*. (1983) 7:183–8.

43. Markov PP, Eliasy A, Pijanka JK, Htoon HM, Paterson NG, Sorensen T, et al. Bulk changes in posterior scleral collagen microstructure in human high myopia. *Mol Vis*. (2018) 24:818–33.

44. Young FA. The nature and control of myopia. *J Am Optom Assoc*. (1977) 48:451–7.

45. Curtin BJ. The myopias: basic science and clinical management. Philadelphia: Harper & Row (1985).

46. Gottlieb MD, Joshi HB, Nickla DL. Scleral changes in chicks with form-deprivation myopia. *Curr Eye Res*. (1990) 9:1157–65. doi: 10.3109/02713689009003472

47. Troilo D, Smith EL III, Nickla DL, Ashby R, Tkatchenko AV, Ostrin LA, et al. IMI - report on experimental models of emmetropization and myopia. *Invest Ophthalmol Vis Sci*. (2019) 60:M31–88. doi: 10.1167/iovs.18-25967

48. Yan F, Wang C, Wilson JA, O'Connell M, Ton S, Davidson N, et al. Visually guided chick ocular length and structural thickness variations assessed by swept-source optical coherence tomography. *Biomed Opt Express*. (2021) 12:6864–81. doi: 10.1364/BOE.433333

49. Kusakari T, Sato T, Tokoro T. Visual deprivation stimulates the exchange of the fibrous sclera into the cartilaginous sclera in chicks. *Exp Eye Res*. (2001) 73:533–46. doi: 10.1006/exer.2001.1064

50. Norton TT, Rada JA. Reduced extracellular matrix in mammalian sclera with induced myopia. *Vis Res*. (1995) 35:1271–81. doi: 10.1016/0042-6989(94)00243-f

51. McBrien NA, Jobling AI, Gentle A. Biomechanics of the sclera in myopia: extracellular and cellular factors. *Optom Vis Sci*. (2009) 86:E23–30. doi: 10.1097/OPX.0b013e3181940669

52. Phillips JR, McBrien NA. Form deprivation myopia: elastic properties of sclera. *Ophthalmic Physiol Opt*. (1995) 15:357–62. doi: 10.1046/j.1475-1313.1995.9500062i.x

frontiers | Frontiers in Medicine

TYPE Original Research
PUBLISHED 10 December 2024
DOI 10.3389/fmed.2024.1469275

OPEN ACCESS

EDITED BY
Pablo De Gracia,
University of Detroit Mercy, United States

REVIEWED BY
Arumugam R. Muralidharan,
Singapore Eye Research Institute (SERI), Singapore
Alexandra Benavente-Perez,
State University of New York, United States

*CORRESPONDENCE
Marita Pauline Feldkaemper
✉ marita.feldkaemper@uni-tuebingen.de

RECEIVED 23 July 2024
ACCEPTED 23 October 2024
PUBLISHED 10 December 2024

CITATION
Liu H, Schaeffel F and Feldkaemper MP (2024) Effects of computer-generated patterns with different temporal and spatial frequencies on choroidal thickness, retinal dopamine and candidate genes in chickens wearing lenses. *Front. Med.* 11:1469275.
doi: 10.3389/fmed.2024.1469275

Effects of computer-generated patterns with different temporal and spatial frequencies on choroidal thickness, retinal dopamine and candidate genes in chickens wearing lenses

Hong Liu[1,2], Frank Schaeffel[1] and Marita Pauline Feldkaemper[1]*

[1]Section of Neurobiology of the Eye, Ophthalmic Research Institute, University of Tübingen, Tübingen, Germany, [2]Aier Institute of Optometry and Vision Science, Aier Eye Hospital Group, Changsha, China

Purpose: Changes in choroidal thickness (ChT) are proposed to predict myopia development but evidence is mixed. We investigated time courses of choroidal responses, following different types of dynamic artificial stimulation in chicks with and without spectacle lenses, as well as changes in retinal dopamine metabolism and expression of candidate genes.

Methods: Chicks were kept in an arena surrounded by computer monitors presenting dynamic checkerboard fields of small, medium and large size. Fields were displayed with different cycle frequencies, as ON (rapid rise, slow decay) or OFF (slow rise, rapid decay) temporal luminance profile. Refractive errors, ocular biometry and ChT were assessed. Dopamine metabolism and candidate gene expression levels were also measured. Stimuli were applied for (1) 3 h with no lens, (2) 3 h and monocular treatment with −7D or +7D lenses, (3) 3 or 7 days.

Results: (1) The smallest fields caused the largest decrease in ChT. (2) Negative lens treatment induced on average 11.7 μm thinner choroids. ChT thinning was enhanced by 10 Hz-ON medium field size flicker which also reduced choroidal thickening with positive lenses. (3) With prolonged treatment, the choroid recovered from initial thinning in all groups although to varying degrees which were dependent on stimulus parameters. Relative ChT changes were positively correlated with the vitreal level of dopamine metabolites. Retinal *EGR-1* mRNA level was positively correlated with choroidal thickness. Retinal melanopsin mRNA was increased by 10 Hz-ON stimulation and choroidal *BMPR1A* mRNA increased with 10 Hz-OFF stimulation. On average, early choroidal thinning did not predict the amount of negative lens-induced eye growth changes after 7 days, whereas later ChT changes showed a weak association.

Conclusion: Negative lenses caused long-lasting choroidal thinning, with some recovery during lens wear, especially after stimulation with 10 Hz. The dynamic stimuli modulated choroidal thinning but effects were small. There was little difference between ON and OFF stimulation, perhaps because the checkerboard patterns were too coarse. 10 Hz cycle frequency increased dopamine release. Less dopamine was correlated with thinner choroids. Result do not exclude a predictive value of choroidal thickening for future refractive development since we almost exclusively tested choroidal thinning effects.

KEYWORDS
choroid, myopia, artificial visual stimuli, dopamine, EGR-1, chicken

1 Introduction

Wallman et al. (1) discovered in the early 90's in chickens that the thickness of the choroid, the highly vascularized layer behind the retina, changes when the plane of focus in the retinal image is shifted. With a positive lens in front of the eye, the choroid thickens within hours, moving the retina closer to the focal plane. With a negative lens, the choroid thins, moving the retina closer to the focal plane. In the long term, defocus-induced choroidal thickness changes are followed by changes in growth of the outer coat of the eye, the sclera, leading to the compensation of lens-induced refractive errors (REs). Similar changes in choroidal thickness (ChT) were found in tree shrews, guinea pigs, marmosets and monkeys even though the effects on refractive state were smaller because the induced ChT changes were smaller and the eyes larger (2–4). A few studies in the chicken model have later addressed the question of whether ChT changes can predict ocular growth rates with all kinds of stimulation, with variable outcomes. While one study (5) showed that baseline ChT was neither related to baseline eye size, nor to subsequent eye growth rates, Nickla and Totonelly (6) measured an inverse correlation between ChT changes and axial eye growth rates in untreated chicken eyes. However, it was consistently found that baseline ChT did not predict the susceptibility to deprivation myopia (6, 7).

Recently, due to the advancements of optical coherence tomography (OCT) imaging, even tiny changes in ChT can be non-invasively measured in human subjects (8). It was found that (1) similar to chickens and monkeys, wearing a positive lens in one eye induced thickening of the choroid both in adults and children (9–11). (2) Studies in children also showed that developmental changes in ChT successfully predicted future myopia development (12). Furthermore, cross-sectional studies demonstrated that myopic children and myopic adults had thinner choroids than non-myopes. An inverse association between ChT changes and changes in eye growth was confirmed by Read et al. (13) who concluded that "Choroidal thickness exhibited an inverse association with the axial eye length changes, implying a potential role for the choroid in eye growth." (3) Atropine, known to inhibit myopia development, also makes the choroid thicker and prevents choroidal thinning that is normally induced by wearing a negative lens (14).

In recent years, evidence has accumulated that visual stimuli other than defocus can also change ChT. However, it remained uncertain whether such changes can reliably predict whether a treatment can control myopia. Short term exposure (3 h) to computer-generated artificial stimuli on a screen that predominantly activate ON pathways caused choroidal thickening in chicks, while stimulation of the OFF pathways caused choroidal thinning (15). ChT returned to baseline after 7 days despite continued treatment (15). Unexpectedly, with both dynamic ON and OFF stimulation on a computer screen, with an underlying repetition frequency of 1 Hz, more myopia was induced by negative lenses than under continuous illumination with comparable brightness. Still, retinal dopamine release was higher with ON than OFF stimulation. The ChT changes measured after short-term exposure did not predict refractive states measured after 7 days. Possible explanations are that (1) the underlying repetition frequency (1 Hz) of the temporal sawtooth-shaped luminance profiles in each of the small fields of the checkerboard stimulus might have induced a myopic shift (16), (2) highly dynamic spatio-temporal pattern seen by the chickens made the retina more responsive to defocus and therefore made the negative lenses more effective, (3) in the long term, it does not matter whether stimulation is more ON or OFF because of adaptation of the ON and OFF pathways. Also, Nickla and Totonelly (6) found that the relationship between choroidal thickening and eye growth inhibition may be disrupted under certain experimental conditions. Given that researchers might rely on the assumption that thicker choroids predict myopia inhibition (1), there is an urgent need (1) to find out under which conditions these predictions remain valid and, (2) which mechanisms and biochemical pathways trigger such changes in ChT and, subsequently, scleral growth.

In the current study, we applied visual stimuli with different dynamic luminance profiles, provided on the computer screens as checkerboard patterns with random phases with respect to each other: (1) rapid ON with slow decay or (2) slow increase with rapid OFF or (3) temporal square wave luminance profiles. The repetition frequencies were either 0 Hz (stationary pattern), or 0.8 Hz, 1.2 Hz, 2.5 Hz, 6.5 Hz, 7.5 Hz, and 10 Hz. Individual fields of the checkerboards subtended either 1.7 deg. of visual angle (small squares, 28 × 28 pixels "SSQ"), 2.9 deg. (medium size squares, 48 × 48 pixels, "MSQ"), or 4.1 deg. (large squares, 68 × 68 pixels "LSQ"). Subsequent changes in ChT, eye growth, and myopia development were studied, including their time courses. To find out whether the presentation of a dynamic pattern itself, without ON or OFF dominance, may increase the sensitivity of the retina to defocus, square wave temporal luminance profiles were also tested.

To learn more about the messengers and biochemical pathways that control ChT and, subsequently, the growth of the sclera, some known markers of myopia development were studied. The time course of expression changes of established retinal and choroidal biomarkers is often unknown. We aimed to find out whether their expression level correlates with changes in eye growth and choroidal thickness after medium-term (3 days) and long-term (7 days) treatment. We focused on mRNA expression changes of the transcription factor early-growth response-1 (*EGR-1*) (17, 18), gap junction delta-2 (*GJD2*) (19), melanopsin (*OPN4*) (20) and neuropsin (*OPN5*) in the retina (21, 22). Choroidal markers shown to correlate with ChT, i.e., retinaldehyde dehydrogenase 2 (*RALDH2*) (23) and bone morphogenic protein receptor 1A (*BMPR1A*) (24) were also measured. In addition, we quantified the vitreal and retinal dopamine content and its metabolites, as they are known to be associated with changes in eye growth (25, 26).

2 Materials and methods

2.1 Animals and rearing conditions

White leghorn chicks were obtained from a local hatchery (Weiss, Kirchberg, Germany) at postnatal day 1. They were raised in a temperature and humidity-controlled animal facility. Water and food

were supplied *ad libitum*. The light cycle was 11:13 light/dark (8:30 AM to 6:30 PM) with an illuminance of approximately 500 lux during the light phase. All experiments were conducted in accordance with the statement of the Association for Research in Vision and Ophthalmology (ARVO) for the use of Animals in Ophthalmic and Vision Research. Procedures were approved by the commission for Animal Welfare of the Medical Faculty of the University of Tübingen. Water and food were supplied *ad libitum* under all experimental conditions.

2.2 Visual stimulation: ON-, OFF- and square wave stimuli

Dynamic ON or OFF or square wave stimuli were developed using Visual C++ 8.0 as previously described (15). Stimuli consisted of a checkerboard pattern in which the fields had a repetitive sawtooth-shaped temporal luminance profile, with ON stimuli generated by a rapid rise in brightness and slow linear decay and OFF with a slow rise and rapid decay. Square wave stimuli with either bright or dark fields with both rapid ON and OFF and 0.5 duty cycle were also used. Cycles in all fields were randomly phase shifted with respect to each other, using the rnd() function in C++. Cycle frequency could be adjusted by selecting the number of pixel brightness steps in the temporal brightness slopes of each field.

For stimulation, chickens were kept in a perspex container ("arena" 60 × 60 cm) as previously described (15). Four computer screens (Acer KG271A, 61 cm; Acer, New Taipei City, Taiwan; resolution 1,920 × 1,080 (3.15 px/mm); refresh frequency 144 Hz), displaying the stimuli, were placed behind the transparent walls. In addition, the stimuli were projected from above on the white cardboard covering the floor by two video projectors (Acer, P1383W, resolution 1,280 × 800, contrast 13,000:1). The backlights of the computer screens were white LEDs and the projectors contained mercury high-pressure lamps. The combined spectrum of the computer screen and projector lamps perceived by the chicks in the arena was continuous, ranging from 380 to 780 nm (Supplementary Figure S1). Average illuminance in the arena was 400 lux. Chicks were kept in the arena during the experiment and housed in the animal facility before and after exposure. Chicks could freely move in the "arena" with water and food supplied in small bowls *ad libitum*.

2.3 Experiments

2.3.1 Effects of short-term dynamic ON or OFF stimulation with different temporal and spatial frequencies on ChT in chickens with normal visual experience

Seven chickens per group were exposed to ON and OFF stimuli for 3 h, from 10:00 AM to 1:00 PM. The duration of 3 h was chosen based on a previous set of experiments that showed significant changes in choroidal thickness after 3 h (15). ChT was determined by spectral domain optical coherence tomography (SD-OCT) before and after the exposure period. The numbers of squared fields in the checkerboard pattern on the screen were 68 × 39 (28 × 28 pixels = 8.9 × 8.9 mm, small squares, "SSQ"), 40 × 22 (48 × 48 pixels = 15.2 × 15.2 mm, medium size squares, "MSQ") or 28 × 16 (68 × 68 pixels = 21.5 × 21.5 mm; large squares, "LSQ"). Naturally, the visual angles of each field varied considerably with the viewing distances of the chickens. If they were in the center of the arena, the viewing distance was about 30 cm, and the visual angles were 1.7 deg. (SSQ), 2.9 deg. (MSQ) and 4.1 deg. (LSQ), equivalent to spatial frequencies of about 0.3, 0.17 and 0.12 cyc/deg.

Cycle frequencies of 0 Hz, 0.8 Hz, 1.2 Hz, 2.5 Hz, 6.5 Hz, 7.5 Hz, and 10 Hz were tested.

2.3.2 Effects of short-term dynamic ON or OFF stimulation with different temporal and spatial frequencies on ChT in chickens treated with lenses

Chicks were treated monocularly with a −7D lens or a +7D lens. The same experimental set-up as described under (2.3.1) was used.

2.3.3 Effects of long-term exposure (7 days) and medium-term exposure (3 days) to ON-, OFF and square wave stimuli on ChT and eye growth

The medium square size (MSQ) of the checkerboard pattern was used. Baseline measurements of refractive error (RE), ocular biometry, and ChT were taken at 8–10 days of age. A −7D lens was placed in front of one eye of the animals in the morning of the following day, the contralateral eye served as internal control. Stimuli were presented daily between 9:00 AM and 6:00 PM, and they spent the remaining time of the day in the dark. After a treatment period of 3 days or 7 days measurements of refraction, biometry, and ChT were taken, and retinal and choroidal samples were collected for high pressure liquid chromatography (HPLC) and quantitative RT-PCR (qRT-PCT) analyses.

2.3.3.1 7 days treatment

Chicks were exposed to checkerboard stimuli (medium square size, MSQ) at different frequencies (1.2 Hz, 10 Hz, or static) and different wave types (ON, OFF, or square). Two different control groups were used: chicks in the room light (RL) control group ("RL-7d," $n = 7$) were raised under white room light (400 lux, spectral range, spectral range of light 380 to 780 nm), while chicks in the second control group ("static-7d," $n = 6$) were placed in an "arena" displaying stationary brightness in the checkerboard patterns. Illuminances for both control groups were approximately 400 lux, as in all other experimental groups. In addition, chicks were randomly assigned to the 1.2-Hz ON stimulus group (1.2-ON-7d, $n = 7$), 1.2-Hz OFF stimulus group (1.2-OFF-7d, $n = 7$), 1.2-Hz square wave stimulus group (1.2-square-7d, $n = 7$), 10-Hz ON stimulus group (10-ON-7d, $n = 7$), 10-Hz OFF stimulus group (10-OFF-7d, $n = 7$) and 10-Hz square wave stimulus group (10-square-7d, $n = 7$).

2.3.3.2 3 days treatment

Since we did not find a significant effect of the 1.2 Hz stimulus on ChT in the 7 day treatment groups, we omitted the 1.2 Hz ON and OFF group. Chicks were monocularly treated with a −7D lens and randomly assigned to one of the following groups: room light group (RL-3d, $n = 7$), static pattern group (static-3d, $n = 7$), 10-Hz ON stimulus group (10-ON-3d, $n = 7$), 10-Hz OFF stimulus group (10-OFF-3d, $n = 7$) and 10-Hz square wave stimulus group (10-square-3d, $n = 6$).

2.4 Measurements

2.4.1 Refractive error and ocular biometry

Refraction and ocular biometry were measured before and after treatment for the medium and long-term treatment. An automated version of infrared photoretinoscopy was used to measure the refractive error (27). Five readings per eye were taken and averaged for analysis. Ocular dimensions were measured using A-scan ultrasonography with a 11 MHz probe as previously described (28). The speed of sound in the lens of the chick was previously determined by Wallman and Adams (29). The cornea was topically anesthetized with one drop of 2% xylocaine solution before measuring. The depth of the anterior chamber (ACD), lens thickness (LT), vitreous chamber depth (VCD) and axial length (AL) were recorded, with five repeated measurements.

2.4.2 Spectral domain optical coherence tomography

OCT represents a highly precise, fast and convenient technique to measure ChT in alert chickens (28). OCT measurements (Spectralis OCT, Heidelberg Engineering, Germany, resolution mode: high speed, scan angle: 30 degrees, scan type: B-scan, 768 × 496 pixels, line scan, eye tracking not engaged, scan rate of the live image 8.8 frames/s, wavelength of measurement 1,060 nm) were taken once per day during 10:00 to 10:30 a.m., as previously described (28). The −7D lens was removed before measurement and cleaned carefully. The measurements were taken in a short time (usually within 1 min), and the lens was immediately put back on after each measurement. To ensure consistent measurements in the same fundal area, we held alert chicks by hand in front of the OCT camera and manually adjusted the position of their heads until the cornea was aligned perpendicular to the optical axis of the OCT camera and the fundal layers could be seen on the screen. Optimal alignment of the chicken eye was assumed when the image of the pupil in the left screen window was centered and the scan of the fundal layers in the right window was horizontally aligned. Scans became tilted when the eyes were not properly aligned. Repeated measurements involved re-alignment of the chick head and the eye in each case. Five images were analyzed for each eye and ChT was measured at 5 positions in each image. The approximate lateral distance between each of the five measurement positions within each image was 80 µm, covering a total lateral distance of about 320 µm. The ChT was measured manually using the publicly available software ImageJ,[1] being determined as the distance between the retinal pigment epithelium layer and the outer boundary of the choroid [as described in Liu et al. (30)].

2.4.3 Sample preparation

The chicks were sacrificed by inhaling an overdose of ether and the eyes were immediately enucleated. The eyeballs were cut perpendicularly into halves with a razor blade, 1 mm posterior to the ora serrata. The anterior segment was discarded, leaving only the posterior eye cup. The vitreous body was then removed and quickly frozen in liquid nitrogen. A circular tissue sample with an 8-mm diameter was cut from the central posterior eye cup using a biopsy punch, as previously described (31). The biopsy samples were consistently taken from the circular region just above the root of the pecten, in the central area. The sample was then transferred to a Petri dish under a dissecting microscope, with the retina facing up. Typically, the retina detached easily and was peeled off with an ophthalmic hook. The pigment epithelium was discarded, and the choroid was separated from the sclera using forceps and a hook. Any small clusters of retinal pigment epithelial cells remaining on the choroid were carefully brushed away under visual control. The retina was separated into two halves, one for high pressure liquid chromatography (HPLC) and one for qRT-PCR analysis, while the choroid was only used for HPLC analysis. Tissues were immediately frozen in liquid nitrogen and stored at −80°C for subsequent analysis.

2.4.4 Measurement of dopamine and metabolites via high pressure liquid chromatography

All vitreal samples were weighed and homogenized in 750 µL mobile phase (Thermo Fisher Scientific, Sunnyvale, CA, United States) using a tissue lyser and 5-mm stainless steel beads (TissureLyser LT, Qiagen, Hilden, Germany) at 50 Hz for 4 min. For retinal samples, 350 µL of mobile phase was added instead. A volume of 50 µL of retinal samples was reserved for protein concentration determination (BCA Protein kit, Thermo Scientific, Rockford, IL, United States). Following homogenization, all samples were centrifuged at 14,000 g for 10 min at 4°C. The resulting supernatant was filtered using a 0.2 µm nylon membrane filter (Thermo Scientific, Rockwood, MI, United States), and 25 µL of the filtered sample were directly injected into the HPLC system. Samples were analyzed for catecholamine and indolamine content via HPLC (Ultimate 3000 LC with electrochemical detection ECD 3000RS, Thermo Fischer Scientific) with coulometric detection utilizing an established HPLC method in our lab (32). In brief, a hypersil C18 column was used (150 mm × 3 mm, 3 µm) together with a test mobile phase (Thermo Fischer Scientific) containing 10% acetonitrile and 1% phosphate buffer. The flow rate was 0.4 mL/min and the potential at the first and second electrode was set to +370 and −200 mV, respectively. Dopamine, 3,4-dihydroxyphenylacetic acid (DOPAC), homovanillic acid (HVA, a metabolite of dopamine), serotonin and 5'-Hydroxyindolylessigsäure (HIAA) concentrations were determined with a high reproducibility (98%). The biogenic amine content in the retina was quantified as nanograms per milligram of protein (ng/mg protein), while in the vitreal, the concentration of the substances was determined relative to the wet weight (ng/100 mg wet weight). As described by others, vitreal DOPAC levels can be used as a sensitive measure of DA release from the retina (33). In addition, vitreal HVA levels can be used as an indirect measure of dopaminergic activity, as it has been shown that vitreal HVA levels correlate significantly with vitreal DOPAC levels (32).

2.4.5 Real-time PCR analysis

Total RNA was extracted from retina and choroid samples using the Qiagen RNeasy Mini Kit (Qiagen, Hilden, Germany), and the resulting RNA was treated with DNase Inactivation Reagent (AM1906, Invitrogen, Waltham, Massachusetts, United States) to eliminate contaminating chromosomal DNA according to the manufacturer's instructions. The concentration of RNA (ng/µL) was determined using the NanoDrop® ND-1000 Spectrophotometer (Thermo Fisher Scientific, Wilmington, United States), and the purity and quality of the nucleic acid were assessed via the OD260/OD280 nm absorption

1 https://imagej.net/software/fiji/

ratio. Subsequently, 1 μg of retinal RNA or 500 ng of choroidal RNA was reverse transcribed to generate first-strand cDNA using a mixture of oligo(dT)15 and random primers. GoScript (Promega, Madison, United States) was used to reverse transcribe the RNA while the addition of a Rnase inhibitor (Thermo Fisher Scientific, Wilmington, United States) prevented RNA degradation.

The primer pair for melanopsin (*OPN4*) (Table 1) was designed using the Primer-BLAST tool (NCBI) (forward primer 5′-TAGGCGTCTGGCTGTACTCT-3′; reverse primer 5′-TGTGTAGGCACGGACTGATG-3′; product length 136 Bp). The primer pairs for amplification of *GJD2*, *OPN5*, *RALDH2* and *BMPR1A*, *β*-actin *(ACTB)* and Hypoxanthinephosphoribosyl-transferase (HPRT) have already been published [*RALDH2* and *EGR-1* (34); *GJD2* (35); *BMPR1A* (36); *OPN5* (21); *BACT* and *HPRT* (37), Table 1].

Efficiency of the primers was calculated with the equation $E = 10^{(-1/\text{slope})}$, where the slope of the standard curve was derived from serial cDNA dilutions. PCR was performed using the an iCycler device (CFX96TM System, BioRad, Hercules, United States), with the cycling conditions set as follows: pre-activation phase for 3 min at 95°C, followed by 39 cycles of 95°C for 10 s, 59°C for 15 s, and 72°C for 15 s, with a final extension at 95°C for 3 min. Melting curve analysis was conducted subsequently. Single pure products were verified with a single peak. PCR was carried out in a 96-well plate with 2 ng of cDNA per well, using the QuantiNova SYBR Green PCR Kit (Qiagen, Hilden, Germany). Triplicate reactions were performed for all samples. Hypoxanthinephosphoribosyl-transferase (*HPRT*) and β-actin (*ACTB*) were used as reference genes. The mRNA expression level was analyzed using mean normalized expression (MNE), which is directly proportional to the amount of the target gene relative to the reference gene. MNE was calculated separately for either *ACTB* or *HPRT* using the mean cycle threshold (CT) value of the target and reference genes and taking the efficiency (*E*) of the PCR reaction into account:

$$\text{MNE} = \left(E_{\text{reference}}\right)^{\text{CTreference,mean}} / \left(E_{\text{target}}\right)^{\text{CTtarget,mean}}$$

2.4.6 Statistics

Data are shown as the mean ± SEM. The changes in axial length, vitreous chamber depth and ChT were also calculated (ΔX, ΔN, lens-treated eye = X; fellow eye = N). The difference in the changes in treated and contralateral control eyes is referred to as the relative change (ΔX − ΔN). A power calculation was undertaken to determine the group sizes required to achieve 80% power in observing a 1 D change in refractive development (when the standard deviation (SD) is approximately 0.6 D), a 0.075 mm change in axial length growth (when SD is 0.045 mm), 0.25 ng difference in retinal dopamine content (when SD is 0.15 ng) and 50 μm ChT change (when SD is 30 μm). With a group size of 7 chicks, differences between treatment groups should become significant at the 5% level. The normal distribution of the variables was confirmed via Shapiro–Wilk normality test.

The interocular differences (lens-treated vs. fellow eye) were analyzed with paired *t*-test. The difference between each two groups (exp. vs. exp., fellow vs. fellow) were compared using two-way mixed analysis of variance (ANOVA), with "eye" and "group" being within- and between-subject factors, respectively. Tukey's multiple comparisons test was applied in *post hoc* analyses. Multifactorial ANOVAs were used to evaluate the impact of image size, character, frequency and lens treatment on ChT changes and the interaction effect of these variables. If a significant main effect of one of the parameters was detected, the data was split and one-way ANOVA was used for comparison, followed by Tukey's multiple comparisons test. ChT measured at different times after stimulation was compared with the respective individual thickness at baseline using a two-way ANOVA with repeated measures and Dunnett's test for multiple comparisons. "time" and "eye" were considered as two within-subject factors. Values of $p < 0.05$ were considered significant. Statistical analyses were done using commercial software JMP 16 (SAS Institute, Cary, NC, United States) and GraphPad prism 8 (San Diego, CA, United States).

3 Results

3.1 Effects of short-term (3 h) dynamic ON/OFF stimulation with different temporal and spatial frequency on changes in ChT

3.1.1 Effects of ON/OFF stimulation in the control group with normal vision

The field sizes of the checkerboard pattern had a significant main effect on short-term ChT changes with the smallest squares (SSQ)

TABLE 1 Primer sequences.

Gene	Primer sequence	
	Forward primer (5′-3′)	Reverse primer (5′-3′)
HPRT	TGGCGATGATGAACAAGGT	GCTACAATGTGGTGTCCTCCC
ACTB	CTGAACCCCAAAGCCAAC	CACCATCACCAGAGTCCATCAC
OPN4	TAGGCGTCTGGCTGTACTCT	TGTGTAGGCACGGACTGATG
RALDH2	GCATCTGCTGCCTTCTCCC	AGGCGAGCTGCTCTCACTG
EGR-1	CTTGACCACGCACATCCGC	GCTGAGACCGAAGCTGCCT
GJD2	TTGGTGTTCATGTTTGCTGTCA	CCAGCCCAAGTGGTTCAGTT
BMPR1A	TGTCACAGGAGGTATTGTTGAAGAG	AAGATGGATCATTTGGCACCAT
OPN5	GGGCTGGCTTCTTCTTTGGCTGTGG	CAGGCAGATAAAGGCATGGTGT

causing the largest decrease in ChT (Multifactorial ANOVA: size: $p < 0.0002$; mean delta ChT: SSQ: −22.8 ± 2.3 μm, MSQ: −11.2 ± 2.2 μm, LSQ: −13.4 ± 1.9 μm) while frequency had no significant effect ($p = 0.2877$) and there was no difference between ON and OFF stimulation ($p = 0.421$). There was a significant interaction between temporal frequency and size (Multifactorial ANOVA: frequency × size: $p = 0.0024$). The data was therefore split according to stimulus size (Figures 1A–C) and frequency (Figures 1D–I). It was found that the sawtooth-shaped temporal luminance profile (ON/OFF) had a significant effect when small squares were used (Figure 1A; $p = 0.0024$; mean ChT change ON: −25.9 μm, OFF: −19.0 μm) and frequency significantly influenced ChT when medium size squares were used (Figure 1B, $p = 0.010$). Only one stimulus (1.2 Hz ON, MSQ) induced choroidal thickening (+4.8 ± 6.5 μm), all others made the choroid thinner. For this reason, medium size square (MSQ) stimuli were used for the medium- and long-term treatment.

Interactions between spatial and temporal frequencies are shown in Figures 1D–I. At 0.8 Hz, the largest checkerboard stimuli (LSQ) caused less choroidal thinning than the smallest (SSQ) with both types, ON and OFF (one-way ANOVA, Figure 1D ON: $p < 0.01$; Figure 1G OFF: $p = 0.0189$). The medium checkerboard stimulus (MSQ) had a similar effect on ChT changes as the large stimulus (LSQ) in the ON condition, and the small (SSQ) stimulus in the OFF condition. At 1.2 Hz the medium size squares (MSQ) induced significantly less choroidal thinning than LSQ and SSQ, and only with the ON stimulus (Figures 1E,H). There was no effect of square size on ChT changes at 10 Hz temporal flicker stimulation (Figures 1F,I).

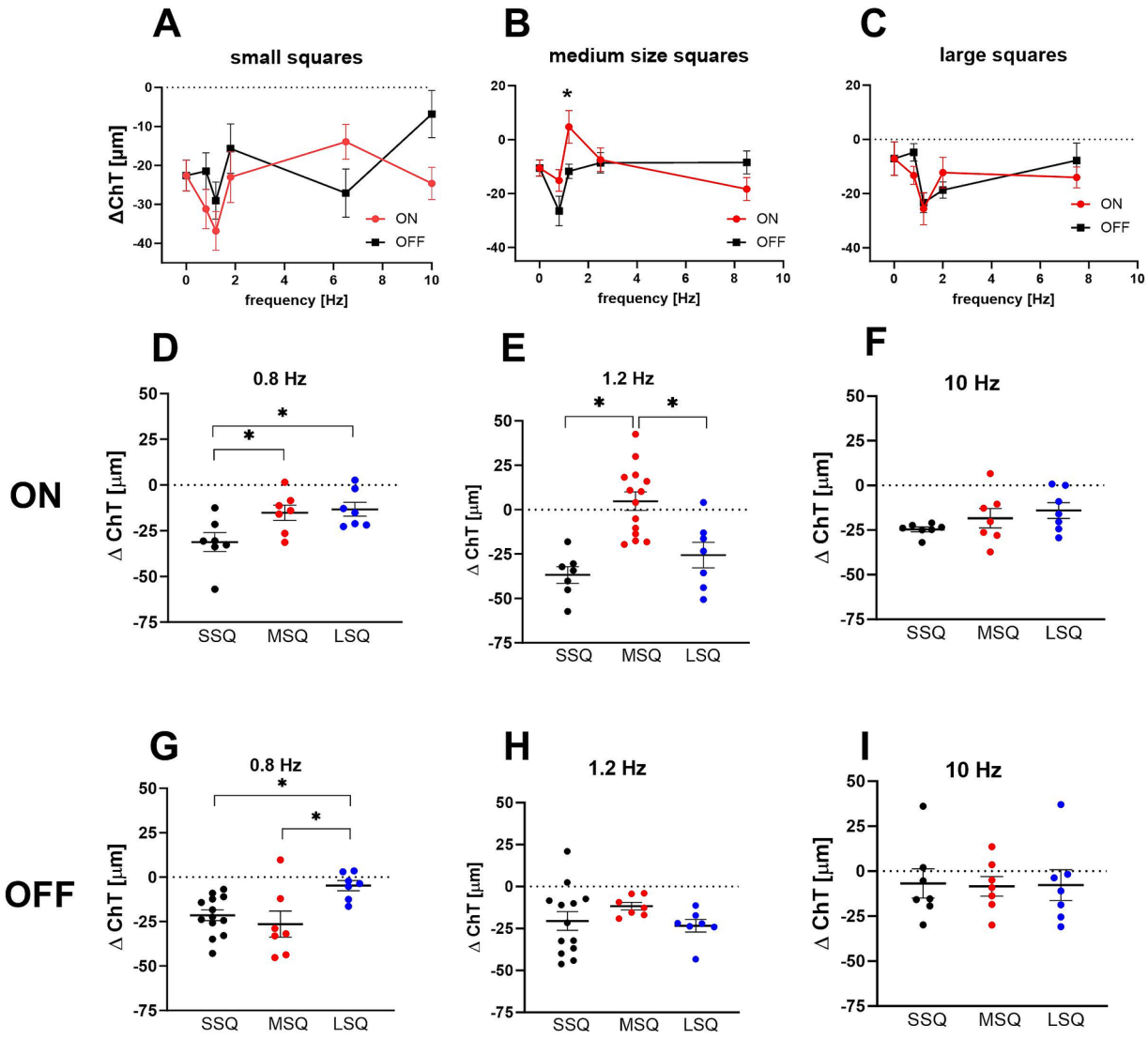

FIGURE 1
(A–C) Effect of short-term dynamic ON/OFF stimuli with different temporal and spatial frequency on changes in choroidal thickness in control chicks. The size of the stimuli had a significant main effect, with the smallest squares causing the largest decrease in ChT. Only one of the stimuli (B: 1.2 Hz ON, MSQ) induced an increase in choroidal thickness (+4.8 ± 6.5 μm) while OFF stimuli at this field size and frequency caused a significantly thinner choroid (−11.7 ± 2.7 μm). Graphs show mean data ± SEM. Un-paired *t*-tests: *$p < 0.05$. **(D–I)** The interaction between temporal and spatial frequency on choroidal thickness changes was highly significant. In combination with 0.8 Hz flicker large stimuli (LSQ) produced significantly smaller changes in choroidal thickness than small stimuli (SSQ) **(C,D)**, whereas under 1.2 Hz flicker choroidal thickness was thickest in the chicks treated with medium size ON stimuli **(E)**. Graphs show mean data ± SEM. One-way ANOVA, Tukey *post hoc* analysis: *$p < 0.05$.

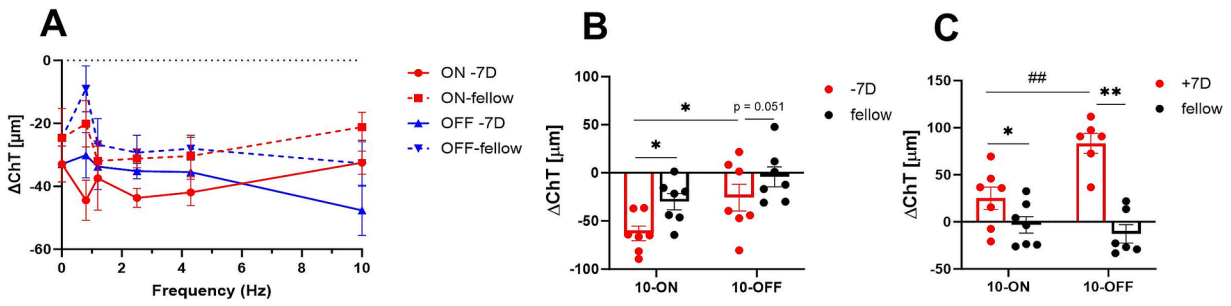

FIGURE 2
(A) Effect of negative lens treatment on choroidal thickness changes under different flicker frequencies (small square size). Three hours of treatment induced on average 11.7 µm more choroidal thinning compared to the contralateral eyes. Also, the flicker frequency of the checkerboard pattern has a significant main effect. The graph shows mean data ± SEM. **(B,C)** Comparison of the effect of plus lens treatment and negative lens treatment on choroidal thickness. Three hours of negative lens treatment induced a significantly larger reduction in choroidal thickness under ON flicker of 10 Hz and medium size checker-board stimuli compared to 10 Hz OFF flicker (10 Hz ON vs. 10 Hz OFF: −62.8 ± 7.6 µm vs. −25.6 ± 13.9 µm), whereas 3 hours of plus lens treatment induced a larger increase under OFF flicker of 10 Hz (trend, $p = 0.052$). Graphs show mean data ± SEM. Paired *t*-test: $^{*}p < 0.05$. Unpaired *t*-test: $^{\#\#}p < 0.01$.

3.1.2 Effects of short-term exposure in chicken with negative lenses (small size checkerboard patterns) and of medium size checkerboard patterns on eyes with negative or positive lenses

Chicks were treated unilaterally with −7D lenses, the contralateral eye was left open and served as control. The small size checkerboard-pattern was used (SSQ). Three hours of negative lens treatment induced on average 11.7 µm thinner choroids compared to the control eyes (Figure 2A). The treatment (negative lens vs. control) and frequency had a significant main effect (multifactorial ANOVA: treatment: $p < 0.0001$; frequency: $p = 0.037$) but the type of flicker (ON/OFF/no flicker) had not (Multifactorial ANOVA: type of flicker: $p = 0.20$).

Medium size checkerboard pattern (MSQ) was used in addition. Three hours of negative lens treatment induced significantly more choroidal thinning with ON flicker, compared to OFF flicker (Figure 2B: 10 Hz ON vs. 10 Hz OFF: −62.8 ± 7.6 µm vs. −25.6 ± 13.9 µm), whereas three hours of positive lens treatment induced a larger increase with ON flicker (Figure 2C: 10 Hz ON vs. 10 Hz OFF: −83.3 ± 10.6 vs. −25.1 ± 12.8 µm).

3.2 Effects of medium- and long-term treatment with ON, OFF and square wave stimuli (medium size, MSQ) on myopia development and eye growth

3.2.1 Refraction

All groups of chicks exhibited a significant myopic shift after 3 or 7 days of lens wear. There was no significant difference in refractive development in the fellow eyes. The negative lens-treated eyes were more myopic after 7 days of treatment under 10 Hz dynamic ON flicker (10-ON) than those under a stationary stimulus, as shown in Figure 3A (ΔRE: −4.66 ± 0.34 D vs. −2.86 ± 0.26 D, $p = 0.03$). Furthermore, 3 days of treatment with 10 Hz ON stimulation induced more myopia than 10 Hz OFF stimulation in the lens treated eye (ΔRE: 10-ON vs. 10-OFF: −2.59 ± 0.24 D vs. −1.78 ± 0.20 D, $p = 0.04$, Figure 3B).

3.2.2 Ocular biometry

After 3 and 7 days of treatment, VCD was significantly longer in negative lens-treated eyes, compared to the contralateral eyes in all groups (Figures 3C,D). Compared to the control group in room light, none of the stimuli had a significant effect on the growth of the vitreous chamber depth, neither in the lens-treated eyes nor in the contralateral control eyes (Figures 3C,D).

As expected, the 7-day treatment induced a significantly greater eye length growth in the negative lens-treated eyes compared to the respective untreated control eyes, but not to the same extent in all groups. A comparison of the treatment groups showed that the change in axial length in the negative lens-treated eyes was significantly greater in the 10-ON group than those in the RL, static, and 1.2-Hz groups (ΔAL: 1.55 ± 0.02 mm in 10-ON vs. 1.25 ± 0.09 mm in RL, $p = 0.002$; vs. 1.23 ± 0.03 mm in static, $p = 0.001$; vs. 1.27 ± 0.06 mm in 1.2-ON, $p = 0.004$, vs. 1.22 ± 0.07 mm in 1.2-OFF, $p = 0.0005$; vs. 1.31 ± 0.04 mm in 1.2-square, $p = 0.03$, Figure 3E). Furthermore, the fellow eyes in the 10-OFF group developed significantly longer eyes compared to RL and 1.2-ON groups (ΔAL: 1.07 ± 0.04 mm in 10-OFF vs. 0.76 ± 0.06 mm in RL, $p = 0.001$; vs. 0.79 ± 0.06 mm in 1.2-ON, $p = 0.004$, Figure 3E).

After 3 days of treatment, the lens-treated eyes were longer than the fellow eyes only in the RL and static stimulus groups. All groups kept under a 10 Hz stimulus, whether ON, OFF, or square, did not have significantly longer axial lengths in the negative lens-treated eyes compared to their fellow eyes. There was no significant difference in axial length between the different groups after only 3 days (Figure 3F).

3.3 Effect of frequency and stimulus pattern on ChT changes

We combined the treatment groups belonging to the same category (same frequency or same stimulus pattern, respectively) to analyze the main effect of flicker frequency on ChT changes on the one hand and stimulus type on the other hand. All stimulus paradigms resulted in initial choroidal thinning, with some recovery over the 7 days (also in

10.3389/fmed.2024.1469275

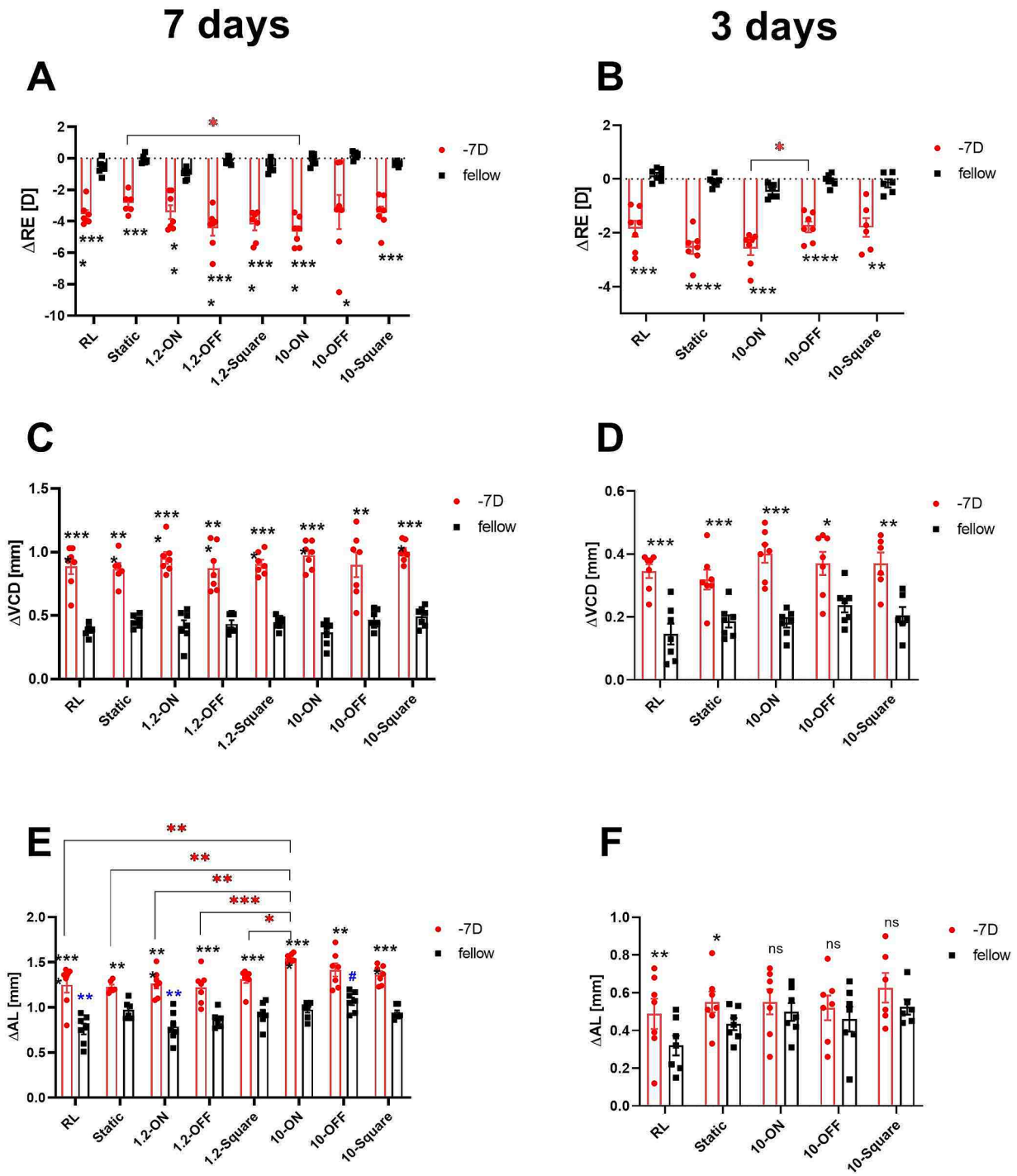

FIGURE 3
Effects of different stimuli on eye growth after treatment for 7 days (A,C,E) and for 3 days (B,D,F). After 7 days of treatment, negative lens-treated eye exposed to 10-Hz ON stimulus were more myopic than those treated with a static pattern **(A)**. The 10 Hz ON stimulus also induced more myopia than the 10-Hz OFF stimulus in the medium-term experiment **(B)**. None of the stimuli influenced the increase in VCD induced by negative lens **(C,D)**. On the contrary, in the long-term experiment, a significant effect on the change in AL in LIM eyes was observed in the 10-ON group, which exhibited longer AL compared to the RL, static, and 1.2-Hz groups **(E)**. In addition, the AL of the fellow eyes in 10-OFF group was longer compared to the RL group. No significant differences were found among the lens treated groups after 3 days of treatment. However, it is worth noting that also no interocular differences between the contralateral control eyes and the −7D lens treated eyes were found in all groups exposed to 10-Hz flicker (ON, OFF, static) **(F)**. Data are shown as mean ± SEM. The black asterisks denote interocular differences assessed via paired *t*-tests. Red asterisks indicate differences among groups determined by Tukey's *post hoc* test. Blue asterisks indicate differences compared with the 10-OFF group (denoted by blue pound symbols). *$p < 0.05$, **$p < 0.01$, ***$p < 0.001$, and ****$p < 0.0001$; ns: not significant.

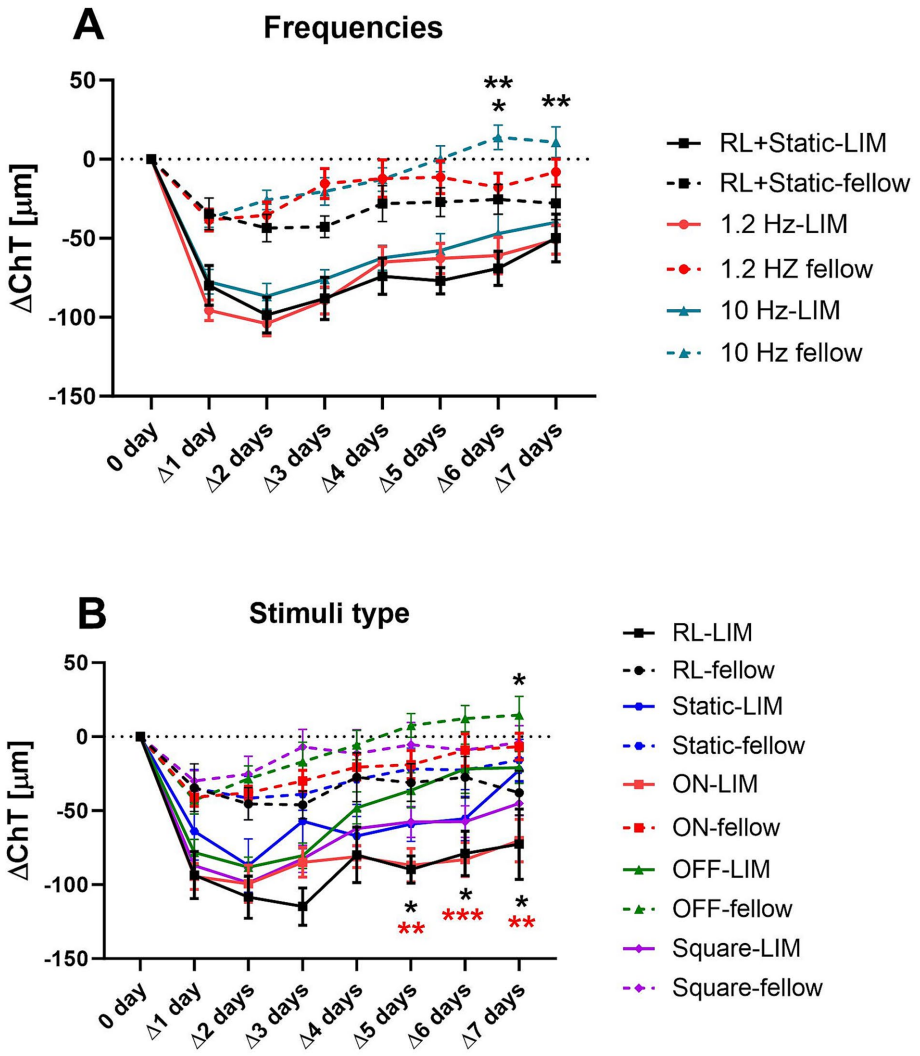

FIGURE 4
Effects of different frequencies **(A)** and wave types **(B)** on the change of ChT (compared to the respective baseline measurement). All stimulus paradigms resulted in initial choroidal thinning, with some recovery over the 7 days. The high frequency stimulation resulted in an increase in ChT in the 10 Hz fellow eyes on the 6th and 7th day **(A)**. When analyzing the effect of different stimulus patterns, only OFF stimuli increased the ChT, in the fellow and lens treated eyes **(B)**. The asterisks in **(A)** indicate the level of significance in comparison to the 10-Hz group, while those in **(B)** indicate the level of significance in comparison to the OFF group. Data were shown as mean ± SEM. *$p < 0.05$, **$p < 0.01$, and ***$p < 0.001$.

room light). Our results showed that the time course of ChT changes was not affected by the frequency of flicker light in the lens treated eyes. But in the fellow eyes, we detected a significant increase in ChT as shown in Figure 4A. Here, the choroid was significantly thicker after 6 days of treatment with 10-Hz flicker (ΔChT: 13.84 ± 7.83 µm) compared to the fellow eyes in the experiment with 1.2 Hz flicker (−17.73 ± 8.76 µm, $p = 0.02$) and also, if compared to fellow eyes in room light or with static patterns (−25.34 ± 9.47 µm, $p = 0.005$). On day 7, the choroid was significantly thicker in fellow eyes at 10 Hz flicker (ΔChT: 10.79 ± 9.64 µm), compared to room light or with static patterns (−27.84 ± 10.41 µm, $p = 0.007$). At 1.2 Hz, the difference to fellow eyes was no longer significant (−8.14 ± 8.27 µm, $p = 0.24$, Figure 4A).

When analyzing the different patterns of stimuli (ON, OFF, square wave, static), we found that, compared to room light, only the OFF stimulus had a significant effect on ChT in both negative lens-treated and fellow eyes. The choroid remained thicker in eyes treated with the OFF stimulus and negative lenses, compared to room light or compared to ON stimulation, at least during the last 3 days of the experiment (ΔChT on the 5th day: −36.26 ± 11.90 µm in the OFF group vs. −89.76 ± 9.20 µm in the RL group, $p = 0.04$, and vs. −86.89 ± 11.25 µm in the ON group, $p = 0.009$; ΔChT on the 6th day: −21.68 ± 16.55 µm in the OFF group vs. −78.91 ± 15.05 µm in the RL group, $p = 0.02$, and vs. −83.11 ± 11.53 µm in the ON group, $p = 0.0007$; ΔChT on the 7th day: −20.85 ± 10.79 µm in the OFF group vs. −72.66 ± 23.67 µm in the RL group, $p = 0.049$, and vs. −70.24 ± 14.35 µm in the ON group, $p = 0.01$, respectively, Figure 4B). Furthermore, in fellow eyes, the choroid was also thicker in eyes treated with the OFF stimulus, compared to in room light on the 7th day (14.60 ± 12.65 µm vs. −37.96 ± 14.89 µm, $p = 0.046$, Figure 4B). No significant changes were detected when compared to ON, square or static pattern stimuli.

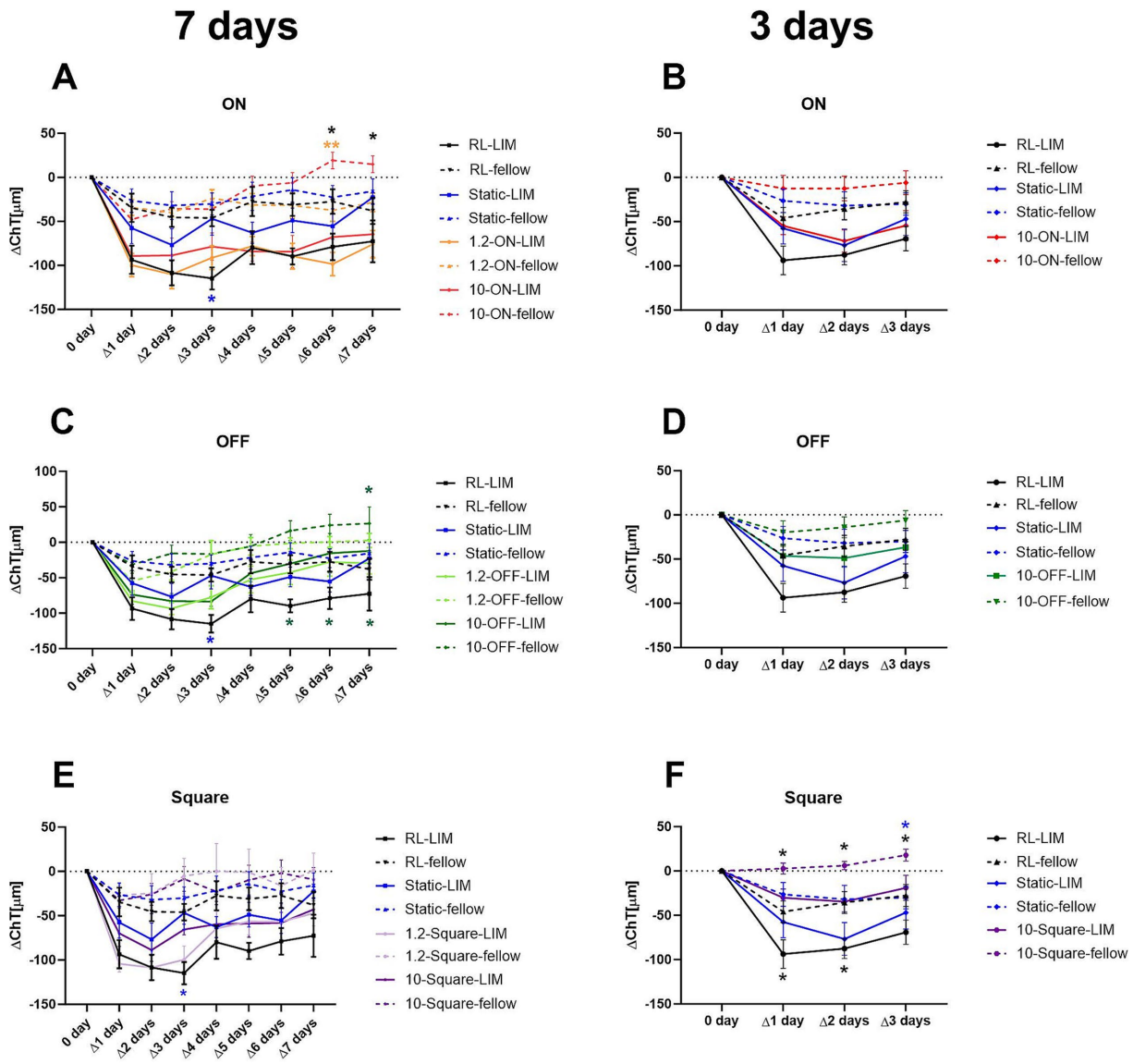

FIGURE 5
Effect of different stimuli on the change of ChT after 7 days **(A,C,E)** and medium-3 days of treatment **(B,D,F)**. In the long-term experiment, the 10-Hz ON stimulus thickened the choroid in the fellow eyes **(A)**, whilst the 10-Hz OFF stimulus increased the ChT in both eyes **(B)**. The square wave stimulus did not have a significant influence on the ChT **(C)**. In the medium-term experiment, no significant differences were detected with ON or OFF stimuli **(B,D)**. However, the choroid was thickened by the square wave stimulus in both eyes **(F)**. Data were shown as mean ± SEM. *$p < 0.05$ and **$p < 0.01$.

3.4 Effects of different stimuli and time on ChT

ChT decreased strongly during the first day of stimulation. This was true for all eyes, including the fellow eyes, but here to a lesser extent. The 10 Hz OFF stimulus had the strongest effect on the ChT. In this group, the choroid was significantly thicker from day 5 to the end of the experiment than in chicks kept under room light (RL vs. 10 Hz-OFF: Δ5 days: −89.76 ± 9.20 μm vs. −30.14 ± 17.40 μm, $p = 0.048$; Δ6 days: −78.91 ± 15.05 μm vs. −15.47 ± 27.81 μm, $p = 0.03$; Δ7 days: −72.66 ± 23.67 μm vs. −12.20 ± 15.82 μm, $p = 0.045$, two-way repeated measures ANOVA with Tukey's test, Figure 5C). A similar effect was observed in the 10 Hz-OFF fellow eyes, although only on the last day. In the 10 Hz ON fellow eyes, ChT was also increased at days 6 and 7 (Δ6 days: 19.37 ± 9.46 μm in 10 Hz-ON group vs. −27.35 ± 13.99 μm in RL group, $p = 0.04$, and vs. −37.46 ± 12.48 μm in 1.2 Hz-ON group, $p = 0.008$; Δ7 days: 14.99 ± 9.54 μm in 10 Hz-ON group vs. −37.96 ± 14.89 μm in RL group, $p = 0.02$, Figure 5A). In contrast, the 1.2 Hz and 10 Hz square wave stimuli had no effect on ChT, neither in the negative lens treated nor the fellow eyes compared to the static and room light groups (Figure 5E). The experiment was repeated, limiting the treatment to 3 days because we wanted to collect samples for gene expression studies comparing the effect of long-term and medium-term treatment. The time course of ChT changes during the first 3 days (Figures 5B,D) was similar to that observed in the long-term treatment experiment (Figures 5A,C). Specifically, there was a rapid decrease in ChT during the first day. ChT changes in the 10 Hz-ON and

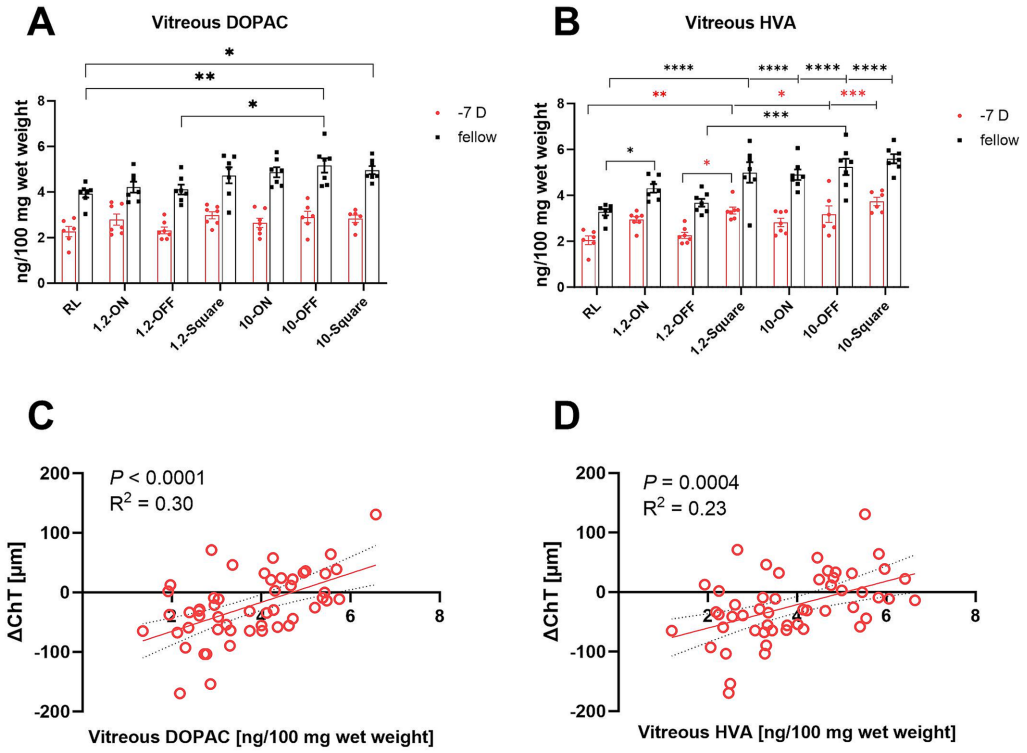

FIGURE 6
Effect of different stimuli on the level of retinal dopamine metabolites. The 10-Hz OFF and 10-Hz square stimuli increased the level of vitreal DOPAC in the fellow eyes **(A)**. All high-frequency patterns and the 1.2-Hz square stimulus increased the amount of HVA in the vitreal in the fellow eyes. The high frequency stimuli also increased the level of vitreal HVA in LIM eyes, except for the 10-Hz ON stimulus. In addition, the fellow eyes in 1.2-ON group contained more vitreal HVA in comparison to the RL group **(B)**. The change in ChT after 7 days (RL, 10-ON, 10-OFF, 10-square group data are shown) were positively correlated with the level of vitreal DOPAC **(C)** and vitreal HVA **(D)**. Data are shown as mean ± SEM. $*p < 0.05$, $**p < 0.01$, $***p < 0.001$, and $****p < 0.0001$.

10 Hz-OFF flicker groups were not significantly different from that in room light and under static stimuli. However, the chicks treated with 10 Hz square wave stimulus had a significantly thicker choroid than those treated with RL during the first 2 days in LIM eyes (RL vs. 10-square: Δ1 day: −93.80 ± 16.13 μm vs. −30.24 ± 9.85 μm, $p = 0.01$; Δ2 days: −87.58 ± 11.16 μm vs. −34.58 ± 11.48 μm, $p = 0.049$, Figure 5F), and during the first 3 days in the fellow eyes (RL vs. 10-square: Δ1 day: −45.94 ± 12.10 μm vs. 2.72 ± 6.14 μm, $p = 0.02$; Δ2 days: −35.56 ± 12.28 μm vs. 6.07 ± 4.65 μm, $p = 0.04$; Δ3 days: −27.69 ± 12.40 μm vs. 17.89 ± 6.73 μm, $p = 0.02$, Figure 5F). In addition, the ChT of the fellow eyes in 10-square group was also thicker than that in the static stimulus group on the 3rd day (Static vs. 10-square: −30.16 ± 12.62 μm vs. 17.89 ± 6.73 μm, $p = 0.02$, Figure 5F).

We also investigated whether initial changes in ChT that occurred on the first day of lens treatment were correlated with later changes in axial length and vitreous chamber depth. For this analysis, the changes in ChT relative to baseline on day 0 were determined separately for each eye. The values of the contralateral control eyes were then subtracted from those of the lens-treated eyes (ΔX − ΔN). We found that initial changes in ChT relative to baseline between the two eyes (ΔX − ΔN: day 1) were not significantly correlated with changes in axial length and vitreous chamber depth after 7 days of treatment (ΔX − ΔN ChT day 1 vs. ΔX − ΔN AL change day 7: $p = 0.099$, $R^2 = 0.0504$). In contrast, relative ChT changes at day 5, day 6 and day 7 showed a significant association with myopia development (Supplementary Figure S2A: AL: $R^2 = 0.1241$, $p < 0.01$; Supplementary Figure S2B: VCD: $R^2 = 0.0977$, $p < 0.05$). After treatment of 3 days, only axial length changes and ChT showed a weak but significant correlation (medium term treatment: $R^2 = 0.0763$, $p < 0.05$).

Interestingly, ChT changed significantly during the 7 days treatment in some groups. Pronounced recovery was observed for both 1.2 Hz and 10 Hz OFF stimulation which showed up as an increase in ChT during the last 3 days of the experiment (Supplementary Table S1).

We also investigated whether initial changes in ChT that occurred on the first day of lens treatment were correlated with later changes in choroidal thickness. In an analysis of the entire data set, a significant correlation between changes on day 1 and changes at each subsequent day was observed. Obviously, animals that showed a large decrease in ChT in eyes with negative lenses, compared to their fellow eyes on day 1 also showed a larger difference on subsequent days. However, the significance of the correlation declined steadily over the week of treatment (Supplementary Table S2). In a separate analysis of this relationship in each of the treatment groups, the predictive power was high during the first 3 days in the animals in the static stimulus group and from day 2 to day 6 in the 10 Hz OFF group but there was no correlation with any other stimulus.

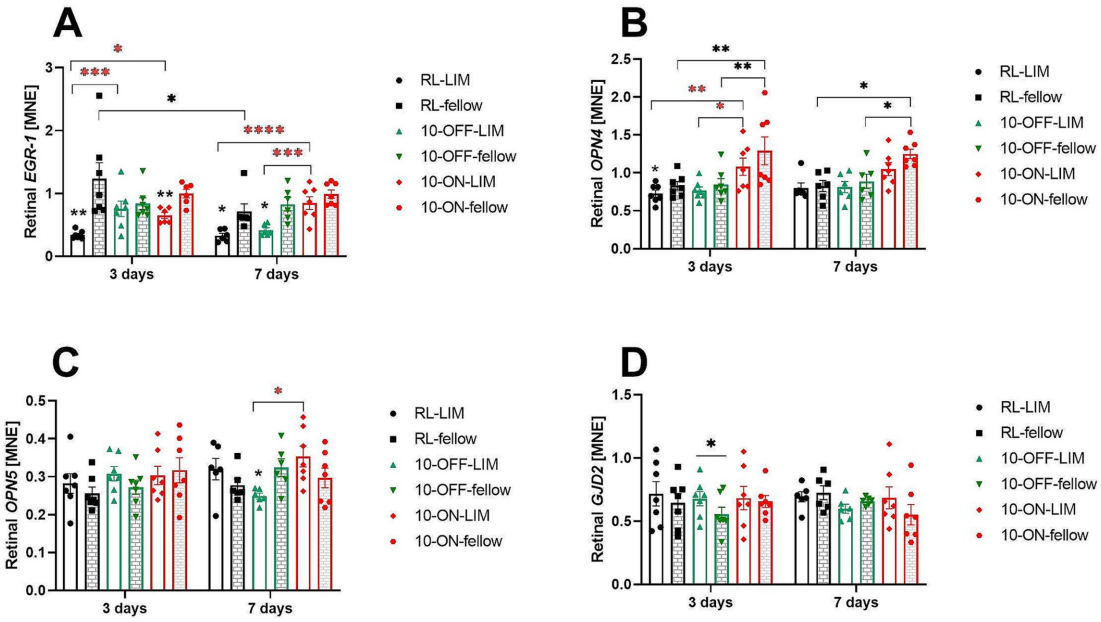

FIGURE 7
The mRNA expression level of myopia candidate genes in the retina after long or short-term treatment. Negative lens treatment significantly decreased retinal *EGR-1* expression in room light (RL), in 10 Hz ON flicker (after 3 days), and in 10 Hz OFF flicker (after 7 days). Compared to the RL-LIM eyes, *EGR-1* mRNA expression in the lens treated eyes was significantly higher, both in the 10-Hz ON and 10-Hz OFF stimuli, after 3 days. This effect persisted in the 10-ON group in the long-term experiment **(A)**. A temporal effect was observed in the fellow eyes of the RL group, as the level of retinal *EGR-1* mRNA decreased over time **(A)**. After 3 days of treatment, the 10-Hz ON stimulus induced a significant increase in the level of retinal *OPN4* mRNA in both eyes, compared to the RL and 10-OFF groups. However, after 7 days of treatment, this effect was observed only in the fellow eyes **(B)**. The expression of retinal *OPN5* mRNA was higher in LIM eyes in the 10-ON group than that in the 10-OFF group **(C)**. In the short-term experiment, only the 10-OFF group showed an interocular effect in the expression of retinal *GJD2* mRNA, which was an elevation in the LIM eyes **(D)**. Data were shown as mean ± SEM. $*p < 0.05$, $**p < 0.01$, $***p < 0.001$, and $****p < 0.0001$.

3.5 Effects of the different visual stimuli on retinal dopamine metabolism

Vitreal levels of dopamine metabolites DOPAC and HVA can be used as a sensitive measure of dopamine release from the retina (33). In line with previous findings (38), negative lens treatment reduced the amount of dopamine metabolites DOPAC and HVA with high significance in all groups (Supplementary Table S3). In addition, frequency (0 Hz, 1.2 Hz, or 10 Hz) and stimuli pattern (ON, OFF, square wave, room light) had a significant main effect on dopamine metabolism (multifactorial ANOVA: DOPAC: treatment and frequency: $p < 0.0001$, Figure 6A; HVA: treatment, frequency and stimuli pattern: $p < 0.0001$, Figure 6B). When vitreal HVA data were grouped according to stimulus type, HVA content was significantly higher when chicks were stimulated with square wave stimuli compared to room light and OFF stimuli, and also higher under ON stimulation than under room light (one-way ANOVA, $p = 0.0002$, Figure 6B). A recent study in our lab (15) found a significant increase in DOPAC and HVA level in chicks kept under 1 Hz-ON vs. 1 Hz-OFF stimulation. Although, there was no significant difference between 1.2 Hz-ON and 1.2 Hz-OFF stimuli in our present study, a similar trend was seen in terms of a higher mean level of vitreal HVA in fellow and −7D lens-treated eyes in the 1.2-ON vs. 1.2 OFF group. When the vitreal HVA data were grouped according to frequency, vitreal HVA was significantly higher under flicker light, compared to room light, and also higher at 10 Hz flicker than at 1.2 Hz flicker (one-way ANOVA, $p < 0.0001$, Figure 6B).

Overall, the largest changes were observed in fellow control eyes under 10 Hz flicker with the OFF stimulus, with significantly higher level of vitreal DOPAC than in room light and 1.2 Hz OFF flicker (10-OFF vs. RL: 5.17 ± 0.31 vs. 3.92 ± 0.17 ng/100 mg wet weight, $p = 0.003$; vs. 1.2-OFF: 4.11 ± 0.21 ng/100 mg wet weight, $p = 0.02$, Figure 6A). Also, the 10 Hz square wave stimulus increased vitreal DOPAC levels in the fellow control eyes. Also, the 1.2 Hz and 10 Hz ON, OFF and square wave stimuli increased the amount of vitreal HVA level in fellow eyes, compared to room light.

In the negative lens-treated eyes, vitreal HVA content was significantly higher in at 10 Hz OFF and 10 Hz square wave stimulation compared to room light (RL vs. 10-OFF: 2.05 ± 0.19 vs. 3.18 ± 0.36 ng/100 mg wet weight, $p = 0.03$; vs. 10-square: 3.73 ± 0.18 ng/100 mg wet weight, $p = 0.0002$, Figure 6B). Vitreal HVA levels were also increased at 1.2 Hz square wave stimulation, compared to room light and to 1.2 Hz OFF stimulation.

After 1 week of treatment, vitreal DOPAC and HVA content were correlated with the changes in ChT (Figures 6C,D) when data from all eyes were pooled. The higher their content, the thicker was the choroid ($p < 0.0001$, $R^2 = 0.30$; $p = 0.0004$, $R^2 = 0.23$, respectively, Figures 6C,D).

3.6 Effects of ON and OFF stimuli and treatment duration on gene expression

3.6.1 Retina

Expression of candidate genes that were previously associated with myopia development was measured after 3 and 7 days of negative lens

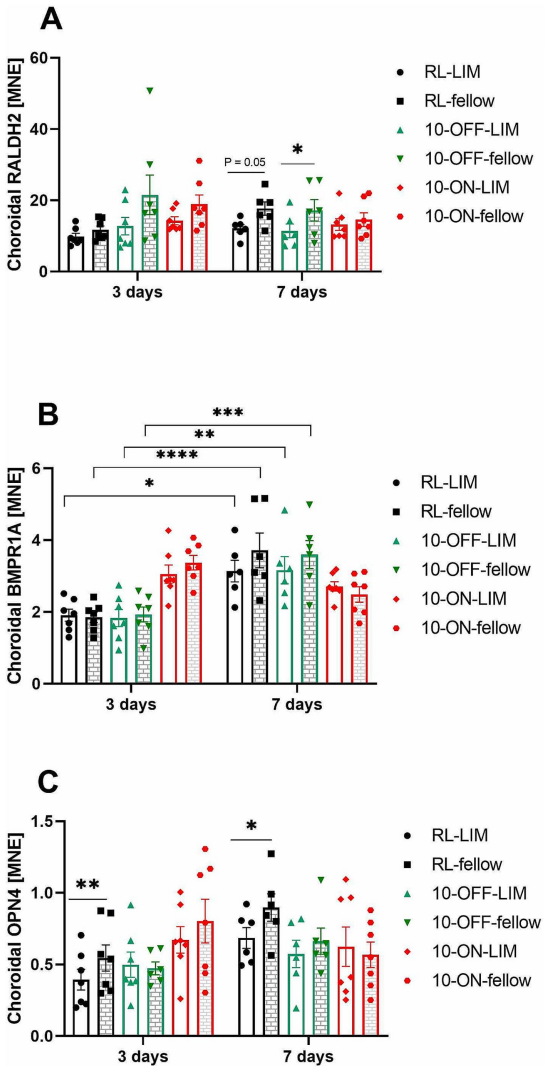

FIGURE 8
The mRNA expression level of myopia-related genes in the choroid after long or short-term treatment. The expression of choroidal *RALDH2* mRNA was decreased by −7D lens in the RL and 10-OFF group after treatment for 7 days **(A)**. In both eyes of the RL and 10-OFF groups, a significant temporal effect was shown in the expression of choroidal *BMPR1A* mRNA, which was elevated over time **(B)**. The expression of choroidal *OPN4* mRNA was found to be decreased in LIM eyes in the RL group **(C)**. Data were shown as mean ± SEM. $*p < 0.05$, $**p < 0.01$, $***p < 0.001$, and $****p < 0.0001$.

treatment, both in room light as well as with 10-Hz ON and 10-Hz OFF flicker light (Figure 7). As found in previous studies (34), *EGR-1* mRNA levels decreased in negative lens-treated eyes. This effect was found in room light, both after 3 days (RL-LIM vs. RL-fellow: 0.34 ± 0.02 vs. 1.24 ± 0.25, $p = 0.01$) and 7 days (RL-LIM vs. RL-fellow: 0.33 ± 0.04 vs. 0.71 ± 0.12, $p = 0.02$, Figure 7A). *EGR-1* mRNA expression was also lower in the negative lens-treated eyes compared to fellow eyes at 10 Hz ON flicker after 3 days of treatment (0.65 ± 0.05 vs. 1.00 ± 0.07, $p = 0.047$) and 10 Hz OFF flicker after 7 days (0.42 ± 0.04 vs. 0.83 ± 0.11, $p = 0.02$). However, *EGR-1* mRNA expression in eyes with negative lenses was still significantly higher at 10 Hz ON (0.65 ± 0.05, $p = 0.02$) and OFF stimulation after 3 days of treatment (0.76 ± 0.12, $p = 0.0009$), compared to room lighting (0.34 ± 0.02). The effect persisted after 7 days with 10 Hz ON stimulation (0.85 ± 0.11, $p < 0.0001$ to RL, $p = 0.0008$ compared to 10 Hz OFF stimulation).

We also found a small reduction in the level of retinal *OPN4* mRNA in eyes with negative lenses after 3 days under room lighting (RL-LIM vs. fellow: 0.73 ± 0.05 vs. 0.83 ± 0.05, $p = 0.03$, Figure 7B). The perhaps most significant finding was that 10 Hz ON exposure stimulated the expression of *OPN4* mRNA in both eyes after 3 days and in fellow eyes after 7 days (Figure 7B). There was no change in the level of retinal *OPN5* mRNA after 3 days of treatment. After 1 week of treatment, retinal *OPN5* mRNA expression was higher in the negative lens-treated eyes after 10 Hz ON stimulation (0.35 ± 0.03) compared to 10 OFF stimulation (0.25 ± 0.01, $p = 0.01$, Figure 7C).

A small increase in retinal *GJD2* mRNA was observed in the eyes treated with negative lenses under 10 Hz OFF stimulation after 3 days, compared to fellow eyes (0.68 ± 0.06 vs. 0.55 ± 0.06, $p = 0.047$, Figure 7D).

After 3 day of treatment, changes in ChT and retinal *EGR-1* mRNA levels were positively correlated, showing that retinal *EGR-1* mRNA levels increase as the choroid thickened. This correlation was significant ($p = 0.007$), although only 17% of the change in ChT was explained by changes in *EGR-1* in mRNA ($R^2 = 0.17$). No such correlation was found after 7 days of treatment, nor for any of the other studied genes.

3.6.2 Choroid

There was no significant change in choroidal *RALDH2* mRNA during 3 days of treatment. However, the level of *RALDH2* expression was significantly lower in the lens treated eyes compared to the fellow eyes with 10 Hz OFF stimulation after 7 days (11.44 ± 1.92 vs. 17.23 ± 3.01, $p = 0.03$, Figure 8A). A similar trend was observed in room lighting (12.18 ± 1.06 vs. 17.72 ± 1.83, $p = 0.05$). After 7 days, also choroidal *BMPR1A* mRNA changed in both eyes, both in room lighting and 10 Hz OFF stimulation (RL-LIM: 3.14 ± 0.30; RL-fellow: 3.72 ± 0.48; 10-OFF-LIM: 3.16 ± 0.38; 10-OFF-fellow: 3.60 ± 0.39). At 7 days, there was a higher level of *BMPR1A* expression compared to 3 days (RL-LIM: 1.91 ± 0.17, $p = 0.01$; RL-fellow: 1.86 ± 0.15, $p < 0.0001$; 10-OFF-LIM: 1.83 ± 0.24, $p = 0.005$; 10-OFF-fellow: 1.93 ± 0.21, $p = 0.0002$, Figure 8B). No temporal effect was found in 10-ON group. An interocular difference was observed in the expression of choroidal *OPN4* mRNA during both the early (LIM vs. fellow: 0.39 ± 0.07 vs. 0.55 ± 0.09, $p = 0.003$) and late periods (LIM vs. fellow: 0.69 ± 0.07 vs. 0.90 ± 0.10, $p = 0.04$, Figure 8C) of treatment in the RL group. This difference was not observed in the other groups.

After treatment for 3 days, ChT change and choroidal *RALDH2* mRNA level were found to be positively correlated. This correlation was significant ($p = 0.045$), although only 10% of the change in ChT can possibly be explained by changes in the amount of choroidal *RALDH2* mRNA expression. No significant correlation was found for the other genes.

4 Discussion

We have investigated how different computer-generated dynamic visual stimuli, assumed to predominantly stimulate retinal ON and OFF pathways, in combination with or without imposed

optical defocus, affect ChT thickness, axial length, refraction and the expression of some biomarkers of myopia, including dopamine. The time kinetics was also studied, by measuring after 3 h, and 3 and 7 days of continued treatment. The potential predictive power of these variables for future refractive development was statistically analyzed.

4.1 Temporal and spatial frequency during ON or OFF stimulation determine changes in ChT

After short-term treatment of 3 h, the effect of ON/OFF stimuli on ChT varied with the field sizes of the dynamic checkerboard patterns and their temporal frequency. Both dynamic ON and OFF stimuli caused choroidal thinning in chicks with normal vision, with the largest effect at the smallest field size used. Only one type of stimulus, a 1.2 Hz pattern cycle checkerboard with medium field sizes of about 2.9 deg. visual angle, led to thickening of the choroid. It is well known that stimulus size plays an important role in the ON/OFF response of retinal ganglion cells (RGCs). With an increase of stimulus size, the amplitudes of both, ON- and OFF-center RGCs, decrease. When a full-field stimulus was presented to mice *in vivo*, approximately half of the OFF-center RGCs altered their sign into either OFF/ON or ON only. The sign switch was derived from the area surround the receptive field (39). In humans, ON and OFF responses in the primary visual cortex have different spatial characteristics: large gratings with low spatial frequencies activate more OFF-dominated neurons, while narrow gratings with high spatial frequencies shifts the responses to ON-dominated neurons (40). ON and OFF ganglion cells exhibit an asymmetrical pattern in their temporal adaptation to photopic and scotopic conditions. Specifically, under photopic conditions, both ON and OFF ganglion cells demonstrate similar temporal characteristics. However, under scotopic conditions, ON cells shift their tuning towards low temporal frequencies, whereas OFF cells respond to higher frequencies (41). In mice, the response of both ON and OFF retinal ganglion cells increased with temporal frequencies ranging from 0.15 to 3 Hz. Beyond 3 Hz, their responses began to decrease (41). In our study, chickens were stimulated under photopic conditions, with an ambient illumainance of 400 lux. Assuming that findings in mice and humans can be extrapolated to birds, a smaller stimulus size combined with relatively low stimulation frequency should induce a stronger response in both ON and OFF cells. In fact, differences between ON and OFF stimulation were only observed with medium-sized fields in the checkerboard at a frequency of 1.2 Hz. In this case, ON stimuli caused thickening of the choroid, and OFF stimuli resulted in choroidal thinning. One reason for the generally not consistent differences between ON versus OFF stimulation in the current study is that the checkerboard fields may have been too large to stimulate antagonistic receptive fields. Diedrich and Schaeffel (42) used multi-electrode recordings in the chick retina and found a visual acuity of the chicks of about 5 cyc/deg. and a rather low maximal contrast sensitivity of about 10 at 1.7 cyc/deg. (10% contrast is detected). The strongest responses of ganglion cells were measured with stimuli of 1.64 cyc/deg. In the current study, we have a minimal 1.7 deg. visual angle (SQS), equivalent to about max 0.3 cyc/deg. It is not known, whether the antagonistic ON/OFF receptive fields are activated at this field size. If not, only temporal ON/OFF signals will be generated.

In young human subjects, a computer-generated dynamic ON stimulus at 1 Hz, similar to the one in the current study increased ChT while the OFF version of it decreased it (15). The authors of this study translated the ON and OFF signals into practical applications for humans: reading white text on a black background stimulates the ON pathway, while reading black text on a white background stimulates the OFF pathway (43). The magnitudes of these effects of contrast polarity on ChT were greater than that of dynamic ON/OFF square stimulations in humans and chicks. This difference in magnitude could be attributed to the significantly smaller size of the stimuli in the former case, as speculated by the authors. Nevertheless, we observed in this study that a medium size ON stimulus was in fact more effective compared to the small size, which was used in the previous study (15), in chickens. The reason for this difference in results between the two studies remains unclear, as the same stimuli were used. The only known difference between the two studies that we are aware of, is the different White Leghorn hybrid line used. Furthermore, our findings revealed that only the OFF stimulus with a frequency of 10 Hz had an enhancing effect on ChT in LIM eyes. The reason could be that the OFF RGCs activate preferential over ON RGCs in a frequency band around 10 Hz, as predicted in a model (44).

The effects of the ON and OFF stimuli on refractive error development also vary. Both the 1-Hz ON and OFF stimuli of small squares promoted the development of LIM in chickens (15). In another study, a 4-Hz OFF stimulus was observed to diminish positive lens-induced hyperopia, while a 4-Hz ON stimulus mitigated the development of LIM in chickens (45). Likewise, blocking the ON response inhibited the progression of LIM, whereas blocking the OFF response prevented the development of positive lens-induced hyperopia (46). In the human visual cortex, ON cortical pathways exhibit higher contrast sensitivity compared to OFF cortical pathways, with this discrepancy escalating with luminance range. The asymmetrical characteristics present in ON and OFF responses add complexity to the assessment of effects, particularly when considering tuning parameters. However, in cases of myopia, where the eye elongates, the ON pathways become less responsive and less sensitive (47).

4.2 Differential effect of high flicker frequency on the initial choroidal response to positive and negative lens treatment

Short term treatment with negative lenses induced a significantly larger response (reduction in choroidal thickness) in the negative lens-treated eyes with 10 Hz ON flicker compared to 10 Hz OFF flicker, whereas 3 h of plus lens treatment induced a larger response (increase in ChT) with stimulation of the ON system. It was already discussed since long that different retinal circuits with different temporal characteristics are involved in the processing of hyperopic and myopic defocus (48), which might than lead to the differential effect of high frequency ON and OFF flicker on the size of the choroidal response as shown in our study. In addition, it was recently discussed that "choroidal thickening induced by positive defocus may

be triggered by metabolic constraints, rather than representing a "third mechanism of focusing the eye" as first proposed by Wallman et al. (1, 49).

4.3 The initial extent of ChT thinning (after 1 day) does not predict the amount of negative lens-induced myopia

ChT is inversely correlated with axial length in myopia (50), as well as with refractive error and visual acuity in high myopes (51, 52). In addition, subfoveal ChT in humans is an independent predictor for myopic maculopathy progression (53). In a large cohort and longitudinal study performed in young adults, the authors found that each 10 μm increase in baseline ChT was associated with a refractive change of 0.006 D/year and of 0.003 mm/year in axial length (54). In addition to forecasting the natural eye growth process, ChT can also be used to predict or assess the effectiveness of myopia control methods, such as repeated low-level red-light therapy (55) and low-concentration atropine (56). Animal experiments have shown that baseline ChT is correlated with baseline refraction and deprivation-induced myopia development in pigmented guinea pigs, but not in the albino ones (57). On the other hand, it has been shown that ChT as an independent parameter cannot predict visual acuity in high myopes after adjustment for spherical equivalent and the presence of pathological myopic lesions (58). Similar evidence has been found in chickens, indicating that baseline ChT is unable to predict the extent of the final myopic shift in form-deprived chickens (7). However, it has been shown to be predictive of ocular growth in chickens with normal vision (6), where a thicker choroid is associated with reduced eye growth. However, this relationship is not as quantitatively precise as the correlation between refractive error and axial length.

A number of studies have shown an association between a treatment-induced reduction in eye length growth and thickening of the choroid. As for example a brief period of normal vision during negative lens-wearing effectively slow down myopia development, inducing a choroid thickening of 91 μm and less axial elongation of 183 μm (59). In addition, the dopamine receptor agonist apomorphine reduces axial elongation by 184 μm and increases choroidal thickness by 42 μm in LIM chickens (60). This may also explain why 0.01% atropine is not effective in slowing myopia progression in children in the long term, as there was no significant increase in ChT after 6 months of use (61).

In our study, the choroidal thickness decreased significantly less in the 10-OFF group. This effect was already seen after 3 h of treatment. The 10 Hz OFF treated chicks also had a thicker choroid after 7 days, but there was no significant difference in the lens-induced myopic shift in this group compared to the control group. It seems that less ChT reduction does not mean less eye growth. This result therefore supports earlier findings of our groups and others that a decrease in choroidal thickness induced by artificial stimuli has no predictive power for the change in eye length growth. With the exception of one stimulus, all artificial stimuli tested in this study led to choroidal thinning. ChT decreased strongly during the first day of stimulation followed by a partial or full recovery at day 7. Initial choroidal thinning (1 day) induced by negative lens wear under a number of artificial stimuli did not predict the amount of myopia induced by negative lenses after 7 days, while ChT changes that occurred later during the treatment period showed a significant association. One has to keep in mind that the extent to which the choroid can thin has a natural lower limit, which potentially had an impact on the results of the correlation analysis. Also, the result of the present study does not provide much information about the predictive power of initial choroidal thickening, since only one stimulus induced this effect (1.2 Hz-ON after 3 h of treatment). A current review article by Ostrin et al. (62) states that "current evidence is not sufficient to speculate that short-term choroidal thickening can be used as a biomarker of treatment efficacy for myopia control therapies." Therefore, future studies should focus on stimuli that thicken the choroid in order to analyze the predictive power of choroidal thickening.

4.4 Influence of artificial stimuli and lens treatment on dopamine metabolism and the correlation with ChT

As expected, negative lens treatment reduced dopamine release as measured by changes in the amount of dopamine metabolites in the vitreous. On the other hand, dopamine release was strongly stimulated by high frequency flicker and also-although to a lesser extent- by low frequency flicker; both in fellow control eyes (DOPAC and HVA) and in the lens-treated eyes (HVA). This result thereby supports previous findings in chicks showing that frequencies around 10 Hz (stroboscopic light (63)) optimally activate dopaminergic amacrine cells and therefore stimulate retinal dopamine release. In addition, a study in guinea pigs demonstrated that 0.5 Hz luminance flicker increase the levels of the dopamine metabolites (64). Interestingly, HVA level was highest in the group of chicks kept under square wave stimulation. However, as HVA levels were equally elevated in both control and lens-treated eyes, the lens-induced effect persisted in all treatment groups.

The amount of dopamine release was positively correlated with choroidal thickness. This result thereby confirms an association between both parameters that was also recently described and discussed in a study by Mathis et al. (65). As no dopamine receptors have been identified in the choroid, it was supposed that a direct effect of the transmitter in this tissue is unlikely (66). However, Mathis et al. showed that retinal and choroidal dopamine levels are correlated, suggesting a role for dopamine in choroidal thickness changes. Further studies are needed to clarify the exact nature of the pathway linking retinal dopamine release to ChT changes.

4.5 Influence of artificial stimuli and lens treatment on candidate gene expression changes and their correlation with changes in ChT

Changes in visual input and signals within the retina can lead to changes in ChT, scleral structure and consequently axial elongation of the eye. With the use of large-scale screening technologies, a number of molecules have been found to be associated with the development or prevention of induced myopia and therefore postulated to play a role in the regulation of ocular growth (67).

Most consistent across studies and animal models were changes in the expression of the immediate early gene *EGR-1* in correlation with induced defocus and deprivation. *EGR-1* knockout mice exhibit axial myopia, highlighting its essential role in eye growth (68). The expression pattern of *EGR-1* aligns with the trajectory of eye growth: it is downregulated in eyes developing LIM (lens-induced myopia) and

upregulated during recovery from LIM (69). In our study, we confirmed that lens treatment reduced the expression of *EGR-1* under room light conditions. Interestingly, we found a significant positive correlation of ChT changes and retinal *EGR-1* mRNA levels after 3 days of treatment, i.e., a low retinal *EGR-1* level was correlated with a thinner choroid. However, whether a causal relationship exists requires further investigation, also because there was no significant correlation between both parameters after 1 week and the extent of the correlation was relatively low (only 17% of the change in ChT could be explained by changes in *EGR-1* expression). Possibly, ChT changes might be regulated at least partly by visual signals derived from the retina, including *EGR-1*. However, after longer treatment, a disassociation takes place. This is also reflected in the increased mRNA expression of *EGR-1* in the LIM retina of the 10-ON groups which does not correspond to a reduced eye growth after 1 week, indicating that *EGR-1* expression may not/not any more correlate with the rate of eye growth after long treatment periods.

The expression of the gap junction protein 2, also known as connexin-36, was found to decrease in the retinas of guinea pigs with FDM (19) and LIM (70) whereas functional connexin-35 increased in the cone-dominated myopic chicken retina (71). In mice, no change in *GJD2* mRNA was found but an increased phosphorylation of connexin-36 which could indicate increased functional gap junction coupling of AII amacrine cells in the rod-dominated myopic mouse retina. This might be a possible adaptation to adjust to the altered noisy signaling status (72). AII amacrine cells (ACs), coupled by connexin-36, segregate signals into ON and OFF pathways. In our study, only the retinas of 10 Hz OFF stimulated chicks showed a higher level of *GJD2* mRNA compared to the fellow eyes after 3 days of treatment. This effect in gene expression in 10 Hz-OFF was not correlated with differential changes in ChT in this treatment group at that time point. In addition, the increase in *GJD2* mRNA expression level was only temporal and not seen after 1 week of treatment.

Violet light has been found to provide protective effects against lens-induced myopia (LIM) and to cause choroidal thickening in mice. These effects are dependent on the function of retinal *OPN5* (73). Violet light exposure also upregulated *EGR-1* expression in the chicken chorio-retinal tissues (74), an effect subsequently confirmed in mice to be mediated by *OPN5* (75). In our study, we observed significantly higher levels of *EGR-1* and *OPN5* mRNA expression in the LIM eyes of the 10-ON group compared to the 10-OFF group after 1 week of treatment. Given that our light source did not emit violet light, it seems plausible that the alteration in *OPN5* and *EGR-1* expression are independent of each other in this particular case.

The blue light sensitive non-visual opsin melanopsin (*OPN4*) is expressed in the choroid and in intrinsically photosensitive ganglion cells (ipRGCs) in the retina which, like rods and cones, provide essential input to dopaminergic amacrine cells (76). *OPN4* knock-out mice exhibit greater hyperopia compared to wildtype mice; however, they are also more susceptible to form-deprivation myopia (FDM) (20). We did not detect any lens-induced changes in retinal *OPN4* expression after one week, but its level was significantly elevated in the 10 Hz ON group compared to the 10 Hz OFF group, in fellow and lens treated eyes after 3 days of treatment. Since short-term experiments showed a significant thinner choroid during short-term 10 Hz ON stimulation (Figure 8B), a higher retinal *OPN4* level might be associated with a thinner choroid, which fits to the *OPN4* knock-out results. It was also observed in *OPN4* knock-out mice that the choroidal thickening in response to the light stimulation was absent (77). In contrast to extensive knowledge about the function of melanopsin in the retina, its role in the choroid is currently unknown. Interestingly, it was recently concluded that melanopsin may regulate diurnal or defocus-induced changes in ChT, "including the intriguing possibility that the choroid may be photosensitive" (78). Indeed, the opsin genes including *OPN4* were found to be expressed in the chick choroid (79). We observed that the *OPN4* mRNA expression was decreased in the LIM eyes compared to the fellow eyes in the RL group, both in short-term and long-term experiment. The expression of *OPN4* in the choroid might therefore play a role in the thickness response.

A significant down-regulation of the bone morphogenetic protein receptor *BMPR1A* was observed in the choroid of chickens after 48 h of treatment with a +10D lens, while no such effect was observed in the retina (24). Interestingly, our study identified a temporal effect on *BMPR1A* mRNA expression. Specifically, prolonged treatment resulted in elevated mRNA levels in both eyes of the RL and 10-OFF groups. In contrast, the 10-ON group exhibited an opposite trend in mRNA expression. The temporal upregulation of BMP is necessary for early ocular lens development in chickens (80). Therefore, the temporal elevation might be related with eye development as well.

5 Summary

In conclusion, our study confirms that negative lens treatment thins the choroid in chickens, and that the effect can be modulated by artificial visual stimuli in their environment. However, the induced increase in ChT with 1.2 Hz ON flicker was too small to generate long-term changes in myopia development. We found that the amplitude of choroidal thinning on day 1 of lens treatment had no predictive value for the amount of myopia that developed in 7 days, whereas relative changes in ChT were predictive from day 5 on. Parameters of the used ON/OFF stimuli tuning, such as field sizes of the checkerboard and cycle frequency induce varying effects on ChT, highlighting the need for careful analysis of these parameters to achieve inhibition of myopia.

Data availability statement

The original contributions presented in the study are publicly available. This data can be found here: https://www.ncbi.nlm.nih.gov/nuccore/XM_046919995.1.

Ethics statement

The animal study was approved by Regierungspraesidium Tuebingen-Veterinaeramt-72016 Tuebingen. The study was conducted in accordance with the local legislation and institutional requirements.

Author contributions

HL: Writing – review & editing, Writing – original draft, Visualization, Investigation, Formal analysis, Data curation. FS: Writing – review & editing, Software, Methodology, Funding acquisition, Conceptualization. MF: Writing – review & editing, Writing – original draft, Supervision, Methodology, Investigation, Funding acquisition, Formal analysis, Data curation, Conceptualization.

Funding

The author(s) declare that financial support was received for the research, authorship, and/or publication of this article. This work was funded by support from the German Research Council (DFG, FE 450/4-1 and SCHA 518/17-1).

Conflict of interest

The authors declare that the research was conducted in the absence of any commercial or financial relationships that could be construed as a potential conflict of interest.

Publisher's note

All claims expressed in this article are solely those of the authors and do not necessarily represent those of their affiliated organizations, or those of the publisher, the editors and the reviewers. Any product that may be evaluated in this article, or claim that may be made by its manufacturer, is not guaranteed or endorsed by the publisher.

Supplementary material

The Supplementary material for this article can be found online at: https://www.frontiersin.org/articles/10.3389/fmed.2024.1469275/full#supplementary-material

SUPPLEMENTARY FIGURE 1
Light spectrum perceived by the chicks in the experimental set up "arena".

SUPPLEMENTARY FIGURE 2
Significant correlation of relative changes in choroidal thickness with axial length **(A)** and vitreous chamber depth **(B)** after 7 days of treatment. Interocular differences between the two eyes are shown (X = lens treated eye; N = normal fellow eye).

References

1. Wallman J, Wildsoet C, Xu A, Gottlieb MD, Nickla DL, Marran L, et al. Moving the retina: choroidal modulation of refractive state. *Vis Res*. (1995) 35:37–50. doi: 10.1016/0042-6989(94)E0049-Q

2. Hung LF, Wallman J, Smith EL 3rd. Vision-dependent changes in the choroidal thickness of macaque monkeys. *Invest Ophthalmol Vis Sci*. (2000) 41:1259–69.

3. Troilo D, Nickla DL, Wildsoet CF. Form deprivation myopia in mature common marmosets (*Callithrix jacchus*). *Invest Ophthalmol Vis Sci*. (2000) 41:2043–9.

4. Troilo D, Nickla DL, Wildsoet CF. Choroidal thickness changes during altered eye growth and refractive state in a primate. *Invest Ophthalmol Vis Sci*. (2000) 41:1249–58.

5. Chen YP, Prashar A, Erichsen JT, To CH, Hocking PM, Guggenheim JA. Heritability of ocular component dimensions in chickens: genetic variants controlling susceptibility to experimentally induced myopia and pretreatment eye size are distinct. *Invest Ophthalmol Vis Sci*. (2011) 52:4012–20. doi: 10.1167/iovs.10-7045

6. Nickla DL, Totonelly K. Choroidal thickness predicts ocular growth in normal chicks but not in eyes with experimentally altered growth. *Clin Exp Optom*. (2015) 98:564–70. doi: 10.1111/cxo.12317

7. Guggenheim JA, Chen YP, Yip E, Hayet H, Druel V, Wang L, et al. Pre-treatment choroidal thickness is not predictive of susceptibility to form-deprivation myopia in chickens. *Ophthalmic Physiol Opt*. (2011) 31:516–28. doi: 10.1111/j.1475-1313.2011.00827.x

8. Chakraborty R, Read SA, Collins MJ. Monocular myopic defocus and daily changes in axial length and choroidal thickness of human eyes. *Exp Eye Res*. (2012) 103:47–54. doi: 10.1016/j.exer.2012.08.002

9. Moderiano D, Do M, Hobbs S, Lam V, Sarin S, Alonso-Caneiro D, et al. Influence of the time of day on axial length and choroidal thickness changes to hyperopic and myopic defocus in human eyes. *Exp Eye Res*. (2019) 182:125–36. doi: 10.1016/j.exer.2019.03.019

10. Read SA, Collins MJ, Sander BP. Human optical axial length and defocus. *Invest Ophthalmol Vis Sci*. (2010) 51:6262–9. doi: 10.1167/iovs.10-5457

11. Chiang ST, Phillips JR, Backhouse S. Effect of retinal image defocus on the thickness of the human choroid. *Ophthalmic Physiol Opt*. (2015) 35:405–13. doi: 10.1111/opo.12218

12. Read SA, Collins MJ, Vincent SJ. Light exposure and eye growth in childhood. *Invest Ophthalmol Vis Sci*. (2015) 56:6779–87. doi: 10.1167/iovs.14-15978

13. Read SA, Fuss JA, Vincent SJ, Collins MJ, Alonso-Caneiro D. Choroidal changes in human myopia: insights from optical coherence tomography imaging. *Clin Exp Optom*. (2019) 102:270–85. doi: 10.1111/cxo.12862

14. Sander BP, Collins MJ, Read SA. The effect of topical adrenergic and anticholinergic agents on the choroidal thickness of young healthy adults. *Exp Eye Res*. (2014) 128:181–9. doi: 10.1016/j.exer.2014.10.003

15. Wang M, Aleman AC, Schaeffel F. Probing the potency of artificial dynamic ON or OFF stimuli to inhibit myopia development. *Invest Ophthalmol Vis Sci*. (2019) 60:2599–611. doi: 10.1167/iovs.18-26471

16. Crewther SG, Barutchu A, Murphy MJ, Crewther DP. Low frequency temporal modulation of light promotes a myopic shift in refractive compensation to all spectacle lenses. *Exp Eye Res*. (2006) 83:322–8. doi: 10.1016/j.exer.2005.12.016

17. Fischer AJ, McGuire JJ, Schaeffel F, Stell WK. Light- and focus-dependent expression of the transcription factor ZENK in the chick retina. *Nat Neurosci*. (1999) 2:706–12. doi: 10.1038/11167

18. Brand C, Burkhardt E, Schaeffel F, Choi JW, Feldkaemper MP. Regulation of Egr-1, VIP, and Shh mRNA and Egr-1 protein in the mouse retina by light and image quality. *Mol Vis*. (2005) 11:309–20.

19. Yang GY, Liu FY, Li X, Zhu QR, Chen BJ, Liu LQ. Decreased expression of gap junction delta-2 (GJD2) messenger RNA and connexin 36 protein in form-deprivation myopia of guinea pigs. *Chin Med J*. (2019) 132:1700–5. doi: 10.1097/CM9.0000000000000319

20. Chakraborty R, Landis EG, Mazade R, Yang V, Strickland R, Hattar S, et al. Melanopsin modulates refractive development and myopia. *Exp Eye Res*. (2021) 214:108866. doi: 10.1016/j.exer.2021.108866

21. Kato M, Sato K, Habuta M, Fujita H, Bando T, Morizane Y, et al. Localization of the ultraviolet-sensor Opn5m and its effect on myopia-related gene expression in the late-embryonic chick eye. *Biochem Biophys Rep*. (2019) 19:100665. doi: 10.1016/j.bbrep.2019.100665

22. Guido ME, Marchese NA, Rios MN, Morera LP, Diaz NM, Garbarino-Pico E, et al. Non-visual opsins and novel photo-detectors in the vertebrate inner retina mediate light responses within the blue spectrum region. *Cell Mol Neurobiol*. (2022) 42:59–83. doi: 10.1007/s10571-020-00997-x

23. Harper AR, Wang X, Moiseyev G, Ma JX, Summers JA. Postnatal chick choroids exhibit increased retinaldehyde dehydrogenase activity during recovery from form deprivation induced myopia. *Invest Ophthalmol Vis Sci*. (2016) 57:4886–97. doi: 10.1167/iovs.16-19395

24. Zhang Y, Liu Y, Hang A, Phan E, Wildsoet CF. Differential gene expression of BMP2 and BMP receptors in chick retina & choroid induced by imposed optical defocus. *Vis Neurosci*. (2016) 33:E015. doi: 10.1017/S0952523816000122

25. Feldkaemper M, Schaeffel F. An updated view on the role of dopamine in myopia. *Exp Eye Res*. (2013) 114:106–19. doi: 10.1016/j.exer.2013.02.007

26. Zhou X, Pardue MT, Iuvone PM, Qu J. Dopamine signaling and myopia development: what are the key challenges. *Prog Retin Eye Res*. (2017) 61:60–71. doi: 10.1016/j.preteyeres.2017.06.003

27. Schaeffel F, Hagel G, Eikermann J, Collett T. Lower-field myopia and astigmatism in amphibians and chickens. *J Opt Soc Am A*. (1994) 11:487–95. doi: 10.1364/JOSAA.11.000487

28. Schaeffel F, Howland HC. Properties of the feedback loops controlling eye growth and refractive state in the chicken. *Vis Res*. (1991) 31:717–34. doi: 10.1016/0042-6989(91)90011-S

29. Wallman J, Adams JI. Developmental aspects of experimental myopia in chicks: susceptibility, recovery and relation to emmetropization. *Vis Res*. (1987) 27:1139–63. doi: 10.1016/0042-6989(87)90027-7

30. Liu H, Schaeffel F, Yang Z, Feldkaemper MP. $GABA_B$ receptor activation affects eye growth in chickens with visually induced refractive errors. *Biomol Ther*. (2023) 13:434. doi: 10.3390/biom13030434

31. Mathis U, Feldkaemper MP, Schaeffel F. Effects of single and repeated intravitreal applications of atropine on choroidal thickness in alert chickens. *Ophthalmic Res*. (2021) 64:664–74. doi: 10.1159/000515755

32. Wang M, Schaeffel F, Jiang B, Feldkaemper M. Effects of light of different spectral composition on refractive development and retinal dopamine in chicks. *Invest Ophthalmol Vis Sci*. (2018) 59:4413–24. doi: 10.1167/iovs.18-23880

33. Megaw P, Morgan I, Boelen M. Vitreal dihydroxyphenylacetic acid (DOPAC) as an index of retinal dopamine release. *J Neurochem*. (2001) 76:1636–44. doi: 10.1046/j.1471-4159.2001.00145.x

34. Simon P, Feldkaemper M, Bitzer M, Ohngemach S, Schaeffel F. Early transcriptional changes of retinal and choroidal TGFbeta-2, RALDH-2, and ZENK following imposed positive and negative defocus in chickens. *Mol Vis*. (2004) 10:588–97.

35. Kihara AH, Paschon V, Cardoso CM, Higa GS, Castro LM, Hamassaki DE, et al. Connexin36, an essential element in the rod pathway, is highly expressed in the essentially rodless retina of *Gallus gallus*. *J Comp Neurol*. (2009) 512:651–63. doi: 10.1002/cne.21920

36. Zhang Y, Liu Y, Wildsoet CF. Bidirectional, optical sign-dependent regulation of BMP2 gene expression in chick retinal pigment epithelium. *Invest Ophthalmol Vis Sci*. (2012) 53:6072–80. doi: 10.1167/iovs.12-9917

37. Gisbert S, Feldkaemper M, Wahl S, Schaeffel F. Interactions of cone abundancies, opsin expression, and environmental lighting with emmetropization in chickens. *Exp Eye Res*. (2020) 200:108205. doi: 10.1016/j.exer.2020.108205

38. Ohngemach S, Hagel G, Schaeffel F. Concentrations of biogenic amines in fundal layers in chickens with normal visual experience, deprivation, and after reserpine application. *Vis Neurosci*. (1997) 14:493–505. doi: 10.1017/S0952523800012153

39. Sagdullaev BT, McCall MA. Stimulus size and intensity alter fundamental receptive-field properties of mouse retinal ganglion cells *in vivo*. *Vis Neurosci*. (2005) 22:649–59. doi: 10.1017/S0952523805225142

40. Jansen M, Jin J, Li X, Lashgari R, Kremkow J, Bereshpolova Y, et al. Cortical balance between ON and OFF visual responses is modulated by the spatial properties of the visual stimulus. *Cereb Cortex*. (2019) 29:336–55. doi: 10.1093/cercor/bhy221

41. Pandarinath C, Victor JD, Nirenberg S. Symmetry breakdown in the ON and OFF pathways of the retina at night: functional implications. *J Neurosci*. (2010) 30:10006–14. doi: 10.1523/JNEUROSCI.5616-09.2010

42. Diedrich E, Schaeffel F. Spatial resolution, contrast sensitivity, and sensitivity to defocus of chicken retinal ganglion cells *in vitro*. *Vis Neurosci*. (2009) 26:467–76. doi: 10.1017/S0952523809990253

43. Aleman AC, Wang M, Schaeffel F. Reading and myopia: contrast polarity matters. *Sci Rep*. (2018) 8:10840. doi: 10.1038/s41598-018-28904-x

44. Kameneva T, Meffin H, Burkitt AN. Differential stimulation of ON and OFF retinal ganglion cells: a modeling study. *Annu Int Conf IEEE Eng Med Biol Soc*. (2010) 2010:4246–9. doi: 10.1109/IEMBS.2010.5627176

45. Crewther DP, Crewther SG. Refractive compensation to optical defocus depends on the temporal profile of luminance modulation of the environment. *Neuroreport*. (2002) 13:1029–32. doi: 10.1097/00001756-200206120-00010

46. Crewther SG, Crewther DP. Inhibition of retinal ON/OFF systems differentially affects refractive compensation to defocus. *Neuroreport*. (2003) 14:1233–7. doi: 10.1097/00001756-200307010-00009

47. Poudel S, Jin J, Rahimi-Nasrabadi H, Dellostritto S, Dul MW, Viswanathan S, et al. Contrast sensitivity of ON and OFF human retinal pathways in myopia. *J Neurosci*. (2023) 44:e1487232023. doi: 10.1523/JNEUROSCI.1487-23.2023

48. Schwahn HN, Schaeffel F. Flicker parameters are different for suppression of myopia and hyperopia. *Vis Res*. (1997) 37:2661–73. doi: 10.1016/S0042-6989(97)00114-4

49. Schaeffel F, Swiatczak B. Mechanisms of emmetropization and what might go wrong in myopia. *Vis Res*. (2024) 220:108402. doi: 10.1016/j.visres.2024.108402

50. Flores-Moreno I, Lugo F, Duker JS, Ruiz-Moreno JM. The relationship between axial length and choroidal thickness in eyes with high myopia. *Am J Ophthalmol*. (2013) 155:314–319.e1. doi: 10.1016/j.ajo.2012.07.015

51. Nishida Y, Fujiwara T, Imamura Y, Lima LH, Kurosaka D, Spaide RF. Choroidal thickness and visual acuity in highly myopic eyes. *Retina*. (2012) 32:1229–36. doi: 10.1097/IAE.0b013e318242b990

52. Ho M, Liu DT, Chan VC, Lam DS. Choroidal thickness measurement in myopic eyes by enhanced depth optical coherence tomography. *Ophthalmology*. (2013) 120:1909–14. doi: 10.1016/j.ophtha.2013.02.005

53. Li Z, Wang W, Liu R, Wang D, Zhang J, Xiao O, et al. Choroidal thickness predicts progression of myopic maculopathy in high myopes: a 2-year longitudinal study. *Br J Ophthalmol*. (2020) 105:1744–450. doi: 10.1136/bjophthalmol-2020-316866

54. Lee SS, Alonso-Caneiro D, Lingham G, Chen FK, Sanfilippo PG, Yazar S, et al. Choroidal thickening during young adulthood and baseline choroidal thickness predicts refractive error change. *Invest Ophthalmol Vis Sci*. (2022) 63:34. doi: 10.1167/iovs.63.5.34

55. Xiong R, Zhu Z, Jiang Y, Wang W, Zhang J, Chen Y, et al. Longitudinal changes and predictive value of choroidal thickness for myopia control following repeated low-level red-light therapy. *Ophthalmology*. (2022) 130:286–96. doi: 10.1016/j.ophtha.2022.10.002

56. Yam JC, Jiang Y, Lee J, Li S, Zhang Y, Sun W, et al. The association of choroidal thickening by atropine with treatment effects for myopia: two-year clinical trial of the low-concentration atropine for myopia progression (LAMP) study. *Am J Ophthalmol*. (2022) 237:130–8. doi: 10.1016/j.ajo.2021.12.014

57. Jiang L, Liu X, Zhou L, Busoy JMF, Khine MT, Dan YS, et al. Choroidal thickness in early postnatal guinea pigs predicts subsequent naturally occurring and form-deprivation myopia. *Invest Ophthalmol Vis Sci*. (2022) 63:10. doi: 10.1167/iovs.63.11.10

58. Gupta P, Cheung CY, Saw SM, Koh V, Tan M, Yang A, et al. Choroidal thickness does not predict visual acuity in young high myopes. *Acta Ophthalmol*. (2016) 94:e709–15. doi: 10.1111/aos.13084

59. Nickla DL. Transient increases in choroidal thickness are consistently associated with brief daily visual stimuli that inhibit ocular growth in chicks. *Exp Eye Res*. (2007) 84:951–9. doi: 10.1016/j.exer.2007.01.017

60. Nickla DL, Totonelly K, Dhillon B. Dopaminergic agonists that result in ocular growth inhibition also elicit transient increases in choroidal thickness in chicks. *Exp Eye Res*. (2010) 91:715–20. doi: 10.1016/j.exer.2010.08.021

61. Ye L, Shi Y, Yin Y, Li S, He J, Zhu J, et al. Effects of atropine treatment on choroidal thickness in myopic children. *Invest Ophthalmol Vis Sci*. (2020) 61:15. doi: 10.1167/iovs.61.14.15

62. Ostrin LA, Harb E, Nickla DL, Read SA, Alonso-Caneiro D, Schroedl F, et al. IMI-the dynamic choroid: new insights, challenges, and potential significance for human myopia. *Invest Ophthalmol Vis Sci*. (2023) 64:4. doi: 10.1167/iovs.64.6.4

63. Rohrer B, Iuvone PM, Stell WK. Stimulation of dopaminergic amacrine cells by stroboscopic illumination or fibroblast growth factor (bFGF, FGF-2) injections: possible roles in prevention of form-deprivation myopia in the chick. *Brain Res*. (1995) 686:169–81. doi: 10.1016/0006-8993(95)00370-6

64. Luo X, Li B, Li T, Di Y, Zheng C, Ji S, et al. Myopia induced by flickering light in guinea pig eyes is associated with increased rather than decreased dopamine release. *Mol Vis*. (2017) 23:666–79.

65. Mathis U, Feldkaemper M, Liu H, Schaeffel F. Studies on the interactions of retinal dopamine with choroidal thickness in the chicken. *Graefes Arch Clin Exp Ophthalmol*. (2022) 261:409–25. doi: 10.1007/s00417-022-05837-w

66. Brown DM, Mazade R, Clarkson-Townsend D, Hogan K, Datta Roy PM, Pardue MT. Candidate pathways for retina to scleral signaling in refractive eye growth. *Exp Eye Res*. (2022) 219:109071. doi: 10.1016/j.exer.2022.109071

67. Tkatchenko TV, Shah RL, Nagasaki T, Tkatchenko AV. Analysis of genetic networks regulating refractive eye development in collaborative cross progenitor strain mice reveals new genes and pathways underlying human myopia. *BMC Med Genet*. (2019) 12:113. doi: 10.1186/s12920-019-0560-1

68. Schippert R, Burkhardt E, Feldkaemper M, Schaeffel F. Relative axial myopia in Egr-1 (ZENK) knockout mice. *Invest Ophthalmol Vis Sci*. (2007) 48:11–7. doi: 10.1167/iovs.06-0851

69. Ashby RS, Zeng G, Leotta AJ, Tse DY, McFadden SA. Egr-1 mRNA expression is a marker for the direction of mammalian ocular growth. *Invest Ophthalmol Vis Sci*. (2014) 55:5911–21. doi: 10.1167/iovs.13-11708

70. Zhu Q, Yang G, Chen B, Liu F, Li X, Liu L. Altered expression of GJD2 messenger RNA and the coded protein connexin 36 in negative lens-induced myopia of guinea pigs. *Optom Vis Sci*. (2020) 97:1080–8. doi: 10.1097/OPX.0000000000001611

71. Banerjee S, Wang Q, Tang G, So C, Shan SW, Li KK, et al. Functional connexin35 increased in the myopic chicken retina. *Vis Neurosci*. (2021) 38:E008. doi: 10.1017/S0952523821000079

72. Banerjee S, Wang Q, Zhao F, Tang G, So C, Tse D, et al. Increased connexin36 phosphorylation in AII Amacrine cell coupling of the mouse myopic retina. *Front Cell Neurosci*. (2020) 14:124. doi: 10.3389/fncel.2020.00124

73. Jiang X, Pardue MT, Mori K, Ikeda SI, Torii H, D'Souza S, et al. Violet light suppresses lens-induced myopia via neuropsin (OPN5). *Proc Natl Acad Sci USA*. (2021) 118:e2018840118. doi: 10.1073/pnas.2018840118

74. Torii H, Kurihara T, Seko Y, Negishi K, Ohnuma K, Inaba T, et al. Violet light exposure can be a preventive strategy against myopia progression. *EBioMedicine*. (2017) 15:210–9. doi: 10.1016/j.ebiom.2016.12.007

75. Jeong H, Lee D, Jiang X, Negishi K, Tsubota K, Kurihara T. Opsin 5 mediates violet light-induced early growth response-1 expression in the mouse retina. *Sci Rep*. (2023) 13:17861. doi: 10.1038/s41598-023-44983-x

76. Zhang DQ, Wong KY, Sollars PJ, Berson DM, Pickard GE, McMahon DG. Intraretinal signaling by ganglion cell photoreceptors to dopaminergic amacrine neurons. *Proc Natl Acad Sci USA*. (2008) 105:14181–6. doi: 10.1073/pnas.0803893105

77. Berkowitz BA, Schmidt T, Podolsky RH, Roberts R. Melanopsin phototransduction contributes to light-evoked choroidal expansion and rod L-type calcium channel function *in vivo*. *Invest Ophthalmol Vis Sci*. (2016) 57:5314–9. doi: 10.1167/iovs.16-20186

78. Stone RA, Wei W, Sarfare S, McGeehan B, Engelhart KC, Khurana TS, et al. Visual image quality impacts circadian rhythm-related gene expression in retina and in choroid: a potential mechanism for ametropias. *Invest Ophthalmol Vis Sci*. (2020) 61:13. doi: 10.1167/iovs.61.5.13

79. Summers JA, Jones KL. Single cell transcriptomics identifies distinct choroid cell populations involved in visually guided eye growth. *Front Ophthalmol*. (2023) 3:1245891. doi: 10.3389/fopht.2023.1245891

80. Shu DY, Lovicu FJ. Insights into bone morphogenetic protein (BMP-) signaling in ocular lens biology and pathology. *Cells*. (2021) 10:2604. doi: 10.3390/cells10102604

frontiers | Frontiers in Medicine

TYPE Original Research
PUBLISHED 14 January 2025
DOI 10.3389/fmed.2024.1479891

OPEN ACCESS

EDITED BY
Pablo De Gracia,
University of Detroit Mercy, United States

REVIEWED BY
Christina Zeitz,
Institut National de la Santé et de la Recherche Médicale (INSERM), France
Alexandra Benavente-Perez,
State University of New York, United States

*CORRESPONDENCE
Teele Palumaa
✉ teele.palumaa@emory.edu

RECEIVED 13 August 2024
ACCEPTED 10 December 2024
PUBLISHED 14 January 2025

CITATION
Palumaa T, Balamurugan S and Pardue MT (2025) Meta-analysis of retinal transcriptome profiling studies in animal models of myopia. *Front. Med.* 11:1479891.
doi: 10.3389/fmed.2024.1479891

Meta-analysis of retinal transcriptome profiling studies in animal models of myopia

Teele Palumaa[1,2]*, Shruti Balamurugan[1] and Machelle T. Pardue[1,3,4]

[1]Department of Ophthalmology, Emory University, Atlanta, GA, United States, [2]Institute of Genomics, University of Tartu, Tartu, Estonia, [3]Atlanta VA Center for Visual and Neurocognitive Rehabilitation, Decatur, GA, United States, [4]Department of Biomedical Engineering, Georgia Institute of Technology, Atlanta, GA, United States

Objective: Myopia prevalence is increasing at alarming rates, yet the underlying mechanistic causes are not understood. Several studies have employed experimental animal models of myopia and transcriptome profiling to identify genes and pathways contributing to myopia. In this study, we determined the retinal transcriptome changes in response to form deprivation in mouse retinas. We then conducted a transcriptome meta-analysis incorporating all publicly available datasets and analyzed how the results related to the genes associated with refractive errors in human genome-wide association studies (GWAS).

Methods: Form deprivation was induced in three male C57BL6/J mice from postnatal day 28 (P28) to P42. Retinal gene expression was analyzed with RNA sequencing, followed by differential gene expression analysis with DESeq2 and identification of associated pathways with the Kyoto Encyclopedia of Genes and Genomes (KEGG). A systematic search identified four similar retinal transcriptomics datasets in response to experimental myopia using chicks or mice. The five studies underwent transcriptome meta-analyses to determine retinal gene expression changes and associated pathways. The results were compared with genes associated with human myopia.

Results: Differential gene expression analysis of form-deprived mouse retinas revealed 235 significantly altered transcripts, implicating the BMP2 signaling pathway and circadian rhythms, among others. Transcriptome-wide meta-analyses of experimental myopia datasets found 427 differentially expressed genes in the mouse model and 1,110 in the chick model, with limited gene overlap between species. Pathway analysis of these two gene sets implicated TGF-beta signaling and circadian rhythm pathways in both mouse and chick retinas. Some pathways associated only with mouse retinal changes included dopamine signaling and HIF-1 signaling pathway, whereas glucagon signaling was only associated with gene changes in chick retinas. The follistatin gene changed in both mouse and chick retinas and has also been implicated in human myopia. TGF-beta signaling pathway and circadian entrainment processes were associated with myopia in mice, chicks, and humans.

Conclusion: This study highlights the power of combining datasets to enhance statistical power and identify robust gene expression changes across different experimental animal models and conditions. The data supports other experimental evidence that TGF-beta signaling pathway and circadian rhythms are involved in myopic eye growth.

KEYWORDS

myopia, transcriptomics, meta-analysis, experimental models, RNA-Seq

1 Introduction

Myopia prevalence rates are increasing worldwide (1) yet the causes for this are not fully known. While there is convincing evidence that the retina is essential for signaling refractive eye growth [see review (2)], the exact mechanisms that regulate this process remain elusive. Current myopia control methods, which include optical and pharmacological treatments and lifestyle changes, are limited in their effect size (3). Therefore, understanding the causal mechanisms regulating refractive development and myopia is essential for optimizing current treatments and developing novel approaches to myopia management.

The field of myopia research has significantly benefitted from studies conducted on animal models that investigate molecular changes associated with myopia development. Two primary methods for inducing experimental myopia are form deprivation and lens-induced myopia, where either a diffuser goggle or a negative-powered lens is placed in front of the experimental eye, resulting in the induction of myopic refractive shift (4, 5). The increasing accessibility and affordability of advanced sequencing technologies have made transcriptome analyses increasingly popular. Several studies have implemented transcriptome profiling of the retinal tissue to identify molecular signatures and cellular pathways associated with myopic eye growth (6–13). However, despite the wealth of data generated, the sample size of each study is usually relatively small, which can limit the statistical power and robustness of findings. In addition to the variability between studies arising from slight differences in experimental protocols, other sources of variation include differences in sequencing methods and analysis pipelines (14). Furthermore, the robustness of retinal changes in response to myopic stimulus can also be evaluated by analyzing samples from different species.

Conducting meta-analyses addresses some of the limitations of transcriptome profiling by retrieving samples from multiple studies that analyze the same experimental condition and applying the same analysis pipelines. Meta-analyses remove variation introduced by applying different analysis pipelines and increase the sample size, thus enhancing statistical power. This approach provides an overview of the most robustly changing genes and pathways across different laboratories and experimental models and has been used in several contexts (15, 16). Identifying these consistent changes can result in a better understanding of the underlying biological processes and mechanisms.

In this article, we first present a transcriptome analysis of retinal changes in a mouse model of form deprivation myopia (FDM). Then, we perform a systematic search and meta-analysis of publicly available transcriptomic datasets related to experimental myopia in animal models. Through this combined approach, we aim to identify key gene expression changes and pathways involved in myopia development, which may provide insights into the robust molecular mechanisms underlying this condition. Furthermore, we compare the transcriptomic changes with genes and pathways associated with human refractive errors to determine which retinal changes in experimental myopia may be associated with the human disease.

2 Materials and methods

2.1 Animals

All animal experiments were approved by the Atlanta Veterans Affairs Institutional Animal Care and Use Committee (protocol V015-14). Male C57BL/6J mice were housed in a standard 12-12 hour light-dark cycle. Food and water were provided *ad libitum*. From postnatal day (P) 28, mice were exposed to FDM by surgically attaching a head-mounted diffuser goggle over the right eye (17). The left eye remained uncovered and served as an internal control. Refractive error, corneal curvature and axial length were measured at P28, P35, and P42. After dilating the eyes with 1% tropicamide, mice were anesthetized (ketamine 80 mg/kg; xylazine 16 mg/kg). Refractive error was measured with an automated infrared eccentric photorefractor (5), corneal radius of curvature was measured using an automated keratometer (18) and axial length with a spectral domain optical coherence tomography system (Bioptigen, Durham, NC, USA). Myopic shift was calculated as the refractive error difference between the goggled and uncovered eye.

2.2 Tissue preparation and RNA sequencing

At P42, mice were sacrificed by cervical dislocation during the light phase; their retinal tissue was immediately collected, flash-frozen on dry ice, and stored at −80°C until further processing. Total RNA was extracted using TRIzol and RNeasy Micro kit RNA extraction methods according to the manufacturers' protocols. RNA quantity was measured with a NanoDrop 1000 (Thermo Fisher Scientific), RNA quality was analyzed with the Agilent 2100 Bioanalyzer using the Pico chip (Agilent Technologies), and samples with an RNA integrity number (RIN) >7.5 were used for RNA sequencing (RNA-Seq). RNA was submitted to Emory Integrated Genomics Core. Following poly-A enrichment, 50-base paired-end libraries were prepared and sequenced on the Illumina HiSeq Sequencing System at 50 M reads per sample. The RNA-Seq data of this study are available in the Gene Expression Omnibus repository, accession number GSE284642, and BioProject, accession number PRJNA1200000.

2.3 RNA sequencing data analysis

FASTQ files were uploaded to the Galaxy web platform (19). Read quality was analyzed with FastQC (20). Reads filtered for low-quality reads and trimmed using Trimmomatic (21). Transcript abundance was quantified with Salmon (22). Count normalization and differential analysis were conducted with DESeq2 (23) in R (24) and an unadjusted p value of <0.05 was considered statistically significant, as this analysis is exploratory in nature with an aim to suggest further hypotheses. Differentially regulated pathways and cellular functions were further analyzed using the KEGG database (25) and GO terms (26) and visualized with pathfindR (27) and ggplot2 (28).

2.4 Systematic search of transcriptomics datasets

A search was conducted on the PubMed, Gene Expression Omnibus (GEO) and BioProject databases using the following search statement: retina* AND (transcriptom* OR "RNA seq*" OR "RNA-seq*" OR microarray) AND (myopia OR "short*sighted*" OR "refractive error" OR "refractive development" OR "ocular growth" OR "eye growth" OR "experimental myopia" OR "lens-induced myopia" OR "image defocus" OR "form*deprivation"). All searches were conducted on June 5, 2024. The results were screened for studies that met the following inclusion criteria:

1. The study used an animal model.
2. The study included samples from control eyes and eyes with experimentally induced myopia.
3. The study analyzed retinal samples. All combined tissue samples, e.g. retina/RPE/choroid were excluded.
4. The study conducted whole-genome transcriptome profiling (RNA-Seq or microarray analysis).

2.5 Data processing and meta-analysis

With this search, six RNA-Seq datasets were identified (Table 1). The unprocessed data files of identified studies in the FASTQ format were located. In two instances, the studies filled the inclusion criteria, yet the raw data was not found nor accessed after contacting the corresponding author. Identified studies used either the chick or mouse model of myopia, and the samples from different species were analyzed separately.

The FASTQ files were imported to the Galaxy platform (19), filtered for low-quality reads, and trimmed using Trimmomatic (21), specifying the adapter parameters to what was used in each experiment. The quality of individual reads was analyzed with FastQC (20) before and after the trimming process. Samples were excluded if the percentage of duplicates, read count, or GC content was >2 standard deviations from the mean of the respective study. Transcript abundance was quantified with Salmon (22), estimates were aggregated to the gene level.

Non-normalized untransformed count matrices of each study were obtained using tximport package (v 1.28.0) (29) in R. Next, ComBat-seq (30) from the sva package (v 3.48.0) (31) was used to remove batch effects between studies, specifying the study identifier as the batch variable and the treatment group (experimental myopia vs. control) as the grouping variable. Manipulations used for myopia induction were not separated in this meta-analysis. Low-abundance transcripts were eliminated by retaining only genes with >10 counts in the number of samples of the smallest experimental group. Differential gene expression between control and experimental myopia samples was conducted using the DESeq2 package (23). An unadjusted p value of <0.05 was considered statistically significant, which does increase type I error risk, but as the analysis has inherently high biological variability, a more stringent criteria could eliminate potentially interesting and relevant findings. Transcripts were annotated using the *Mus musculus GRCm38* Ensembl v91 release or the *Gallus gallus* GRCg7b Ensembl v112 release genome assemblies. Differentially expressed pathways and cellular functions were further analyzed using the KEGG database (25), and visualized with pathfindR (27) and ggplot2 (28). Principal component analyses (PCA) of experiments were performed on the variance-stabilized counts of the RNA-Seq data using DESeq2 (23). PCA coordinates were extracted, considering treatment and batch as grouping factors.

Genes associated with refractive errors from genome-wide association studies (GWAS) were retrieved from the GWAS Catalog (32). Single nucleotide variants (SNVs) and their corresponding mapped genes were obtained for traits "myopia" (Experimental Factor Ontology [EFO] trait HP_0000545) and "abnormality of refraction" (EFO trait HP_0000539). Pathways enriched for genes associated with a genetic predisposition to myopia were determined using the KEGG database (25) and visualized with pathfindR (27) and ggplot2 (28).

3 Results

3.1 Transcriptomic changes in response to FDM in the mouse retina

Form deprivation was induced in three male mice from postnatal day (P) 28 by placing a translucent goggle in front of the right eye with a head-mounted pedestal, while the contralateral left eye remained uncovered and served as a control eye (17). By P42, the form-deprived eyes developed myopia, as their refractive error was on average 1.37 ± 0.87 D [mean ± standard deviation (SD)] more myopic than the contralateral uncovered eyes (P28 vs. P42 $p = 0.008$, one-way ANOVA with Šidák's correction for multiple comparisons; Figure 1A). We did not observe statistically significant changes in axial length and corneal radius of curvature between the control and form-deprived eyes (two-way repeated measures ANOVA, age x eye interaction effect $p > 0.05$; Figures 1B, C), which is not uncommon as the magnitude of changes is very small (33, 34).

The retinas of these animals were submitted for RNA-Seq analysis. Upon quality control, one sample was removed as its read duplication level was >2 SD from the mean of the study. Differential gene expression analysis showed that 235 transcripts were differentially expressed between the control and experimental retinas (Figure 2A and Supplementary Table 1). Among the most highly upregulated transcripts were several crystallins (*Cry*), such as *Cryaa*, *Cryba1*, *Cryba2*, *Cryba4*, *Crybb1*, *Crybb2* and *Crygs*. Upregulation of different crystallin transcripts has been also demonstrated previously in chick compound retina/RPE/choroid tissue in response to FDM (35) and in chick retinas after FDM and LIM induction (36). Among the downregulated genes were paraoxonase 1 (*Pon1*), an antioxidative protein associated with lower activity in AMD (37) and potentially linked to oxidative stress, which has been reported in myopia (38); and retinoic acid early transcript 1E (*Raet1e*), which is intriguing as retinoic acid signaling has been implicated in myopia (39).

The genes were further analyzed for enriched pathways using the KEGG database and GO biological process terms. The enriched pathways included various cell signaling pathways, e.g. thyroid

TABLE 1 Experimental myopia retinal transcriptome profiling studies identified.

#	References	BioProject accession number	Species	Myopia model	Animal age at the start of treatment	Myopia induction duration	Control group	No. of samples (experimental + control)	Sex
1	Karouta et al. (7)	PRJNA678523	Chick	FDM	7 days	4 and 24 h	Age-matched untreated controls	15 (7 + 8)	M
2	Li et al. (2)	PRJNA832969	Mouse (C57BL/6J)	FDM	3 weeks	4 weeks	Contralateral untreated eye	12 (6 + 6, each sample 3 retinas pooled)	M
3	Shan et al. (45)	PRJNA766764	Chick	LIM (−10D)	4 days	24 and 48 h	Contralateral untreated eye	12 (6 + 6)	*Not collected*
4	Stone et al. (10)	PRJNA946718	Chick	FDM	Newly hatched	24–44 h (every 4 h)	Contralateral untreated eye	72 (36 + 36)	M and F
5	*Current article*		Mouse (C57BL/6J)	FDM	4 weeks	2 weeks	Contralateral untreated eye	5 (2 + 3)	M
Not included									
	Tkatchenko et al. (6)	–	Marmoset	LIM (−5D)	74 ± 5 days	10 days and 5 weeks	Contralateral eye with plano lens	24 (12 + 12)	M and F
	Ji et al. (9)	PRJNA994038 (*not found on June 5, 2024*)	Mouse (C57BL/6J)	LIM (−25D)	4 weeks	4 weeks	Contralateral untreated eye	6 (3 + 3)	*Not stated*

FDM, form-deprivation myopia; LIM, lens-induced myopia.

10.3389/fmed.2024.1479891

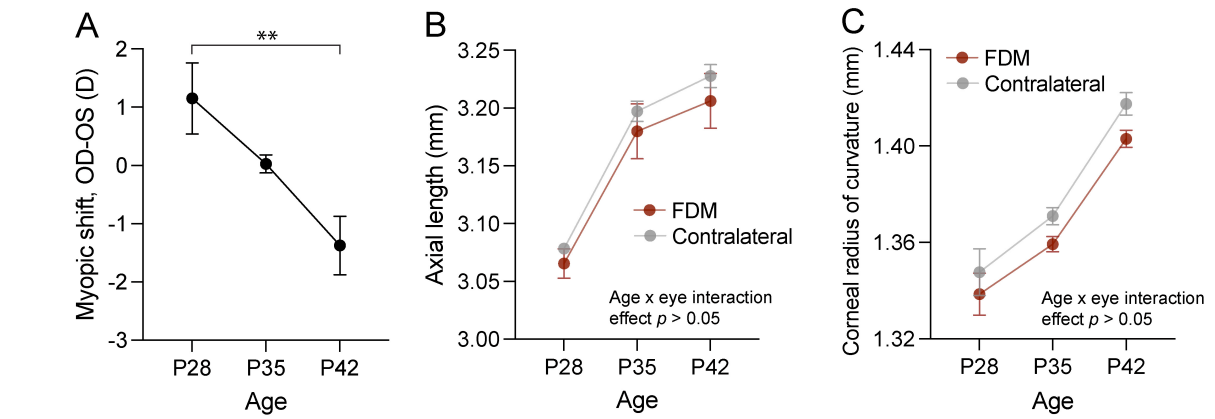

FIGURE 1
Ocular changes in response to form deprivation in mice used in the RNA sequencing experiment. **(A)** The myopic shift, expressed as the interocular difference in refractive error, showed relative myopia in the form-deprived eye of wild-type C57BL/6J mice after two weeks of form deprivation. Axial length **(B)** and corneal curvature **(C)** dynamics in response to form deprivation revealed no interaction effect between age and form deprivation. Data are mean ± SEM, $n = 3$. In **(A)**, statistical analysis was performed using one-way ANOVA with Šidák's correction for multiple comparisons. In **(B, C)**, two-way repeated measures ANOVA was used. ** $p < 0.01$. FDM, form-deprivation myopia.

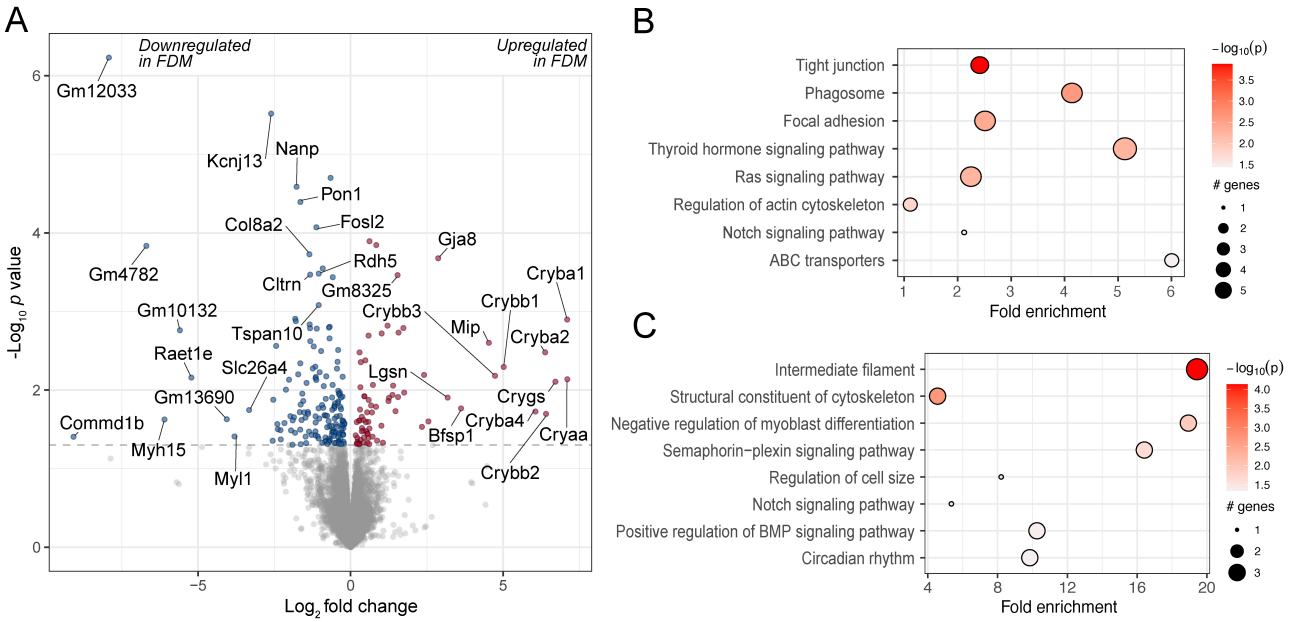

FIGURE 2
Differentially expressed genes and enriched pathways in FDM mouse retinas. **(A)** A volcano plot of genes differentially regulated in FDM retinas from wild-type mice, illustrating the $\log_2$ effect size and unadjusted log-transformed p values. The gray dashed horizontal line indicates an unadjusted p value of 0.05. Genes with significant changes are highlighted in red (upregulated) and blue (downregulated), with a selection of gene names indicated. A selection of KEGG pathways **(B)** and GO terms **(C)** enriched for the differentially regulated genes are highlighted.

hormone and Ras signaling pathways. Thyroid hormone signaling has also been implicated in prior studies investigating the retinal response to experimental myopia (10, 40). A key gene in the Ras signaling pathway, *RASGRF1*, has been associated with myopia (41), and there is evidence that its downstream pathway, the MAPK pathway, is differentially regulated in myopic retinas (11). They also included the regulation of the BMP signaling pathway, which has been associated with experimental myopia in previous studies in the retina and choroid (42), as well as the sclera (43, 44) (Figures 2B, C, Supplementary Tables 2, 3).

3.2 Identification of publicly available retinal transcriptomics datasets of experimental myopia

To increase the number of experimental samples and thereby increase the statistical power of our analysis, while simultaneously reducing the variation induced by conducting experiments in different laboratories in different species and using slightly different RNA-Seq protocols, we sought to combine and analyze all similar

experiments conducted to date. We performed systematic searches in PubMed, GEO, and BioProject to identify studies employing transcriptome profiling to study retinal gene expression in response to experimental myopia in animal models. These searches yielded 71, 42, and 8 results, respectively. After screening the articles for inclusion criteria (see Materials and methods), we determined six suitable studies: two using mice (8, 9), three using chicks (7, 10, 45), and one using marmosets (6) as experimental animals. Four of the studies were included in the meta-analysis, as well as the RNA-Seq experiment presented earlier (Table 1).

There were several global differences between the studies conducted in mouse and chick models regarding the developmental stage of animals and the duration of myopia induction. The experiments conducted in mice used juvenile animals aged between 3 and 4 weeks, while chicks were as young as newly hatched to 7 days old. In mice, myopia was induced for a total of 2 to 4 weeks, while in chicks, the induction was limited to 4–48 h. Four of the five studies induced myopia with form deprivation, and one study in chicks used a −10D lens. Four studies used the contralateral eye as a control eye, while one used age-matched untreated animals. Three of the studies used only male animals, one used male and female, and the sex of animals in one study was not collected (see an overview in Table 1).

Since the chick and mouse samples differed not only in the experimental animal used but also in the developmental stage and myopia induction length, we conducted two separate meta-analyses, one including samples from mouse studies and one including all samples from chick studies. In these two sets of samples, we analyzed the effect of experimental myopia on the retinal transcriptome. A total of 9 control and 8 experimental myopia samples were identified using the mouse model, and 49 control and 50 experimental myopia samples in the chick model. After removing samples with outliers regarding sequencing read quality metrics (see Materials and methods; Supplementary Tables 4, 5), a total of nine control and seven myopia mouse samples, and 46 control and 45 myopia chick samples were included in the downstream analysis.

3.3 Meta-analysis of retinal transcriptomics datasets of experimental myopia

Samples from all included studies underwent the same analysis pipeline to ensure the results were directly comparable. Principal component analyses (PCA) of the individual studies did not indicate a clear clustering of the experimental samples by myopia treatment (Supplementary Figure 1). In studies that used the contralateral eye as a control, the samples from the same experimental animal were clustered together (Supplementary Figures 1B, C, E). In the only study using experimental animals of both sexes, there was clear clustering based on sex (Supplementary Figure 1D).

Next, we combined the two studies conducted in mice and the three studies conducted in chicks separately by applying batch correction and normalization using ComBat-seq (30). Before batch correction and normalization, we observed the expected batch effects, revealed by the sample distribution in PCA (Figures 3A, C). After data processing, the samples were clustered significantly closer, while a certain level of segregation between samples remained (Figures 3B, D).

The meta-analysis of 16 mouse retinal samples identified 427 differentially regulated genes (unadjusted p value <0.05, Figure 4A, Supplementary Table 6). Among the enriched KEGG pathways, significant changes were observed in signaling pathways such as TGF-beta (Figures 4B, C, Supplementary Table 7), which is critical in ocular growth and myopia development (42, 46). In addition, among the enriched pathways were dopaminergic, GABAergic and serotonergic synapse and circadian entrainment. The genes contributing to these pathways largely overlapped and included G-protein gamma subunit genes *Gng3* and *Gng4* (Figure 4C), which contribute to various receptor signaling pathways (47).

A significantly larger number of samples, a total of 91, were included in the meta-analysis of chick retinal responses to experimental myopia. We found that 1,110 genes were differentially regulated (Figure 5A, Supplementary Table 8), a larger proportion of them (54%), with highest changes in significance, were downregulated. Among those genes was vasoactive intestinal polypeptide (*VIP*), which is expressed in a subset of amacrine cells (48), and its downregulation in response to myopia has been shown in macaque retinas (48), chick retinas (45) and chick retina/RPE complex (49). Furthermore, intravitreal administration of VIP reduced the magnitude of FDM, while VIP antagonists abolished FDM development in chicks (50). The most significantly downregulated gene was urotensin-2B (*UTS2B*; Benjamini-Hochberg adjusted p value 1.05E-35). *UTS2B* encodes for urotensin II-related peptide (URP), and the downregulation of prepro-URP has been reported previously in chick retina (45) and retina/RPE complex (49). In addition to its vasoactive properties, URP is also known to induce cell proliferation (51). To our knowledge, the effect of URP in the retina is not well understood. Also among the top downregulated genes was brain-derived neurotrophic factor (*BDNF*), which has been established as neuroprotective agent in the retina (52–54). While the exact role of BDNF in myopia has not been clearly identified to date, lower levels of BDNF have been found in the aqueous humor of myopic individuals (55), and polymorphisms in the noncoding RNA gene BDNF-AS, the antisense RNA of BDNF, have been associated with myopia (56).

In line with a higher number of differentially expressed genes, the gene set was enriched for more pathways (Figures 5B, C, Supplementary Table 9). Similarly to the mouse model, the TGF-beta pathway and circadian entrainment pathways were prominent. Among the pathways that were overrepresented in the genes changing in chick retinas, but not in mouse retinas, were the HIF-1 signaling pathway as well as glucagon signaling.

Next, we sought to understand to what extent the genes and pathways differentially regulated in the mouse and chick retinas overlap. Furthermore, we wanted to determine how the findings from experimental myopia models compare to the knowledge about refractive error genetics in humans. To this end, we analyzed the results of the meta-analyses in the context of genes implicated in refractive errors in GWAS studies (Supplementary Table 10), defined as being mapped in the proximity of genetic loci associated

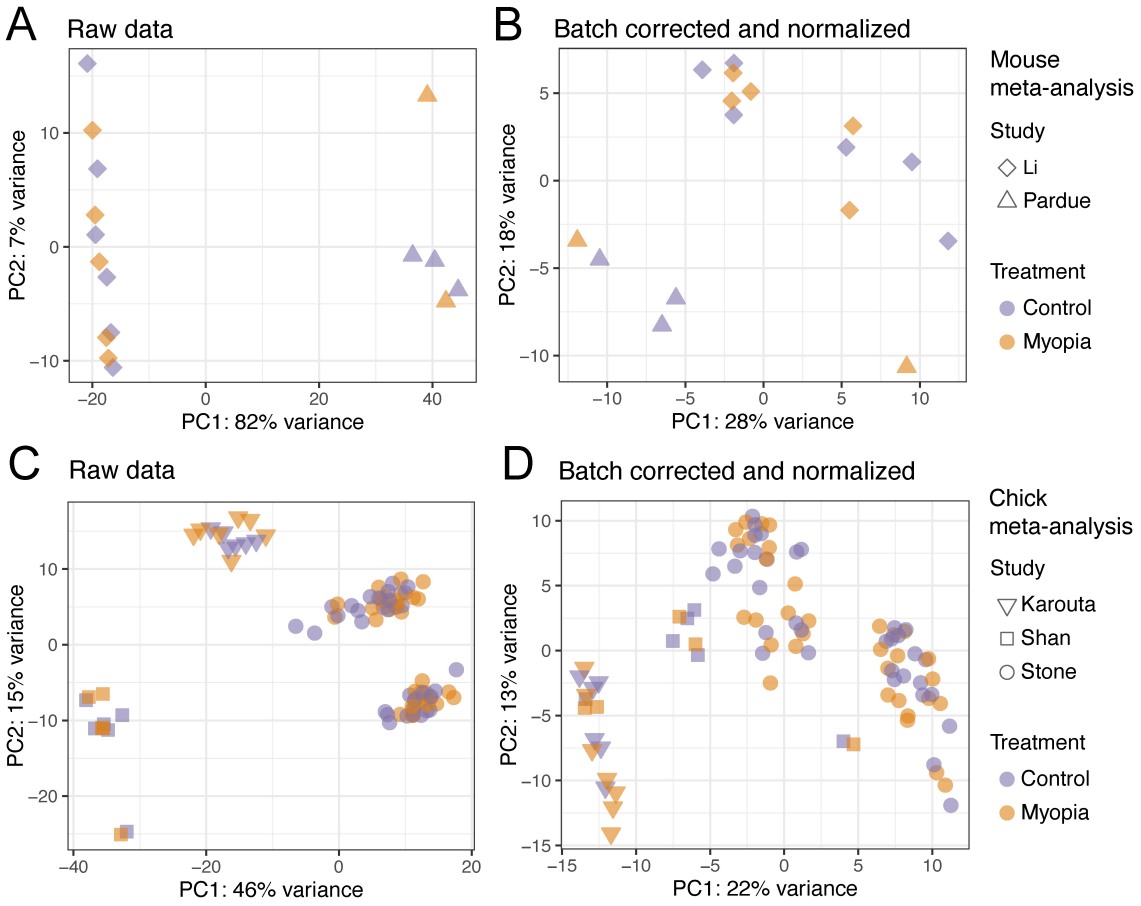

FIGURE 3
Principal component analysis of the samples included in the RNA-sequencing meta-analysis. The raw RNA-Seq datasets of the studies using the mouse model of myopia **(A)** and chick model of myopia **(C)** before any processing. The RNA-Seq samples of the mouse **(B)** and chick studies **(D)** after batch correction and normalization.

with refractive error and myopia. Regarding gene-level changes, we found that one gene, follistatin (*Fst*), was downregulated in mouse and chick retinas, and has also been implicated in refractive error in humans (Figure 6A, Supplementary Table 11). The impact of light perception and photoreceptors also seems to be conserved in the mechanisms. In particular, we observed that the gene encoding for melanopsin (*Opn4*) was downregulated in both mouse and chick retinas (Figure 6A). In addition, genes associated with photoreceptor function and phototransduction, such as *Vsx1* and *Rdh5*, were changing in chick retinas and are also implicated in refractive errors in humans (Figure 6A).

We further explored the pathways enriched for the genes changing in mouse and chick retinas, as well as those overrepresented in human refractive error susceptibility genes (Supplementary Table 12), with a subset highlighted for their relevance in retinal and refractive development (Figure 6B, Supplementary Table 13). Pathways associated with all three analyses included, again, the TGF-beta signaling pathway and circadian entrainment processes. These findings reveal the mechanistic similarities between experimental myopia in mouse and chick retinas and our knowledge of refractive error genetics in humans. They highlight the complexities of myopia as a multifactorial condition influenced by both conserved and species-specific pathways.

4 Discussion

Myopia is a growing healthcare concern, and a better mechanistic understanding of the disorder is required to design novel and effective management approaches. The increasing number of publicly available studies employing transcriptome profiling in experimental myopia provides the opportunity to combine the studies in meta-analyses, which increases the power of the analysis and allows the detection of consistent changes across experimental protocols and techniques. Here, we performed two meta-analyses on two retinal transcriptome profiling studies of mouse experimental myopia and three retinal transcriptome profiling studies of chick experimental myopia. During the final stages of manuscript preparation, another dataset by Stone et al. (57) was published, which was not included in this analysis.

We identified 427 and 1,110 differentially expressed genes in the mouse and chick retinas upon experimental myopia, respectively. The gene *Opn4*, encoding for melanopsin, a

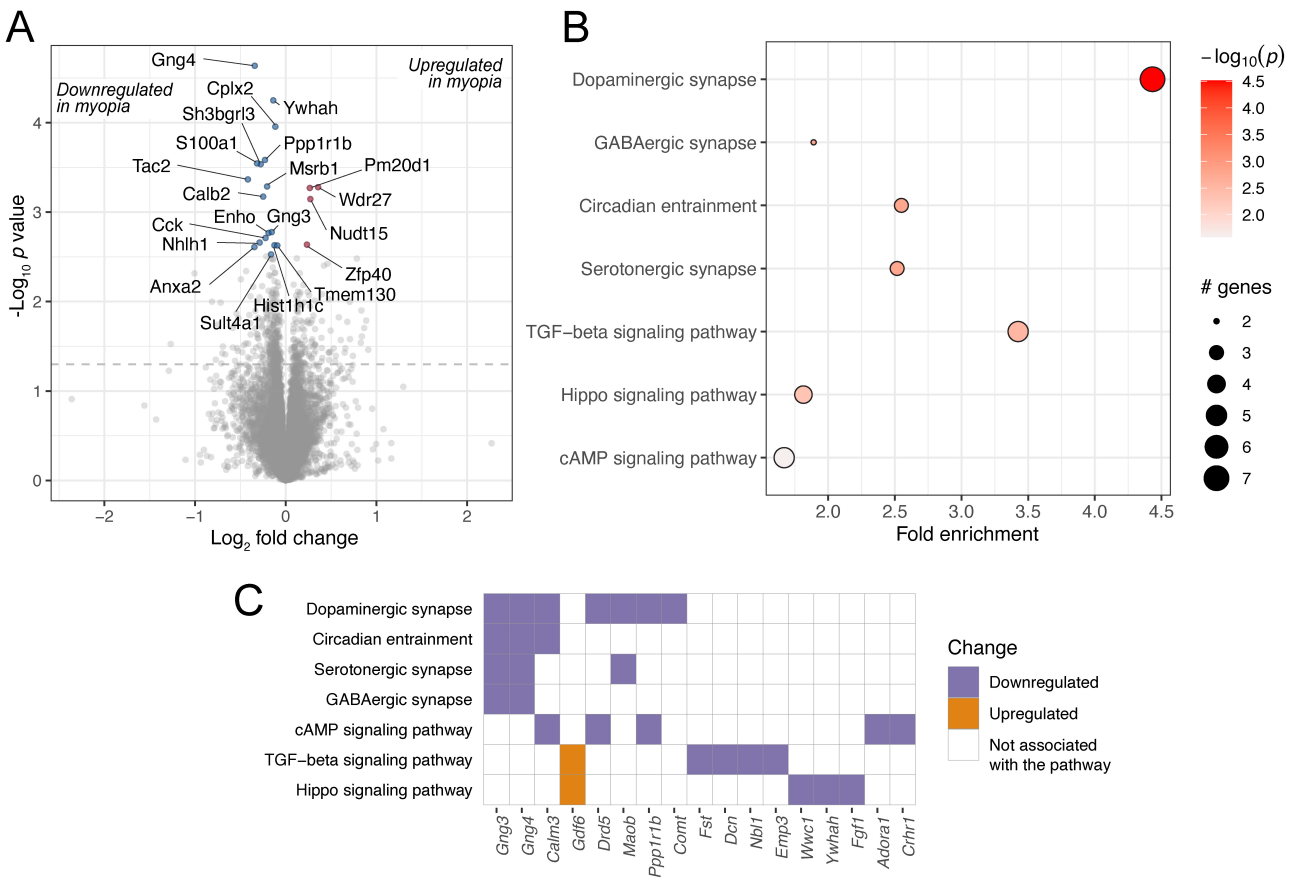

FIGURE 4
Genes and pathways differentially regulated in mouse retinas in response to experimental myopia. **(A)** A volcano plot of genes differentially regulated in response to experimental myopia in mouse retinas, indicating the $\log_2$ effect size and unadjusted log-transformed *p* values. The gray dashed horizontal line indicates an unadjusted *p* value of 0.05. A selection of genes significantly changing are highlighted in red (upregulated) and blue (downregulated), with the gene names indicated. **(B)** A selection of KEGG pathways enriched for the differentially regulated genes are highlighted. **(C)** The genes contributing to the pathways illustrated in **(B)** are shown on the horizontal axis, colors represent the directionality of gene expression change in experimental myopia.

photopigment expressed in the photosensitive retinal ganglion cells, regulating primarily the non-visual light responses (58, 59), was downregulated in the retinas of both species. Melanopsin has been found to have a strong effect on refractive development in the mouse model, where knock-out of the gene results in more hyperopic refractions and an aberrant response to FDM (60, 61). The involvement of visual processing in myopia pathogenesis is indicated by the fact that we identified the gene *Vsx1*, essential for terminal differentiation of subsets of OFF bipolar cells, to be downregulated in chick experimental myopia (Supplementary Table 7) and is also implicated in refractive errors in humans (GWAS Catalog). The knock-out of *Vsx1* has been demonstrated to render mice less susceptible to FDM (62). Another gene differentially regulated in mouse and chick retinas, and involved in visual processing, was dopamine receptor 1 (*Drd1*). It has been shown in mice that the activation of retinal dopamine 1 receptor inhibits FDM development (63).

In the meta-analyses, we found that across species, which also differed in the duration of myopia induction and developmental stage, the TGF-beta pathway was differentially regulated, and the pathway was also enriched for genes associated with human refractive errors. The TGF-beta superfamily comprises cytokines, including TGF-beta, bone morphogenic proteins (BMPs), and several others. We observed downregulation of BMP2 and BMP4 in chick myopia, similar to previous studies (49), and these genes are also implicated in human myopia (Figure 6A). The only gene that was differentially regulated in both mouse and chick retinas and is also implicated in human refractive errors, was follistatin. The primary role of follistatin is to bind and neutralize members of the TGF-beta superfamily, including BMP2 and BMP4 (64), further implying the importance of this pathway in myopia pathogenesis.

Another pathway consistently changing in all three gene sets was circadian entrainment. How exactly circadian rhythms may affect myopia development is unclear, but there is evidence that multiple processes associated with refractive error display daily rhythmicity, including axial length (65, 66) and choroidal thickness (66), and the daily rhythm of axial length is altered in chicks developing experimental myopia (67, 68). In addition, data suggest a difference in behavioral circadian rhythms in myopic individuals. In particular, some studies indicate that myopic children have later sleep timing (69–71), shorter sleep duration (70, 72) and worse sleep quality (70, 73). The mechanisms underlying

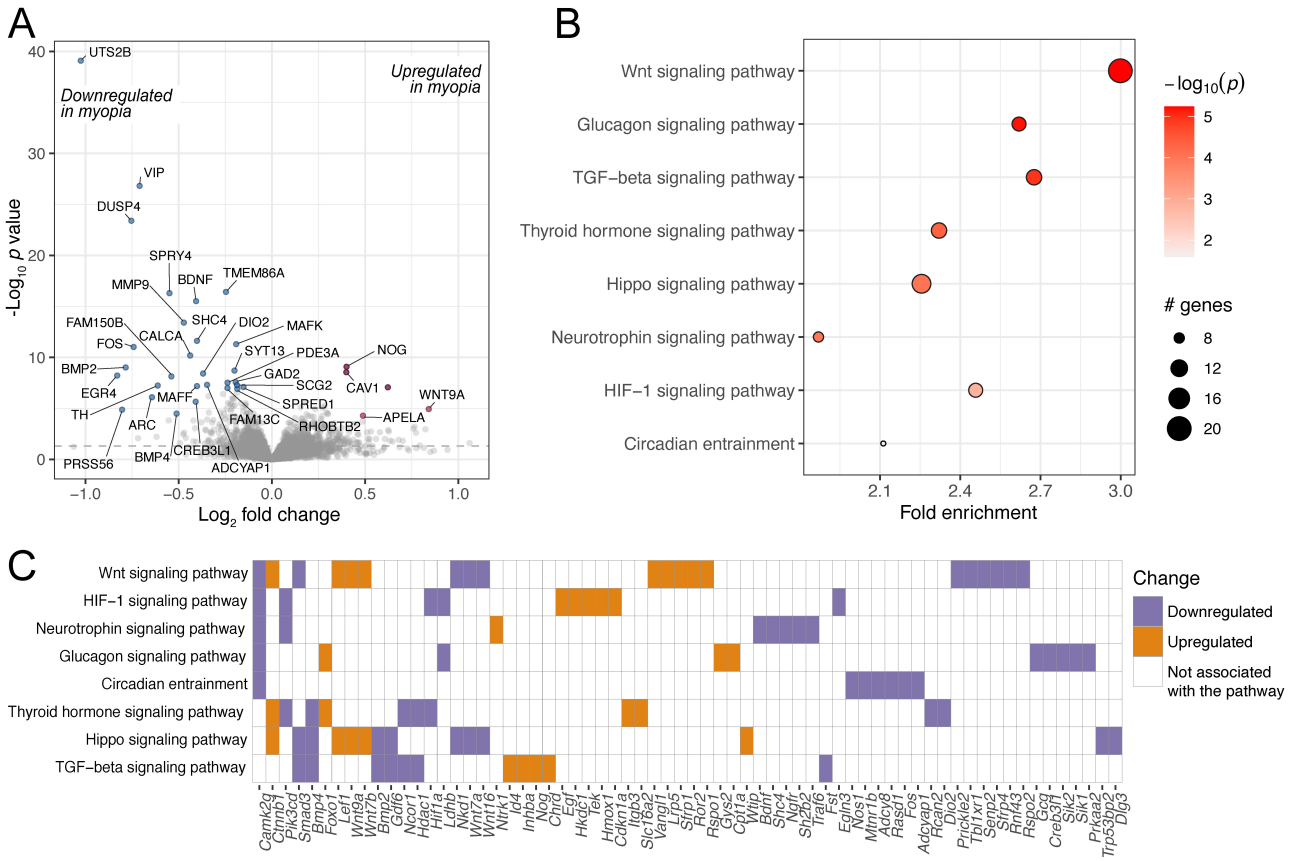

FIGURE 5
Genes and pathways differentially regulated in chick retinas in response to experimental myopia. **(A)** A volcano plot of genes differentially regulated in response to experimental myopia in chick retinas, indicating the $\log_2$ effect size and unadjusted log-transformed *p* values. The gray dashed horizontal line indicates an unadjusted *p* value of 0.05. A selection of genes significantly changing are highlighted in red (upregulated) and blue (downregulated), with the gene names indicated. **(B)** A selection of KEGG pathways enriched for the differentially regulated genes are highlighted. **(C)** The genes contributing to the pathways illustrated in **(B)** are shown on the horizontal axis, colors represent the directionality of gene expression change in experimental myopia.

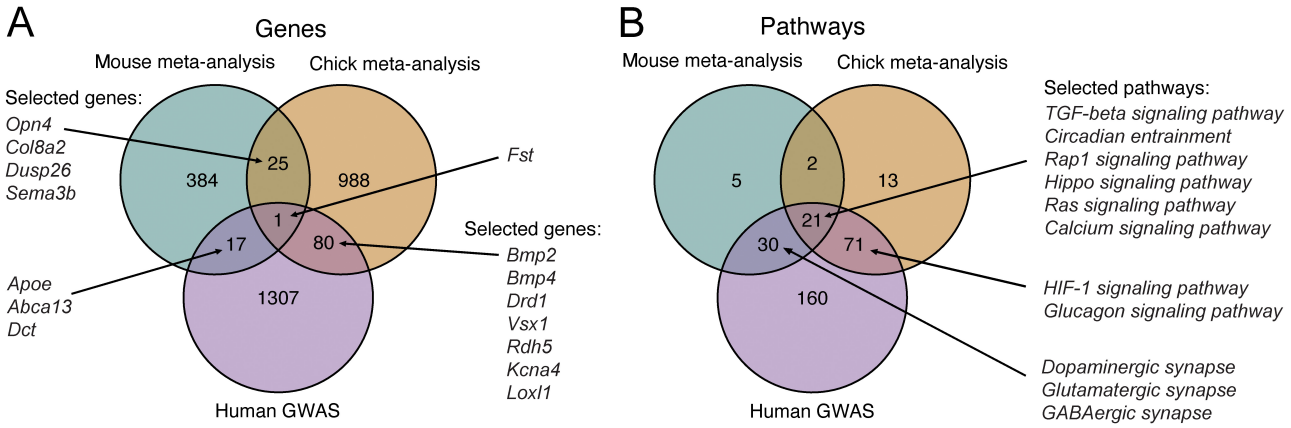

FIGURE 6
Overlap between genes and enriched pathways differentially regulated in experimental myopia in mouse and chick retinas, and those implicated in refractive error in human GWA studies. **(A)** Venn diagram of genes differentially regulated in experimental myopia in the mouse and chick retina and genes implicated in refractive error in humans show one gene associated with all three gene groups. **(B)** Venn diagram of pathways enriched for genes in **(A)**. A subset of genes and pathways most relevant in the context of the retina and refractive development are illustrated on the graphs. GWAS, genome-wide association study.

the association between myopia and circadian rhythms require further investigation.

Among the pathways associated with retinal gene changes in mouse and human myopia was dopamine signaling. While the overall dopamine signaling pathway was not overrepresented in the genes differentially regulated in chick retinas, tyrosine hydroxylase (*TH*), the rate-limiting enzyme in dopamine synthesis, was significantly downregulated in myopic chick retinas (Figure 5A). The relevance of dopamine signaling in myopia pathogenesis has been documented in several studies. For example, systemic administration of dopamine precursor L-DOPA resulted in attenuation of myopic shift in FDM (74), while the knock-out of *Th* in the mouse led to more myopic refractions (75). Furthermore, the dopamine receptor subtypes have been demonstrated to play distinct roles in myopic eye growth (76, 77).

One pathway overrepresented in the genes changing in chick retinas, was the HIF-1 signaling pathway, which has been associated with myopic signals in several studies (78, 79). Another such pathway involved glucagon signaling. The activation of glucagon signaling was demonstrated to inhibit experimental myopia in chicks (80). There is also evidence for the importance of glucagon signaling in the mouse retina. In particular, it has been demonstrated that glucagon increases inhibitory post-synaptic currents in rod bipolar cells in a dopamine-dependent manner, and this effect is abolished in retinas after 3 weeks of FDM (81), suggesting a potential neuromodulatory role for glucagon signaling also in the mouse retina.

In addition to studying myopia using experimentally induced models, other studies have taken advantage of the differences in the extent of myopia between different mouse strains (82), or of mouse models of diseases associated with myopia, such as complete congenital stationary night blindness (cCSNB) (11). Analyzing the retinal transcriptome of different mouse strains that vary in refractive error, Tkatchenko et al. (82) found the involvement of dopamine receptor signaling and phototransduction pathway in baseline myopia. Using three mouse models of cCSNB, Zeitz et al. (11) found that retinal genes differentially regulated were enriched for terms such as mitogen-activated protein kinase (MAPK) pathway and synaptic signaling. Similar to the results we obtained from the meta-analyses, *Bdnf* and *Tgfb2* transcripts were both downregulated in cCSNB models (11). A previous meta-analysis by Riddell et al. (83) studied the transcriptome changes of chick eye tissues in response to optically-induced refractive errors. Interestingly, they found an enrichment of genes associated with the complement cascade (83), which we did not detect. The discrepancy may originate from the tissues included in the analyses, while we only included retinal datasets, Riddell et al. included also the RPE and choroid (83). Collectively, these data highlight both similarities and differences in the molecular pathways underlying myopia across species and models, emphasizing the value of studying diverse experimental systems to gain a comprehensive understanding of myopia development and its underlying mechanisms.

There are several limitations to the meta-analyses presented in this article. First, the number of samples from different sexes was not balanced, in fact, only one study used male and female experimental animals. In that particular study, PCA revealed a strong effect of sex on the retinal transcriptome (Supplementary Figure 1D), and therefore, it is unclear to what extent the results are generalizable across sexes. Second, with this analysis, we identified the most robustly changing retinal transcripts, without differentiating between early and late responses to myopic stimulus, nor the differential effects of FDM and LIM. As new datasets are published and the number of samples increases, these analyses will be very interesting to perform, to further understand the intricacies of the molecular signatures in retinal responses to myopic stimuli.

Data availability statement

The original dataset presented in the study is deposited in the Gene Expression Omnibus repository, accession number GSE284642, and BioProject, accession number PRJNA1200000. These data can be found here: https://www.ncbi.nlm.nih.gov/geo/query/acc.cgi?acc=GSE284642. Publicly available datasets were analyzed in this study. These data can be found in BioProject, accession numbers PRJNA678523, PRJNA832969, PRJNA766764, and PRJNA946718.

Ethics statement

The animal study was approved by the Atlanta Veterans Affairs Medical Center Institutional Animal Care and Use Committee (protocol V015-14). The study was conducted in accordance with the local legislation and institutional requirements.

Author contributions

TP: Conceptualization, Data curation, Formal analysis, Investigation, Visualization, Writing – original draft, Writing – review & editing. SB: Formal analysis, Investigation, Writing – original draft, Writing – review & editing. MP: Conceptualization, Funding acquisition, Project administration, Supervision, Writing – original draft, Writing – review & editing.

Funding

The author(s) declare financial support was received for the research, authorship, and/or publication of this article. This research was funded by the NIH R01 EY016435 (MTP) VA Merit Award RX003134 (MTP) and the European Union Horizon Europe research and innovation program under the Marie Skłodowska-Curie grant agreement No. 101153901 (TP).

Conflict of interest

The authors declare that the research was conducted in the absence of any commercial or financial relationships that could be construed as a potential conflict of interest.

Publisher's note

All claims expressed in this article are solely those of the authors and do not necessarily represent those of their affiliated

organizations, or those of the publisher, the editors and the reviewers. Any product that may be evaluated in this article, or claim that may be made by its manufacturer, is not guaranteed or endorsed by the publisher.

Author disclaimer

Views and opinions expressed are however those of the author(s) only and do not necessarily reflect those of the European Union or European Research Executive Agency (REA). Neither the European Union nor the granting authority can be held responsible for them.

Supplementary material

The Supplementary Material for this article can be found online at: https://www.frontiersin.org/articles/10.3389/fmed.2024.1479891/full#supplementary-material

References

1. Holden BA, Fricke TR, Wilson DA, Jong M, Naidoo KS, Sankaridurg P, et al. Global prevalence of myopia and high myopia and temporal trends from 2000 through 2050. *Ophthalmology.* (2016) 123:1036–42. doi: 10.1016/j.ophtha.2016.01.006

2. Brown DM, Mazade R, Clarkson-Townsend D, Hogan K, Datta Roy PM, Pardue MT. Candidate pathways for retina to scleral signaling in refractive eye growth. *Exp Eye Res.* (2022) 219:109071. doi: 10.1016/j.exer.2022.109071

3. Wildsoet CF, Chia A, Cho P, Guggenheim JA, Polling JR, Read S, et al. IMI – interventions for controlling myopia onset and progression report. *Invest Ophthalmol Vis Sci.* (2019) 60:M106–31. doi: 10.1167/iovs.18-25958

4. Schaeffel F, Feldkaemper M. Animal models in myopia research. *Clin Exp Optom.* (2015) 98:507–17. doi: 10.1111/cxo.12312

5. Schaeffel F, Burkhardt E, Howland HC, Williams RW. Measurement of refractive state and deprivation myopia in two strains of mice. *Optom Vis Sci.* (2004) 81:99–110. doi: 10.1097/00006324-200402000-00008

6. Tkatchenko TV, Troilo D, Benavente-Perez A, Tkatchenko AV. Gene expression in response to optical defocus of opposite signs reveals bidirectional mechanism of visually guided eye growth. *PLoS Biol.* (2018) 16:e2006021. doi: 10.1371/journal.pbio.2006021

7. Karouta C, Kucharski R, Hardy K, Thomson K, Maleszka R, Morgan I, et al. Transcriptome-based insights into gene networks controlling myopia prevention. *FASEB J.* (2021) 35:e21846. doi: 10.1096/fj.202100350RR

8. Li Y, Lu Y, Du K, Yin Y, Hu T, Fu Q, et al. RNA-sequencing analysis reveals the long noncoding RNA profile in the mouse myopic retina. *Front Genet.* (2022) 13:1014031. doi: 10.3389/fgene.2022.1014031

9. Ji S, Ye L, Yuan J, Feng Q, Dai J. Integrative transcriptome and proteome analyses elucidate the mechanism of lens-induced myopia in mice. *Invest Ophthalmol Vis Sci.* (2023) 64:15. doi: 10.1167/iovs.64.13.15

10. Stone RA, Tobias JW, Wei W, Schug J, Wang X, Zhang L, et al. Diurnal retinal and choroidal gene expression patterns support a role for circadian biology in myopia pathogenesis. *Sci Rep.* (2024) 14:533. doi: 10.1038/s41598-023-50684-2

11. Zeitz C, Roger JE, Audo I, Michiels C, Sánchez-Farías N, Varin J, et al. Shedding light on myopia by studying complete congenital stationary night blindness. *Prog Retin Eye Res.* (2023) 93:101155. doi: 10.1016/j.preteyeres.2022.101155

12. Tkatchenko AV, Walsh PA, Tkatchenko TV, Gustincich S, Raviola E. Form deprivation modulates retinal neurogenesis in primate experimental myopia. *Proc Natl Acad Sci U S A.* (2006) 103:4681–6. doi: 10.1073/pnas.0600589103

13. Schippert R, Schaeffel F, Feldkaemper MP. Microarray analysis of retinal gene expression in chicks during imposed myopic defocus. *Mol Vis.* (2008) 14:1589–99. Available at: http://www.molvis.org/molvis/v14/a189

14. Arora S, Pattwell SS, Holland EC, Bolouri H. Variability in estimated gene expression among commonly used RNA-seq pipelines. *Sci Rep.* (2020) 10:2734. doi: 10.1038/s41598-020-59516-z

15. Botos MA, Arora P, Chouvardas P, Mercader N. Transcriptomic data meta-analysis reveals common and injury model specific gene expression changes in the regenerating zebrafish heart. *Sci Rep.* (2023) 13:5418. doi: 10.1038/s41598-023-32272-6

16. Hosseini SF, Bakhtiarizadeh MR, Salehi A. Meta-analysis of RNA-Seq datasets highlights novel genes/pathways involved in fat deposition in fat-tail of sheep. *Front Vet Sci.* (2023) 10:1159921. doi: 10.3389/fvets.2023.1159921

17. Faulkner AE, Kim MK, Iuvone PM, Pardue MT. Head-mounted goggles for murine form deprivation myopia. *J Neurosci Methods.* (2007) 161:96–100. doi: 10.1016/j.jneumeth.2006.10.011

18. Schaeffel F. Test systems for measuring ocular parameters and visual function in mice. *Front Biosci.* (2008) 13:4904-11. doi: 10.2741/3049

19. Afgan E, Baker D, Batut B, van den Beek M, Bouvier D, Cech M, et al. The Galaxy platform for accessible, reproducible and collaborative biomedical analyses: 2018 update. *Nucleic Acids Res.* (2018) 46:W537–44. doi: 10.1093/nar/gky379

20. Andrews S. *FastQC: a quality control tool for high throughput sequence data.* (2010). Available at: http://www.bioinformatics.babraham.ac.uk/projects/fastqc

21. Bolger AM, Lohse M, Usadel B. Trimmomatic: a flexible trimmer for Illumina sequence data. *Bioinformatics.* (2014) 30:2114–20. doi: 10.1093/bioinformatics/btu170

22. Patro R, Duggal G, Love MI, Irizarry RA, Kingsford C. Salmon provides fast and bias-aware quantification of transcript expression. *Nat Methods.* (2017) 14:417–9. doi: 10.1038/nmeth.4197

23. Love MI, Huber W, Anders S. Moderated estimation of fold change and dispersion for RNA-seq data with DESeq2. *Genome Biol.* (2014) 15:550. doi: 10.1186/s13059-014-0550-8

24. R Core Team. *R: A language and environment for statistical computing*. Vienna: R Foundation for Statistical Computing (2021). Available at: https://www.R-project.org/

25. Kanehisa M, Goto S, KEGG. Kyoto encyclopedia of genes and genomes. *Nucleic Acids Res.* (2000) 28:27–30. doi: 10.1093/nar/28.1.27

26. Raudvere U, Kolberg L, Kuzmin I, Arak T, Adler P, Peterson H, et al. g:Profiler: a web server for functional enrichment analysis and conversions of gene lists (2019 update). *Nucleic Acids Res.* (2019) 47:W191–8. doi: 10.1093/nar/gkz369

27. Ulgen E, Ozisik O, Sezerman OU. pathfindR: an R package for comprehensive identification of enriched pathways in omics data through active subnetworks. *Front Genet.* (2019) 10:858. doi: 10.3389/fgene.2019.00858

28. Wickham H. *ggplot2: Elegant Graphics for Data Analysis*. Cham: Springer Publishing Company, Incorporated (2016). https://dl.acm.org/doi/book/10.5555/2967391 (accessed June 3, 2024).

29. Soneson C, Love MI, Robinson MD. Differential analyses for RNA-seq: transcript-level estimates improve gene-level inferences [version 2; peer review: 2 approved]. *F1000Res.* (2016) 4:1521. doi: 10.12688/f1000research.7563.2

30. Zhang Y, Parmigiani G, Johnson WE. ComBat-seq: batch effect adjustment for RNA-seq count data. *NAR Genom Bioinform.* (2020) 2:lqaa078. doi: 10.1093/nargab/lqaa078

31. Leek JT, Johnson WE, Parker HS, Jaffe AE, Storey JD. The sva package for removing batch effects and other unwanted variation in high-throughput experiments. *Bioinformatics.* (2012) 28:882–3. doi: 10.1093/bioinformatics/bts034

32. Sollis E, Mosaku A, Abid A, Buniello A, Cerezo M, Gil L, et al. The NHGRI-EBI GWAS catalog: knowledgebase and deposition resource. *Nucleic Acids Res.* (2022) 51:D977–85. doi: 10.1093/nar/gkac1010

33. Mazade R, Palumaa T, Pardue MT. Insights into myopia from mouse models. *Annu Rev Vis Sci.* (2024) 10:213–38. doi: 10.1146/annurev-vision-102122-102059

34. Pardue MT, Stone RA, Iuvone PM. Investigating mechanisms of myopia in mice. *Exp Eye Res.* (2013) 114:96–105. doi: 10.1016/j.exer.2012.12.014

35. Ishibashi K, Fujii S, Escaño MFT, Sekiya Y, Yamamoto M. Up-regulation of crystallin mRNAs in form-deprived chick eyes. *Exp Eye Res.* (2000) 70:153–8. doi: 10.1006/exer.1999.0765

36. Ashby RS, Megaw PL, Morgan IG. Changes in retinal αB-crystallin (cryab) RNA transcript levels during periods of altered ocular growth in chickens. *Exp Eye Res.* (2010) 90:238–43. doi: 10.1016/j.exer.2009.10.011

37. Baskol G, Karakucuk S, Oner AO, Baskol M, Kocer D, Mirza E, et al. Serum paraoxonase 1 activity and lipid peroxidation levels in patients with age-related macular degeneration. *Ophthalmologica.* (2006) 220:12–6. doi: 10.1159/000089269

38. Mérida S, Villar VM, Navea A, Desco C, Sancho-Tello M, Peris C, et al. Imbalance between oxidative stress and growth factors in human high myopia. *Front Physiol.* (2020) 11:463. doi: 10.3389/fphys.2020.00463

39. Brown DM Yu J, Kumar P, Paulus QM, Kowalski MA, Patel JM, Kane MA, et al. Exogenous all- *trans* retinoic acid induces myopia and alters scleral biomechanics in mice. *Invest Ophthalmol Vis Sci.* (2023) 64:22. doi: 10.1167/iovs.64.5.22

40. Stone RA, McGlinn AM, Baldwin DA, Tobias JW, Iuvone PM, Khurana TS. Image defocus and altered retinal gene expression in chick: clues to the pathogenesis of ametropia. *Invest Ophthalmol Vis Sci.* (2011) 52:5765–77. doi: 10.1167/iovs.10-6727

41. Chen T, Shan G, Ma J, Zhong Y. Polymorphism in the RASGRF1 gene with high myopia: a meta-analysis. *Mol Vis.* (2015) 21:1272–80. Available at: http://www.molvis.org/molvis/v21/1272

42. Li H, Wu J, Cui D, Zeng J. Retinal and choroidal expression of BMP-2 in lens-induced myopia and recovery from myopia in guinea pigs. *Mol Med Rep.* (2016) 13:2671–6. doi: 10.3892/mmr.2016.4843

43. Li H, Cui D, Zhao F, Huo L, Hu J, Zeng J. BMP-2 is involved in scleral remodeling in myopia development. *PLoS ONE.* (2015) 10:e0125219. doi: 10.1371/journal.pone.0125219

44. Wang Q, Zhao G, Xing S, Zhang L, Yang X. Role of bone morphogenetic proteins in form-deprivation myopia sclera. *Mol Vis.* (2011) 17:647–57. Available at: http://www.molvis.org/molvis/v17/a74

45. Shan SW, Wang PF, Cheung JKW Yu F, Zheng H, Luo S, Yip SP, et al. Transcriptional profiling of the chick retina identifies down-regulation of *VIP* and *UTS2B* genes during early lens-induced myopia. *Mol Omics.* (2022) 18:449–59. doi: 10.1039/D1MO00407G

46. Tedja MS, Haarman AEG, Meester-Smoor MA, Kaprio J, Mackey DA, Guggenheim JA, et al. IMI – myopia genetics report. *Invest Ophthalmol Vis Sci.* (2019) 60:M89–M105. doi: 10.1167/iovs.18-25965

47. Betke KM, Wells CA, Hamm HE. GPCR mediated regulation of synaptic transmission. *Prog Neurobiol.* (2012) 96:304–21. doi: 10.1016/j.pneurobio.2012.01.009

48. Stone RA, Laties AM, Raviola E, Wiesel TN. Increase in retinal vasoactive intestinal polypeptide after eyelid fusion in primates. *Proc Natl Acad Sci U S A.* (1988) 85:257–60. doi: 10.1073/pnas.85.1.257

49. McGlinn AM, Baldwin DA, Tobias JW, Budak MT, Khurana TS, Stone RA. Form-deprivation myopia in chick induces limited changes in retinal gene expression. *Invest Ophthalmol Vis Sci.* (2007) 48:3430–6. doi: 10.1167/iovs.06-1538

50. Pickett Seltner RL, Stell WK. The effect of vasoactive intestinal peptide on development of form deprivation myopia in the chick: a pharmacological and immunocytochemical study. *Vision Res.* (1995) 35:1265–70. doi: 10.1016/0042-6989(94)00244-G

51. Malagon MM, Molina M, Gahete MD, Duran-Prado M, Martinez-Fuentes AJ, Alcain FJ, et al. Urotensin II and urotensin II-related peptide activate somatostatin receptor subtypes 2 and 5. *Peptides.* (2008) 29:711–20. doi: 10.1016/j.peptides.2007.12.015

52. Afarid M, Torabi-Nami M, Zare B. Neuroprotective and restorative effects of the brain-derived neurotrophic factor in retinal diseases. *J Neurol Sci.* (2016) 363:43–50. doi: 10.1016/j.jns.2016.02.024

53. Unoki K, LaVail MM. Protection of the rat retina from ischemic injury by brain-derived neurotrophic factor, ciliary neurotrophic factor, and basic fibroblast growth factor. *Invest Ophthalmol Vis Sci.* (1994) 35:907–15.

54. Lambuk L, Mohd Lazaldin MA, Ahmad S, Iezhitsa I, Agarwal R, Uskoković V, et al. Brain-derived neurotrophic factor-mediated neuroprotection in glaucoma: a review of current state of the art. *Front Pharmacol.* (2022) 13:875662. doi: 10.3389/fphar.2022.875662

55. Wang X, Mingwu L, Zheng R, Cui T, Qin J, Su Z, et al. High irisin and low BDNF levels in aqueous humor of high myopia. *Adv Clin Exp Med.* (2021) 30:893–904. doi: 10.17219/acem/125428

56. Musolf AM, Simpson CL, Moiz BA, Long KA, Portas L, Murgia F, et al. Caucasian families exhibit significant linkage of myopia to chromosome 11p. *Invest Ophthalmol Vis Sci.* (2017) 58:3547–54. doi: 10.1167/iovs.16-21271

57. Stone RA, Tobias JW, Wei W, Carlstedt X, Zhang L, Iuvone PM, et al. Diurnal gene expression patterns in retina and choroid distinguish myopia progression from myopia onset. *PLoS ONE.* (2024) 19:e0307091. doi: 10.1371/journal.pone.0307091

58. Hattar S, Liao HW, Takao M, Berson D, Yau K. Melanopsin-containing retinal ganglion cells: architecture, projections, and intrinsic photosensitivity. *Science.* (2002) 295:1065–70. doi: 10.1126/science.1069609

59. Palumaa T, Gilhooley M, Jagannath A, Hankins MW, Hughes S, Peirson SN. Melanopsin: photoreceptors, physiology and potential. *Curr Opin Physiol.* (2018) 5:68–74. doi: 10.1016/j.cophys.2018.08.001

60. Chakraborty R, Landis EG, Mazade R, Yang V, Strickland R, Hattar S, et al. Melanopsin modulates refractive development and myopia. *Exp Eye Res.* (2022) 214:108866. doi: 10.1016/j.exer.2021.108866

61. Liu A-L, Liu Y-F, Wang G, Shao Y-Q, Yu C-X, Yang Z, et al. The role of ipRGCs in ocular growth and myopia development. *Sci Adv.* (2022) 8:eabm9027. doi: 10.1126/sciadv.abm9027

62. Chakraborty R, Park HN, Aung MH, Tan CC, Sidhu CS, Iuvone PM, et al. Comparison of refractive development and retinal dopamine in OFF pathway mutant and C57BL/6J wild-type mice. *Mol Vis.* (2014) 20:1318–27. Available at: http://www.molvis.org/molvis/v20/1318

63. Shu Z, Chen K, Wang Q, Wu H, Zhu Y, Tian R, et al. The role of retinal dopamine D1 receptors in ocular growth and myopia development in mice. *J Neurosci.* (2023) 43:8231–42. doi: 10.1523/JNEUROSCI.1196-23.2023

64. Parfenova OK, Kukes VG, Grishin DV. Follistatin-like proteins: structure, functions and biomedical importance. *Biomedicines.* (2021) 9:999. doi: 10.3390/biomedicines9080999

65. Stone RA, Quinn GE, Francis EL, Ying G, Flitcroft DI, Parekh P, et al. Diurnal axial length fluctuations in human eyes. *Invest Ophthalmol Vis Sci.* (2004) 45:63–70. doi: 10.1167/iovs.03-0294

66. Nickla DL, Wildsoet C, Wallman J. Visual influences on diurnal rhythms in ocular length and choroidal thickness in chick eyes. *Exp Eye Res.* (1998) 66:163–81. doi: 10.1006/exer.1997.0420

67. Weiss S, Schaeffel F. Diurnal growth rhythms in the chicken eye: relation to myopia development and retinal dopamine levels. *J Comp Physiol A.* (1993) 172:263–70. doi: 10.1007/BF00216608

68. Nickla DL. The phase relationships between the diurnal rhythms in axial length and choroidal thickness and the association with ocular growth rate in chicks. *J Comp Physiol A.* (2006) 192:399–407. doi: 10.1007/s00359-005-0077-2

69. Chakraborty R, Seby C, Scott H, Tang V, Kemps E, Anstice N, et al. Delayed melatonin circadian timing, lower melatonin output, and sleep disruptions in myopic, or short-sighted, children. *Sleep.* (2024) 47:zsad265. doi: 10.1093/sleep/zsad265

70. Ayaki M, Torii H, Tsubota K, Negishi K. Decreased sleep quality in high myopia children. *Sci Rep.* (2016) 6:33902–33902. doi: 10.1038/srep33902

71. Xu S, Zong Z, Zhu Y, Zhang X, Zhang Y, Wang X, et al. Association between sleep-wake schedules and myopia among Chinese school-aged children and adolescents: a cross-sectional study. *BMC Ophthalmol.* (2023) 23:135. doi: 10.1186/s12886-023-02874-9

72. Jee D, Morgan IG, Kim EC. Inverse relationship between sleep duration and myopia. *Acta Ophthalmol.* (2016) 94:e204–10. doi: 10.1111/aos.12776

73. Peng W, Sun SM, Wang F, Sun YN. Comparison of factors associated with myopia among middle school students in urban and rural regions of Anhui, China. *Optom Vis Sci.* (2022) 99:702. doi: 10.1097/OPX.0000000000001933

74. Landis EG, Chrenek MA, Chakraborty R, Strickland R, Bergen M, Yang V, et al. Increased endogenous dopamine prevents myopia in mice. *Exp Eye Res.* (2020) 193:107956. doi: 10.1016/j.exer.2020.107956

75. Bergen MA, Park HN, Chakraborty R, Landis EG, Sidhu C, He L, et al. Altered refractive development in mice with reduced levels of retinal dopamine. *Invest Ophthalmol Vis Sci.* (2016) 57:4412–9. doi: 10.1167/iovs.15-17784

76. Huang F, Zhang L, Wang Q, Yang Y, Li Q, Wu Y, et al. Dopamine D1 receptors contribute critically to the apomorphine-induced inhibition of form-deprivation myopia in mice. *Invest Ophthalmol Vis Sci.* (2018) 59:2623. doi: 10.1167/iovs.17-22578

77. Huang F, Wang Q, Yan T, Tang J, Hou X, Shu Z, et al. The role of the dopamine D2 receptor in form-deprivation myopia in mice: studies with full and partial D2 receptor agonists and knockouts. *Invest Ophthalmol Vis Sci.* (2020) 61:47. doi: 10.1167/iovs.61.6.47

78. Wu H, Chen W, Zhao F, Zhou Q, Reinach PS, Deng L, et al. Scleral hypoxia is a target for myopia control. *Proc Nat Acad Sci.* (2018) 115:E7091–100. doi: 10.1073/pnas.1721443115

79. Wu W, Su Y, Hu C, Tao H, Jiang Y, Zhu G, et al. Hypoxia-induced scleral HIF-2α upregulation contributes to rises in MMP-2 expression and myopia development in mice. *Invest Ophthalmol Vis Sci.* (2022) 63:2. doi: 10.1167/iovs.63.8.2

80. Vessey KA, Lencses KA, Rushforth DA, Hruby VJ, Stell WK. Glucagon receptor agonists and antagonists affect the growth of the chick eye: a role for glucagonergic regulation of emmetropization? *Invest Ophthalmol Vis Sci.* (2005) 46:3922–31. doi: 10.1167/iovs.04-1026

81. Tapia F, Peñaloza V, Silva-Olivares F, Sotomayor-Zárate R, Schmachtenberg O, Vielma AH. Glucagon increases retinal rod bipolar cell inhibition through a D1 dopamine receptor-dependent pathway that is altered after lens-defocus treatment in mice. *Invest Ophthalmol Vis Sci.* (2024) 65:46. doi: 10.1167/iovs.65.1.46

82. Tkatchenko TV, Shah RL, Nagasaki T, Tkatchenko AV. Analysis of genetic networks regulating refractive eye development in collaborative cross progenitor strain mice reveals new genes and pathways underlying human myopia. *BMC Med Genomics.* (2019) 12:113. doi: 10.1186/s12920-019-0560-1

83. Riddell N, Crewther SG. Novel evidence for complement system activation in chick myopia and hyperopia models: a meta-analysis of transcriptome datasets. *Sci Rep.* (2017) 7:9719. doi: 10.1038/s41598-017-10277-2

frontiers | Frontiers in Medicine

TYPE Original Research
PUBLISHED 10 February 2025
DOI 10.3389/fmed.2025.1496210

OPEN ACCESS

EDITED BY
Pablo De Gracia,
University of Detroit Mercy, United States

REVIEWED BY
Fuensanta Vera-Diaz,
New England College of Optometry, United States
Brian Vohnsen,
University College Dublin, Ireland

*CORRESPONDENCE
Geunyoung Yoon
gyoon2@central.uh.edu

RECEIVED 13 September 2024
ACCEPTED 21 January 2025
PUBLISHED 10 February 2025

CITATION
Degre Kendrick C, Pusti D and Yoon G (2025) Quantifying monochromatic and polychromatic optical blur anisotropy in the periphery of myopes and emmetropes using a radial asymmetry metric.
Front. Med. 12:1496210.
doi: 10.3389/fmed.2025.1496210

Quantifying monochromatic and polychromatic optical blur anisotropy in the periphery of myopes and emmetropes using a radial asymmetry metric

Chloe Degre Kendrick, Dibyendu Pusti and Geunyoung Yoon*

College of Optometry, University of Houston, Houston, TX, United States

Purpose: The goal of this study is to characterize peripheral blur anisotropy resulting from monochromatic and chromatic aberrations along multiple meridians of myopic and emmetropic eyes using a newly developed quantitative metric.

Methods: A scanning Shack-Hartmann-based wavefront sensor was used to measure lower- and higher-order monochromatic aberrations along the horizontal and vertical meridians of 20 healthy adult subjects (10 myopes, and 10 emmetropes). Monochromatic and polychromatic blur asymmetry magnitude and orientation were quantified using a novel metric based on the optical transfer function. Published population averages of longitudinal and transverse chromatic aberration were used for polychromatic blur asymmetry calculations.

Results: Blur anisotropy magnitude and orientation differed between refractive groups at several peripheral retinal locations under monochromatic and polychromatic conditions. Myopes were significantly more likely to have vertically oriented blur than emmetropes under monochromatic conditions in the temporal peripheral retina beyond 20°. These differences were minimized when chromatic aberrations were included, though the trend remained the same.

Implications: A trend of more vertical optical blur in the temporal periphery of myopes strengthens the hypothesis that myopes experience different peripheral optical blur than emmetropes, though the small sample size of the current study limits generalizability of the results. A thorough account of peripheral blur across the visual field may lead to a better understanding of the cues that the peripheral visual system might rely on during processes such as accommodation, emmetropization, and myopization.

KEYWORDS

myopia, emmetropization, optical anisotropy, radial asymmetry metric, peripheral blur, chromatic aberration, higher-order aberrations, astigmatism

1 Introduction

Myopia, or optical near-sightedness, is one of the leading causes of visual impairment worldwide and is linked with severe eye comorbidities that can cause permanent blindness such as maculopathy, retinal detachment, and glaucoma (1, 2). This is especially concerning due to the steadily growing prevalence of myopia, which is estimated to affect 50% of the world

population by 2050 (3). Genetic factors are a known predictor of myopia development (4, 5), however, lifestyle and environment have also been shown to play a role (6). Much work has been done to identify the environmental risk factors for myopia, such as education and time spent outdoors (7–9), although the mechanism by which axial elongation occurs is still largely unexplained. Foundational animal research has found that the emmetropization and myopization processes can be impacted by visual experience, however, the precise processes by which the eye uses visual input to regulate growth in humans are not yet well understood (10–13).

The relative peripheral hyperopia (RPH) theory is one such hypothetical mechanism originating from non-human primate research suggesting that larger amounts of RPH may trigger axial elongation even when the fovea is well-corrected for defocus due to detection of residual defocus in the periphery (14). Furthermore, RPH in myopes is increased when using traditional single-vision correction (15, 16), which is thought to be an explanation for myopia progression in children wearing correction optimized only for foveal refraction. A strong association found between RPH and myopia in humans supports this theory (17, 18). In response, several treatments have been developed with the aim of reducing RPH, which have shown varying degrees of success in slowing myopia progression (19). However, longitudinal studies have not been able to predict myopia development from peripheral refraction before onset, suggesting that relative peripheral hyperopia may be an aftereffect of axial elongation, rather than a cause of myopization (20). This has prompted an investigation into other potential visual signals, such as blur orientation, that the periphery might detect as a cue for accommodation or axial elongation (21).

While peripheral refraction (i.e., lower-order aberrations) has been the primary focus in myopia control research so far, it is noteworthy that higher-order aberrations and chromatic aberrations also play a significant role in both peripheral retinal image quality and blur perception (22–25). Peripheral optical aberrations, including asymmetric aberrations such as astigmatism and coma, significantly increase in magnitude with retinal eccentricity (22, 26). Coma alone, and astigmatism when it is combined with defocus, both produce asymmetric optical blur on the retina. Notably, the blur orientation caused by astigmatism also changes direction depending on the sign of defocus it is combined with. This asymmetric blur has been hypothesized to serve as an orientational signal that aids the visual system in defocus detection and emmetropization (21, 27–29). Zheleznyak recently reported that the directionality of peripheral blur varies between refractive error groups, indicating a potential association with the development of refractive errors such as myopia (29, 30). However, this work has investigated population averages of monochromatic aberrations in the temporal peripheral retina alone. Furthermore, myopes have more relative hyperopic defocus in the periphery (17) as a consequence of their more elongated eyes, which is hypothesized to impact the shape of blur on the retina. However, the retina does not necessarily expand uniformly with myopization (31), necessitating investigation of ocular aberrations and optical quality across multiple meridians of the eye. There have been several reports of optical quality in the periphery (17, 18, 22, 24, 26, 27, 29, 30, 32–34), however, peripheral optical blur anisotropy and orientation have not been quantified using individuals' ocular aberrations nor has there been an assessment of blur anisotropy in the nasal, superior or inferior areas of the retina.

This study aims to bridge these gaps by evaluating peripheral blur anisotropy across multiple ocular meridians while accounting for individuals' higher-order aberration profiles. Longitudinal and transverse chromatic aberrations (LCA, TCA) are also considered in this work due to their impact on image quality (35). While LCA is mostly constant across the retina (32) TCA varies in magnitude depending on retinal eccentricity and alters blur orientation differently along different meridians (36). Furthermore, a recent study evaluating peripheral blur anisotropy at different wavelengths found differences in blur anisotropy between population-averaged aberration profiles of myopes, emmetropes, and hyperopes in the temporal peripheral retina (30).

Previous metrics have described blur anisotropy using a ratio based on the two-dimensional modulation transfer function (MTF). Zheleznyak first described optical anisotropy as the ratio of MTFs for horizontal to vertical gratings (27). Ji et al. described peripheral blur anisotropy as the ratio of overall horizontal to vertical contrast calculated by vector analysis of each modulus of the MTF filtered by the spatial resolution limit (21). Zheleznyak recently took a similar approach, by calculating the ratio of the area under the horizontal MTF divided by the area under the vertical MTF (29). The drawback of a "horizontal to vertical" (H:V) ratio-based method is that it cannot be used to quantify diagonal aberrations. Therefore, a new metric capable of characterizing blur anisotropy across the entire retina would enhance our understanding of how peripheral optics impact peripheral retinal image quality.

The current study aims to address these topics by characterizing the magnitude and orientation of peripheral blur in myopic and emmetropic individuals, considering monochromatic and population-averaged chromatic aberrations across multiple meridians of the eye. A new metric is proposed that can be used to characterize peripheral blur anisotropy and orientation in an effort to elucidate how an individual's lower- and higher-order aberrations may interact with chromatic aberrations to contribute to peripheral blur on the retina. A more comprehensive characterization of peripheral blur in myopic and emmetropic eyes is an important step towards understanding how peripheral optics might impact mechanisms behind emmetropization and myopization.

2 Materials and methods

2.1 Subject demographics

The left eyes of 20 healthy subjects between the ages of 19 and 35 (mean: 24.8 ± 4.1) years old were included in the study (9 females and 11 males). All participants satisfied the study's inclusion criteria, which required having healthy eyes, with no history of ocular diseases or surgeries, and no current use of medications. Most of the participants were university students and included members of our laboratory team. Subjects were sorted into two groups of ten subjects each based on cycloplegic on-axis defocus error as measured by the Shack-Hartmann wavefront sensor (26). Myopes had a mean defocus of -4.78 ± 1.47 D and emmetropes had a mean spherical refraction of 0.06 ± 0.53 D. All procedures adhered to the ethical standards of the Declaration of Helsinki and received approval from the Institutional Review Board for human subject research at the University of Rochester in Rochester, NY, USA.

2.2 Wavefront measurements

Each subject underwent cycloplegia and pupil dilation with one drop each of 1% tropicamide and 2.5% phenylephrine 30 min prior to wavefront measurements. Participants were positioned with a bite bar and then instructed to fixate on the center of a Maltese cross target that was co-aligned with the optical axis of a custom-built scanning Shack-Hartmann wavefront sensor for the duration of each meridional scan measurement (26). The fixation target was viewed with a cold mirror, and a lens was inserted into the optical path to correct for subjective refractive error and to control any residual accommodation remaining after cycloplegia. This inserted lens power was not included in the wavefront sensor measurement. Subjects maintained normal central fixation for the duration of each meridional scan. Wavefront data was collected using an 850 nm laser. Measured aberrations were then converted to the equivalent magnitude at 555 nm, which is the peak of the photopic CIE luminous efficiency function (37) i.e. the wavelength that the human eye is most sensitive to. For polychromatic conditions, defocus was converted to the equivalent magnitude for individual wavelengths. Further details on the measurement device can be found in a previously published paper (26). Each meridional scan was completed within five seconds, and a pupil camera was used to monitor proper alignment between the eye and the optical axis of the device during each measurement.

The measurement ranges for ocular aberrations were as follows: horizontal meridian from -30 degrees to +30 degrees in 5 degree steps and vertical meridian from -18 degrees to +18 degrees in 6 degree steps. Negative values signify nasal and inferior retinal locations, respectively, while 0 degrees designates the fovea for all scans. Zernike aberrations and wavefronts were calculated from the acquired Shack-Hartmann spot patterns at each retinal eccentricity using a 5.5 mm diameter circular pupil. A circular pupil was used for both foveal and eccentric measurements, similar to the 'small circle' strategy previously described by Lundström et al. (22). A point spread function (PSF) was likewise calculated from the wavefront for each individual at each tested location.

2.3 Chromatic aberrations

Population averages of longitudinal and transverse chromatic aberrations (LCA, TCA) induced by dispersion of light in the visible spectrum were included in our polychromatic calculations to simulate the peripheral blur that our subjects might experience in natural lighting conditions. LCA presents as wavelength-dependent defocus blur and has been shown to be relatively constant across the retina (25, 38). On the other hand, TCA increases with retinal eccentricity and has the effect of blurring the retinal image along the meridian that it is measured along. For example, TCA will cause horizontal blur along the horizontal meridian of a diffraction-limited model eye and vertical blur along the vertical meridian. TCA variation between subjects has been attributed to dislocation of the pupil center from the visual axis and TCA has been consistently found to vary linearly with eccentricity (36, 39). Furthermore, Rynders et al. found that on average, the pupil is well-centered in the human eye (40) i.e. average TCA at fovea of a population is zero. Therefore, we assumed that there was no TCA on-axis and simply applied 0.41 arcmins of TCA for every degree of eccentricity in every direction, though some previous work has found that the location of lowest TCA may be offset from the fovea (36). LCA was calculated for wavelengths between 405 and 695 nm. For the unweighted polychromatic condition, all wavelengths were equally weighted. A weighted condition with peak focus at 555 nm, corresponding to the peak of the human spectral sensitivity function (V_λ) (37, 41) was also included.

Monochromatic calculations included only diffraction and Zernike aberrations obtained from wavefront measurements. Finally, we have used previously published cone sampling data to limit the spatial frequencies that are included in calculating blur anisotropy and orientation for all conditions (42). The asymmetries in cone spacing along the horizontal and vertical meridians were included in our processing.

2.4 Radial asymmetry metric

A radial asymmetry metric (RAM) used to quantify the radial asymmetry of the optical transfer function (OTF) was developed to quantitatively characterize peripheral optical blur in terms of magnitude and orientation. Unlike previous metrics (21, 29) which restrict the assessment of blur anisotropy to the ratio between horizontal and vertical components, the new RAM separately quantifies the magnitude of radial asymmetry and the directional bias of the blur (i.e., orientation). This approach provides greater flexibility, enabling the characterization of diagonal aberrations in addition to horizontal and vertical ones, across any meridian of the eye. Furthermore, this approach takes image quality into account by calculating anisotropy directly from the shape of the two-dimensional OTF matrix.

RAM magnitude, i.e., the radial asymmetry of the OTF, was quantified across the horizontal and vertical meridians of the eye in five- and six-degree intervals, respectively. To do so, first, the OTF matrix was calculated from the Fourier transform of the PSF in Matlab (The MathWorks, Natick, MA). The radial asymmetry of the original OTF (Figure 1A) was then quantified by rotating the OTF by 90 degrees (Figure 1B), and then calculating the sum of the difference between the original and rotated OTF matrices (Figure 1C). It is possible to assess the radial asymmetry of the OTF in this way because of the mirror symmetry property between the first and third quadrant (and second and fourth quadrant) of the OTF matrix in the frequency domain. For example, if the original OTF was perfectly symmetric, the sum of the difference between the original and rotated OTF matrices would be equal to zero. The value was normalized by dividing the sum of the difference map (Figure 1C) by the sum of the OTF matrix of a diffraction-limited system, for that particular retinal eccentricity. In this way, the final value for RAM magnitude represents how much total asymmetry is present in the image along every direction at that specific location on the retina, with a maximum possible value of 1.

RAM orientation was also derived from the OTF by calculating the sum of the original OTF (Figure 1A) for each angular direction between 1 and 180 degrees in 1-degree angular sections. In other words, the image quality, in terms of contrast, was assessed for each axial direction of the retinal image, where a higher value indicated higher contrast or better image quality. These values were plotted along with a running average (Matlab function 'smooth', R2024a) to minimize the impact of noise from the matrix calculations (Figure 1D), and the axis corresponding to the maximum value from the running average was used for subsequent

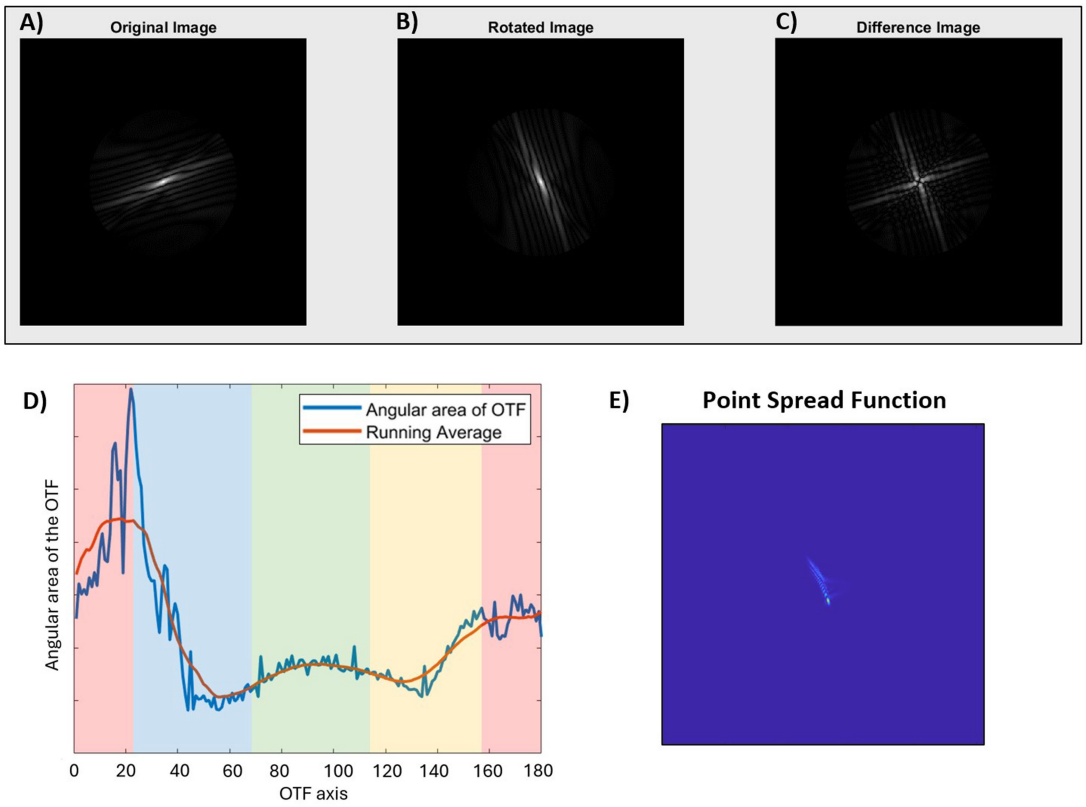

FIGURE 1
Quantification of radial asymmetry metric (RAM) magnitude **(A–C)** and orientation **(D)** of the optical transfer function (OTF), and the corresponding point spread function **(E)**. **(A)** Original OTF displaying radial asymmetry. **(B)** OTF after a 90-degree rotation to analyze asymmetry, and **(C)** Asymmetry matrix equal to the sum of the differences between the original and rotated OTF matrices. **(D)** Plot of the angular area of the OTF as a function of axis for the same OTF as shown in figure. The colored bands indicate the RAM orientation for the corresponding PSF where green is horizontal, red is vertical, blue is diagonal 135°, and yellow is diagonal 45°. **(E)** The PSF corresponding to the original image in figure. In this example, the OTF axis of maximum angular area of the OTF is 20 degrees. After accounting for the 90-degree rotation between OTF and PSF (20 + 90 = 110), the final RAM orientation is vertical (V), corresponding to a vertically blurred PSF.

calculations. The axis was then converted to the retinal image perspective by subtracting (or adding) 90 degrees, so that the final reported value corresponds to the axis of blur orientation on the retina. This is analogous to the axis of maximum blur of the PSF (Figure 1E). For ease of reporting and statistical analysis, RAM orientation results were batched into one of four categories: horizontal blur (H: 1 to 22.5 and 157.5 to 180 degrees), vertical blur (V: 67.5 to 112.5 degrees), or diagonal blur (D45: 22.5 to 67.5 degrees; D135: 112.5 to 157.5 degrees).

Zernike coefficients up to fifth-order aberrations were computed for central 40 degrees along the horizontal, vertical, and diagonal meridians of a simple model eye Zemax (Ansys, Canonsburg, PA). The corresponding PSFs were mapped by eccentricity and meridian (Figure 2A). RAM magnitude and blur anisotropy (Figure 2B) as described by Ji et al. (21) were computed based on the simulated on-axis and peripheral aberrations. Cone sampling limits were not included in this simulation. Figure 2 illustrates two notable differences between these two metrics. First, the RAM magnitude is the same along every meridian for the model eye, while the blur anisotropy metric does not identify anisotropy present along the diagonal meridians. This is because the blur anisotropy metric relies on quantifying anisotropy using a ratio of H:V components while the RAM quantifies overall radial asymmetry, which is the same across all meridians of a perfect model eye. Second, the blur anisotropy metric reaches a stable value beyond 10 degrees, while the RAM identifies 10 degrees as the location of peak difference with a gradual fall off towards 20 degrees. Again, the blur anisotropy calculation does not consider optical quality (or size) of the MTF. In other words, the blur anisotropy values can be the same for very different retinal image quality. Because the RAM is based on the overall size of the OTF, optical quality is accounted for in the magnitude calculation. Therefore, neither optical quality nor diagonal aberrations, which are prevalent along diagonal meridians of the model eye as shown in the corresponding PSFs (Figure 2A), can be quantified using the previous MTF-based ratio metric. Unlike the blur anisotropy metric however, RAM cannot describe magnitude and orientation in a single value. Therefore, RAM magnitude values should be interpreted alongside RAM orientation values to understand the complete description of the blur shape. For RAM magnitude shown in Figure 2B (left) RAM orientation was H along the horizontal meridian, V along the vertical meridian, D45 along the diagonal 45° meridian, and D135 along the diagonal 135° meridian.

2.5 Data processing and statistical analysis

Zernike analysis for each subject at each retinal location was performed using custom-built software. Lower-order aberrations

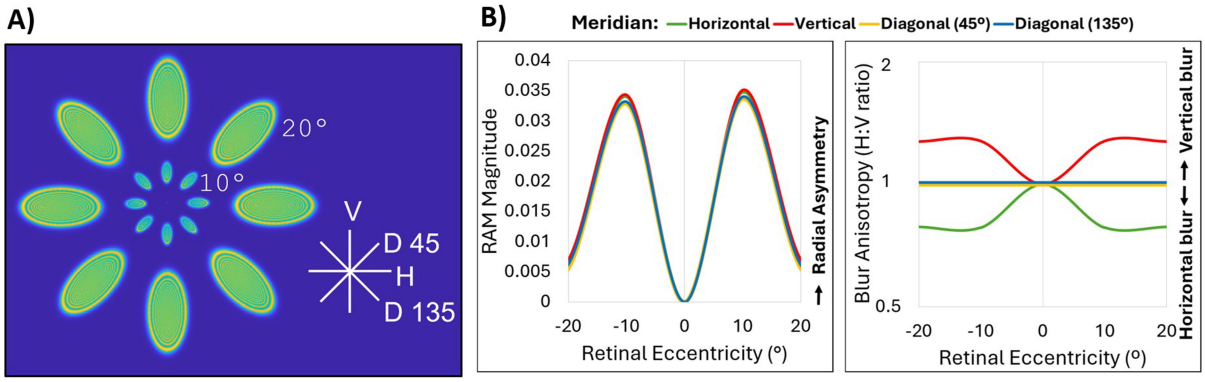

FIGURE 2
Comparison of RAM and blur anisotropy H:V ratio metrics. **(A)** Point spread functions for up to fifth-order Zernike aberrations of 0°, 10°, and 20° eccentricity obtained from a simple Zemax model eye along the horizontal (H), vertical (V), diagonal 45° (D 45), and diagonal 135° (D135) meridians. The model eye was diffraction-limited on axis with a pupil size of 4 mm and a flat retinal surface. Peripheral aberrations consisted mainly of defocus, astigmatism and coma. **(B)** Comparison of OTF-based radial asymmetry metric (RAM, left) and MTF-based H:V ratio blur anisotropy metric (right) for horizontal (green), vertical (red), diagonal 45° (yellow), and diagonal 135° (blue) meridians. All lines for RAM magnitude, and the diagonal meridian lines for blur anisotropy, overlap.

(defocus and astigmatism) were corrected at the fovea for each subject to achieve a best-corrected image in terms of optical quality. The applied foveal correction was then applied to every peripheral point so that the final aberration data represented the Zernike coefficients of a well-corrected eye, similar to as if aberrations were measured with spectacle correction. This process is necessary so that peripheral blur in myopes who would typically wear refractive correction could be compared with peripheral blur in emmetropes.

JMP Pro 17 was used for all statistical analysis. A Wilcoxon nonparametric two-sample test was used to compare RAM magnitude means between refractive error groups at each eccentricity. A contingency analysis and likelihood ratio statistic following a chi-square distribution was used to compare categorical RAM blur orientation between refractive error groups at each eccentricity. A p-value <0.05 was considered significant and a Z-score of 1.96 was used to calculate 95% confidence intervals.

3 Results

3.1 RAM magnitude

Three conditions were evaluated for blur anisotropy as shown in Figure 3: monochromatic (top row), polychromatic (middle row), and polychromatic weighted by the human spectral sensitivity function, V_λ (bottom row). Overall, RAM magnitude increased with eccentricity across both horizontal and vertical meridians. This was true for both refractive error groups across all three optical conditions. The addition of V_λ-weighted chromatic aberrations decreased the RAM magnitude at all eccentricities. RAM magnitude was further reduced for the unweighted polychromatic condition.

Generally, the RAM magnitude was similar between myopes and emmetropes at most retinal locations (Figure 3). RAM magnitude tended to be larger in emmetropes than myopes in the nasal retina beyond 20°, though this difference was only statistically significant at nasal 30° across all three conditions ($p < 0.05$), and at nasal 25° for Vλ-weighted polychromatic. Unweighted polychromatic blur anisotropy also statistically differed between refractive groups at nasal 10° (Figure 3, middle row), the only place where myopes had significantly larger RAM magnitude than emmetropes.

3.2 RAM blur orientation

The percentage of subjects with vertical blur (as opposed to horizontal or diagonal blur) is reported in Figure 4 for the same conditions as previously described. Overall, the prevalence of vertical blur decreased with the addition of chromatic aberration in the horizontal periphery (Figure 4, left column) and increased the prevalence of vertical blur in the vertical periphery (Figure 4, right column).

Along the horizontal meridian, monochromatic conditions resulted in 100% of myopes having vertical blur at nasal 30° and temporal 30° retina compared to only 70 and 60% of myopes, respectively (Figure 4, top left). The temporal retina showed a clear trend of more myopes than emmetropes with vertical blur beyond 20°. This trend reached statistically significant differences beyond 20° for monochromatic and at 20° and 25° for the polychromatic condition (Figure 4, bottom row). V_λ-weighted polychromatic blur orientation showed the same trend, though only reaching statistical significance at 30° temporal (Figure 4, middle row).

Along the vertical meridian, there was only one retinal location per condition that had significant differences in blur orientation between myopes and emmetropes: 6° temporal for monochromatic, 6° nasal for polychromatic and 12° nasal for V_λ-weighted polychromatic. These differences did not appear to be part of a larger trend as the two closest rental eccentricities on either side of the locations differing between refractive groups did not exhibit similar differences between groups.

4 Discussion

This study quantified the magnitude and orientation of peripheral blur in myopic and emmetropic individuals, considering the effects of

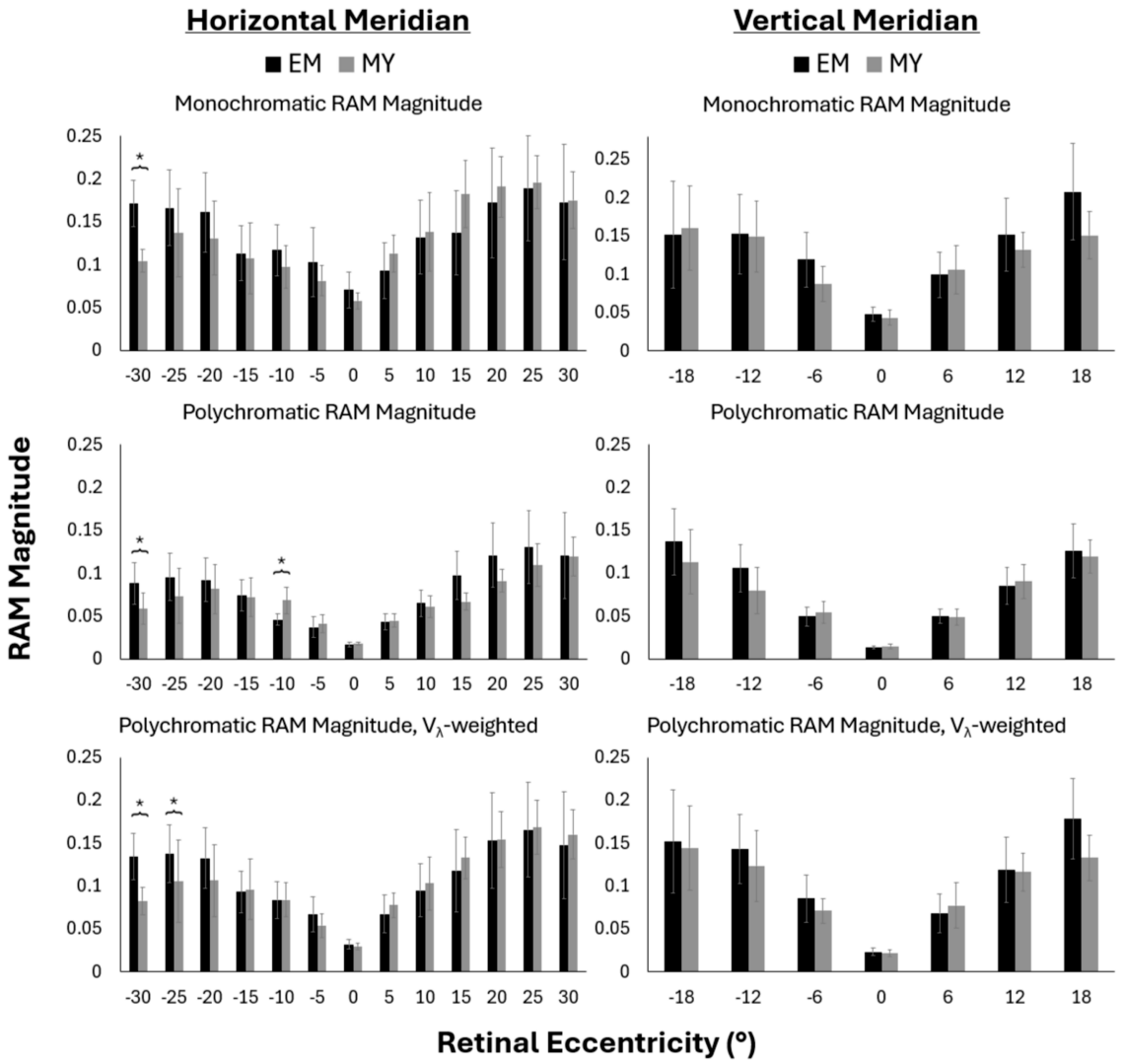

FIGURE 3
Monchromatic (top), polychromatic (middle), V_λ-weighted polychromatic (bottom), RAM magnitude along the horizontal (left) and vertical (right) meridians for emmetropes (EM) and myopes (MY). Negative values represent nasal and inferior retinal eccentricities across the horizontal and vertical meridians, respectively. Error bars represent 95% confidence intervals. *p-value<0.05.

both monochromatic and chromatic aberrations across multiple retinal meridians, using a newly developed OTF-based metric. We confirmed that the magnitude of radial asymmetry increased with temporal, nasal, superior, and inferior eccentricity in both myopes and emmetropes. The magnitude of radial asymmetry of optical blur appeared to differ between myopes and emmetropes in the nasal peripheral retina, though a small sample size limits the statistical power of this observation. Our findings also indicate that the orientation of peripheral blur is significantly different between myopes and emmetropes in the temporal peripheral retina between 20° and 30°.

Previous studies have reported increasing blur anisotropy bias between horizontal and vertical MTF as eccentricity increases in the temporal peripheral retina (21, 29, 30). This is mostly attributed to an increase in defocus, astigmatism, and asymmetric higher-order aberrations such as coma in the periphery (18, 22, 24, 26, 34). We similarly found that optical blur in the temporal peripheral retina became more radially asymmetric as retinal eccentricity increased. We also found this to be true in the nasal, superior, and inferior retina, for all conditions. Furthermore, we observed an interesting trend that emmetropes had more radially asymmetric blur in the nasal peripheral retina than myopes, and that the difference increased with eccentricity between 20° and 30° for monochromatic and both polychromatic conditions (Figure 3, left column). Interestingly, these differences were most pronounced (reaching statistical significance at 25° and 30°) for the V_λ-weighted condition (Figure 3, bottom left). This finding is compelling when considering peripheral blur anisotropy as a potential visual cue for emmetropization. However, this trend was not observed in the temporal retina, nor along the vertical meridian.

Recently, Zheleznyak et al. investigated chromatic cues for the sign of defocus in the peripheral retina using a large population-averaged aberration dataset and an MTF-based H:V ratio metric (30). They found that, in the temporal retina, green and red light caused vertical blur in myopes but horizontal blur in emmetropes. Our results similarly indicate that myopes have more vertical blur than emmetropes in the temporal retina when the full visual spectrum is

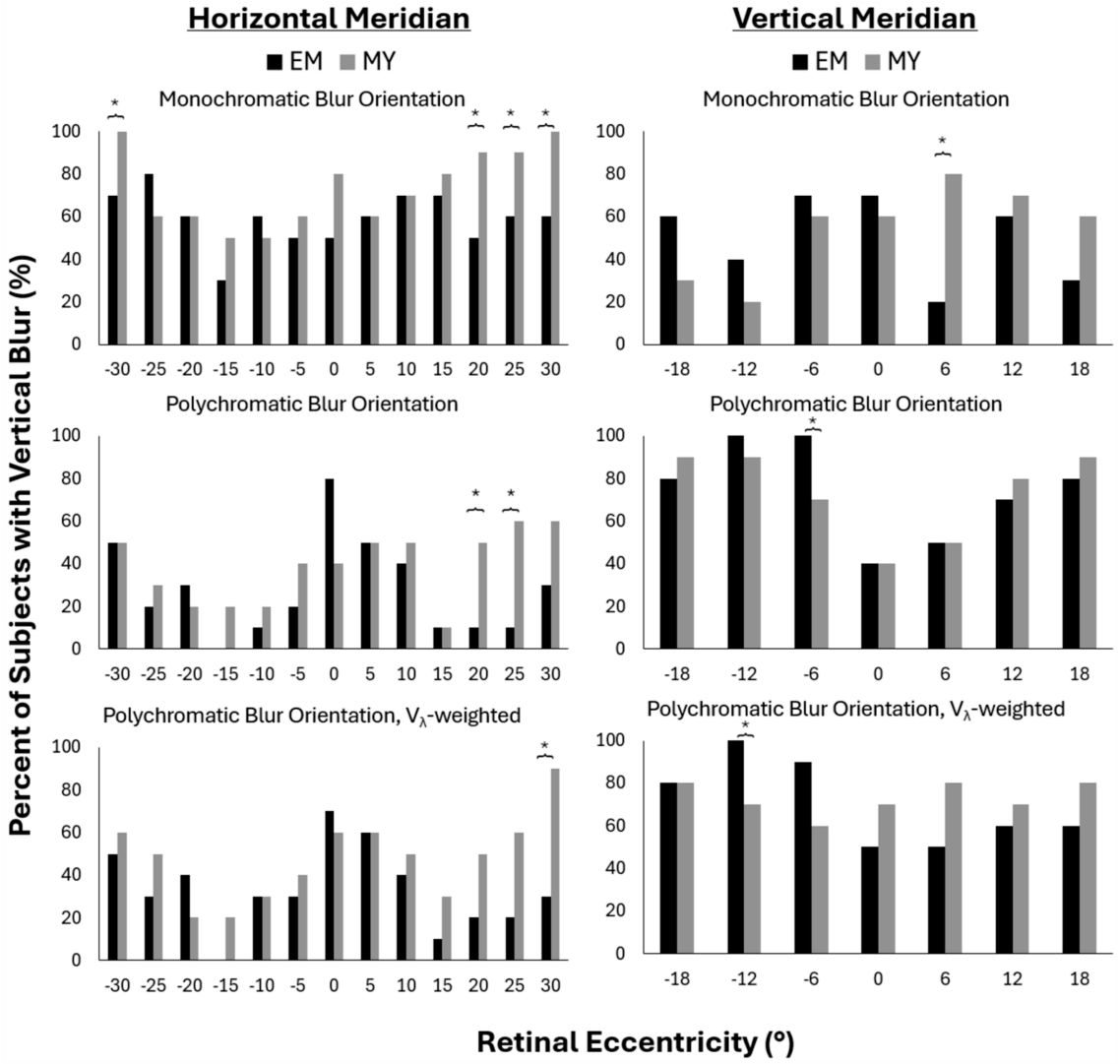

FIGURE 4
Percent of subjects with vertical blur for monochromatic (top), polychromatic (middle) and V_λ-weighted polychromatic (bottom) conditions along the horizontal (left) and vertical (right) meridians in emmetropes (EM) and myopes (MY). Negative values represent nasal and inferior retinal eccentricities across the horizontal and vertical meridians, respectively. *p-value<0.05.

considered. Alternatively, Zheleznyak et al. also found that blue light alone produced a horizontal blur signal in both emmetropes and myopes in the horizontal periphery. It is important to note that there are several differences between these two studies that should be considered when comparing results. Firstly, we examined the overall impact of monochromatic and chromatic aberrations from the visible spectrum on the OTF and peripheral blur rather than the impact of individual wavelengths of light. This approach provides a straightforward representation of how optical blur appears on the retina under real-life conditions, where many wavelengths of light are present simultaneously. Secondly, we used data from individuals, however, our sample sizes were small, which limits the statistical power of our study. In contrast, Zheleznyak et al. used a large population-averaged dataset, which may provide more generalizable results. Lastly, we used a 5.5 mm circular pupil for all Zernike analysis rather than a more realistic elliptical shape. A key advantage of using a circular pupil that fits into the larger ellipse created by measuring eccentric aberrations is that Zernike coefficients can be directly compared between different eccentricities (22). However, previous studies have concluded that pupil ellipticity does not significantly impact the MTF for eccentricities less than 30° (24) which is the maximum eccentricity we measured in this study. Despite the small sample size and the methodological differences between our study and previous studies, we found similar trends, which suggests that our findings are robust.

Overall, radial asymmetry decreased when chromatic aberrations were added. The effect was larger for the unweighted polychromatic condition compared to the V_λ-weighted condition. In other words, the interaction of chromatic aberrations and monochromatic aberrations resulted in a more symmetric blur shape. One explanation is that radially symmetric LCA had more impact on the blur asymmetry than asymmetric TCA at the tested retinal eccentricities. However, this relationship might be reversed at higher eccentricities where TCA increases while LCA remains the same (36, 38). Similarly, the addition

of chromatic aberrations appeared to standardize blur orientation across refractive groups, reducing the prevalence of vertical blur in the temporal periphery of myopes and increasing the prevalence of horizontal blur in both myopes and emmetropes in the horizontal periphery. Likewise, the percentage of subjects with vertical blur increased with chromatic aberrations along the vertical meridian. This was expected as TCA increases horizontal blur along the horizontal meridian and increased vertical blur along the vertical meridian. Notably, the impact of this common factor was great enough to minimize some of the statistical differences we found between groups under monochromatic conditions, though not enough to fully eliminate them. This suggests that blur orientation bias may still be markedly different between refractive error groups under natural conditions when the full visible spectrum is contributing to optical blur, especially at larger eccentricities.

We did not find any differences between refractive groups in magnitude of blur asymmetry along the vertical meridian (Figure 3, right column), and there were only standalone differences in blur orientation (Figure 4, right column). The lack of significant differences is not necessarily surprising considering that orientation only differed between refractive groups at eccentricities beyond 18° along the horizontal meridian. Aberration measurement along the vertical meridian was restricted to ±18 degrees because of the physical limitations of the scanning wavefront sensor. This is primarily due to the protrusion of the upper and lower eyelids, making it especially difficult to measure beyond 18° in the inferior retina. Alternative methods to measure aberrations or characterize the shapes of the optical surfaces of the eye beyond that range are necessary to gain a deeper understanding of optical blur in the superior and inferior periphery.

There was only one instance where RAM magnitude was found to be significantly larger in myopes than emmetropes. This was found at 10° nasal retina with unweighted chromatic aberration (Figure 3, middle left). This location is near the optic disc of the eye which is approximately at 15° nasal retina. Studies of peripheral refraction have observed localized relative myopic defocus near the optic disc of emmetropes (33). This, along with the knowledge that myopes are more likely to have a tilted optic disc (43) as well as relative peripheral hyperopia, may help to explain the significant difference found between groups at this retinal location. This finding suggests that myopes may experience different optical conditions near the optic disc compared to emmetropes, though finer sampling of monochromatic aberrations around the optic disc would be necessary to draw a conclusion.

Previous work has used MTF-based metrics to describe blur anisotropy in the periphery (21, 29), however, this strategy comes with notable limitations. While the MTF contains contrast information about the retinal image, it disregards phase information which has been shown to be important for image recognition (44), especially for broadband stimuli when higher-order aberrations are present as is the case in everyday viewing of the natural world (45). Therefore, we based our metric on the OTF which contains both contrast and phase information. Secondly, the combined effect of spectral sensitivity and decreased cone spacing in the periphery has not been included in peripheral blur studies. These conditions were included since it is not currently known if or how blur anisotropy is detected locally on the retina. We therefore used previously published cone sampling data to limit the spatial frequencies that are included in calculating blur anisotropy and orientation (42), and included a V_λ-weighted version of the polychromatic condition (41) to simulate cone spectral sensitivity. The cone sampling limit truncated the OTF to only include lower spatial frequencies at higher retinal eccentricities, while the V_λ-weighted polychromatic condition, a function of the spectral sensitivity of cone photoreceptors, specified how much impact each wavelength would have on the final retinal image quality metric. The function V_λ has a Gaussian shape with a maximum at 555 nm. Finally, H:V ratio-based metrics are limited to describing only the horizontal and vertical components of blur, which ignores the impact of aberrations that cause diagonal blur. Though not included in this work, characterization of oblique meridians is likely to yield diagonally oriented blur as shown in Figure 2A, especially when chromatic aberrations are included, due to oblique astigmatism and TCA. Therefore, the RAM described in this paper is sufficiently versatile for application to any ocular meridian of interest without bias.

Our findings also have implications for how we evaluate emerging myopia treatments. While multifocal and orthokeratology lenses are designed to decrease refractive error on the retina, they have also been found to increase higher-order aberrations on the peripheral retina (46, 47). At the same time, recent studies have claimed that contrast reduction could have a protective effect against myopia progression (48). Characterization of peripheral aberrations and consequently, blur anisotropy, with current myopia treatments may lead to a better understanding of why some optical treatments are more effective than others. Most importantly, this kind of understanding can aid the development of better and more effective myopia interventions.

Several factors were included in this analysis to reinforce the quality of the results of this study. First, individual higher-order aberrations were used to ensure that results are applicable to individual eyes. When higher-order aberrations are averaged across a large population, the individual variations tend to be minimized, leading to an underestimation of their true impact. This occurs because higher-order aberrations, other than spherical aberration, are somewhat randomly distributed within a normal population at fovea (49) and in the periphery (22). In other words, averaging these aberrations across many individuals effectively neutralizes the unique differences present in each person's eye. These foveal individual differences are likely translated to the periphery as well, emphasizing the value of considering individualized optical treatment if peripheral optics are found to be a factor in myopia development or progression. Furthermore, some research has found that higher-order aberrations may vary between myopes and emmetropes (34). Specifically, Mathur, et al. found that the rate of change of coma increasing with eccentricity is greater in myopes than emmetropes. Notably, coma induces asymmetric blur on the retina. Secondly, multi-meridional analysis is similarly important to this investigation as imaging studies have shown that asymmetries exist in the shape of eye between different meridians (31, 32). Lastly, it is currently unknown if anisotropy or blur orientation signals are used by the retina. However, if the signal is detected and used, it may be by cone photoreceptors which have wavelength-dependent sensitivity. Therefore, chromatic aberrations, eccentricity-specific cone sampling, and the cone spectral sensitivity function were included to simulate realistic ocular optical conditions.

A limitation of our study is the small sample size, which may affect the generalizability of our findings. Additionally, while we measured aberrations along horizontal and vertical meridians, future studies should include a more comprehensive mapping of

the peripheral retina, including diagonal meridians, to capture the full extent of peripheral aberrations. Population averages of chromatic aberration were used for the inclusion of both LCA and TCA in this study. Direct measurement of these factors, specifically in the periphery, may lead to more conclusive results, though some preliminary investigation by our lab has shown that the inaccuracy caused by using population-averaged chromatic aberration is minimal. A very recent study found that blur anisotropy was resistant to pupil changes for pupils larger than 1.5 mm at 30 deg. eccentricity (30). While pupil size was not a primary outcome of this study, it would be interesting for future work to assess how blur anisotropy changes with pupillary fluctuations. Finally, and most essentially, longitudinal studies are necessary to determine if there is a causal relationship between peripheral blur and refractive error.

In conclusion, our study provides valuable insights into the peripheral optical blur experienced by myopes and emmetropes under both monochromatic and polychromatic conditions. Our versatile metric can be used to precisely characterize peripheral blur orientation in any ocular meridian, which provides a useful alternative to other commonly used metrics, especially in cases where diagonal aberrations are present. The differences in peripheral blur orientation between our small groups of myopes and emmetropes underscore the importance of considering how peripheral visual signals, other than simply relative peripheral defocus, might impact myopization and emmetropization. By providing a comprehensive account of monochromatic and polychromatic peripheral blur in individual subjects, this study strengthens our knowledge of the peripheral visual signals available to the physiological systems that regulate eye growth. Future research should continue to explore these factors across different populations and under varying optical conditions to further improve our understanding and therefore lead to better myopia intervention strategies.

Data availability statement

The raw data supporting the conclusions of this article will be made available by the authors, without undue reservation.

Ethics statement

The studies involving humans were approved by the University of Rochester Institutional Review Board for human subject research. The studies were conducted in accordance with the local legislation and institutional requirements. The participants provided their written informed consent to participate in this study.

Author contributions

CD: Conceptualization, Data curation, Formal analysis, Investigation, Methodology, Software, Validation, Writing – original draft, Writing – review & editing. DP: Conceptualization, Data curation, Writing – review & editing, Investigation, Methodology. GY: Conceptualization, Funding acquisition, Methodology, Resources, Supervision, Validation, Writing – review & editing, Investigation, Software.

Funding

The author(s) declare that financial support was received for the research, authorship, and/or publication of this article. Funding for this research was provided by the NIH/NEI R01EY034151, NIH/NEI P30EY007551, and Meta.

Acknowledgments

We would like to acknowledge Flaum Eye Institute at University of Rochester, the site of data collection for this work.

Conflict of interest

The authors declare that the research was conducted in the absence of any commercial or financial relationships that could be construed as a potential conflict of interest.

The author(s) declared that they were an editorial board member of Frontiers, at the time of submission. This had no impact on the peer review process and the final decision.

Publisher's note

References

1. Ohno-Matsui K, Lai TYY, Lai CC, Cheung CMG. Updates of pathologic myopia. *Prog Retin Eye Res*. (2016) 52:156–87. doi: 10.1016/j.preteyeres.2015.12.001

2. Pan CW, Cheung CY, Aung T, Cheung CM, Zheng YF, Wu RY, et al. Differential associations of myopia with major age-related eye diseases: the Singapore Indian eye study. *Ophthalmology*. (2013) 120:284–91. doi: 10.1016/j.ophtha.2012.07.065

3. Holden BA, Fricke TR, Wilson DA, Jong M, Naidoo KS, Sankaridurg P, et al. Global prevalence of myopia and high myopia and temporal trends from 2000 through 2050. *Ophthalmology*. (2016) 123:1036–42. doi: 10.1016/j.ophtha.2016.01.006

4. Edwards MH. Effect of parental myopia on the development of myopia in Hong Kong Chinese. *Ophthalmic Physiol Opt*. (1998) 18:477–83. doi: 10.1046/j.1475-1313.1998.00388.x

5. PACELLA R, MCLELLAN J, GRICE K, del E, WIGGS J, GWIAZDA J. Role of genetic factors in the etiology of juvenile-onset myopia based on a longitudinal study of refractive error. *Optom Vis Sci*. (1999) 76:381–6. doi: 10.1097/00006324-199906000-00017

6. Enthoven CA, Tideman JWL, Polling JR, Tedja MS, Raat H, Iglesias AI, et al. Interaction between lifestyle and genetic susceptibility in myopia: the generation R study. *Eur J Epidemiol*. (2019) 34:777–84. doi: 10.1007/s10654-019-00512-7

7. Morgan IG, Wu PC, Ostrin LA, Tideman JWL, Yam JC, Lan W, et al. IMI risk factors for myopia. *Invest Ophthalmol Vis Sci*. (2021) 62:3. doi: 10.1167/iovs.62.5.3

8. Theophanous C, Modjtahedi B, Batech M, Marlin D, Luong T, Fong D. Myopia prevalence and risk factors in children. *Clin Ophthalmol*. (2018) 12:1581–7. doi: 10.2147/OPTH.S164641

9. Gwiazda JE, Hyman L, Norton TT, Hussein ME, Marsh-Tootle W, Manny R, et al. Accommodation and related risk factors associated with myopia progression and their interaction with treatment in COMET children. *Invest Ophthalmol Vis Sci*. (2004) 45:2143–51. doi: 10.1167/iovs.03-1306

10. Irving EL, Callender MG, Sivak JG. Inducing ametropias in hatchling chicks by defocus—aperture effects and cylindrical lenses. *Vis Res*. (1995) 35:1165–74. doi: 10.1016/0042-6989(94)00235-E

11. Smith EL 3rd, Hung LF. The role of optical defocus in regulating refractive development in infant monkeys. *Vis Res*. (1999) 39:1415–35. doi: 10.1016/S0042-6989(98)00229-6

12. Whatham AR, Judge SJ. Compensatory changes in eye growth and refraction induced by daily wear of soft contact lenses in young marmosets. *Vis Res*. (2001) 41:267–73. doi: 10.1016/S0042-6989(00)00250-9

13. Smith EL 3rd, Hung LF. Form-deprivation myopia in monkeys is a graded phenomenon. *Vis Res*. (2000) 40:371–81. doi: 10.1016/S0042-6989(99)00184-4

14. Smith EL 3rd, Hung LF, Huang J. Relative peripheral hyperopic defocus alters central refractive development in infant monkeys. *Vis Res*. (2009) 49:2386–92. doi: 10.1016/j.visres.2009.07.011

15. Tabernero J, Vazquez D, Seidemann A, Uttenweiler D, Schaeffel F. Effects of myopic spectacle correction and radial refractive gradient spectacles on peripheral refraction. *Vis Res*. (2009) 49:2176–86. doi: 10.1016/j.visres.2009.06.008

16. Lin Z, Martinez A, Chen X, Li L, Sankaridurg P, Holden BA, et al. Peripheral defocus with single-vision spectacle lenses in myopic children. *Optom Vis Sci*. (2010) 87:4–9. doi: 10.1097/OPX.0b013e3181c078f1

17. Mutti DO, Sholtz RI, Friedman NE, Zadnik K. Peripheral refraction and ocular shape in children. *Invest Ophthalmol Vis Sci*. (2000) 41:1022–1030.

18. Osuagwu UL, Suheimat M, Atchison DA. Peripheral aberrations in adult hyperopes, emmetropes and myopes. *Ophthalmic Physiol Opt*. (2017) 37:151–9. doi: 10.1111/opo.12354

19. Jonas JB, Ang M, Cho P, Guggenheim JA, He MG, Jong M, et al. IMI prevention of myopia and its progression. *Invest Ophthalmol Vis Sci*. (2021) 62:6. doi: 10.1167/iovs.62.5.6

20. Atchison DA, Li SM, Li H, Li SY, Liu LR, Kang MT, et al. Relative peripheral hyperopia does not predict development and progression of myopia in children. *Invest Ophthalmol Vis Sci*. (2015) 56:6162–70. doi: 10.1167/iovs.15-17200

21. Ji Q, Yoo YS, Alam H, Yoon G. Through-focus optical characteristics of monofocal and bifocal soft contact lenses across the peripheral visual field. *Ophthalmic Physiol Opt*. (2018) 38:326–36. doi: 10.1111/opo.12452

22. Lundstrom L, Gustafsson J, Unsbo P. Population distribution of wavefront aberrations in the peripheral human eye. *J Opt Soc Am A Opt Image Sci Vis*. (2009) 26:2192–8. doi: 10.1364/JOSAA.26.002192

23. Lundstrom L, Manzanera S, Prieto PM, Ayala DB, Gorceix N, Gustafsson J, et al. Effect of optical correction and remaining aberrations on peripheral resolution acuity in the human eye. *Opt Express*. (2007) 15:12654–61. doi: 10.1364/OE.15.012654

24. Romashchenko D, Rosen R, Lundstrom L. Peripheral refraction and higher order aberrations. *Clin Exp Optom*. (2020) 103:86–94. doi: 10.1111/cxo.12943

25. Atchison DA, Smith G. Chromatic dispersions of the ocular media of human eyes. *J Opt Soc Am A Opt Image Sci Vis*. (2005) 22:29–37. doi: 10.1364/JOSAA.22.000029

26. Pusti D, Degre Kendrick C, Wu Y, Ji Q, Jung HW, Yoon G. Widefield wavefront sensor for multidirectional peripheral retinal scanning. *Biomed Opt Express*. (2023) 14:4190–204. doi: 10.1364/BOE.491412

27. Zheleznyak L, Barbot A, Ghosh A, Yoon G. Optical and neural anisotropy in peripheral vision. *J Vis*. (2016) 16:1. doi: 10.1167/16.5.1

28. Pusti D, Patel NB, Ostrin LA, Nti AN, das S, Yoon G. Peripheral choroidal response to localized defocus blur: influence of native peripheral aberrations. *Invest Ophthalmol Vis Sci*. (2024) 65:14. doi: 10.1167/iovs.65.4.14

29. Zheleznyak L. Peripheral optical anisotropy in refractive error groups. *Ophthalmic Physiol Opt*. (2023) 43:435–44. doi: 10.1111/opo.13104

30. Zheleznyak L, Liu C, Winter S. Chromatic cues for the sign of defocus in the peripheral retina. *Biomed Opt Express*. (2024) 15:5098–114. doi: 10.1364/BOE.537268

31. Verkicharla PK, Mathur A, Mallen EAH, Pope JM, Atchison DA. Eye shape and retinal shape, and their relation to peripheral refraction. *Ophthalmic Physiol Opt*. (2012) 32:184–99. doi: 10.1111/j.1475-1313.2012.00906.x

32. Jaeken B, Lundström L, Artal P. Peripheral aberrations in the human eye for different wavelengths: off-axis chromatic aberration. *J Opt Soc Am A*. (2011) 28:1871–9. doi: 10.1364/JOSAA.28.001871

33. Lan W, Lin Z, Yang Z, Artal P. Two-dimensional peripheral refraction and retinal image quality in Emmetropic children. *Sci Rep*. (2019) 9:16203. doi: 10.1038/s41598-019-52533-7

34. Mathur A, Atchison DA, Charman WN. Myopia and peripheral ocular aberrations. *J Vis*. (2009) 9:p. 15 1-12. doi: 10.1167/9.10.15

35. Ravikumar S, Thibos LN, Bradley A. Calculation of retinal image quality for polychromatic light. *J Opt Soc Am A Opt Image Sci Vis*. (2008) 25:2395–407. doi: 10.1364/JOSAA.25.002395

36. Winter S, Sabesan R, Tiruveedhula P, Privitera C, Unsbo P, Lundström L, et al. Transverse chromatic aberration across the visual field of the human eye. *J Vis*. (2016) 16:9. doi: 10.1167/16.14.9

37. International Organization for Standardization. Photometry - The CIE System of Physical Photometry. *ISO/CIE 23539* (2023). doi: 10.25039/IS0.CIE.23539.2023

38. Fernandez-Alonso M, Finch AP, Love GD, Read JCA. Ocular accommodation and wavelength: the effect of longitudinal chromatic aberration on the stimulus-response curve. *J Vis*. (2024) 24:11. doi: 10.1167/jov.24.2.11

39. Thibos LN. Calculation of the influence of lateral chromatic aberration on image quality across the visual field. *J Opt Soc Am A*. (1987) 4:1673–80. doi: 10.1364/JOSAA.4.001673

40. Rynders M, Lidkea B, Chisholm W, Thibos LN. Statistical distribution of foveal transverse chromatic aberration, pupil centration, and angle psi in a population of young adult eyes. *J Opt Soc Am A Opt Image Sci Vis*. (1995) 12:2348–57. doi: 10.1364/JOSAA.12.002348

41. Schnapf JL, Kraft TW, Baylor DA. Spectral sensitivity of human cone photoreceptors. *Nature*. (1987) 325:439–41. doi: 10.1038/325439a0

42. Watson AB. A formula for human retinal ganglion cell receptive field density as a function of visual field location. *J Vis*. (2014) 14:15. doi: 10.1167/14.7.15

43. Zhang F, Liu X, Wang Y, Wang Q, Zheng M, Chang F, et al. Characteristics of the optic disc in young people with high myopia. *BMC Ophthalmol*. (2022) 22:477. doi: 10.1186/s12886-022-02719-x

44. Sarver EJ, Applegate RA. The importance of the phase transfer function to visual function and visual quality metrics. *J Refract Surg*. (2004) 20:S504–7. doi: 10.3928/1081-597X-20040901-19

45. Bex PJ, Makous W. Spatial frequency, phase, and the contrast of natural images. *J Opt Soc Am A Opt Image Sci Vis*. (2002) 19:1096–106. doi: 10.1364/JOSAA.19.001096

46. Fedtke C, Ehrmann K, Thomas V, Bakaraju RC. Peripheral refraction and aberration profiles with multifocal lenses. *Optom Vis Sci*. (2017) 94:876–85. doi: 10.1097/OPX.0000000000001112

47. Tomiyama ES, Hu C, Marsack JD, Richdale K. Greater higher order aberrations induced by toric orthokeratology versus soft toric multifocal contact lens wear. *Ophthalmic Physiol Opt*. (2021) 41:726–35. doi: 10.1111/opo.12839

48. Rappon J, Chung C, Young G, Hunt C, Neitz J, Neitz M, et al. Control of myopia using diffusion optics spectacle lenses: 12-month results of a randomised controlled, efficacy and safety study (CYPRESS). *Br J Ophthalmol*. (2023) 107:1709–15. doi: 10.1136/bjo-2021-321005

49. Salmon TO, van de Pol C. Normal-eye Zernike coefficients and root-mean-square wavefront errors. *J Cataract Refract Surg*. (2006) 32:2064–74. doi: 10.1016/j.jcrs.2006.07.022

frontiers | Frontiers in Medicine

TYPE Original Research
PUBLISHED 22 April 2025
DOI 10.3389/fmed.2025.1523211

OPEN ACCESS

EDITED BY
Pablo De Gracia,
University of Detroit Mercy, United States

REVIEWED BY
Alexandra Benavente-Perez,
State University of New York, United States
Gopa Kumar Gopinadhan Nair,
University of Southern California, United States
Marquis Walker,
James Madison University, United States

*CORRESPONDENCE
Safal Khanal
✉ skhanal@uab.edu

RECEIVED 05 November 2024
ACCEPTED 17 March 2025
PUBLISHED 22 April 2025

CITATION
Sanchez NC, Roig-Lopez JL, Mobley JA and Khanal S (2025) Proteomic signatures of retinal pigment epithelium-derived exosomes in myopic and non-myopic tree shrew eyes. *Front. Med.* 12:1523211. doi: 10.3389/fmed.2025.1523211

Proteomic signatures of retinal pigment epithelium-derived exosomes in myopic and non-myopic tree shrew eyes

Nilda C. Sanchez[1], Jose Luis Roig-Lopez[1], James A. Mobley[2,3] and Safal Khanal[1]*

[1]School of Optometry, Department of Optometry and Vision Science, University of Alabama at Birmingham, Birmingham, AL, United States, [2]Heersink School of Medicine, Department of Anesthesiology and Perioperative Medicine, University of Alabama at Birmingham, Birmingham, AL, United States, [3]Heersink School of Medicine, O'Neal CCC Mass Spectrometry and Proteomics Shared Resource, University of Alabama at Birmingham, Birmingham, AL, United States

Purpose: The retinal pigment epithelium (RPE) transmits growth signals from the neural retina to the choroid in the emmetropization pathway, but the underlying molecular mechanisms remain poorly understood. Here, we compared the proteomic profiles of RPE-derived exosomes between myopic and non-myopic eyes of tree shrews, dichromatic mammals closely related to primates.

Methods: Four myopic (159–210 days of visual experience, DVE) and seven non-myopic eyes (156–210 DVE) of tree shrews were included. Non-cycloplegic refractive error was measured with Nidek autorefractor, and axial ocular component dimensions were recorded with LenStar. Tissue was collected, yielding RPE-lined eyecups, which were subsequently incubated in L-15 culture media for 2 h. The RPE-derived exosomes were then enriched and purified from the incubation media by double ultracentrifugation and characterized by imaging and molecular methods. Exosomal proteins were identified and quantified with mass spectrometry, examined using GO and KEGG analyses, and compared between myopic and non-myopic samples.

Results: Out of 506 RPE exosomal proteins identified, 48 and 41 were unique to the myopic and non-myopic samples, respectively. There were 286 differentially expressed proteins in the myopic samples, including 79 upregulated and 70 downregulated. The top three upregulated proteins were Histone H4 (Fold Change, FC = 3.04, $p = 0.09$), PTB 1 (FC = 2.59, $p = 0.08$) and Histone H3.1 (FC = 2.59, $p = 0.13$), while the top three downregulated proteins were RPS5 (FC = −2.41, p=0.004), ACOT7 (FC=-2.15, $p = 0.04$) and CRYBB2 (FC = −2.14, $p = 0.05$). Other differentially expressed proteins included LUM, VCL, SEPTIN11, GPX3, SPTBN1, SEPTIN7, RPL10A, KCTD12, FGG, and FMOD. Proteomic analysis revealed a low abundance of ATP6V1B2 and crystallin beta B2, and a significant depletion of the crystallin protein family (crystallin A2, A3, and B3 subunits) in the myopic samples. The enrichment analyses showed extracellular matrix, cytoskeletal dynamic, and cell-matrix adhesion as the primary components associated with the RPE exosomal proteins in myopic eyes.

Conclusion: Using standard molecular and imaging techniques, this study provides the first demonstration of the *ex-vivo* RPE exosome biogenesis from tree shrew eyes. The results showed distinct differential expressions of the RPE exosomal proteins between the myopic and non-myopic eyes, with several proteins unique to each group. Future targeted proteomic studies of identified candidate exosomal protein signatures could elucidate the molecular

mechanism of RPE exosome-mediated growth signal transmission in the emmetropization pathway.

KEYWORDS

myopia, exosomes, retinal pigment epithelium, tree shrews, emmetropization

Introduction

In postnatally developing eyes, a visually guided emmetropization mechanism uses visual cues to control the rate of axial eye growth to achieve and maintain a good focus on the retina (emmetropia). Experimental alterations of visual cues, for example, by imposing defocus (1, 2) or changing the spectral composition of light (3–6), produce a compensatory modulation of eye growth, causing the eye to deviate from emmetropia. These vision-dependent changes in eye growth can occur in a regionally selective manner (7, 8) and without the need for accommodation (9, 10) or central connections to the brain (11), suggesting that the emmetropization mechanism is local to the eye and operates along the retina-choroid-sclera pathway, whereby the neurosensory retina [likely amacrine cells (12, 13)] produces a cascade of growth stimulatory (GO) or inhibitory (STOP) signals that trigger changes in choroidal thickness and scleral remodeling to control eye size and refractive state (14, 15). In the past few decades, certain environmental factors, likely related to the modern world, have led to a failure in emmetropization in an increasingly large number of individuals, causing a rapid rise in myopia prevalence worldwide (16). The mechanistic basis of this failure is not fully understood due largely to an incomplete understanding of the molecular mechanisms involved in the early retinal growth signaling pathway of emmetropization (17).

There is growing evidence that the retinal pigment epithelium (RPE) plays a critical role in the emmetropization mechanism (18). The anatomical location of the RPE—with the neurosensory retina on the apical side and the choroid on the basal side—allows it to serve as a conduit for growth signals between the retina and the choroid (15, 19, 20). During experimental manipulations of image focus, the RPE secretes growth-regulatory factors and shows bi-directional changes in gene expressions (18). For instance, eye growth-promoting stimuli cause downregulation of the BMP2 (21–25), while growth-inhibiting stimuli cause upregulation (21, 23, 25). These results provide compelling evidence for RPE-mediated control of eye growth, although how the RPE transmits signaling information related to eye growth remains unknown.

Exosomes are nano-sized extracellular membrane-bound vesicles (30–100 nm) that could be involved in growth signal transmission across the RPE. All eukaryotic cells release exosomes from their endosomal compartments, except perhaps the mature erythrocytes (26). Studies have reported exosome biogenesis in a variety of bodily fluids (27), including tears and aqueous humor (28, 29). Although previously thought of as a means of cellular waste disposal, recent evidence points to the major physiological function of exosomes in mediating intercellular communication through the delivery of cargo to neighboring or distant cells (30, 31). Their cargo contains proteins, nucleic acids, and lipids unique to the cell of origin and can readily cross RPE tight junctions and retinal blood barriers (32), making them candidate growth signaling molecules. Proteomic evidence supports the biogenesis of exosomes from the RPE (33, 34), likely occurring on the apical side and mediated by the inhibition of G-protein coupled receptor (GPR)143 (35), which acts as a direct competitive antagonist receptor of dopamine—a potent myopia-protective neurotransmitter molecule (35, 36). Interestingly, the apical surface of the RPE also contains Na+/K+/ATPase, a known exosomal marker (37) whose expression levels have been linked to myopia (38, 39). In addition, the RPE apical surface is known to release several neurotransmitters, such as epidermal growth factor (40) and αβ crystalline (41, 42) that are implicated in the regulation of eye growth and refractive state.

These results lead to our hypothesis that exosomes released by the RPE may serve as candidate messengers to facilitate communication of growth signals from the neurosensory retina to the choroid. In this study, we provide preliminary evidence of *ex-vivo* RPE exosome biogenesis from the myopic and non-myopic tree shrew eyes. In addition, we demonstrate differential expression patterns of several RPE exosomal proteins in myopic eyes and highlight major cellular pathways by which RPE exosomes may facilitate growth signal transmission in the emmetropization mechanism.

Methods

Animals

Tree shrews (*Tupaia belangeri*) used in this study were raised by their mothers in the Tree Shrew Core at the University of Alabama at Birmingham. The colony is maintained on a 14-h light-on/10-h light-off cycle. Since tree shrews are born with their eyes closed, we designate the day of eye-opening (~3 weeks after birth) as the first day of visual experience (DVE). The age range of animals in this study was 156 to 210 DVE. All procedures were performed in adherence with the ARVO Statement for the Use of Animals in Ophthalmic and Vision Research and were approved by the Institutional Animal Care and Use Committee of the University of Alabama at Birmingham.

Experimental groups

Nine tree shrews (five males/four females) were the subjects in this study. All animals within a group came from a different litter and were 156 to 210 DVE at the time of tissue collection. Individual eyes were categorized into myopic ($n = 4$ eyes) and

TABLE 1 Characteristics of the experimental groups.

	Myopic ($n = 4$)	Non-myopic ($n = 7$)	p-value*
Days of Visual Experience (DVE, range)	159–210	156–210	
Right eye: left eye	3:1	4:3	
Male: female	3:1	3:4	
Spherical equivalent refractive error {D, mean [Sphere +(Cylinder/2)] ± SD}	−9.26 ± 5.98	0.45 ± 0.64	0.002
Vitreous chamber depth (mm)	3.05 ± 0.05	2.37 ± 0.10	0.0003

*Two sample t-test.

non-myopic (control, $n = 7$ eyes) groups based on their non-cycloplegic refractive error. In myopic eyes, myopia was previously induced either by a −5 D lens or narrow-band cyan light, stimuli that are known to induce myopia in these animals (3, 43, 44). Non-myopic eyes were from animals raised in standard colony lighting who were near emmetropic after having completed their initial emmetropization process or had recovered from previous treatments to become near emmetropic. The average (mean ± SD) spherical equivalent refractive error (SER) was −9.26 ± 5.98 D for the myopic group and 0.45 ± 0.64 D for the non-myopic group (Table 1). The difference in SER between the groups was consistent with the difference in vitreous chamber depth (myopic: 3.05 ± 0.05 mm; non-myopic: 2.37 ± 1.04 mm).

Measurements of refractive error and ocular component dimensions

Non-cycloplegic refractive error was measured in awake and gently restrained animals in a dimly illuminated room using the Nidek infrared autorefractor (ARK-700A, Marco Ophthalmic, Jacksonville, FL, www.marco.com). To record these measurements, animals were aligned with the instrument using a pedestal installed on their skull, as described previously (45). A set of 10 measurements was taken, out of which five measurements with the highest quality scores were averaged to obtain the final SER. All refractive values were corrected for the "small eye artifact" (46) previously shown to be about +4 D in tree shrews (47). As with previous studies, we used non-cycloplegic data to quantify the SER because they have been shown to provide a valid estimate of refractive error in these species (48).

Following the measurement of refractive errors, axial ocular component dimensions were measured in awake and gently restrained animals with the LenStar (LS-900, Haag-Streit, www.haag-streit.com) using tree shrew-specific refractive indices (49). This optical biometer uses low-coherence interferometry to measure the dimensions of axial components. From these components, one can also calculate the vitreous chamber depth as the distance between the posterior lens surface and the internal limiting membrane of the retina. Three measurements were averaged to obtain the final measurement of axial components.

RPE tissue preparation

After the animals were terminally anesthetized (17.5 mg ketamine and 1.2 mg xylazine, followed by 50 mg xylazine, intramuscular injection), eyes were enucleated and immediately put into a 10 cm Petri dish with sterile phosphate-buffered saline (PBS) for washing (Figure 1). Eyes were then transferred to a 6-well plate containing 4 mL of fresh PBS solution and dissected into an eyecup using a dissecting microscope and an 18 G needle. An incision was made in the sclera, ∼1.0 mm behind the limbal boundary. Then, the anterior segment, including the cornea, iris, ciliary body, and crystalline lens, was removed. The retina was then detached from the remaining posterior segment eyecup, gently tugging on the zonule of Zinn, and then progressively peeled away, avoiding fragmentation. The eyecup with only RPE-choroid-sclera complex (RPE-lined eyecup) was washed twice with PBS and transferred to the upper chamber of 0.4 μm transwell insert of a 24-well plate (Corning, Cat# 3450, USA). Approximately 200 μl of L-15 media was added on top of the eyecup located in the upper chamber and 500 μl of media in the lower chamber of the insert. This allowed the eyecup to immerse in media, maintaining a normal flow of fluids on the RPE monolayer during incubation. The eyecup with media was then incubated at 37°C for 2 h, using a protocol modified from a previous report (35). After 2 h, the conditioning media was collected and centrifuged at 800 × g for 5 min at 4°C. The supernatant was then transferred to a new tube and stored at −80°C before enriching exosomes.

Exosome enrichment and characterization

The RPE exosomes were isolated and purified using the double ultracentrifugation method (50). First, the eyecup conditioning media (∼200 μl) was thawed and centrifuged at 1,000 × g for 10 min at 4°C. The supernatant was then transferred to an ultracentrifuge tube (#361623, for fixed angle rotor) and diluted to a volume of 4.5 mL using PBS before centrifuging the diluted sample at 10,000 × g for 30 min at 4°C using a fixed angle rotor. The supernatant was collected in an ultra-clear ultracentrifuge tube (#344057, for a swinging bucket rotor) and centrifuged in a swinging bucket rotor at 100,000 × g for 60 min at 4°C. After ultracentrifugation, the pellets were washed twice with 4.5 mL of PBS and briefly air-dried by flipping tubes upside down on Kimwipe (1–3 min). The excess PBS on the tube wall was wiped off using Kimwipe without disturbing the pellet/bottom of the tube. The pellet was then reconstituted in 40 μl of PBS by pipetting up and down ∼20 times gently, and resuspended samples were prepared for quality checks and proteomic analysis.

Three phenotyping methods were used to characterize the enriched exosomes: transmission electron microscopy (TEM, Tecnai Spirit T12), CD63 enzyme-linked immunoassay, and nanoparticle tracking analysis (NTA), as recommended by the International Society for Extracellular Vesicles (51). The

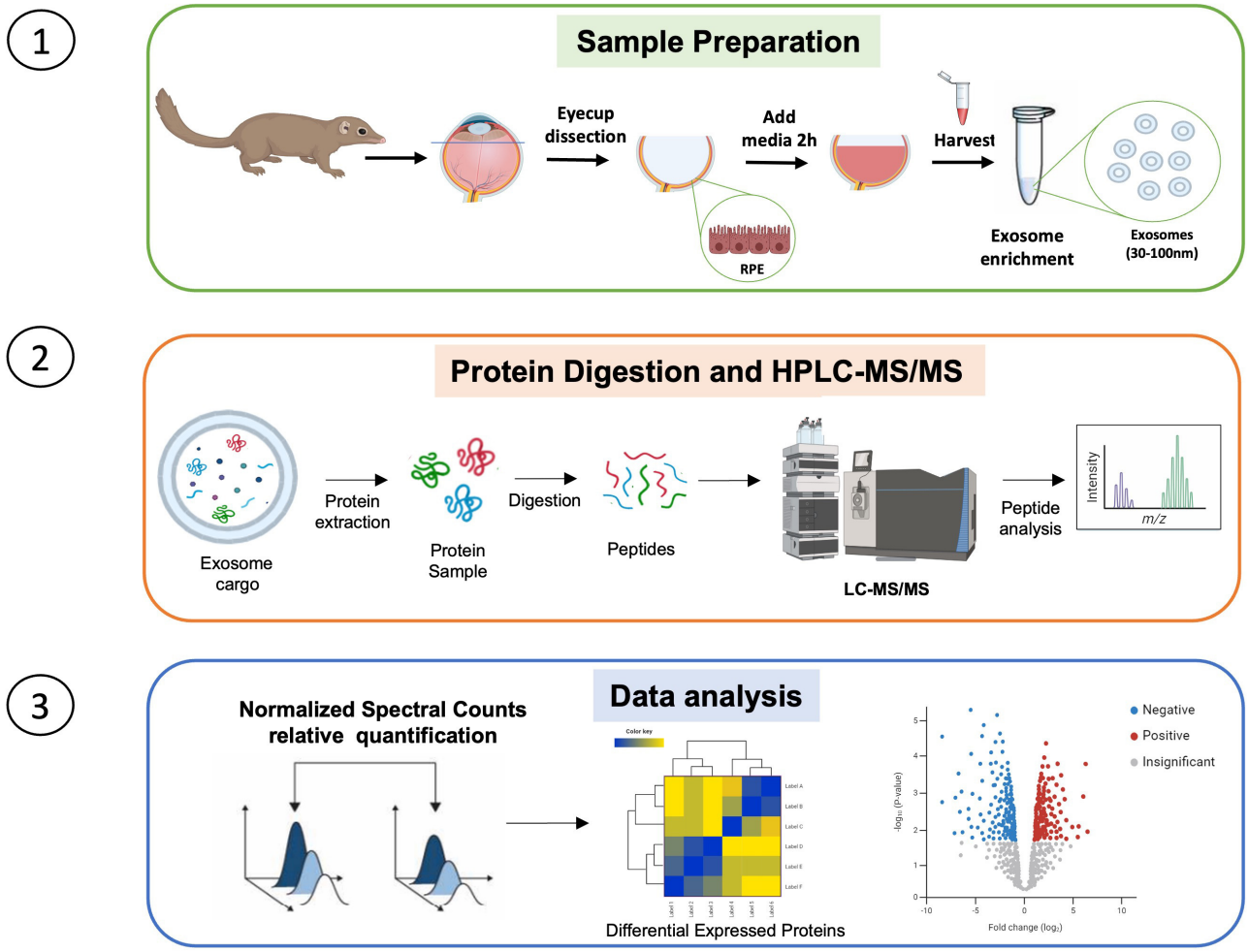

FIGURE 1
Graphical illustration of experimental methodology showing sample preparation, protein digestion and extraction, and data analysis. Created with BioRender.com.

morphology of particles in the samples was visualized with transmission electron microscopy (TEM, Tecnai Spirit T12) after preparing the samples according to a previously published protocol (27). We also evaluated CD63 expression [a molecular marker of exosomes (27)] in the samples using ExoELISA-ULTRA CD63 Kit (#EXEL-ULTRA-CD63-1, System Biosciences, SBI) following the manufacturer's instructions.

Nanoparticle tracking analysis

The size and concentration of exosomes released from RPE-lined eyecups were measured with NTA using NanoSight NS300 (Malvern Instruments Inc., Westborough, MA) equipped with a 488nm laser and integrated automated fluidics. Five 60-s videos were recorded of each sample with the camera level set at 13 and the detection threshold set at 5. The temperature was set at 25°C and monitored throughout the measurements. Videos recorded for each sample were analyzed with NTA software version 3.4.4 to determine the concentration and size of measured particles with corresponding standard errors. For analysis, auto settings were used for blur, minimum track length, and minimum expected particle size. The NanoSight system was calibrated with polystyrene latex microbeads of 50, 100, and 200 nm (Thermo Scientific Inc.) before analysis. Exosome samples were diluted at 1:50 in PBS and 1 mL was used for NanoSight analysis. Sterile PBS (Gibco #20012-027) was used as a diluent to avoid contaminating particles. Five measurement runs were performed for each sample and averaged to obtain the final data. Results of NTA were displayed as frequency distribution graphs showing the number of particles per milliliter. The concentration of particles was calculated to determine the mean ± SD number of exosomes in the myopic and non-myopic samples.

Mass spectrometry

Sample preparation

Proteomics analysis was carried out as previously referenced with minor changes (52) under section 2.5 nLC-ESI-MS2 under Protein IDs for GeLC. All protein extracts were attained using M-PER™ Mammalian Protein Extraction Reagent (Thermo Fisher

Scientific, Cat. # 78501) and quantified using Pierce BCA Protein Assay Kit (Thermo Fisher Scientific, Cat.# PI23225). As was experimentally determined, a set amount of protein per sample was diluted to 35 μL using NuPAGE LDS sample buffer (1× final conc., Invitrogen, Cat.# NP0007). Proteins were reduced with DTT and denatured at 70°C for 10 min prior to loading everything onto Novex NuPAGE 10% Bis-Tris Protein gels (Invitrogen, Cat.# NP0315BOX) and separated (35 min at 200 constant V). The gels were stained overnight with a Novex Colloidal Blue Staining kit (Invitrogen, Cat.# LC6025). Following de-staining, each entire lane was cut into multiple MW fractions (3–8 fractions, as is experimentally determined to be optimal) and equilibrated in 100 mM ammonium bicarbonate (AmBc), each gel plug was digested overnight with Trypsin Gold, Mass Spectrometry Grade (Promega, Cat.# V5280) following manufacturer's instruction. Peptide extracts were reconstituted in 0.1% Formic Acid (FA)/ddH_2O at 0.1 μg/μL.

Protein quantification

Peptide digests (8 μL each) were injected onto a 1,260 Infinity nHPLC stack (Agilent Technologies) and separated using a 75-micron I.D. × 15 cm pulled tip C-18 column (Jupiter C-18 300 Å, 5 microns, Phenomenex). This system ran in line with a Thermo Q Exactive HFx mass spectrometer, equipped with a Nanospray FlexTM ion source (Thermo Fisher Scientific), and all data was collected in CID mode. The nHPLC was configured with binary mobile phases that included solvent A (0.1%FA in ddH_2O), and solvent B [0.1%FA in 15% ddH_2O/85% Acetonitrile (ACN)], programmed as follows; 10 min at 5%B (2 μL/min, load), 90 min at 5%-40%B (linear: 0.5 nL/min, analyze), 5 min at 70%B (2 μL/min, wash), 10 min at 0%B (2 μL/min, equilibrate). Following each parent ion scan (300–1,200 m/z at 60k resolution), fragmentation data (MS2) was collected on the topmost intense 10 ions at 7.5K resolution. For data-dependent scans, charge state screening and dynamic exclusion were enabled with a repeat count of 2, repeat duration of 30 s, and exclusion duration of 90 s.

MS data conversion and searches

The XCalibur RAW files were collected in profile mode, centroided, and converted to MzXML using ReAdW v. 3.5.1. The mgf files were created using MzXML2Search (included in TPP v. 3.5) for all scans. The data were searched using SEQUEST (Thermo Fisher Scientific), which is set for three maximum missed cleavages, a precursor mass window of 20 ppm, trypsin digestion, variable modification C at 57.0293, and M at 15.9949 as a base setting, with additional post-translational modifications (ex: Phos, Ox, GlcNAc, etc.) that may be applied later as determined to be of importance experimentally. Searches were performed with a species-specific subset of the UniProtKB database.

Peptide filtering, grouping, and quantification

The list of peptide IDs generated based on SEQUEST search results was filtered using Scaffold (Protein Sciences, Portland Oregon). Scaffold filters and groups all peptides to generate and retain only high-confidence IDs while also generating normalized spectral counts (N-SCs) across all samples for relative quantification. The filter cut-off values were set with a minimum peptide length of >5 AAs, with no MH+1 charge states, with peptide probabilities of >80% C.I., and with the number of peptides per protein ≥2. The protein probabilities were set to a >99.0% C.I., and an false discovery rate (FDR) < 1.0. Scaffold incorporates the two most common methods for statistical validation of large proteome datasets, the FDR and protein probability (53–55). Relative quantification across experiments was performed via spectral counting (56, 57), and when relevant, spectral count abundances were normalized between samples (58).

Data and statistical analysis

Proteomic data analysis

For proteomic data generated, two separate non-parametric statistical analyses were performed between each pair-wise comparison. These non-parametric analyses include 1) the calculation of weight values by significance analysis of microarray (SAM; cut off >|0.8| combined with, 2) *T*-Test (single tail, unequal variance, cut off $p < 0.05$), which are then sorted according to the highest statistical relevance in each comparison. For SAM (59, 60), whereby the weight value (W) is a statistically derived function that approaches significance as the distance between the means (μ1-μ2) for each group increases, and the SD (δ1-δ2) decreases using the formula, W=(μ1-μ2)/(δ1-δ2). For protein abundance ratios determined with N-SCs, we set a 1.5–2.0-fold change (FC) as the threshold for significance, determined empirically by analyzing the inner-quartile data from the control experiments using ln-ln plots, where the Pearson's correlation coefficient (R) is 0.98, and >99% of the normalized intensities fell between the set fold change. In each case, all three tests (SAM, *T*-test, or FC) needed to pass to be considered significant.

Systems analysis

The Gene Ontology (GO) assignments and pathway analysis were performed using the ShinyGO 0.77 online tool (61). The results were verified with other online tools: Database for Annotation, Visualization, and Integrated Discovery and g: Profiler online tool (62). In addition, functional annotation clustering and Kyoto Encyclopedia of Genes and Genomes (KEGG) pathway mapping were performed. Protein networks and interactomes were analyzed with the STRING 9.1 public database (63).

Results

Characterization of exosomes released by RPE-lined eyecups

Figure 2 illustrates the phenotypic characterization of exosomes isolated from the RPE-lined eyecups of myopic and non-myopic tree shrew eyes. The TEM images of the samples showed homogeneous round-shaped membraned vesicles on exosome-enriched samples (Figure 2A). The particle size was in the range expected for exosomes (64) and peaked at 72.3 ± 2.3 nm for

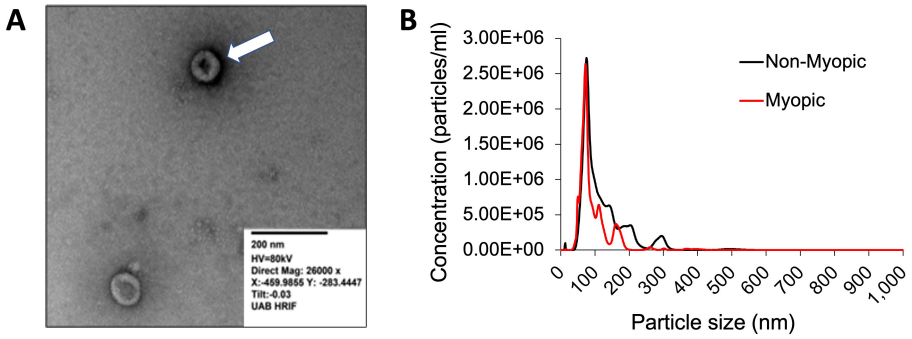

FIGURE 2
The phenotypic characterization of exosomes released by RPE-lined eyecups. **(A)** Homogeneous round-shaped membraned vesicles with diameters of 30–150 nm characteristic of exosomes were observed in transmission electron microscopy (scale: 200 nm). **(B)** Concentration of particles as a function of their size on Nanoparticle Tracking Analysis (NTA) of exosomes enriched samples: non-myopic (black line) and myopic (red line). The peak size of particles was 72.3 nm for non-myopic samples and 67.6 nm for myopic samples.

the non-myopic sample and 67.6 ± 2.3 for the myopic sample (Figure 2B). The size heterogeneity between the myopic and non-myopic samples may be related to biological roles, such as cellular processes, disease mechanisms, or cargo content and delivery (65, 66). The mean ± SD concentration of particles was $1.43 \pm 0.06 \times 10^8$ particles/mL in the non-myopic sample and $9.4 \pm 0.37 \times 10^7$ particles/mL in the myopic sample. The presence of the CD63, a molecular marker of exosomes (51), was measured by ExoELISA-ULTRA CD63 Kit (#EXEL-ULTRA-CD63-1, System Biosciences, SBI). The samples were positive for CD63, with a range of exosome abundance from 4×10^8 to 7×10^8 across samples.

Proteomic profile of RPE exosomes from myopic and non-myopic eyes

A total of 506 proteins were identified across the myopic and non-myopic RPE exosome samples. Out of these, 417 were common, 48 were uniquely expressed in the myopic samples and 41 were uniquely expressed in the non-myopic samples (Figure 3A; Supplementary Tables S1, S2). The enrichment analysis for KEGG, GO cellular components, and GO molecular functions performed on ShinyGO 0.77 for uniquely expressed proteins are shown in Figures 3B–D for myopic samples and Figures 4A–C for non-myopic samples. The RPE exosomal proteins uniquely expressed in myopic samples were linked to the metabolism of carbohydrates and amino sugars with phosphoglucomutase and phosphotransferase molecular activity which contribute to the upregulation of glycolysis pathway in target cells (Supplementary Table S1). Other notable GO cellular components associated with myopic RPE exosomal proteins were extracellular matrix, intracellular vesicles, and focal adhesion and paracrine factors related to extracellular matrix remodeling. Examples of identified proteins in these categories were Heat shock protein family B (small) member 1(HSPB1), Transforming growth factor-beta-induced protein (TGFBI), Myocilin (MYOC), Apolipoprotein A-IV (APOA4), Thrombospondin-1 (THBS1), protein phosphatase 1 catalytic subunit beta (PPP1CB), Myosin binding protein C2 (MYBPC2), Phosphoglucomutase-like protein 5 (PGM5), and Collagen type VI alpha 3 chain (COL6A3; Supplementary Tables S1, S2).

In the non-myopic samples, the uniquely expressed proteins were involved in the metabolism of tricarboxylic acid and pyruvate (Figure 4A). In addition, mitochondrial components with pyruvate dehydrogenase enzymatic activity, chaperone complex, and tricarboxylic acid cycle (TCA) enzymes were the most enriched cellular components (Figures 4B, C). Examples of identified proteins in these categories were Dihydrolipoyl dehydrogenase, mitochondrial (DLD), Pyruvate dehydrogenase E1 component subunit alpha (PDHA1), Succinyl-CoA ligase [ADP-forming] (SUCLA2), T-complex protein 1 subunit beta (TCPB), Beta-crystallin A2, A3, B1, B3 (CRYBA2, CRYBA3, CRYB1 and CRYB3; Supplementary Tables S3, S4). These analyses suggest that the proteomic profile of RPE exosomes from myopic eyes shows a differential expression pattern, which likely supports altered metabolic requirements of the myopic retina and extracellular matrix remodeling process.

Identification of proteins differentially expressed in RPE exosomes from myopic eyes

The comparison of proteomic profiles of RPE exosomes between myopic and non-myopic eyes exhibited 286 differentially expressed proteins. Out of these, 79 were significantly upregulated and 70 were significantly downregulated (Supplementary Tables S5, S6). Table 2 summarizes the top 41 differential expressed proteins, including 21 upregulated, 16 downregulated, and 3 undetected in myopic samples. The heatmap of these proteins showed several protein clusters that were upregulated and downregulated in myopic samples compared with non-myopic samples (Figure 5A).

A volcano plot was constructed to display the top 41 differentially expressed proteins (Figure 5B). Above the horizontal threshold line ($p = 0.05$), the significantly upregulated proteins (≥1.5 FC, myopic/non-myopic) are shown as red dots and the

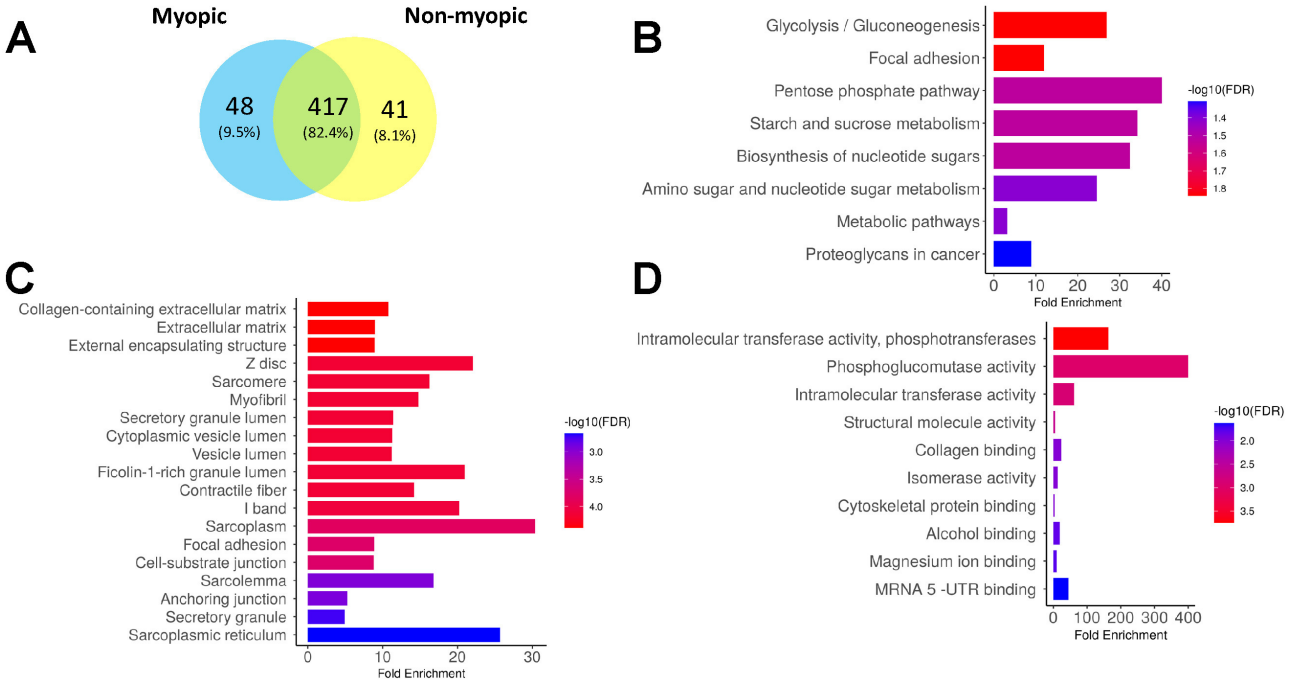

FIGURE 3
Proteomic profiles of RPE exosomes from myopic samples. **(A)** Venn diagram displaying all identified RPE exosomal proteins across the myopic and non-myopic samples. Enrichment analysis from KEGG **(B)**, GO cellular components **(C)** and GO molecular functions **(D)** for 48 unique RPE exosomal proteins identified in myopic samples. All enrichment analysis were performed with ShinyGo 0.77 online tool.

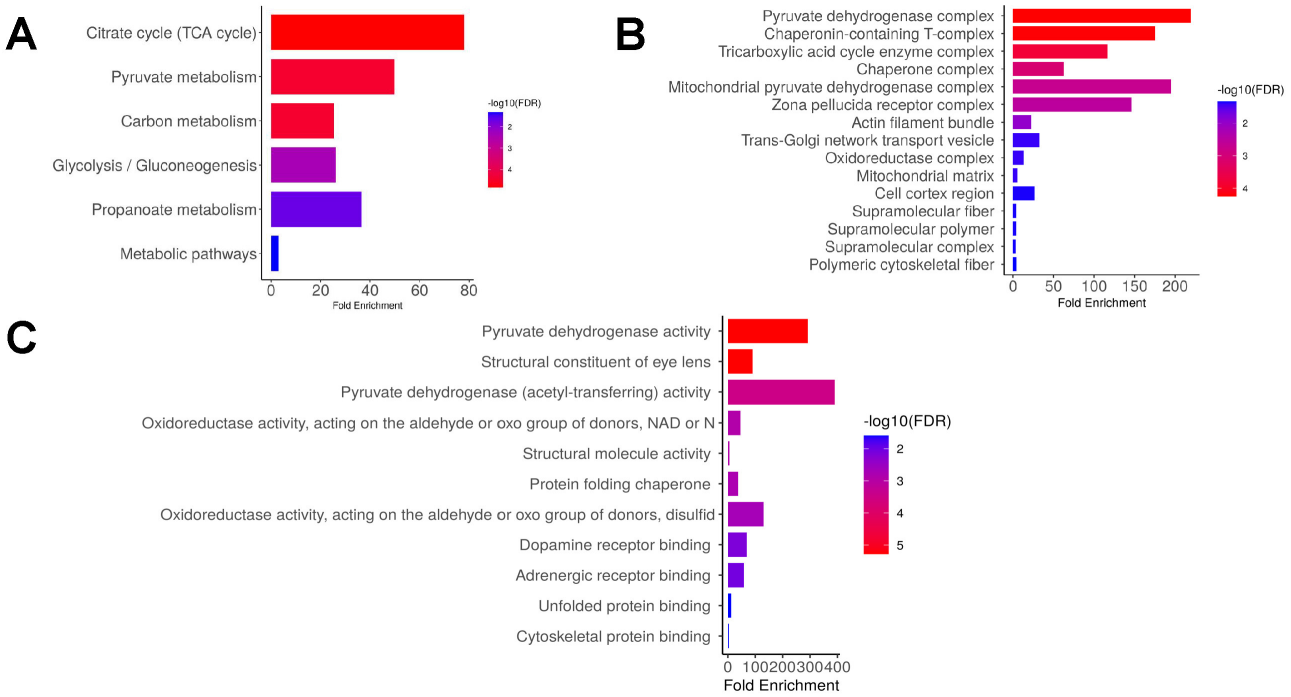

FIGURE 4
Proteomic profiles of RPE exosomes from non-myopic samples. Enrichment analysis from KEGG **(A)**, GO cellular components **(B)** and GO molecular functions **(C)** for 41 unique RPE exosomal proteins identified in non-myopic samples. All enrichment analysis were performed with ShinyGo 0.77 online tool.

10.3389/fmed.2025.1523211

TABLE 2 Differentially expressed RPE exosomal proteins in myopic eyes.

Protein names	Accession number	Gene symbol	SAM	T-test	Fold Change (Myopic/ Non-myopic)	Expression level in myopic eyes
Histone H4	P62805	H4C9	0.686	0.098	3.04	Upregulated
PTB domain-containing engulfment adapter protein 1	Q9UBP9	GULP1	1.036	0.076	2.59	
Histone H3.1	P68431	H3C10	0.626	0.137	2.59	
AP-2 complex subunit alpha-1	O95782	AP2A1	0.863	0.107	2.43	
Lumican	P51884	LUM	1.445	0.014	2.27	
Vinculin	P18206	VCL	0.693	0.092	2.22	
Septin 11, isoform CRA_b	D6RGI3	SEPTIN11	0.937	0.036	2.19	
Glutathione peroxidase 3	P22352	GPX3	0.921	0.058	2.12	
Spectrin beta chain, non-erythrocytic 1	Q01082	SPTBN1	0.730	0.030	1.94	
Septin-7	Q16181	SEPTIN7	0.882	0.014	1.91	
60S ribosomal protein L10a	P62906	RPL10A	0.579	0.090	1.84	
BTB/POZ domain-containing protein KCTD12	Q96CX2	KCTD12	0.715	0.070	1.82	
Fibrinogen gamma chain	P02679	FGG	0.828	0.014	1.80	
Osteoglycin OG	Q7Z532	OGN	0.498	0.094	1.79	
Fibromodulin	Q06828	FMOD	0.580	0.100	1.73	
Phosphoglycerate kinase 1	P00558	PGK1	0.683	0.032	1.70	
Septin-2	Q15019	SEPTIN2	0.780	0.038	1.70	
Alpha-actinin-4	O43707	ACTN4	0.491	0.097	1.65	
Glutathione S-transferase Mu 3	P21266	GSTM3	0.875	0.018	1.64	
Gelsolin	P06396	GSN	0.793	0.034	1.57	
Myomesin-1	P52179	MYOM1	0.918	0.007	1.50	
Cell growth-inhibiting protein 34	Q08ES8	RPL11	−0.677	0.048	−1.53	Downregulated
Arrestin-C	P36575	ARR3	−0.487	0.100	−1.57	
V-type proton ATPase subunit B, brain isoform	P21281	ATP6V1B2	−0.452	0.087	−1.59	
Alpha-crystallin A chain	P02489	CRYAA	−0.644	0.031	−1.61	
CDC37 protein	Q6FG59	CDC37	−0.810	0.042	−1.64	
Phosphoserine aminotransferase	Q9Y617	PSAT1	−0.581	0.072	−1.70	
Alpha-crystallin B chain	P02511	CRYAB	−0.529	0.071	−1.75	
6-phosphogluconate dehydrogenase, decarboxylating	P52209	PGD	−0.625	0.042	−1.79	
Phosphatidylethanolamine-binding protein 1	P30086	PEBP1	−0.525	0.069	−1.80	
Opsin 1 (Cone pigments), medium-wave-sensitive	B7ZLG5	OPN1MW	−0.526	0.067	−1.81	

(Continued)

TABLE 2 (Continued)

Protein names	Accession number	Gene symbol	SAM	T-test	Fold Change (Myopic/ Non-myopic)	Expression level in myopic eyes
Histidine triad nucleotide-binding protein 1	P49773	HINT1	−0.530	0.060	−1.83	
Retinol dehydrogenase 10	Q8IZV5	RDH10	−0.487	0.078	−1.86	
Poly(rC)-binding protein 2	Q15366	PCBP2	−1.174	0.006	−2.10	
ADP-ribosylation factor 3	P61204	ARF3	−0.661	0.073	−2.12	
Beta-crystallin B2	P43320	CRYBB2	−0.628	0.051	−2.14	
Cytosolic acyl coenzyme A thioester hydrolase	O00154	ACOT7	−0.745	0.045	−2.15	
40S ribosomal protein S5	P46782	RPS5	−1.246	0.004	−2.41	
Beta-crystallin A2	P53672	CRYBA2				Undetectable
Beta-crystallin A3	P05813	CRYBA1				
Beta-crystallin B3	P26998	CRYBB3				

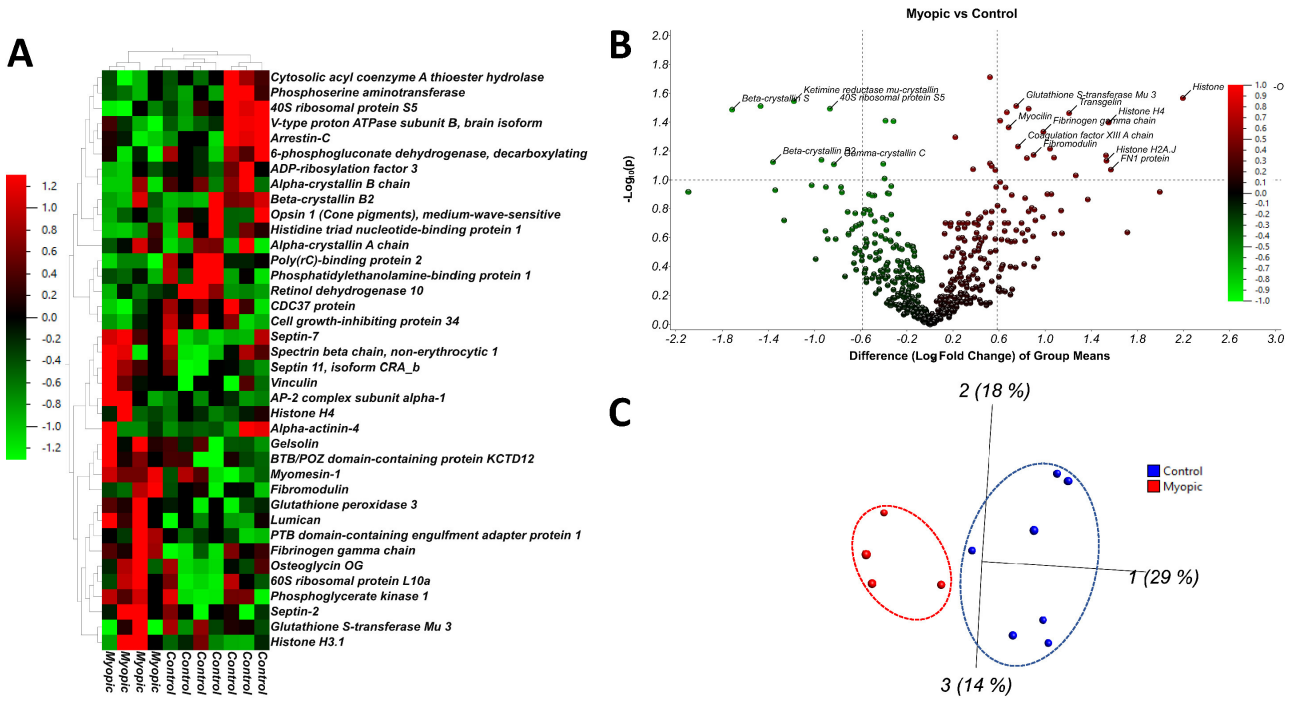

FIGURE 5
Differential expression patterns of top 38 RPE exosomal proteins in myopic eyes. **(A)** Heatmap of these proteins comparing expression levels between myopic and non-myopic (control) eyes. The box color indicates $\log_2$ fold changes showing upregulation in red and downregulation in green. **(B)** Volcano plot illustrating top 40 significantly differentially abundant proteins selected by Qlucore Stats. The $-\log_{10}$ (Benjamini–Hochberg corrected *P*-value) is plotted against the $\log_2$ (fold change, FC: myopic/non-myopic). The non-axial vertical lines denote ±1.5-fold change while the non-axial horizontal line denotes $p = 0.05$, which is the significance threshold (prior to logarithmic transformation). Volcano plot shows significantly upregulated proteins with red dots (FC≥1.5) into the right of the non-axial vertical right line and significantly downregulated proteins as green dots (FC≤-1.5) into the left of the non-axial vertical line. **(C)** 3D Principal component analysis (PCA) shows that myopic (red) and non-myopic (control, blue) samples are well distinguished by two defined clusters.

significantly downregulated proteins (≤-1.5 FC, myopic/non-myopic) are shown as blue dots. Out of the differentially expressed proteins, the most abundant proteins in the myopic samples were Histone H4 (H4C9, FC = 3.04), PTB domain containing engulfment adaptor protein 1 (GULP1, FC = 2.59), Histone H3.1 (H3C10, FC = 2.59), Lumican (LUM, FC = 2.27), Vinculin (VSL, FC = 2.2), Septin-2,7,11 (SEPTIN 2,7,11, FC = 1.70 to 2.19), Gelsolin (GSN, FC = 1.57), Alpha-actin 4 (ACTN4, FC

= 1.65), Fribomodulin (FMOD, FC = 1.73), and Fibrinogen gamma chain (FGG, FC = 1.80). Similarly, the least abundant proteins were Cell growth-inhibiting protein 34 (FC = 1.53), Arrestin-C (FC = −1.57), Alpha-crystallin A and B chains (FC = −1.61 to −1.75), Opsin 1 medium-wave-sensitive (FC = −1.81), Retinol dehydrogenase 10 (FC = −1.86), Poly(rC)-binding protein 2 (FC = −2.10), 40S ribosomal protein S5 (RPS5, FC = −2.41), Cytosolic acyl coenzyme A thioester hydrolase (ACOT7, FC = −2.15) and Beta-crystallin B2 protein (CRYBB2, FC = −2.14) (Figure 5B and Table 2). The principal component analysis of the exosome protein data showed two well-defined clusters for the myopic and non-myopic groups (Figure 5C).

Functional analysis of the top 41 differentially expressed RPE exosome proteins in the myopic eyes

The functional GO analysis of the top 41 differentially expressed proteins showed that the upregulated RPE exosomal proteins in myopic eyes were closely related to cytokinesis, glycan metabolism, and nucleosome activation pathways, including some previously reported in eye growth regulation, such as oxidative stress (67), TGF-β receptor signaling (68), and plasminogen activation (69) (Figure 6A). The most significant biological process was the response to lipid hydroperoxide. The results suggested that the upregulated protein groups could be involved in the cytoskeleton organization mediated by SEPTIN proteins and increased resistance to remodel the extracellular matrix (Supplementary Figure S1B). On the contrary, the downregulated RPE exosomal proteins in myopic eyes were mostly related to lens development, visual perception, sensory system development, and nucleotide catabolism (Figure 6B). Although the KEGG and GO analyses for the downregulated proteins in myopia did not show results in ShinyGO sorting for cellular components, these proteins were found to be related to the structure of the eye lens when they were sorted by molecular functions (Supplementary Figure S1D).

The ingenuity pathway analysis by category of diseases and biomarkers of 41 differentially expressed RPE exosomal proteins in myopic samples showed 35 members altered in cancer, organismal injury, and abnormalities, 23 in neurological diseases, and 13 members involved in ophthalmic diseases including conditions related to abnormal morphology of the eye (Supplementary Table S7). The top canonical pathways for differentially expressed RPE exosomal proteins in myopia were related to integrin signaling, Ras homolog family member A (RHOA) signaling, cell junction signaling, and phototransduction pathway (Supplementary Table S8).

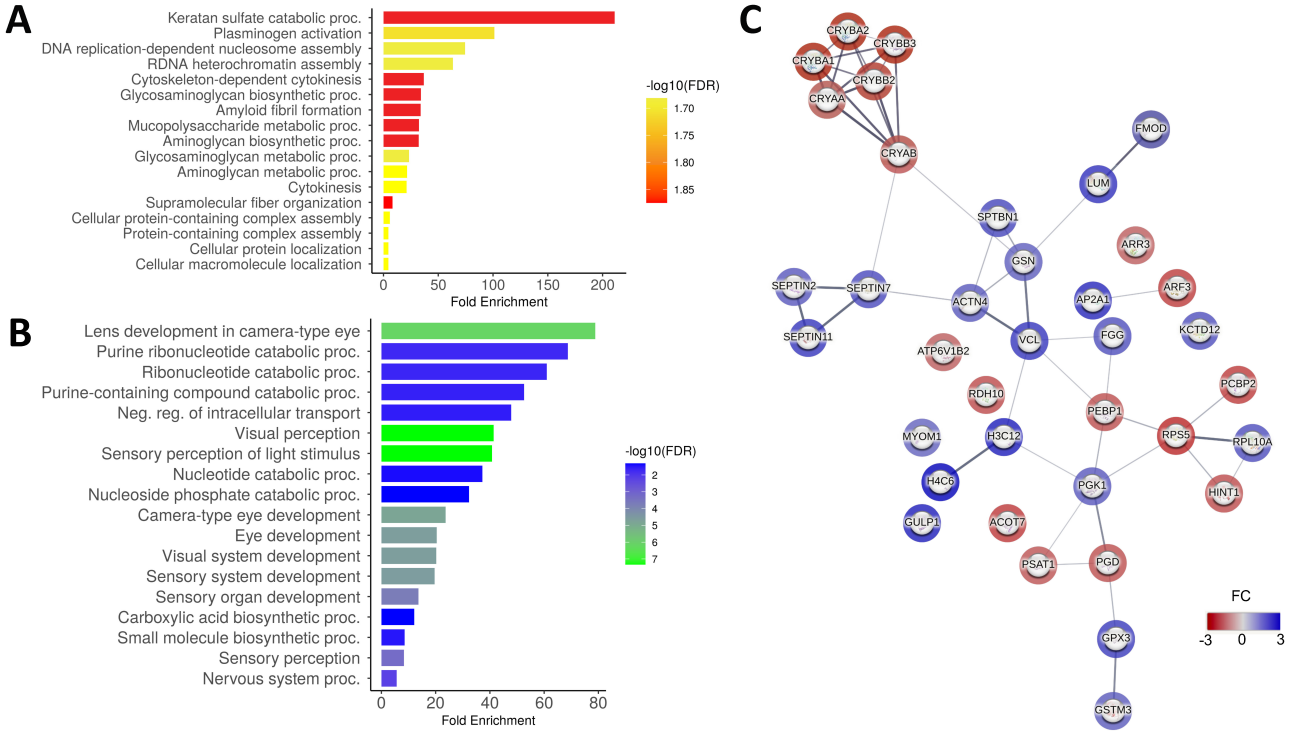

FIGURE 6
Enrichment analyses and networks interactions of top 41 differentially expressed RPE exosomal proteins in the myopic eyes. GO analysis for biological processes of 21 significantly upregulated proteins **(A)** and 17 significantly downregulated proteins and 3 undetected proteins **(B)** in myopic samples performed with the ShinyGO 0.77 online tool. **(C)** Protein–protein interaction network on STRING database of top 41 differentially expressed proteins. Fold changes are in border color of the circles: upregulated proteins in blue and downregulated proteins in red.

A

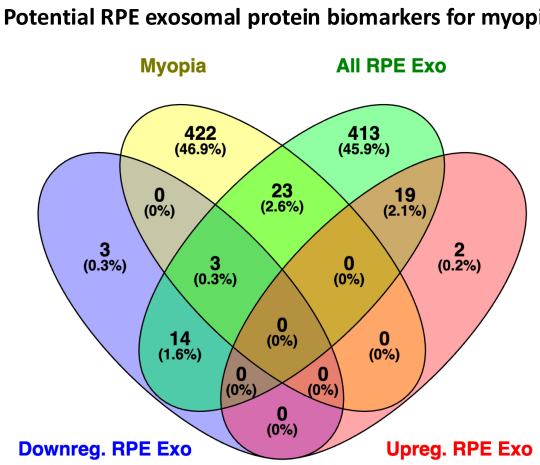

B

Protein biomarkers	Gene Symbol	Downreg. RPE Exosomes	Myopia	High Myopia	RPE Apical Side
ATPase H+ transporting V1 subunit B2	ATP6V1B2	X	X	X	
Crystallin Beta B2	CRYBB2	X	X		
Crystallin Alpha B	CRYAB	X			X
Phosphatidylethanolamine binding protein 1	PEBP1	X			X

FIGURE 7
Profile of RPE exosomal proteomics compared with published data. **(A)** Venn diagram showing significantly downregulated RPE exosomal proteins in myopic samples (blue), significantly upregulated RPE exosomal proteins in myopic samples (red), and all identified RPE exosomal proteins (green) in this study compared with all myopia monarch proteins listed on STRING database (yellow). **(B)** Common proteins between the current study and published data: all myopia monarch and high myopia proteins listed on STRING database, and RPE apical side-released proteins reported previously (33).

An interaction network model for differentially expressed RPE exosomal proteins in myopia eyes

To identify the candidate protein networks involved in myopia, we used the top 41 differentially expressed RPE exosomal proteins to construct a protein-protein interaction (PPI) network model using the STRING database where nodes were defined with a score $\geq$ 0.4 (Figure 6C). The border color indicates fold change of differentially expressed proteins in myopic samples compared with non-myopic samples: upregulated proteins in blue and downregulated proteins in red. Closer connectivity between each node was represented by shorter distances and the number of connective lines that joined each circle. The connectivity was the most pronounced in the SEPTIN and Beta-crystalline protein interaction groups (Figure 6C).

Identification of potential RPE exosome protein biomarkers of myopia

We also compared the proteomic profile of RPE exosomes from myopic eyes with data deposited on the STRING database for myopia (448 genes), high myopia (41 genes) (63), and previously reported proteomic data from the apical side of the RPE (55 proteins) (33). We found 23 common proteins with the STRING database (Figure 7A), although these proteins did not show significant expressions on myopic samples. Three significantly downregulated RPE exosomal proteins in our myopic samples were common with the previous reports: ATPase H+ transporting V1 subunit B2 (ATP6V1B2), Crystallin beta B2 (CRYBB2), and Arrestin 3 (ARR3) (Figure 7A). Proteins ATP6V1B2 (70), CRYBB2 (68), and ARR3 (71) have been previously associated with myopia and/or high myopia (Figure 7B), suggesting that myopia could be linked with reduced expression levels of these RPE exosomal proteins. Two other previously reported RPE-derived apical exosomal proteins (33), Phosphatidylethanolamine binding protein 1 (PEPB1) and Crystallin alpha B (CRYAB) (72), were significantly downregulated in our myopic samples (Figure 7B and Supplementary Figure S2B). Protein CRYAB was also downregulated in an animal model of myopia induced by form deprivation (72).

Discussion

In this preliminary study, we provided the first demonstration of RPE exosome biogenesis in tree shrew eyes using an innovative *ex vivo* model. By characterizing the proteomic profiles of exosomes released by the RPE in myopic and non-myopic eyes, we further showed that myopia is associated with proteomic alterations in RPE-derived exosomes. Additionally, we identified several RPE exosomal proteins as candidate biomarkers that could play a role in mediating growth signal communication across the RPE in the control of eye growth and refractive state.

There is prior evidence that proteomic profiles of exosomes are altered in myopia (28, 73, 74). However, these studies quantified protein expression levels in exosomes derived from ocular fluids such as aqueous or vitreous humor, so they are unlikely to represent exosomal characteristics and changes involved in the retina-choroid-sclera growth signaling pathway of emmetropization. The RPE is a critical mediator of growth signals between the neurosensory retina and the choroid (18, 20). It has been shown that exosomes derived from the RPE contain numerous signaling proteins in normal physiological conditions (33) including oxidative stress-induced signaling phosphoproteins (34). The RPE monolayer can potentially serve as receptors of putative signaling molecules like dopamine, retinoic acid, and adenosine and mediators of associated growth signals into the choroid (15, 36). Therefore, the mechanistic investigation of RPE-derived exosomes and exosomal proteomic profiles could provide insights into potential protein biomarkers involved in intracellular signaling of growth information in the emmetropization mechanism.

Exosomal proteins secreted by the RPE exclusively in myopic eyes

Among the 48 RPE exosomal proteins uniquely expressed in myopic eyes, we identified several family members of previously reported cytoskeletal and structural proteins related to myopia: Myosin-binding protein C (MYBPC) and Tropomyosin 1α4 (TPM4) (76), extracellular matrix proteins like Collagen alpha 3(VI) chain (COL6A3) (75), and Apolipoproteins A-IV and B (APOA4 and APOB) (74, 76). Additionally, this group of uniquely expressed RPE exosomal proteins in myopia included Thrombospondin 1 (THBS1), Keratocan (KERA), and Myocilin (MYOC) that were reportedly downregulated in the sclera of myopic tree shrew eyes (70). Considering that the same set of proteins was observed both in the RPE and sclera, the translocation of these proteins might facilitate growth signal transmission to affect the extracellular matrix remodeling in the sclera (77). Indeed, the cellular components of uniquely expressed myopic RPE exosomal proteins were primarily related to extracellular matrix, intracellular vesicles, and focal adhesion, indicating a potential role in extracellular matrix remodeling. These results suggest that the RPE exosomes likely serve as a facilitator of cellular communication to trigger morphological changes in the sclera.

Exosomal proteins secreted by the RPE exclusively in non-myopic eyes

The proteomic analysis revealed 41 RPE exosomal proteins uniquely expressed in non-myopic eyes. These proteins may have a role in the homeostatic maintenance of growth inhibitory STOP signals to produce optimal "physiological" eye growth (78, 79). For example, the unique expression of Beta-arrestin-2 (ARRB2) in non-myopic eyes is consistent with its role in the regulation of dopamine D2 receptor activity. It has been shown that ARRB2 is involved in the desensitization and internalization of dopamine D2 receptors (137) and that the activation and inactivation of these receptors could lead to myopia development and inhibition, respectively (138, 139).

Three members of the crystallin β family—CRYBB3, CRYBA2, and CRYBA1—were exclusively expressed in the non-myopic samples. These crystallin proteins are part of the α, β, and γ crystallin superfamily, which plays a crucial role in maintaining the transparency of the crystalline lens. Interestingly, members of this protein superfamily are also found in posterior ocular structures, such as the RPE, photoreceptor inner and outer segments, and the outer nuclear layer of the retina (140, 141). Studies have shown that these crystallin proteins in the RPE respond to light intensity (142) and oxidative stress (143), similar to the αβ crystallins in the lens. Furthermore, the presence of these crystallin proteins in non-myopic eyes aligns with previous findings of αβ crystallins in exosomes derived from the apical surface of human RPE cells (42). These crystallins were also localized in the interphotoreceptor matrix, suggesting their uptake from the extracellular space as part of a protective response to oxidative damage and neural stress (42). Additionally, there is evidence of signaling interactions between the lens and the posterior segment (80–82). Collectively, these findings imply that the crystallins observed could play a role in exosome-mediated intercellular communication between photoreceptors and the RPE within the emmetropization pathway.

Upregulation of RPE exosomal proteins in myopic eyes

In myopic eyes, the RPE exosomes exhibited higher levels of PTB domain-containing engulfment adapter protein 1 (GULP1) and Adaptor-related protein complex 2 (AP2A1) compared to non-myopic eyes. GULP1 is essential for phagocytosis of apoptotic cells, transport of glycosphingolipids and cholesterols, and endosomal trafficking of various low-density lipoprotein receptor-related protein 1 (LRP1) ligands (83). In contrast, AP2A1, a subunit of the adaptor protein complex 2 (AP-2), plays a role in clathrin-mediated endocytosis and helps facilitate the internalization of LRP1 and its ligands by promoting the formation of clathrin-coated vesicles (84). LRP1 functions as a scavenger of tissue inhibitors of metalloproteinases (TIMP), both of which are found in the RPE (144, 145). The upregulation of GULP1 and AP2A1 could lead to greater removal of TIMP by LRP1 in the RPE cells (85), promoting transforming growth factor (TGF)-β activation and oxidative stress and potentially contributing to myopia development (146). LRP1 deficiency has been shown to be associated with myopia phenotype through TGF-β activity (86, 87).

The RPE exosomes of myopic eyes showed upregulation of several structural proteins: actin filament binding protein, Vinculin (VCL); a filament-forming cytoskeletal GTPase, Septin family proteins (SEPTIN2, SEPTIN 7, and SEPTIN11); and focal adhesion cytoskeleton protein, βII spectrin (SPTBN1). Vinculin and βII spectrin proteins are known to be involved in cell-cell adhesion (88, 89). Additionally, Vinculin regulates cell-matrix adhesion and E-cadherin expression on cellular surfaces and potentiates mechanosensing by the E-cadherin complex (88). SEPTIN11 promotes cell motility and cell adhesion by activating the RhoA protein (90) and the Septin protein family plays a potential role

in cytokinesis (91). Other upregulated RPE exosomal proteins in myopic eyes were Lumican (LUM) and Fibromodulin (FMOD), closely related members of the extracellular matrix leucine-rich repeat glycoprotein/proteoglycan family. These proteins bind to fibrils allowing assembly of the collagen network in the extracellular matrix (92). LUM is a keratan sulfate proteoglycan that promotes fibroblast-myofibroblast transition. It has been reported to increase transcription of alpha-smooth muscle actin, matrix metallopeptidase 9, Collagen I, plasminogen activator inhibitor 1, and TGF-β *in vitro* (93), and play several roles in ocular diseases (94). LUM helps to maintain stability and tension of the extracellular matrix in the sclera by interacting with collagen fibers (95). This interaction of LUM with collagen fibers could be involved in myopiagenesis as its gene mutation and polymorphism have been associated with myopia in humans (96) and animal models (97). For example, LUM mutant zebrafish eyes exhibited ocular enlargement primarily due to disruption of collagen fibril arrangement leading to scleral thinning and reduced stiffness (97). Additionally, double knockouts of LUM and FMOD were found to cause axial eye elongation, retinal detachment, and scleral thinning, suggesting that both proteins are critical for scleral ensemble and functioning and may underlie morphological changes in the sclera of myopic eyes (98). The proteoglycans discussed in this section have also been identified in various retinal layers, including the RPE and interphotoreceptor matrix (147). Therefore, the increased levels of these proteins in RPE exosomes from myopic eyes may indicate a compensatory response to the heightened potency of GO signals in the early emmetropization pathway, or a protective mechanism aimed at maintaining the integrity of RPE, interphotoreceptor matrix, and other retinal layers.

Proteomic analyses of RPE exosomes in myopic eyes also showed an upregulation of Alpha Actinin-4 (ACTN4) and Gelsolin (GSN), proteins previously linked with the biological basis of myopia (76). These results suggest that cytoskeletal structural proteins and coagulation pathways may have a role in myopia development. Another highly expressed exosomal protein in the myopic eyes was glutathione S-transferase mu 3 (GSTM3), a potent antioxidant enzyme that reduces glutathione and prevents neurotoxicity by cellular oxidative stress (99). It has been found that the suppression of the GSTM3 gene is associated with age-related cataract formation by oxidative stress in the lens (100). An overexpression of GSTM3 on myopic exosomes could be part of the neuroprotective response of RPE cells to counter feedback from the oxidative stress loop triggered by TGF-β (101), which is a known growth factor involved in myopiagenesis (68).

The upregulated RPE exosomal proteins were mainly involved in keratan sulfate catabolism, plasminogen activation, cytokinesis, and glycosaminoglycan and aminoglycan metabolism. The enhancement of these metabolic pathways is consistent with the reduced expression of glycosaminoglycans and proteoglycans in the sclera of myopic eyes (102, 103). Moreover, plasminogen protein has been proposed as a molecular marker of high myopia in humans (69). Proteins Fibromodulin (FMOD), Fibrinogen beta chain (FGB), and Fibrinogen gamma chain (FGG), which were upregulated in myopic eyes in this study, have also been reported to be upregulated in the retina of myopic rabbits (104). Since fibrinogen stimulates tissue plasminogen activators against plasminogen, (105) and plasminogen activators, like matrix metalloproteases, are mediators of extracellular proteolysis (106), they could act in similar ways to produce extracellular matrix remodeling in myopia.

Downregulation of RPE exosomal proteins in myopic eyes

The RPE of myopic eyes released exosomes with lower levels of proteins encoded by genes whose mutations are reportedly linked with myopia, such as Opsin 1 medium-wave-sensitive (OPN1MW) (107–109), Arrestin-C (ARR3) (71), α crystallin A and B (72, 110), and Retinol dehydrogenase 10 (RDH10) (111). Opsins are light-activated G-protein coupled transmembrane receptors that allow activation of the phototransduction pathway (112). These visual pigments contribute to human color vision (113). Opsin gene deficiency is related to color blindness (114) and its protein dysfunction is associated with cone dystrophy and myopia (108, 115, 116). ARR3 or cone-arrestin is a G-protein-coupled receptor that binds to phosphorylated opsins, after activation of the phototransduction pathway (117). ARR3 gene mutations are associated with high myopia (118). While the lower abundances of OPN1MW and ARR3 proteins in RPE exosomes of myopic eyes could indicate potential retinal dysfunction in myopia (119), it is unlikely that these proteins are packaged by the RPE cells into exosomes. Rather, exosomes that originate from cone photoreceptors are the likely source of these proteins. Presumably, the photoreceptor-derived exosomes were attached to the apical surface of the RPE and were harvested with RPE-derived exosomes.

α crystallin proteins were also downregulated in RPE exosomes of myopic eyes. These proteins belong to the small heat shock protein (HSP20) family and act as molecular chaperones. Downregulation of CRYAA mRNA and protein has been reported in high-myopic patients (110). CRYAB is known to be secreted by exosome-dependent pathways from polarized human RPE cells; they play a protective function in the interphotoreceptor matrix and confer resistance to heat and oxidative stress in cells (120, 121). Oxidative stress of retinal cells associated with myopia may initiate a downregulation of CRYAA and CRYAB secretion in the RPE exosomes. Similar results have been reported in the retina of an experimental glaucoma model, which showed significantly reduced expression of CRYAB (122). Another member of the crystallin protein family, CRYBB2, was found to be downregulated in our myopic samples. Notably, CRYBB2 has also been previously shown to be secreted in exosomes from the apical side of the RPE (33). Like other crystallin proteins, CRYBB2 has been demonstrated to help protect the RPE against oxidative stress (141). The reduced levels of crystallin proteins in RPE exosomes from myopic eyes may suggest a diminished capacity to respond to oxidative stress, potentially contributing to the dysregulation of eye growth and the development of myopia.

Another downregulated exosomal protein, RDH10, is a member of the retinol dehydrogenases family. RDH10 is mainly expressed in photoreceptors and RPE cells and reduces all-trans-retinal to all-trans-retinol during phototransduction (123). The RPE contains metabolic enzymes required for retinal signaling and metabolites like 11-cis-retinal that play a key role in the retinoid visual cycle (124). Retinoic acid, a metabolic precursor

of vitamin A, has been implicated in ocular growth (15, 125) and is highly expressed in the myopic retina (126–128). It has also been shown that the extracellular matrix remodeling process in myopia could be regulated by the cell differentiation function of retinoic acid (129). Furthermore, mutations in genes related to retinoic acid metabolism like RDH5 have been found to be associated with refractive errors and myopia (111, 130, 131). Deficiency of RDH5 also results in upregulation of MMP-2 and TGF-β2, promoting the epithelial-mesenchymal transition of RPE cells and myopia development (132). These findings are consistent with our observation of reduced expression levels of RDH10 in RPE exosomes of myopic eyes, indicating their role in extracellular matrix remodeling in myopia. We found that the downregulation of these RPE exosomal proteins inhibited signaling pathways related to lens development, eyes and sensory system development, visual perception, and sensory perception of the light stimulus and was associated with processes related to purine, nucleotide/nucleoside catabolism, and carboxylic acid biosynthesis, suggesting possible metabolic alterations in myopia.

Candidate RPE exosomal signaling pathways and protein biomarkers in myopia

A comparison of our proteomics data set with published literature and the String database (63) revealed two potential exosomal protein biomarkers that were downregulated in myopic eyes: ATP6V1B2 and CRYBB2. The former has been associated with early-onset high myopia (133), while the latter has been associated with induced myopia (72). As stated previously, lower levels of CRYBB2 could be due to the oxidative stress environment of myopia eyes, enhanced by the downregulation of antioxidant genes (67) by TGF-β signaling (68). Another potential biomarker is phosphatidylethanolamine binding protein 1 (PEBP1), a Raf kinase inhibitor protein, which plays a role in cell cycle, growth, and proliferation (148). PEPB1 has been previously reported in exosomes released by the apical side of the RPE in normal physiological conditions (33) and was significantly downregulated in our myopic samples. Apart from these proteins, several other downregulated proteins in our dataset were consistently associated with myopia in the literature, providing an indirect validation of the proteomic analysis of myopic eyes (63, 76). These proteins were MYOC, ATP6V1A, RHOA, SAG, GNAT2, GNB3, COL12A1 and TGFBI.

The ingenuity pathway analysis illustrated that the differentially expressed RPE exosomal proteins of myopic eyes were involved in pathways related to phototransduction, neurotransmitters, and signal transduction, all of which are implicated in the emmetropization mechanism (15). The top canonical signaling pathways relevant to RPE exosomal proteins in myopic eyes were integrin signaling, RHOA, and cell junction pathways. Although protein RHOA was reported to be upregulated in the sclera of myopic eyes (134), it was not differentially expressed in RPE exosomes of myopic eyes in this study. Since activation of integrins and cell-cell junctions promote cell cycle progression and cell proliferation (135), these pathways likely produce changes in extracellular matrix remodeling leading to myopia (77, 136).

Ex-vivo ocular assay: an innovative method with significant implications for ocular biology research

A recent comprehensive report on the causes, prevention, and treatment of myopia, released by The National Academies of Sciences, Engineering, and Medicine, highlighted the need for the development of *in vitro* experimental models that can accelerate understanding of the mechanisms of emmetropization and myopia as well as identification of candidate messengers involved in the retinoscleral signaling process (17). By successfully implementing an innovative *ex vivo* assay to explore the pathogenesis of myopia, the present study has established a model that is as simple as an *in vitro* assay but with the potential to yield more robust and physiologically relevant findings. This *ex vivo* assay model should facilitate high-impact studies of ocular mechanisms (for example, pharmacological manipulation experiments) and significantly aid in advancing the understanding of and future discoveries in ocular biology (35).

This study has several limitations, including small sample size, two different experimental myopia paradigms, and few control eyes that had recovered from prior treatments. In addition, while the neurosensory retina was carefully separated from the RPE to isolate RPE-derived exosomes, it is likely that exosomes from non-RPE cells, such as photoreceptors, were also enriched in the conditioning media. Consequently, the enriched sample was likely composed primarily, but not exclusively, of RPE exosomes. Nevertheless, the findings provide original evidence for the potential role of RPE exosomes in myopiagenesis, opening up a new avenue for understanding the molecular mechanisms behind emmetropization and myopia. Further targeted experiments are necessary to validate candidate RPE exosomal protein biomarkers and pathways identified in this study and test these proteomic signatures across different growth-modulatory conditions (e.g., induced myopia vs. recovery from myopia) and experimental models (e.g., form-deprivation, lens-induced, and limited-bandwidth). Ultimately, a thorough proteomic characterization of RPE exosomes in myopia could provide key insights into the molecular mechanism of RPE exosome-mediated growth signal transmission in the emmetropization pathway.

Data availability statement

The original contributions presented in the study are publicly available. The global mass spectrometry proteomics data presented in this study have been deposited to the ProteomeXchange Consortium via the PRIDE partner repository, accession number PXD062092.

Ethics statement

The animal study was approved by UAB Institutional Animal Care and Use Committee. The study was conducted in accordance with the local legislation and institutional requirements.

Author contributions

NS: Data curation, Formal analysis, Investigation, Writing – original draft. JR-L: Formal analysis, Investigation, Methodology, Resources, Writing – review & editing. JM: Formal analysis, Resources, Software, Validation, Visualization, Writing – review & editing. SK: Conceptualization, Funding acquisition, Investigation, Project administration, Resources, Supervision, Writing – original draft, Writing – review & editing.

Funding

The author(s) declare that financial support was received for the research and/or publication of this article. This study was supported by UAB High Resolution Imaging Facility and research grants from the National Institute of Health/National Eye Institute (R21EY036536 to SK), E. Matilda Ziegler Foundation for the Blind (SK), UAB Core Grant for Vision Research (P30EY003039), and UAB Vision Science Research Center Pilot Grant (SK).

Acknowledgments

The authors thank Dr. Kyoko Kojima for technical assistance and Dr. Rafael Grytz and Dr. Timothy J. Gawne for donating tree shrew eyes.

Conflict of interest

The authors declare that the research was conducted in the absence of any commercial or financial relationships that could be construed as a potential conflict of interest.

Generative AI statement

The author(s) declare that no Gen AI was used in the creation of this manuscript.

Publisher's note

Supplementary material

The Supplementary Material for this article can be found online at: https://www.frontiersin.org/articles/10.3389/fmed.2025.1523211/full#supplementary-material

References

1. Schaeffel F, Glasser A, Howland HC. Accommodation, refractive error and eye growth in chickens. *Vision Res.* (1988) 28:639–57. doi: 10.1016/0042-6989(88)90113-7

2. Norton TT, Siegwart JT Jr, Amedo AO. Effectiveness of hyperopic defocus, minimal defocus, or myopic defocus in competition with a myopiagenic stimulus in tree shrew eyes. *Invest Ophthalmol Vis Sci.* (2006) 47:4687–99. doi: 10.1167/iovs.05-1369

3. Norton TT, Khanal S, Gawne TJ. Tree shrews do not maintain emmetropia in initially-focused narrow-band cyan light. *Exp Eye Res.* (2021) 206:108525. doi: 10.1016/j.exer.2021.108525

4. Khanal S, Norton TT, Gawne TJ. Amber light treatment produces hyperopia in tree shrews. *Ophthalmic Physiol Opt.* (2021) 41:1076–86. doi: 10.1111/opo.12853

5. Wang M, Schaeffel F, Jiang B, Feldkaemper M. Effects of light of different spectral composition on refractive development and retinal dopamine in chicks. *Invest Ophthalmol Vis Sci.* (2018) 59:4413–24. doi: 10.1167/iovs.18-23880

6. Liu R, Qian YF, He JC, Hu M, Zhou XT Dai JH, et al. Effects of different monochromatic lights on refractive development and eye growth in guinea pigs. *Exp Eye Res.* (2011) 92:447–53. doi: 10.1016/j.exer.2011.03.003

7. Smith EL, Hung LF, Huang J, Blasdel TL, Humbird TL, Bockhorst KH. Effects of optical defocus on refractive development in monkeys: evidence for local, regionally selective mechanisms. *Invest Ophthalmol Vis Sci.* (2010) 51:3864–73. doi: 10.1167/iovs.09-4969

8. Diether S, Schaeffel F. Local changes in eye growth induced by imposed local refractive error despite active accommodation. *Vision Res.* (1997) 37:659–68. doi: 10.1016/S0042-6989(96)00224-6

9. Schaeffel F, Troilo D, Wallman J, Howland HC. Developing eyes that lack accommodation grow to compensate for imposed defocus. *Vis Neurosci.* (1990) 4:177–83. doi: 10.1017/S0952523800002327

10. Schmid KL, Wildsoet CF. Effects on the compensatory responses to positive and negative lenses of intermittent lens wear and ciliary nerve section in chicks. *Vision Res.* (1996) 36:1023–36. doi: 10.1016/0042-6989(95)00191-3

11. Wildsoet CF, Schmid KL. Optical correction of form deprivation myopia inhibits refractive recovery in chick eyes with intact or sectioned optic nerves. *Vision Res.* (2000) 40:3273–82. doi: 10.1016/S0042-6989(00)00138-3

12. Fischer AJ, McGuire JJ, Schaeffel F, Stell WK. Light- and focus-dependent expression of the transcription factor ZENK in the chick retina. *Nat Neurosci.* (1999) 2:706–12. doi: 10.1038/11167

13. Ashby RS, Feldkaemper MP. Gene expression within the amacrine cell layer of chicks after myopic and hyperopic defocus. *Invest Ophthalmol Vis Sci.* (2010) 51:3726–35. doi: 10.1167/iovs.09-4615

14. Troilo D, Smith EL 3rd, Nickla DL, Ashby R, Tkatchenko AV, Ostrin LA, et al. IMI - report on experimental models of emmetropization and myopia. *Invest Ophthalmol Vis Sci.* (2019) 60:M31–88. doi: 10.1167/iovs.18-25967

15. Brown DM, Mazade R, Clarkson-Townsend D, Hogan K, Datta Roy PM, Pardue MT. Candidate pathways for retina to scleral signaling in refractive eye growth. *Exp Eye Res.* (2022) 219:109071. doi: 10.1016/j.exer.2022.109071

16. Liang J, Pu Y, Chen J, Liu M, Ouyang B, Jin Z, et al. Global prevalence, trend and projection of myopia in children and adolescents from 1990 to 2050: a comprehensive systematic review and meta-analysis. *Br J Ophthalmol.* (2024) 109:bjo-2024-325427. doi: 10.1136/bjo-2024-325427

17. National Academies of Sciences, Engineering, and Medicine. *Myopia: Causes, Prevention, and Treatment of an Increasingly Common Disease*. Washington, D.C.: National Academies Press (2024).

18. Zhang Y, Wildsoet CF. RPE and choroid mechanisms underlying ocular growth and myopia. *Prog Mol Biol Transl Sci.* (2015) 134:221–40. doi: 10.1016/bs.pmbts.2015.06.014

19. Boulton M, Dayhaw-Barker P. The role of the retinal pigment epithelium: topographical variation and ageing changes. *EYE.* (2001) 15:384–9. doi: 10.1038/eye.2001.141

20. Rymer J, Wildsoet CF. The role of the retinal pigment epithelium in eye growth regulation and myopia: a review. *Vis Neurosci.* (2005) 22:251–61. doi: 10.1017/S0952523805223015

21. Zhang Y, Phan E, Wildsoet CF. Retinal defocus and form-deprivation exposure duration affects RPE BMP gene expression. *Sci Rep*. (2019) 9:7332. doi: 10.1038/s41598-019-43574-z

22. He L, Frost MR, Siegwart JT Jr, Norton TT. Altered gene expression in tree shrew retina and retinal pigment epithelium produced by short periods of minus-lens wear. *Exp Eye Res*. (2018) 168:77–88. doi: 10.1016/j.exer.2018.01.005

23. Goto S, Zhang Y, Vyas SA, Zhu Q, Wildsoet CF. Changes in expression in BMP2 and two closely related genes in guinea pig retinal pigment epithelium during induction and recovery from myopia. *Biomolecules*. (2023) 13:1373. doi: 10.3390/biom13091373

24. Zhang Y, Liu Y, Ho C, Wildsoet CF. Effects of imposed defocus of opposite sign on temporal gene expression patterns of BMP4 and BMP7 in chick RPE. *Exp Eye Res*. (2013) 109:98–106. doi: 10.1016/j.exer.2013.02.010

25. Zhang Y, Liu Y, Wildsoet CF. Bidirectional, optical sign-dependent regulation of BMP2 gene expression in chick retinal pigment epithelium. *Invest Ophthalmol Vis Sci*. (2012) 53:6072–80. doi: 10.1167/iovs.12-9917

26. Pant S, Hilton H, Burczynski ME. The multifaceted exosome: biogenesis, role in normal and aberrant cellular function, and frontiers for pharmacological and biomarker opportunities. *Biochem Pharmacol*. (2012) 83:1484–94. doi: 10.1016/j.bcp.2011.12.037

27. Théry C, Amigorena S, Raposo G, Clayton A. Isolation and characterization of exosomes from cell culture supernatants and biological fluids. *Curr Protoc Cell Biol*. (2006) 3:3Unit 3.22. doi: 10.1002/0471143030.cb0322s30

28. Tsai CY, Chen CT, Lin CH, Liao CC, Hua K, Hsu CH, et al. Proteomic analysis of exosomes derived from the aqueous humor of myopia patients. *Int J Med Sci*. (2021) 18:2023–9. doi: 10.7150/ijms.51735

29. Grigor'eva AE, Tamkovich SN, Eremina AV, Tupikin AE, Kabilov MR, Chernykh VV, et al. Exosomes in tears of healthy individuals: isolation, identification, and characterization. *Biochem (Mosc) Suppl Ser B Biomed Chem*. (2016) 10:165–72. doi: 10.1134/S1990750816020049

30. Gurung S, Perocheau D, Touramanidou L, Baruteau J. The exosome journey: from biogenesis to uptake and intracellular signalling. *Cell Commun Signal*. (2021) 19:47. doi: 10.1186/s12964-021-00730-1

31. Ludwig AK, Giebel B. Exosomes: small vesicles participating in intercellular communication. *Int J Biochem Cell Biol*. (2012) 44:11–5. doi: 10.1016/j.biocel.2011.10.005

32. Zhang Z, Mugisha A, Fransisca S, Liu Q, Xie P, Hu Z. Emerging role of exosomes in retinal diseases. *Front Cell Dev Biol*. (2021) 9:643680. doi: 10.3389/fcell.2021.643680

33. Klingeborn M, Dismuke WM, Skiba NP, Kelly U, Stamer WD, Bowes Rickman C. Directional exosome proteomes reflect polarity-specific functions in retinal pigmented epithelium monolayers. *Sci Rep*. (2017) 7:4901. doi: 10.1038/s41598-017-05102-9

34. Biasutto L, Chiechi A, Couch R, Liotta LA, Espina V. Retinal pigment epithelium (RPE) exosomes contain signaling phosphoproteins affected by oxidative stress. *Exp Cell Res*. (2013) 319:2113–23. doi: 10.1016/j.yexcr.2013.05.005

35. Locke CJ, Congrove NR, Dismuke WM, Bowen TJ, Stamer WD, McKay BS. Controlled exosome release from the retinal pigment epithelium in situ. *Exp Eye Res*. (2014) 129:1–4. doi: 10.1016/j.exer.2014.10.010

36. Zhou X, Pardue MT, Iuvone PM, Qu J. Dopamine signaling and myopia development: what are the key challenges. *Prog Retin Eye Res*. (2017) 61:60–71. doi: 10.1016/j.preteyeres.2017.06.003

37. Lobato-Álvarez JA, Roldán ML, López-Murillo TDC, González-Ramírez R, Bonilla-Delgado J, Shoshani L. The apical localization of Na+, K+-ATPase in cultured human retinal pigment epithelial cells depends on expression of the β2 subunit. *Front Physiol*. (2016) 7:450. doi: 10.3389/fphys.2016.00450

38. Wu S, Guo D, Wei H, Yin X, Zhang L, Guo B, et al. Disrupted potassium ion homeostasis in ciliary muscle in negative lens-induced myopia in guinea pigs. *Arch Biochem Biophys*. (2020) 688:108403. doi: 10.1016/j.abb.2020.108403

39. Murphy MJ, Crewther SG. Ouabain inhibition of Na/K-ATPase across the retina prevents signed refractive compensation to lens-induced defocus, but not default ocular growth in young chicks. *F1000Res*. (2013) 2:97. doi: 10.12688/f1000research.2-97.v1

40. Dong L, Shi XH, Li YF, Jiang X, Wang YX, Lan YJ, et al. Blockade of epidermal growth factor and its receptor and axial elongation in experimental myopia. *FASEB J*. (2020) 34:13654–70. doi: 10.1096/fj.202001095RR

41. Ashby RS, Megaw PL, Morgan IG. Changes in retinal αB-crystallin (cryab) RNA transcript levels during periods of altered ocular growth in chickens. *J End-to-End-test*. (2010) 36:821–6. doi: 10.1016/j.endend.2010.02.045

42. Sreekumar PG, Kannan R, Kitamura M, Spee C, Barron E, Ryan SJ, et al. αB crystallin is apically secreted within exosomes by polarized human retinal pigment epithelium and provides neuroprotection to adjacent cells. *PLoS ONE*. (2010) 5:e12578. doi: 10.1371/journal.pone.0012578

43. Norton TT, Amedo AO, Siegwart JT Jr. The effect of age on compensation for a negative lens and recovery from lens-induced myopia in tree shrews (*Tupaia glis* belangeri). *Vision Res*. (2010) 50:564–76. doi: 10.1016/j.visres.2009.12.014

44. Khanal S, Norton TT, Gawne TJ. Limited bandwidth short-wavelength light produces slowly-developing myopia in tree shrews similar to human juvenile-onset myopia. *Vision Res*. (2022) 204:108161. doi: 10.1016/j.visres.2022.108161

45. Siegwart JT Jr, Norton TT. Goggles for controlling the visual environment of small animals. *Lab Anim Sci*. (1994) 44:292–4.

46. Glickstein M, Millodot M. Retinoscopy and eye size. *Science*. (1970) 168:605–6. doi: 10.1126/science.168.3931.605

47. Norton TT, Wu WW, Siegwart JT Jr. Refractive state of tree shrew eyes measured with cortical visual evoked potentials. *Optom Vis Sci*. (2003) 80:623–31. doi: 10.1097/00006324-200309000-00006

48. Norton TT, Siegwart JT, German AJ, Robertson J, Wu WW. Comparison of cycloplegic streak retinoscopy with autorefractor measures in tree shrew eyes with, and without, induced myopia. *Invest Ophthalmol Vis Sci*. (2000) 41:S563.

49. El Hamdaoui M, Gann DW, Norton TT, Grytz R. Matching the lenstar optical biometer to A-scan ultrasonography for use in small animal eyes with application to tree shrews. *Exp Eye Res*. (2019) 180:250–9. doi: 10.1016/j.exer.2018.12.008

50. Doyle LM, Wang MZ. Overview of extracellular vesicles, their origin, composition, purpose, and methods for exosome isolation and analysis. *Cells*. (2019) 8:727. doi: 10.3390/cells8070727

51. Théry C, Witwer KW, Aikawa E, Alcaraz MJ, Anderson JD, Andriantsitohaina R, et al. Minimal information for studies of extracellular vesicles 2018 (MISEV2018): a position statement of the international society for extracellular vesicles and update of the MISEV2014 guidelines. *J Extracell Vesicles*. (2018) 7:1535750. doi: 10.1080/20013078.2018.1535750

52. Ludwig MR, Kojima K, Bowersock GJ, Chen D, Jhala NC, Buchsbaum DJ, et al. Surveying the serologic proteome in a tissue-specific kras(G12D) knockin mouse model of pancreatic cancer. *Proteomics*. (2016) 16:516–31. doi: 10.1002/pmic.201500133

53. Keller A, Nesvizhskii AI, Kolker E, Aebersold R. Empirical statistical model to estimate the accuracy of peptide identifications made by MS/MS and database search. *Anal Chem*. (2002) 74:5383–92. doi: 10.1021/ac025747h

54. Nesvizhskii AI, Keller A, Kolker E, Aebersold R. A statistical model for identifying proteins by tandem mass spectrometry. *Anal Chem*. (2003) 75:4646–58. doi: 10.1021/ac0341261

55. Weatherly DB, Atwood JA 3rd, Minning TA, Cavola C, Tarleton RL, Orlando R. A Heuristic method for assigning a false-discovery rate for protein identifications from Mascot database search results. *Mol Cell Proteomics*. (2005) 4:762–72. doi: 10.1074/mcp.M400215-MCP200

56. Old WM, Meyer-Arendt K, Aveline-Wolf L, Pierce KG, Mendoza A, Sevinsky JR, et al. Comparison of label-free methods for quantifying human proteins by shotgun proteomics. *Mol Cell Proteomics*. (2005) 4:1487–502. doi: 10.1074/mcp.M500084-MCP200

57. Liu H, Sadygov RG, Yates JR 3rd. A model for random sampling and estimation of relative protein abundance in shotgun proteomics. *Anal Chem*. (2004) 76:4193–201. doi: 10.1021/ac0498563

58. Beissbarth T, Hyde L, Smyth GK, Job C, Boon WM, Tan SS, et al. Statistical modeling of sequencing errors in SAGE libraries. *Bioinformatics*. (2004) 20:i31–9. doi: 10.1093/bioinformatics/bth924

59. Golub TR, Slonim DK, Tamayo P, Huard C, Gaasenbeek M, Mesirov JP, et al. Molecular classification of cancer: class discovery and class prediction by gene expression monitoring. *Science*. (1999) 286:531–7. doi: 10.1126/science.286.5439.531

60. Xu BJ, Shyr Y, Liang X, Ma LJ, Donnert EM, Roberts JD, et al. Proteomic patterns and prediction of glomerulosclerosis and its mechanisms. *J Am Soc Nephrol*. (2005) 16:2967–75. doi: 10.1681/ASN.2005030262

61. Ge SX, Jung D, Yao R. ShinyGO: a graphical gene-set enrichment tool for animals and plants. *Bioinformatics*. (2020) 36:2628–9. doi: 10.1093/bioinformatics/btz931

62. Huang DW, Sherman BT, Lempicki RA. Systematic and integrative analysis of large gene lists using DAVID bioinformatics resources. *Nat Protoc*. (2009) 4:44–57. doi: 10.1038/nprot.2008.211

63. Szklarczyk D, Kirsch R, Koutrouli M, Nastou K, Mehryary F, Hachilif R, et al. The STRING database in 2023: protein-protein association networks and functional enrichment analyses for any sequenced genome of interest. *Nucleic Acids Res*. (2023) 51:D638–46. doi: 10.1093/nar/gkac1000

64. Schorey JS, Cheng Y, Singh PP, Smith VL. Exosomes and other extracellular vesicles in host-pathogen interactions. *EMBO Rep*. (2015) 16:24–43. doi: 10.15252/embr.201439363

65. Caponnetto F, Manini I, Skrap M, Palmai-Pallag T, Di Loreto C, Beltrami AP, et al. Size-dependent cellular uptake of exosomes. *Nanomedicine*. (2017) 13:1011–20. doi: 10.1016/j.nano.2016.12.009

66. Kalluri R, LeBleu VS. The biology, function, and biomedical applications of exosomes. *Science*. (2020) 367:eaau6977. doi: 10.1126/science.aau6977

67. Zhu X, Li D, Du Y, He W, Lu Y. DNA hypermethylation-mediated downregulation of antioxidant genes contributes to the early onset of cataracts in highly myopic eyes. *Redox Biol*. (2018) 19:179–89. doi: 10.1016/j.redox.2018.08.012

68. Zhu X, Du Y, Li D, Xu J, Wu Q, He W, et al. Aberrant TGF-β1 signaling activation by MAF underlies pathological lens growth in high myopia. *Nat Commun.* (2021) 12:2102. doi: 10.1038/s41467-021-22041-2

69. Wen K, Shao X, Li Y, Li Y, Li Y, Wang Q, et al. The plasminogen protein is associated with high myopia as revealed by the iTRAQ-based proteomic analysis of the aqueous humor. *Sci Rep.* (2021) 11:8789. doi: 10.1038/s41598-021-88220-9

70. Frost MR, Norton TT. Alterations in protein expression in tree shrew sclera during development of lens-induced myopia and recovery. *Invest Ophthalmol Vis Sci.* (2012) 53:322–36. doi: 10.1167/iovs.11-8354

71. Gu L, Cong P, Ning Q, Jiang B, Wang J, Cui H. The causal mutation in ARR3 gene for high myopia and progressive color vision defect. *Sci Rep.* (2023) 13:8986. doi: 10.1038/s41598-023-36141-0

72. Zhou X, Ye J, Willcox MDP, Xie R, Jiang L, Lu R, et al. Changes in protein profiles of guinea pig sclera during development of form deprivation myopia and recovery. *Mol Vis.* (2010) 16:2163–74.

73. You J, Wu Q, Xu G, Gu C, Allen E, Zhu T, et al. Exosomal microRNA profiling in vitreous humor derived from pathological myopia patients. *Invest Ophthalmol Vis Sci.* (2023) 64:9. doi: 10.1167/iovs.64.1.9

74. Xue M, Ke Y, Ren X, Zhou L, Liu J, Zhang X, et al. Proteomic analysis of aqueous humor in patients with pathologic myopia. *J Proteomics.* (2021) 234:104088. doi: 10.1016/j.jprot.2020.104088

75. Jobling AI, Nguyen M, Gentle A, McBrien NA. Isoform-specific changes in scleral transforming growth factor-β expression and the regulation of collagen synthesis during myopia progression. *J Biol Chem.* (2004) 279:18121–6. doi: 10.1074/jbc.M400381200

76. Riddell N, Crewther SG. Integrated comparison of GWAS, transcriptome, and proteomics studies highlights similarities in the biological basis of animal and human myopia. *Invest Ophthalmol Vis Sci.* (2017) 58:660–9. doi: 10.1167/iovs.16-20618

77. Harper AR, Summers JA. The dynamic sclera: extracellular matrix remodeling in normal ocular growth and myopia development. *Exp Eye Res.* (2015) 133:100–11. doi: 10.1016/j.exer.2014.07.015

78. Guo L, Frost MR, Siegwart JT Jr, Norton TT. Scleral gene expression during recovery from myopia compared with expression during myopia development in tree shrew. *Mol Vis.* (2014) 20:1643–59.

79. Guo L, Frost MR, Siegwart JT Jr, Norton TT. Gene expression signatures in tree shrew sclera during recovery from minus-lens wear and during plus-lens wear. *Mol Vis.* (2019) 25:311–28.

80. Smith JN, Walker HM, Thompson H, Collinson JM, Vargesson N, Erskine L. Lens-regulated retinoic acid signalling controls expansion of the developing eye. *Development.* (2018) 145:dev167171. doi: 10.1242/dev.167171

81. Huang J, Liu Y, Oltean A, Beebe DC. Bmp4 from the optic vesicle specifies murine retina formation. *Dev Biol.* (2015) 402:119–26. doi: 10.1016/j.ydbio.2015.03.006

82. Beebe D, Garcia C, Wang X, Rajagopal R, Feldmeier M, Kim JY, et al. Contributions by members of the TGFbeta superfamily to lens development. *Int J Dev Biol.* (2004) 48:845–56. doi: 10.1387/ijdb.041869db

83. Kiss RS, Ma Z, Nakada-Tsukui K, Brugnera E, Vassiliou G, McBride HM, et al. The lipoprotein receptor-related protein-1 (LRP) adapter protein GULP mediates trafficking of the LRP ligand prosaposin, leading to sphingolipid and free cholesterol accumulation in late endosomes and impaired efflux. *J Biol Chem.* (2006) 281:12081–92. doi: 10.1074/jbc.M600621200

84. Lau AW, Chou MM. The adaptor complex AP-2 regulates post-endocytic trafficking through the non-clathrin Arf6-dependent endocytic pathway. *J Cell Sci.* (2008) 121:4008–17. doi: 10.1242/jcs.033522

85. Carreca AP, Pravatà VM, Markham M, Bonelli S, Murphy G, Nagase H, et al. TIMP-3 facilitates binding of target metalloproteinases to the endocytic receptor LRP-1 and promotes scavenging of MMP-1. *Sci Rep.* (2020) 10:12067. doi: 10.1038/s41598-020-69008-9

86. Aldahmesh MA, Khan AO, Alkuraya H, Adly N, Anazi S, Al-Saleh AA, et al. Mutations in LRPAP1 are associated with severe myopia in humans. *Am J Hum Genet.* (2013) 93:313–20. doi: 10.1016/j.ajhg.2013.06.002

87. Liu S, Chen T, Chen B, Liu Y, Lu X, Li J. Lrpap1 deficiency leads to myopia through TGF-β-induced apoptosis in zebrafish. *Cell Commun Signal.* (2022) 20:162. doi: 10.1186/s12964-022-00970-9

88. Le Clainche C, Dwivedi SP, Didry D, Carlier MF. Vinculin is a dually regulated actin filament barbed end-capping and side-binding protein. *J Biol Chem.* (2010) 285:23420–32. doi: 10.1074/jbc.M110.102830

89. Yang P, Yang Y, Sun P, Tian Y, Gao F, Wang C, et al. βII spectrin (SPTBN1): biological function and clinical potential in cancer and other diseases. *Int J Biol Sci.* (2021) 17:32–49. doi: 10.7150/ijbs.52375

90. Fu L, Wang X, Yang Y, Chen M, Kuerban A, Liu H, et al. Septin11 promotes hepatocellular carcinoma cell motility by activating RhoA to regulate cytoskeleton and cell adhesion. *Cell Death Dis.* (2023) 14:280. doi: 10.1038/s41419-023-05726-y

91. Kim DS, Hubbard SL, Peraud A, Salhia B, Sakai K, Rutka JT. Analysis of mammalian septin expression in human malignant brain tumors. *Neoplasia.* (2004) 6:168–78. doi: 10.1593/neo.03310

92. Svensson L, Närlid I, Oldberg A. Fibromodulin and lumican bind to the same region on collagen type I fibrils. *FEBS Lett.* (2000) 470:178–82. doi: 10.1016/S0014-5793(00)01314-4

93. Xiao D, Liang T, Zhuang Z, He R, Ren J, Jiang S, et al. Lumican promotes joint fibrosis through TGF-β signaling. *FEBS Open Bio.* (2020) 10:2478–88. doi: 10.1002/2211-5463.12974

94. Tsui MC, Liu HY, Chu HS, Chen WL, Hu FR, Kao WWY, et al. The versatile roles of lumican in eye diseases: a review. *Ocul Surf.* (2023) 29:388–97. doi: 10.1016/j.jtos.2023.06.012

95. Wu J, Zhao Y, Fu Y, Li S, Zhang X. Effects of lumican expression on the apoptosis of scleral fibroblasts: *in vivo* and *in vitro* experiments. *Exp Ther Med.* (2021) 21:495. doi: 10.3892/etm.2021.9926

96. Lin HJ, Wan L, Tsai Y, Chen WC, Tsai SW, Tsai FJ. The association between lumican gene polymorphisms and high myopia. *EYE.* (2010) 24:1093–101. doi: 10.1038/eye.2009.254

97. Yeh LK, Liu CY, Kao WWY, Huang CJ, Hu FR, Chien CL, et al. Knockdown of zebrafish lumican gene (zlum) causes scleral thinning and increased size of scleral coats. *J Biol Chem.* (2010) 285:28141–55. doi: 10.1074/jbc.M109.043679

98. Chakravarti S, Paul J, Roberts L, Chervoneva I, Oldberg A, Birk DE. Ocular and scleral alterations in gene-targeted lumican-fibromodulin double-null mice. *Invest Ophthalmol Vis Sci.* (2003) 44:2422–32. doi: 10.1167/iovs.02-0783

99. Hayes JD, McLellan LI. Glutathione and glutathione-dependent enzymes represent a co-ordinately regulated defence against oxidative stress. *Free Radic Res.* (1999) 31:273–300. doi: 10.1080/10715769900300851

100. Li B, Zhou J, Zhang G, Wang Y, Kang L, Wu J, et al. Relationship between the altered expression and epigenetics of GSTM3 and age-related cataract. *Invest Ophthalmol Vis Sci.* (2016) 57:4721–32. doi: 10.1167/iovs.16-19242

101. Liu RM, Desai LP. Reciprocal regulation of TGF-β and reactive oxygen species: a perverse cycle for fibrosis. *Redox Biol.* (2015) 6:565–77. doi: 10.1016/j.redox.2015.09.009

102. Summers JA, Palmer L. Choroidal regulation of scleral glycosaminoglycan synthesis during recovery from induced myopia. *Invest Ophthalmol Vis Sci.* (2007) 48:2957–66. doi: 10.1167/iovs.06-1051

103. Yuan Y, Li M, Chen Q, Me R, Yu Y, Gu Q, et al. Crosslinking enzyme lysyl oxidase modulates scleral remodeling in form-deprivation myopia. *Curr Eye Res.* (2018) 43:200–7. doi: 10.1080/02713683.2017.1390770

104. Moon CE, Ji YW, Lee JK, Han K, Kim H, Byeon SH, et al. Retinal proteome analysis reveals a region-specific change in the rabbit myopia model. *Int J Mol Sci.* (2023) 24:1286. doi: 10.3390/ijms24021286

105. Thelwell C, Longstaff C. The regulation by fibrinogen and fibrin of tissue plasminogen activator kinetics and inhibition by plasminogen activator inhibitor 1. *J Thromb Haemost.* (2007) 5:804–11. doi: 10.1111/j.1538-7836.2007.02422.x

106. Cuzner ML, Opdenakker G. Plasminogen activators and matrix metalloproteases, mediators of extracellular proteolysis in inflammatory demyelination of the central nervous system. *J Neuroimmunol.* (1999) 94:1–14. doi: 10.1016/S0165-5728(98)00241-0

107. Neitz M, Wagner-Schuman M, Rowlan JS, Kuchenbecker JA, Neitz J. Insight from OPN1LW gene haplotypes into the cause and prevention of myopia. *Genes.* (2022) 13:942. doi: 10.3390/genes13060942

108. Orosz O, Rajta I, Vajas A, Takács L, Csutak A, Fodor M, et al. Myopia and late-onset progressive cone dystrophy associate to LVAVA/MVAVA exon 3 interchange haplotypes of opsin genes on chromosome X. *Invest Ophthalmol Vis Sci.* (2017) 58:1834–42. doi: 10.1167/iovs.16-21405

109. Hagen LA, Arnegard S, Kuchenbecker JA, Gilson SJ, Neitz M, Neitz J, et al. The association between L:M cone ratio, cone opsin genes and myopia susceptibility. *Vision Res.* (2019) 162:20–8. doi: 10.1016/j.visres.2019.06.006

110. Zhu XJ, Zhou P, Zhang KK, Yang J, Luo Y, Lu Y. Epigenetic regulation of αA-crystallin in high myopia-induced dark nuclear cataract. *PLoS ONE.* (2013) 8:e81900. doi: 10.1371/journal.pone.0081900

111. Tedja MS, Wojciechowski R, Hysi PG, Eriksson N, Furlotte NA, Verhoeven VJM, et al. Genome-wide association meta-analysis highlights light-induced signaling as a driver for refractive error. *Nat Genet.* (2018) 50:834–48. doi: 10.1038/s41588-018-0127-7

112. Yee DC, Shlykov MA, Västermark A, Reddy VS, Arora S, Sun EI, et al. The transporter-opsin-G protein-coupled receptor (TOG) superfamily. *FEBS J.* (2013) 280:5780–800. doi: 10.1111/febs.12499

113. Sabesan R, Schmidt BP, Tuten WS, Roorda A. The elementary representation of spatial and color vision in the human retina. *Sci Adv.* (2016) 2:e1600797. doi: 10.1126/sciadv.1600797

114. Neitz J, Neitz M. The genetics of normal and defective color vision. *Vision Res.* (2011) 51:633–51. doi: 10.1016/j.visres.2010.12.002

115. Greenwald SH, Kuchenbecker JA, Rowlan JS, Neitz J, Neitz M. Role of a dual splicing and amino acid code in myopia, cone dysfunction and cone dystrophy associated with L/M opsin interchange mutations. *Transl Vis Sci Technol.* (2017) 6:2. doi: 10.1167/tvst.6.3.2

116. McClements M, Davies WIL, Michaelides M, Young T, Neitz M, MacLaren RE, et al. Variations in opsin coding sequences cause x-linked cone dysfunction syndrome with myopia and dichromacy. *Invest Ophthalmol Vis Sci.* (2013) 54:1361–9. doi: 10.1167/iovs.12-11156

117. Peterson YK, Luttrell LM. The diverse roles of arrestin scaffolds in G protein–coupled receptor signaling. *Pharmacol Rev.* (2017) 69:256–97. doi: 10.1124/pr.116.013367

118. Széll N, Feher T, Maróti Z, Kalmár T, Latinovics D, Nagy I, et al. Myopia-26, the female-limited form of early-onset high myopia, occurring in a European family. *Orphanet J Rare Dis.* (2021) 16:45. doi: 10.1186/s13023-021-01673-z

119. Huang Y, Chen X, Zhuang J, Yu K. The role of retinal dysfunction in myopia development. *Cell Mol Neurobiol.* (2023) 43:1905–30. doi: 10.1007/s10571-022-01309-1

120. Mambula SS, Stevenson MA, Ogawa K, Calderwood SK. Mechanisms for Hsp70 secretion: crossing membranes without a leader. *Methods.* (2007) 43:168–75. doi: 10.1016/j.ymeth.2007.06.009

121. Yaung J, Jin M, Barron E, Spee C, Wawrousek EF, Kannan R, et al. alpha-Crystallin distribution in retinal pigment epithelium and effect of gene knockouts on sensitivity to oxidative stress. *Mol Vis.* (2007) 13:566–77.

122. Liu H, Bell K, Herrmann A, Arnhold S, Mercieca K, Anders F, et al. Crystallins play a crucial role in glaucoma and promote neuronal cell survival in an in vitro model through modulating Müller cell secretion. *Invest Ophthalmol Vis Sci.* (2022) 63:3. doi: 10.1167/iovs.63.8.3

123. Chen C, Tsina E, Cornwall MC, Crouch RK, Vijayaraghavan S, Koutalos Y. Reduction of all-trans retinal to all-trans retinol in the outer segments of frog and mouse rod photoreceptors. *Biophys J.* (2005) 88:2278–87. doi: 10.1529/biophysj.104.054254

124. Choi EH, Daruwalla A, Suh S, Leinonen H, Palczewski K. Retinoids in the visual cycle: role of the retinal G protein-coupled receptor. *J Lipid Res.* (2021) 62:100040. doi: 10.1194/jlr.TR120000850

125. Summers J. "Retinoic acid in ocular growth regulation." In: *Vitamin A*. IntechOpen (2019). doi: 10.5772/intechopen.84586

126. McFadden SA, Howlett MHC, Mertz JR. Retinoic acid signals the direction of ocular elongation in the guinea pig eye. *Vision Res.* (2004) 44:643–53. doi: 10.1016/j.visres.2003.11.002

127. Mertz JR, Wallman J. Choroidal retinoic acid synthesis: A possible mediator between refractive error and compensatory eye growth. *Exp Eye Res.* (2000) 70:519–27. doi: 10.1006/exer.1999.0813

128. Troilo D, Nickla DL, Mertz JR, Summers Rada JA. Change in the synthesis rates of ocular retinoic acid and scleral glycosaminoglycan during experimentally altered eye growth in marmosets. *Invest Ophthalmol Vis Sci.* (2006) 47:1768–77. doi: 10.1167/iovs.05-0298

129. Li C, McFadden SA, Morgan I, Cui D, Hu J, Wan W, et al. All-trans retinoic acid regulates the expression of the extracellular matrix protein fibulin-1 in the guinea pig sclera and human scleral fibroblasts. *Mol Vis.* (2010) 16:689–97.

130. Martínez-Albert N, Bueno-Gimeno I, Gené-Sampedro A. Risk factors for myopia: a review. *J Clin Med.* (2023) 12:6062. doi: 10.3390/jcm12186062

131. Verhoeven VJM, Hysi PG, Wojciechowski R, Fan Q, Guggenheim JA, Höhn R, et al. Genome-wide meta-analyses of multiancestry cohorts identify multiple new susceptibility loci for refractive error and myopia. *Nat Genet.* (2013) 45:314–8. doi: 10.1038/ng.2554

132. Mao YM, Lan CJ, Tan QQ, Zhou GM, Xiang XL, Lin J, et al. All-trans retinoic acid regulates the expression of MMP-2 and TGF-β2 via RDH5 in retinal pigment epithelium cells. *Int J Ophthalmol.* (2023) 16:849–54. doi: 10.21203/rs.3.rs-1804289/v1

133. Wang Y, Xiao X, Li X, Yi Z, Jiang Y, Zhang F, et al. Genetic and clinical landscape of ARR3-associated MYP26: the most common cause of Mendelian early-onset high myopia with a unique inheritance. *Br J Ophthalmol.* (2023) 107:1545–53. doi: 10.1136/bjo-2022-321511

134. Yuan Y, Zhu C, Liu M, Ke B. Comparative proteome analysis of form-deprivation myopia in sclera with iTRAQ-based quantitative proteomics. *Mol Vis.* (2021) 27:494–505.

135. Hirata H, Dobrokhotov O, Sokabe M. Coordination between cell motility and cell cycle progression in keratinocyte sheets via cell-cell adhesion and Rac1. *iScience.* (2020) 23:101729. doi: 10.1016/j.isci.2020.101729

136. Metlapally R, Wildsoet CF. Scleral mechanisms underlying ocular growth and myopia. *Prog Mol Biol Transl Sci.* (2015) 134:241–8. doi: 10.1016/bs.pmbts.2015.05.005

137. Masri B, Salahpour A, Didriksen M, Ghisi V, Beaulieu JM, Gainetdinov RR, et al. Antagonism of dopamine D2 receptor/beta-arrestin 2 interaction is a common property of clinically effective antipsychotics. *Proc Natl Acad Sci U S A.* (2008) 105:13656–61. doi: 10.1073/pnas.0803522105

138. Huang F, Shu Z, Huang Q, Chen K, Yan W, Wu W, et al. Retinal dopamine D2 receptors participate in the development of myopia in mice. *Invest Ophthalmol Vis Sci.* (2022) 63:24. doi: 10.1167/iovs.63.1.24

139. Huang F, Wang Q, Yan T, Tang J, Hou X, Shu Z, Wan F, Yang Y, Qu J, Zhou X. The role of the dopamine D2 receptor in form-deprivation myopia in mice: studies with full and partial D2 receptor agonists and knockouts. *Invest Ophthalmol Vis Sci.* (2020) 61:47. doi: 10.1167/iovs.61.6.47

140. Xi J, Farjo R, Yoshida S, Kern TS, Swaroop A, Andley UP. A comprehensive analysis of the expression of crystallins in mouse retina. *Mol Vis.* (2003) 9:410–9.

141. Li M, Liu S, Huang W, Zhang J. Physiological and pathological functions of βB2-crystallins in multiple organs: a systematic review. *Aging.* (2021) 13:15674–87. doi: 10.18632/aging.203147

142. Sakaguchi H, Miyagi M, Darrow RM, Crabb JS, Hollyfield JG, Organisciak DT, et al. Intense light exposure changes the crystallin content in retina. *Exp Eye Res.* (2003) 76:131–3. doi: 10.1016/s0014-4835(02)00249-x

143. lge CS, Priglinger SG, Neubauer AS, Kampik A, Zillig M, Bloemendal H, et al. Retinal pigment epithelium is protected against apoptosis by alphaB-crystallin. *Invest Ophthalmol Vis Sci.* (2002) 43:3575–82.

144. Hollborn M, Birkenmeier G, Saalbach A, Iandiev I, Reichenbach A, Wiedemann P, et al. Expression of LRP1 in retinal pigment epithelial cells and its regulation by growth factors. *Invest Ophthalmol Vis Sci.* (2004) 45:2033–8. doi: 10.1167/iovs.03-0656

145. Ruiz A, Brett P, Bok D. TIMP-3 is expressed in the human retinal pigment epithelium. *Biochem Biophys Res Commun.* (1996) 226:467–74. doi: 10.1006/bbrc.1996.1379

146. Ku H, Chen JJ, Chen W, Tien PT, Lin HJ, Wan L, et al. The role of transforming growth factor beta in myopia development. *Mol Immunol.* (2024) 167:34–42. doi: 10.1016/j.molimm.2024.01.011

147. Low SWY, Connor TB, Kassem IS, Costakos DM, Chaurasia SS. Small leucine-rich proteoglycans (SLRPs) in the retina. *Int J Mol Sci.* (2021) 22:7293. doi: 10.3390/ijms22147293

148. Schoentgen F, Jonic S. PEBP1/RKIP behavior: a mirror of actin-membrane organization. *Cell Mol Life Sci.* (2020) 77:859–74. doi: 10.1007/s00018-020-03455-5

frontiers | Frontiers in Medicine

TYPE Original Research
PUBLISHED 04 August 2025
DOI 10.3389/fmed.2025.1504560

OPEN ACCESS

EDITED BY
Pablo De Gracia,
University of Detroit Mercy, United States

REVIEWED BY
Emiliano Teran,
Autonomous University of Sinaloa, Mexico
Liwei Ma,
Shenyang Aier Excellence Eye Hospital Co, Ltd, China

*CORRESPONDENCE
Victor Rodriguez-Lopez
✉ victor.rl@io.cfmac.csic.es

RECEIVED 30 September 2024
ACCEPTED 18 July 2025
PUBLISHED 04 August 2025

CITATION
Rodriguez-Lopez V, Dotor-Goytia P, Moreno E and Vinas-Pena M (2025) Differences in perceived chromatic aberration between emmetropic and myopic eyes using adaptive optics.
Front. Med. 12:1504560.
doi: 10.3389/fmed.2025.1504560

Differences in perceived chromatic aberration between emmetropic and myopic eyes using adaptive optics

Victor Rodriguez-Lopez*, Paulina Dotor-Goytia, Elena Moreno and Maria Vinas-Pena

Institute of Optics, Spanish National Research Council (IO-CSIC), Madrid, Spain

Introduction: The study of polychromatic visual perception is challenging due to the number of entangled factors involved in the process, from the cues within visual information from the outside world, to the ocular optics, the retinal properties, and neural adaptation processes in the brain.

Methods: In this study, we used an adaptive optics (AO)- based polychromatic visual simulator to investigate the perception of combined optical cues and its dependence on refractive error. Subjective best focus was obtained as the average of 3 repeated measurements for (1) polychromatic and five monochromatic wavelengths in the visible (450–670 nm); (2) three different visual stimuli (conventional binary sunburst, natural outdoor image, natural indoor image); and (3) under natural aberrations (no-AO) and corrected aberrations (AO) conditions. Repeatability was determined as the standard deviation across repetitions. Chromatic difference of focus (CDF) was calculated for Green-Blue (G-Blue, 550–470 nm) and Green-Red (G-Red, 550–700 nm). Longitudinal chromatic aberration (LCA) was estimated using a polynomial regression fit of the best subjective focus curves as a function of the wavelength. Nine young adults (28 $\pm$ 6 years) with different refractive profiles (6 myopic and 3 emmetropic) participated in this study.

Results: CDF showed different trends in the G-Red and the G-Blue regions, especially for the binary stimulus and after AO-correction of aberrations. However, in the myopic group, CDF was similar in absolute value for G-Blue and G-Red (0.61 $\pm$ 0.34 and 0.73 $\pm$ 0.58, respectively, $p > 0.05$ Mann-Whitney U test), whereas, in the emmetropic group, the chromatic difference was greater for G-Blue than for G-Red (0.58 $\pm$ 0.32 D and 0.22 $\pm$ 0.38 D, respectively, $p < 0.05$ Mann-Whitney U test). There was no effect of correcting natural aberrations. LCA does not vary with refractive error.

Discussion: Overall, the results of this study suggest that the refractive profile may influence how visual information with specific chromatic properties is perceived and processed, potentially shaping visual mechanisms involved in chromatic defocus perception.

KEYWORDS

myopia, chromatic defocus, longitudinal chromatic aberration, blur perception, refractive error, adaptive optics, monochromatic high-order aberrations

1 Introduction

The study of polychromatic visual information processing is challenging. First, visual inputs from the outside world are rarely well-defined homogeneous patches of light or dark, but are typically a mixture of polychromatic large-and small-scale structures (1–3) that interact with the dynamics of visual function (i.e., accommodation, binocular vision, eye movements, and adaptation, among others) (4–8). Furthermore, ocular optics is far from being a diffraction-limited system, and retinal image quality is degraded by the effects of monochromatic and chromatic aberrations, and their interactions (9–11). Finally, prolonged exposure to a degraded stimulus (i.e., a blurred retinal image) alters visual perception (12, 13) by shifting blur discrimination thresholds, more prominently in myopes than in emmetropes (14, 15).

Visual information processing, which is modulated by ocular dynamics, is essential for defocus detection (16, 17) and thus for vision. Accommodation, monochromatic high-order aberrations (HOAs), peripheral defocus, astigmatism, and chromatic aberrations are thought to modulate the sign and magnitude of defocus on the retina, and may also alter the temporal and spatial integration of defocus signals across the retina (18). Optical defocus leads to a proportional degradation of contrast at the edges of the images, a potential cue for the retina that would use edge contrast to determine the focal plane, and color contrast to identify the sign of defocus (3). However, retinal blur has been identified as the primary even-error stimulus for accommodation (19–21), the accommodative response becomes more precise when aberrations are corrected, and the presence of higher amounts of HOAs produces an increase in accommodative lag (22), similar to the increased accommodative lag found in myopes (23).

Ocular aberrations also play an important role in visual perception, and their correction could either improve retinal image quality and visual performance (24, 25) or reduce it due to adaptation. One study (26) reported that the presence of HOAs results in different point spread functions for hyperopic and myopic defocus, suggesting that these differences may be used by the visual system to determine the correct direction of focus shift. However, the relationship between aberrations and refractive error is inconclusive. Some studies have suggested a slightly higher amount of monochromatic aberrations in myopic eyes (27–29), while others have found no correlation between aberrations and refractive error (30–34) and others have found higher levels of HOAs in hyperopes (35). It seems likely that increased axial growth is accompanied by geometrical changes in the ocular components, resulting in changes in the aberration pattern and magnitude (36). In any case, if increased high-order aberrations occur in myopes, they seem to be more pronounced in high myopia (37), and related to structural changes.

In addition, chromatic cues may aid in detecting the sign of defocus. Broadband light produces color fringes on the retinal image, which may provide a signed chromatic signal of whether the defocus is hyperopic or myopic (3), as shown in a variety of animal models (18). Chromatic dispersion causes short wavelengths to focus in front of long wavelengths, creating a chromatic focus difference between them, known as longitudinal or axial chromatic aberration (LCA) (38). LCA causes long wavelengths to be focused on a more hyperopic plane than shorter wavelengths, so that the total refraction of the eye varies inversely with wavelength. Ocular LCA shows low intersubject variability, with subjective LCA (≈ 2D in the visible range) being significantly higher (by 0.50 D in the 488–700 nm range) than objective LCA (measured using reflectometric methods), likely due to differences in the retinal reflection planes and the retinal image focal plane (39, 40). Polychromatic optical quality in the phakic eye depends on the delicate balance between monochromatic and chromatic aberrations (41–43), which may be an important factor in myopic eyes because the human eye can use chromatic defocus as a directional cue for accommodation to both moving and stationary objects (44, 45). However, some individuals are able to accommodate in the absence of chromatic aberration, suggesting the existence of other achromatic cues that drive accommodation (46). Recently, Swiatczak and Schaeffel suggested that the human retina uses this difference in focus in the blue and the red to determine the sign of defocus, and hypothesized that the myopic retina has lost the ability to respond to LCA (47). Strikingly, the amount of both subjective and objective LCA was independent of the presence of HOAs (39), at least in a young emmetropic sample.

Adaptive optics (AO) based visual simulators operating at multiple wavelengths, with complementary AO elements for blur manipulation, allow to simulate vision under very different conditions, using a variety of psychophysical paradigms (i.e., method of limits, constant stimuli, adaptive staircase methods, among others), and artificial and naturalistic stimuli (Gabor patches, gratings, letters, natural images). AO allows to explore the limits of spatial vision imposed by the ocular optics (24) and to bypass them to study the neural adaptation processes in the brain, as well as to test the visual response to different optical cues in combination with relevant ocular properties (i.e., aberrations, accommodation, neural adaptation). Recently, a filter-based Badal LCA compensator incorporated into an AO scanning laser ophthalmoscope (AOSLO) allowed the independent and simultaneous control of focus at different wavelengths, so it can be tuned to compensate for the LCA of each individual eye (48), paving the way for more effective ways to modulate LCA, and understand its impact. The aim of this study is to investigate differences in the visual perception of stimuli with different spectral and spatial content in monochromatic and chromatic conditions, while controlling the subject's monochromatic high-order aberrations using an AO-based polychromatic visual simulator. In particular, we investigate differences in the perceived best focus of subjects with different refractive errors in young adults.

2 Methods

Through-focus (TF) optical and visual quality with different stimuli (binary black and white, grayscale natural images) using five monochromatic and one polychromatic conditions was tested in a polychromatic (AO) based simulator. The subjective best focus for the same conditions was measured in 9 subjects, with different refractive errors, while controlling their ocular aberrations.

2.1 Stimuli: binary and natural images

Three different stimuli were used to evaluate the influence of visual information on the perception of the best focus in monochromatic and polychromatic conditions. Figure 1A shows the three stimuli used in the study (top row) and their corresponding frequency spectrum calculated

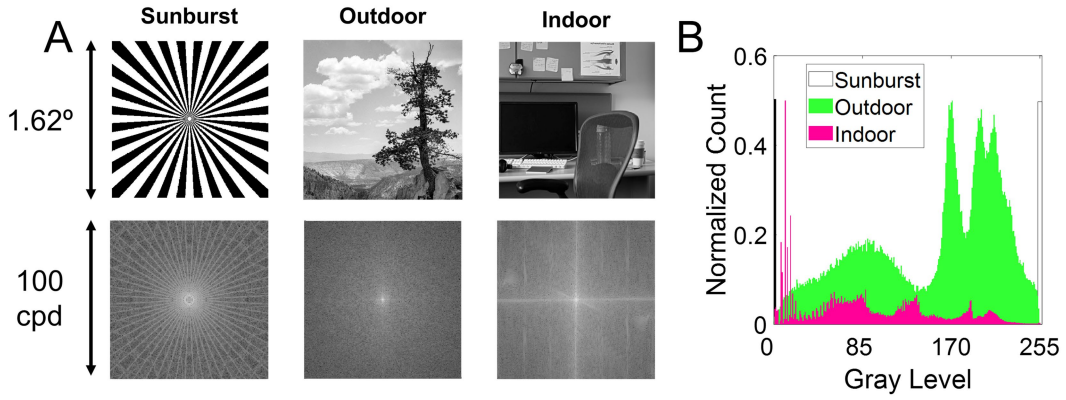

FIGURE 1
Visual stimuli. **(A)** Top row, stimuli used in the study. Bottom row, the frequency spectrum calculated as the magnitude of the Fourier transform. The stimuli are (1) Sunburst, a binary mask; (2) Outdoor, a natural grayscale image depicting an outdoor scene of a distant tree; and (3) Indoor, a natural grayscale image depicting an indoor scene of an office. **(B)** Histogram of the three images.

as the magnitude of the Fourier transform of the images (bottom row). Figure 1B shows the histograms of the three images. Stimuli subtended 1.62 degrees when viewed through the AO system.

2.2 Polychromatic adaptive optics visual simulator

On-bench measurements and visual testing were performed with a custom-developed polychromatic AO system at the Institute of Optics (Spanish National Research Council, IO-CSIC, Madrid, Spain). The system has been described in detail in previous publications (39, 49, 50). The current configuration of the system consists of 9 different channels, of which the following were used in this study. (1) The illumination channel, with light coming from the supercontinuum laser source (SC400 femtopower 1,060 supercontinuum laser; Fianium Ltd., United Kingdom) in combination with a dual acousto-optic tunable filter module (Gooch & Housego, United Kingdom) that delivers light in multiple wavelengths through 2 different fiber outputs (visible and near-infrared). (2) The AO channel, consisting of the Hartmann-Shack wavefront sensor (microlens array 40 × 32, 3.6 mm effective diameter, centered at 1,062 nm; HASO 32 OEM, Imagine Eyes, France) and the electromagnetic deformable mirror (52 actuators, 15-mm effective diameter, 50 μm stroke; MIRAO, Imagine Eyes, France) to measure and correct the high-order aberrations (HOAs). In this study, it was used to compensate for the system aberrations and to measure and correct the aberrations of the subjects. The system aberrations were corrected at 827 nm. (3) The psychophysical channel uses a Digital Micro-Mirror Device (DMD, DLP® Discovery™ 4,100 0.7 XGA; Texas Instruments, United States) placed in a conjugate retinal plane to display visual stimuli subtending 1.62 angular degrees. The DMD was monochromatically illuminated with light coming from the supercontinuum laser source, and with white light coming from a white light fiber lamp (OSL2B—3,200 K; Thorlabs, Germany). (4) The pupil monitoring channel consists of an infrared camera conjugated to the pupil of the eye, in combination with an infrared LEDs ring. (5) The Badal optometer channel corrects for defocus and allows for through-focus psychophysical testing. All optoelectronic elements of the system were automatically controlled and synchronized by custom software written in Visual C++ and C# (Microsoft, United States) and MATLAB (MathWorks, United States).

2.3 On-bench testing

TF optical quality was evaluated on-bench in the same AO system using an artificial eye placed at the position of the subject's eye using a 3-D micrometer stage. Single-pass TF retinal images of the three stimuli were collected on an artificial eye equipped with an objective lens (50.8 mm of focal length) and a CCD camera (DCC1545M, High Resolution USB2.0 CMOS Camera, Thorlabs, Germany) acting as a "retina," in place of the subject's eye. The stimuli were displayed in the DMD, illuminated with light from the supercontinuum laser source for monochromatic illumination and the white light lamp for polychromatic illumination, for a pupil diameter of 5 mm. Each stimulus was displayed in the DMD on a black background and projected onto the retina of the system (i.e., the CCD camera). The vergence of the system was varied from −0.75 to +0.75 D in steps of 0.25 D by changing the position of the Badal system. TF images were acquired for the wavelengths 480, 550, 633 nm and white light and for all stimuli, while correcting for the higher order aberrations of the system (RMS < 0.05 microns over the entire range).

2.4 *In vivo* experimental testing

To find the subjective best focus, subjects adjusted the position of the Badal system using a keyboard until the stimulus was perceived focused using the methods of limits (precision 0.01 D steps) while viewing the stimulus illuminated at a series of wavelengths in visible light (450, 480, 500, 550, 633 and 670 nm) as well as in white light. The luminance of the stimulus was approximately 20 cd/m^2 throughout the tested spectral range (450–670 nm), therefore in the photopic range at all wavelengths. Equiluminance across wavelengths and white light was ensured during calibration. Subjects were instructed to use the keyboard to find the position where the stimulus appeared sharp. Subjects first performed a trial run using the reference wavelength of 550 nm to familiarize themselves with the test. The starting point of

the Badal was randomly chosen between +1.00 and +1.50 D (placed beyond the optical infinity) beyond the subject's best focus reported in the first trial to avoid any accommodative response (e.g., if the best focus at 550 nm in the first trial was −2.00 D, the starting point for finding the best focus at 550 nm was between −0.50 and −1.00 D). The best focus search was repeated 3 times for each wavelength. Measurements were later performed for each stimulus randomly for all wavelengths and white light. Later, subjects performed the same task but with AO correction. The state of the deformable mirror, which compensated for the ocular aberrations of each eye, was determined in a closed-loop operation at 880 nm and applied to measurements at all wavelengths (39). Aberrations were monitored throughout the experiment to ensure a residual RMS < 0.1 microns in all cases and all subjects.

The subjective best focus was obtained for each of the monochromatic and polychromatic light sources, three stimuli, in the presence of natural aberrations and with AO correction. Subjects were stabilized with a dental impression and the pupil of the eye was aligned with the optical axis of the instrument using the line of sight as a reference, while the natural pupil was viewed on the monitor with a pupil camera. An artificial pupil was used to maintain the same pupil diameter (5 mm) across subjects (subjects' pupil size was greater than 5 mm − 5.49 ± 0.33 mm). The room lights were turned off during the measurements. Breaks were taken every 30 min, and subjects could stop if they needed additional rest. The entire experimental session lasted approximately 2 h.

2.5 Subjects

Nine subjects were tested monocularly in the AO system. Subjects were healthy young adults (28.2 ± 6.0 years), with refractive errors ranging from −6.25 to +1.00 D (astigmatism < 0.50 D in all cases). Subjects were classified into myopes (spherical refractive error higher than −0.5 D) and emmetropes (spherical refractive error lower −0.50 and +1.00 D). Refractive error was determined from their current prescription and adjusted, if necessary, using traditional subjective refraction, i.e., the fogging technique. There was no difference in the refractive error from the current prescription in any of the subjects. The RMS of 3rd order and higher aberrations (at 5 mm pupil diameter) in the subjects ranged from 0.07 to 0.54 µm. Figure 2A summarizes the refractive and aberration profile of the subjects, ranked according to the magnitude of their refractive error.

All subjects were informed of the nature and possible consequences of the study and provided written informed consent. All protocols met the tenets of the Declaration of Helsinki and were previously approved by the Bioethics Committee of the Spanish National Research Council (CSIC).

A

Subject	Group	Spherical Equivalent	Age	RMS (µm)
S1	Myope	-6.25	42	0.46
S2	Myope	-5.00	30	0.88
S3	Myope	-2.25	31	0.31
S4	Myope	-2.00	25	0.63
S5	Myope	-1.00	23	0.55
S6	Myope	-1.00	24	0.59
S7	Emmetrope	+0.25	23	0.35
S8	Emmetrope	+0.50	27	0.08
S9	Emmetrope	+1.00	29	0.26

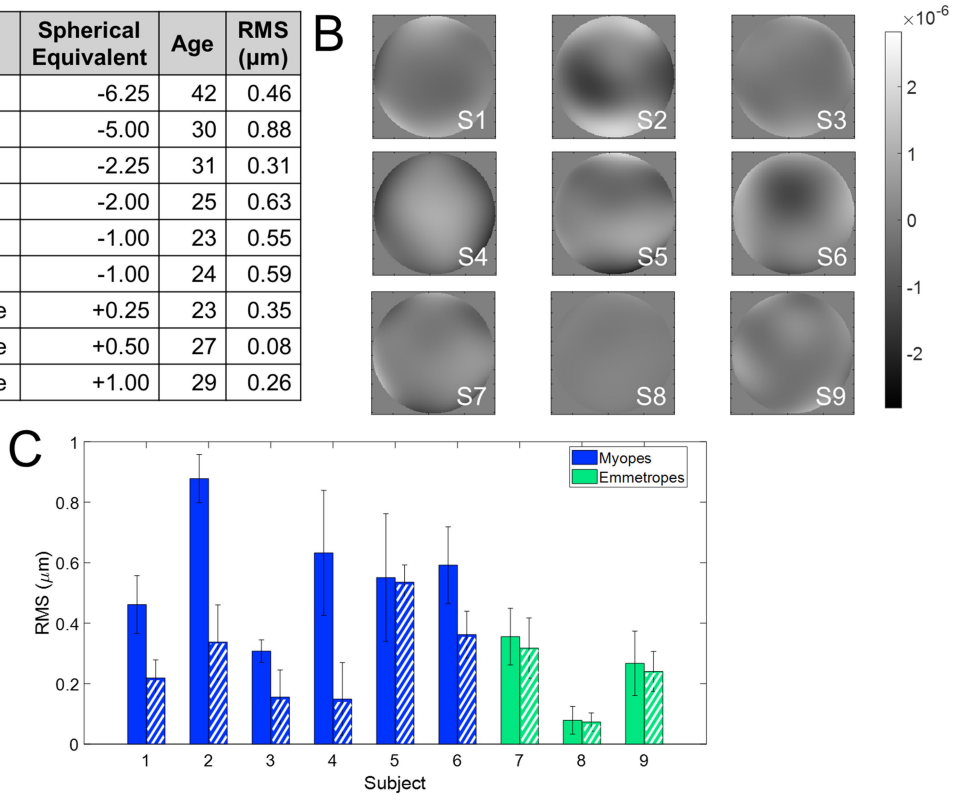

FIGURE 2
Refractive profile of the subjects enrolled in the study. **(A)** Demographics of the subjects enrolled in the study. The RMS wavefront error is with astigmatism and high-order aberrations. **(B)** Wavefront aberration maps. The scale bar is microns. **(C)** RMS wavefront error. Solid bars show the RMS with all aberrations except for piston, tilts, and defocus, and dashed bars show only high-order aberrations. Blue indicates myopes and green emmetropes.

2.6 Data analysis

On-bench testing: TF optical quality was obtained from the images of each stimulus on-bench. The image quality metric was obtained from the correlation coefficient (correlation of each of the TF images with the image in the best focus for each wavelength under the same conditions: laser power, pupil diameter, and exposure time) of the image series. Only the region of interest (where the stimulus was located in the camera image) was analyzed and converted to grayscale before estimating the correlation. The correlation metric is expected to peak at 0 D in all conditions. To provide a quantitative estimate of the degradation for both wavelength and defocus sign –myopic (negative) and hyperopic (positive)–, the absolute value of the slope of the linear regression adjustment between the negative defocus values and the correlation metric and the positive defocus values and the correlation metric was calculated. This analysis was performed considering only defocus values within the range of ±0.5 D (from −0.5 to 0.0 D for negative defocus, and from 0.0 to +0.5 D for positive defocus). The slope is an indicator of image degradation as defocus increases. A higher slope value means that the decrease in the correlation metric is greater and therefore the degradation is also greater.

In vivo testing: The subjective best focus in each condition was obtained directly from the Badal system readings. The average and the standard deviation across the 3 repeated measurements provided the subjective best focus and its repeatability for all conditions, respectively. In addition, the chromatic difference of focus curves was obtained from them by shifting the best focus curves on the vertical axis so that they crossed zero at 550 nm (the reference wavelength). The chromatic difference in focus (CDF) was fitted to a quadratic regression. The Green-Blue (G-Blue) difference was estimated as the chromatic difference in focus between green and blue (550 and 480 nm) using the adjustments for each refractive error group. Similarly, the Green-Red G-Red difference was estimated as the chromatic difference in focus between green and red (550 and 700 nm) using the adjustments for each refractive error group. Finally, the longitudinal chromatic aberration (LCA) was estimated by fitting these chromatic differences of focus curves within the visible region (from 470 to 700 nm). A Mann–Whitney U-test two-tailed was used to analyze the statistical significance of the differences between the results of the different conditions, and of different refractive error groups. A linear mixed model with Bonferroni correction was applied to account for multiple comparisons. The significance level was set at 5% ($p = 0.05$). MATLAB (Math-works Inc., Natick, United States) was used for analysis. Spearman correlation was used to compare psychophysical data to explore trends in visual perception.

3 Results

3.1 Through-focus on-bench image analysis

Figure 3 shows the on-bench through-focus (TF) image series acquired for the different conditions tested in a range of 1.20 D (± 0.60 D, Figure 3A), while AO-correcting the HOAs of the system. The residual Root Mean Square (RMS) after AO-correction was less than 0.05 microns for all conditions, and only the defocus term changed when the Badal system was varied (Figure 3B). Figure 3C shows the slope of the correlation metric as a function of defocus for negative and positive defocus and all wavelengths and stimuli as a bar graph (see Data Analysis section in Methods). A higher value of the slope indicates a greater decrease in the correlation metric and therefore a greater degradation. For each wavelength, the slope for negative defocus (lighter color) is on the left, and the slope for positive defocus (darker color) is on the right. For all stimuli and wavelengths, the slope for positive defocus is higher than for myopic defocus (0.103 vs. 0.079 on average), meaning that positive defocus degrades the images slightly more than negative defocus. In addition, the slope is lower for the outdoor natural stimulus than for the other two (0.017 for outdoor vs. 0.042 for indoor and 0.213 for sunburst), indicating less degradation of the outdoor images than the binary/indoor images. The sunburst had the steepest slope and therefore the highest degradation (0.256 for positive defocus in the red wavelength).

3.2 Subjects' profile

Figure 2 shows the refractive and aberration profiles of the subjects who participated in the experiment, grouped according to their refractive error (from higher myopia to higher hyperopia). Figure 2A shows the demographic information, Figure 2B the wavefront aberration map of all subjects participating in the study, and Figure 2C a comparison of the RMS of HOAs + astigmatism (solid bars) and RMS of HOAs only (dashed bars). The RMS of HOAs + astigmatism ranged from 0.08 to 0.88 μm (mean 0.46 ± 0.24 μm), whereas the RMS of HOAs only ranged from 0.08 to 0.53 μm (0.26 ± 0.14 μm).

3.3 Polychromatic subjective best focus

Figure 4 shows the subjective best focus for all wavelengths, stimuli, and subjects measured in Experiment 1, with natural aberrations. Blue represents myopes (S1 to S6; refractive error higher than −0.50 D) and green represents emmetropes (S7 to S9; between −0.50 and 1.00 D). Figure 4A shows the subjective best focus for the three stimuli (Sunburst, black; Indoor, dark gray; Outdoor, light gray) for each wavelength, and the corresponding fit for each subject. Figure 4B shows the individual data clustered stimuli.

Similar to previous experiments using the same experimental setup (39), the variability of the best focus task was very low (0.06 D on average, both in the presence of natural aberrations, and after AO-correction). As expected, the subjective best focus for green (550 nm) was highly correlated with that for white light, both in the presence of natural aberrations ($\rho = 0.98$; slope = 1.00; y-intercept = 0.22) and after AO-correction ($\rho = 0.97$; slope = 0.94; y-intercept = −0.13). As expected, shorter wavelengths were focused on more negative (myopic) focus, and longer wavelengths on more positive (hyperopic) focus. Subjective best focus with natural aberrations and AO-correction was highly correlated ($\rho = 0.97$; slope = 0.95; y-intercept = −0.39).

Figure 5 and Table 1 summarize the chromatic difference of focus (CDF) for the two refractive groups (myopes in blue; emmetropes in green) and the effect of AO-correction of natural aberrations. Figure 4A reports the subjective best focus (from Badal direct readings) obtained with the eye's natural aberrations, and Figure 4B with AO-correction of high order aberrations. CDFs curves for emmetropes (green) remained relatively flat in the red region and becomes progressively steeper toward

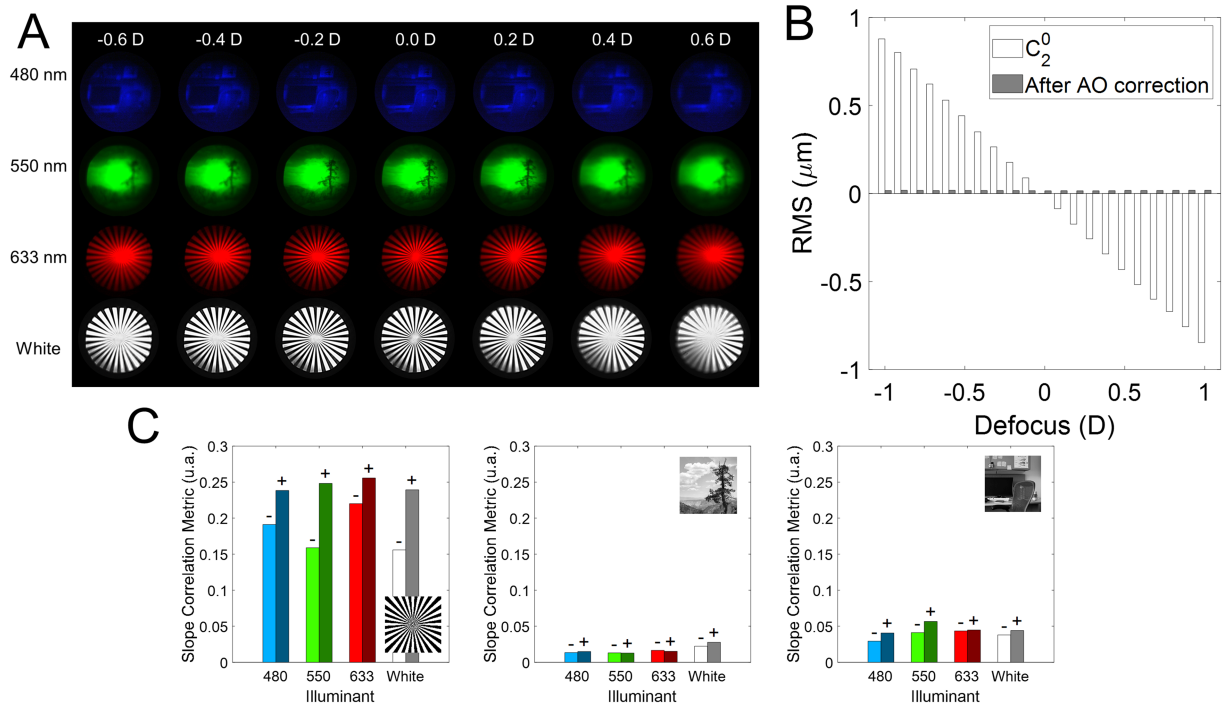

FIGURE 3
On-bench TF images analysis. **(A)** Illustrative examples of the TF images for different illumination (480, 550, 633 nm, and white light) and stimulus conditions. **(B)** Optical quality throughout the experiments. The defocus coefficient term of the wavefront at the pupil plane of the system measured with the wavefront sensor (white bars, c_2^0), and the residual RSM after AO correction (gray bars) of the HOAs + astigmatism of the system. **(C)** Absolute value of the slope of the linear regression fit of the correlation and defocus in the range ±0.50 D. A higher value of the slope indicates a greater degradation as a function of defocus. A minus sign is placed over the negative defocus slope bars (values < 0.00 D) and a positive sign over the positive defocus slope bars (values > 0.00 D).

the blue region, whereas myopes (blue) exhibited markedly steep slopes for both the blue and red regions. A linear mixed model confirmed main effect of refractive error on CDF. In the presence of natural aberrations, CDF-Green-Blue is significantly lower than the Green-Red, whereas for myopes both are similar. AO-correction of ocular aberrations changes that partially. CDF-Green-Blue for emmetropes significantly increased, reaching higher values than myopes for the same range, whereas the increment for the Green-Red regions was lower. Myopes remained insensitive to the AO-correction effect.

The effect of the different stimuli is shown in Figure 5. With natural aberrations (Figure 5A), myopes showed mean G-Blue and G-Red values of 0.61 ± 0.34 and 0.73 ± 0.58 D, respectively ($p = 0.31$, U = 130, effect size r = 0.061, Mann–Whitney U test) whereas emmetropes showed 0.58 ± 0.32 and 0.22 ± 0.38 D, respectively ($p = 0.049$, U = 63, effect size r = 0.108, Mann–Whitney U test), significantly higher for G-Blue than for G-Red. The inter-group difference was significant for G-Red ($p = 0.028$, U = 124, effect size r = 0.08), but not for G-Blue ($p = 0.77$, U = 87, effect size r = 0.011). These differences were greater when using natural images (0.66 D outdoor and 0.46 D indoor) than the binary stimulus (0.23 D). On average, the CDF curves at 670 nm differed by 0.51 D.

AO correction (Figure 5B) accentuated inter-group differences in the G-Blue region (−0.22 at 480 nm on average, and particularly −0.80 D for the binary stimulus) while reducing separation at G-Red region (~0D at 670 nm). Within emmetropes, G-Blue remained higher than G-Red (p = 0.04, U = 64, effect size r = 0.113, Mann–Whitney U test); within groups, G-Red still differed although not statistically ($p = 0.05$, U = 119, r = 0.071) but G-Blue did not ($p = 0.11$, U = 49, r = −0.06). In addition, no significant differences arose natural and AO conditions inside either refractive group (all $p > 0.05$ in, U ranged from 21 to 173, Mann Whitney U test). For reference, the results of a previous study (39), performed in the same system and experimental conditions are shown in the figure (gray bars): 0.53 D and 0.99 D for the G-Blue and G-Red, respectively in the presence of aberrations, and 0.75 D and 0.74 after AO-correction of HOAs. The sample in that study consisted of five young subjects (28.6 ± 1.9 years) with spherical errors ranging from 0 and −4.50 D (−1.15 ± 0.95 D).

3.4 Subjective longitudinal chromatic aberration

Subjective longitudinal chromatic aberration (LCA) was estimated from the polynomial fitting of the CDF curves for the extremes of the spectral range (from 480 to 700 nm). Figure 6A shows the average across stimuli for each refractive error group and with natural aberrations and aberrations compensated. On average, subjective LCA is similar for both refractive groups when using the binary stimuli, and AO-correction of HOAs does not modify that trend. Results are slightly different with natural images, where AO-correction of HOAs increases subjective LCA total amount, particularly for emmetropic subjects, as shown in Figure 2A. There was no statistical difference as a function of the stimulus, refractive error, or aberration condition ($p > 0.05$ for all comparisons, U ranged from 23 to 35, Mann Whitney U test). These findings were further supported by the linear mixed model, which did not identify any significant fixed effects for these factors.

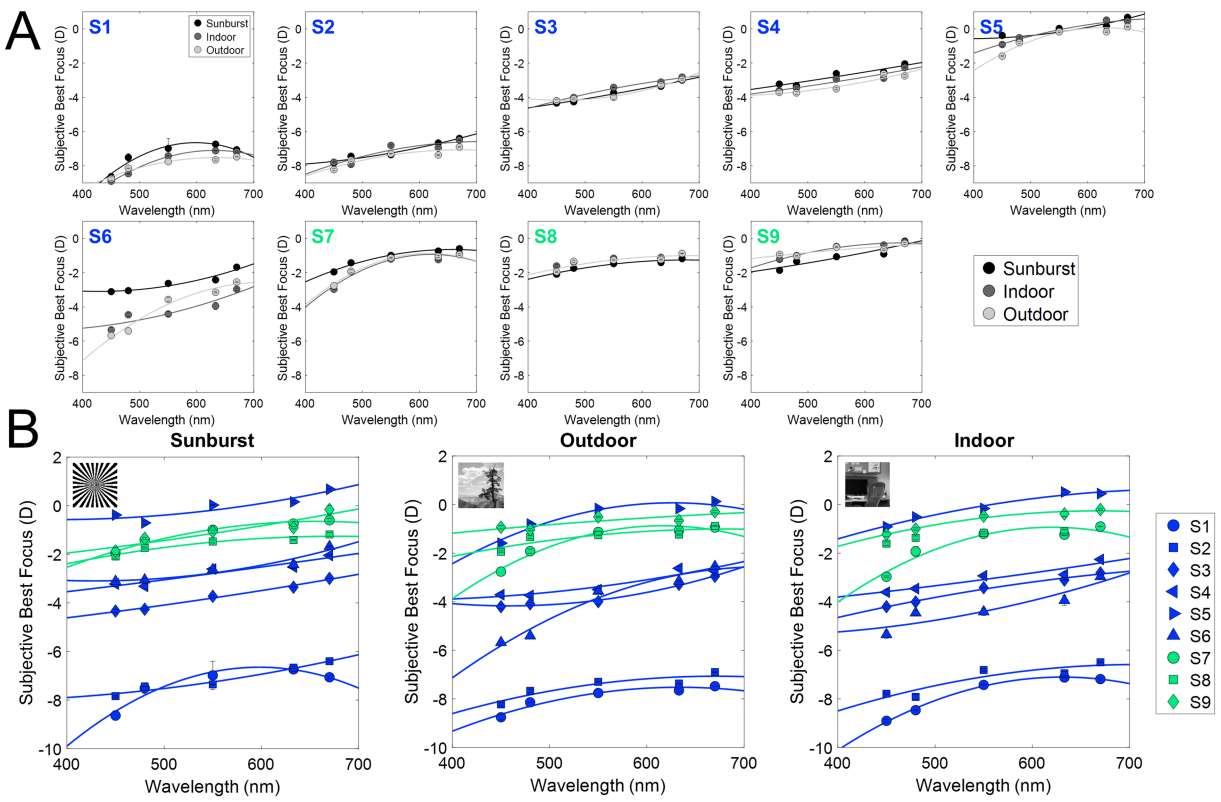

FIGURE 4
Subjective best focus for different wavelengths and stimuli in the presence of natural aberrations and after AO-correction. **(A)** Individual chromatic defocus curves (CDF) for the three stimuli tested. **(B)** Individual results for all subjects as a function of the stimulus (black, binary; dark gray, indoor gray scale; light gray, outdoor gray scale). Blue markers represent myopes (S1 to S6, ranked by increasing refractive error), and green markers represent emmetropes (S7 to S9).

4 Discussion

In this study, we investigated the differences in the perception of polychromatic optical cues and their dependence on refractive error, in the presence of natural aberrations and after their aberration correction, (a) to shed light on the perception of polychromatic large-and small-scale structures; (b) to test differences between emmetropic and myopic eyes in chromatic aberration and the impact of monochromatic aberrations, and (c) to investigate the visual perception of these features.

In this study, we present differences in the perception of chromatic defocus when using binary or natural stimuli, in monochromatic and polychromatic conditions. On average, G-Blue CDF (480–550 nm) was higher than G-Red CDF (555–700 nm) in emmetropes, while myopes showed the opposite trend (Figure 5). In addition, the G-Red CDF was significantly different for myopes and emmetropes (see Figure 5C). The use of different stimuli increased these differences, with natural images showing the largest differences (binary 0.23 D; indoor 0.46 D; outdoor 0.66 D). AO correction of HOAs had no effect on the G-Blue CDF on myopes, regardless of the stimuli, but increased G-Blue CDF in emmetropes when viewing the binary or the indoor stimuli. Removal of aberrations reduced the G-Red CDF obtained with the binary (emmetropes and myopes) and outdoor (myopes) stimuli, and increased it with the indoor (emmetropes and myopes) and outdoor (emmetropes) stimuli, indicating differences in perception related to the refractive profile.

4.1 Polychromatic subjective best focus

Overall, our results are consistent with previous reports of subjective best focus measurements at different wavelengths, when using a high-contrast stimulus, similar to the binary image used here (10, 39, 51–53), with very low variability in the subjective best focus setting (<0.10 D), both in the presence of natural aberrations and after AO-correction. Similarly, the subjective best focus task showed very low variability across subjects, stimuli, and illumination conditions, and the subjective best focus for green illuminant was correlated with that for white light, both in the presence/absence of HOAs.

The chromatic difference of focus (CDF) curve for emmetropes is flatter in the red but becomes increasingly steep in the blue, in agreement with previous studies (43). Here, myopes show steeper curves for both the blue and red regions (Figure 5). In the presence of natural aberrations, the CDF curves of emmetropes and myopes showed differences in the G-Red part of the curves, both on average and for each stimulus. These differences were greater for the CDF curves obtained with natural images than for the binary stimulus, suggesting perceptual differences associated to the refractive error and the visual information presented. The model proposed by Schaeffel and Swiatczak (54), in which the retina uses a closed-loop negative feedback system based on image defocus to modulate eye growth (16, 54), receiving contributions from spatial frequency information (stimulatory pathway) and defocus in different

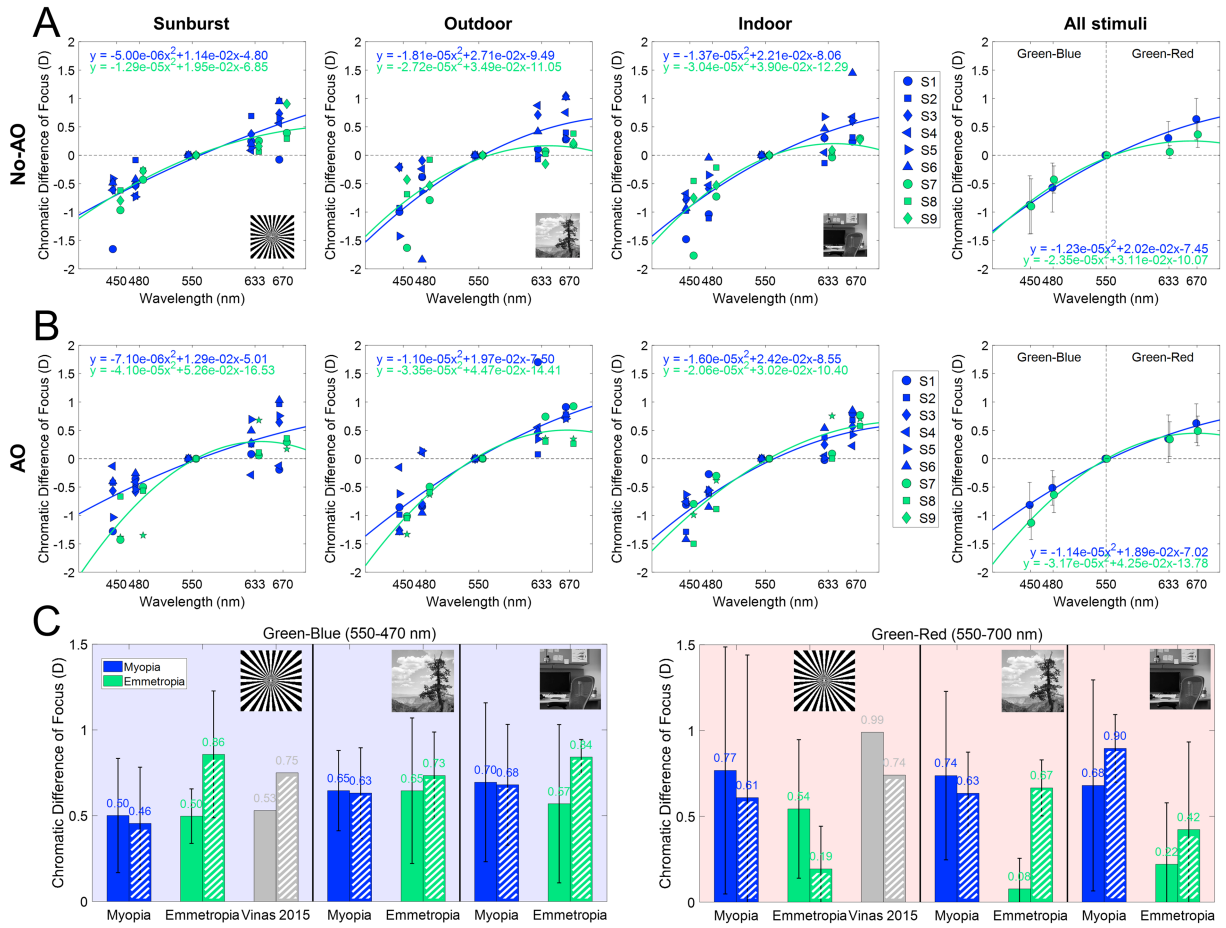

FIGURE 5
Chromatic difference of focus curves (470–700 nm). **(A)** Chromatic difference of focus curves (centered at 550 nm) for each stimulus and group. **(B)** AO-corrected chromatic difference of focus fitting curves (centered at 550 nm) for each stimulus and group. **(C)** Chromatic difference of focus for green-blue (550–470 nm) and green-red (550–700 nm) for all conditions, both with natural aberrations and with AO-correction. Dashed bars are AO correction data. Data from Vinas et al. (39) are shown as gray bars.

TABLE 1 Summary of the chromatic difference of focus for all conditions and groups of subjects.

Condition	Spectral region	Group	Mean ± SD (D)	*p*	U	Effect size r
Natural Aberrations	Green-Blue (480–550 nm)	Emmetropes	0.22 ± 0.38	0.77	87	0.011
		Myopes	0.61 ± 0.34			
	G-Red (550–700 nm)	Emmetropes	0.58 ± 0.32	0.03*	124	0.08
		Myopes	0.73 ± 0.58			
AO Correction	Green-Blue (480–550 nm)	Emmetropes	0.81 ± 0.24	0.11	49	−0.06
		Myopes	0.59 ± 0.31			
	G-Red (550–700 nm)	Emmetropes	0.42 ± 0.36	0.05	119	0.071
		Myopes	0.71 ± 0.50			

Descriptive and inferential results from Mann-Whitney U tests. An * represents that the values are statistically different.

chromatic planes (inhibitory pathway), motivated the study of chromatic blur perception to more complex stimuli, with different refractive errors, and AO natural aberrations correction. In particular, the fact that the spatial frequency component of the visual target has been reported as a potential cause of myopia development (55) motivated the use of indoor and outdoor grayscale images.

4.2 Chromatic difference of focus for blue and red

When compared with the results of a previous study performed with the same system and experimental conditions (sunburst stimuli), we find similar trends in the CDF curves, but slightly higher differences within spectral ranges (0.53 D and 0.99 D for the G-Blue and G-Red, and 0.75

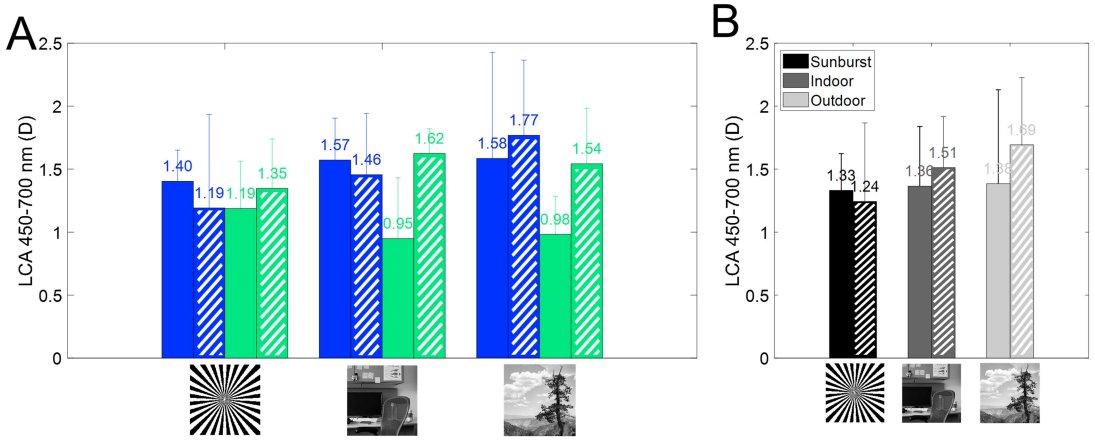

FIGURE 6
Longitudinal chromatic aberration (LCA) from 450 to 700 nm. Dashed bars represent AO correction. **(A)** Subjective LCA for myopes (blue) and emmetropes (green), for all three stimuli, with and without correction of HOAs. **(B)** Average subjective LCA as a function of the stimulus.

D and 0.74 after AO-correction of HOAs). These differences can be attributed to the sample used (young subjects, with spherical errors ranging between 0 and −4.50 D), whereas our sample is clustered by refractive error. In addition, the previous study used a linear fit, which may have misrepresented the extremes of the spectral range, especially the red region. In emmetropes, the average G-Blue CDF across stimuli was significantly higher than the average G-Red CDF ($0.58 \pm 0.32 > 0.22 \pm 0.38$ D; $p < 0.05$, U = 63, Mann–Whitney U test), whereas in myopes there was a reversed non-significant trend ($0.61 \pm 0.34 < 0.73 \pm 0.58$ D, respectively). Similarly, there were statistical differences between refractive error groups in the G-Red ($p < 0.05$, U = 124, Mann–Whitney U test), but not in the G-Blue ($p > 0.05$, Mann–Whitney U test). The chromatic difference of focus for all stimuli shows that myopes perceive red defocus differently than emmetropes. In fact, myopes do not show differences in the chromatic difference of focus between G-Blue and G-Red, whereas emmetropes do. These results suggest that the mechanism that uses chromatic defocus as an optical cue is somehow disrupted in myopes, as suggested by other authors (54).

According to the Indiana chromatic eye model (56), the G-Blue focus difference in an emmetropic eye should be larger than the G-Red (0.69 vs. 0.45 D, respectively). However, experimental data do not agree with this prediction. In a previous work (39), we showed an opposite trend (G-Blue 0.53 D and G-Red 0.99 D), and AO-correcting aberrations balance these results (0.75 D and 0.74 D, respectively). In the current study (Figure 5), the G-Blue CDF is significantly different for emmetropes and myopes when testing natural outdoor images, but not when testing indoor or binary images. Correction of natural aberrations has a significant effect on emmetropes for both binary and indoor natural images, with a significant increase in the G-Blue CDF. On the other hand, G-Red CDF was significantly lower for emmetropes than for myopes, regardless of stimulus type, with similar results for outdoor natural and binary images, and higher for indoor natural images. AO-correction of aberrations significantly increased the G-Red CDF for myopes obtained with the outdoor natural images, exceeding that of the indoor natural image. These results indicate that myopic eyes do not use the blue and red focus information, whereas emmetropes do, regardless of the stimuli, consistent with the hypothesis that the myopic retina does not respond to chromatic blur in the sense that it does not use the red-blue focus difference as a cue for emmetropization (3, 47).

4.3 Impact of high-order aberrations in chromatic blur

Correction of HOAs of the subjects slightly modified those trends, highlighting differences in the blue and red regions between emmetropes and myopes, especially for the binary stimulus (Figures 5A,B). The results of our study show that natural aberrations have an impact on the perceived chromatic aberration across stimuli in emmetropes, but not in myopes. AO-correction of monochromatic aberrations increases the differences in the chromatic difference of focus for the binary stimuli, while it decreases for the natural image stimuli for emmetropic eyes. Again, myopic eyes appear to be insensitive to changes in the perceived stimuli (Figure 5B). High-order aberrations in the optics of the eye can provide an odd error cue as the point spread function changes shape with the same absolute spherical equivalent refractive error, but a different sign.

4.4 Subjective LCA and refractive error

Although some variability was found, there was no statistical difference as a function of the stimulus, refractive error, or aberration condition ($p > 0.05$ for all comparisons). Furthermore, there is no influence of the refractive error on the magnitude of LCA (Figure 6B), either with natural aberrations or compensated aberrations. This result is in agreement with a previous report (57) showing that LCA was not correlated with refractive error ($r^2 = 0.024$). The results are also slightly different for natural images, where AO-correction of HOAs increased the total amount of subjective LCA, particularly for emmetropic subjects.

4.5 Limitations of the study

There are limitations to this study. First, accommodation was not paralyzed during the measurements. However, the goal of this study was to test the chromatic perception under the most natural conditions possible, given the limitations of the AO system. Therefore, we chose to maintain accommodation functionality during the measurements. However, the influence of accommodation was expected to be minimal

because the subjective best focus was always found from a positive defocus. The effect of accommodation on chromatic perception remains a topic for future research, as it may provide insight into the underlying perceptual mechanisms.

Another limitation of this study was the modest sample size. Measurements in an adaptive optics system are typically long and tedious, and recruiting subjects is challenging. Nonetheless, the findings of this study provide new insights into the differences in chromatic perception between myopes and emmetropes and pave the way for the development of more efficient and rapid testing methods that can be implemented with a larger sample sizes.

Overall, the results of this study suggest that the refractive profile may influence the perception of visual information with specific chromatic properties, leading to differences in the processing of these properties. However, future work should focus on disentangling other mechanisms involved in the perception of polychromatic optical cues, such as accommodation dynamics, refractive error, and age range.

Data availability statement

The original contributions presented in the study are included in the article/supplementary material, further inquiries can be directed to the corresponding author.

Ethics statement

The studies involving humans were approved by Bioethics Committee of the Spanish National Research Council. The studies were conducted in accordance with the local legislation and institutional requirements. The participants provided their written informed consent to participate in this study.

Author contributions

VR-L: Conceptualization, Data curation, Formal analysis, Investigation, Methodology, Validation, Visualization, Writing – original draft, Writing – review & editing. PD-G: Data curation, Investigation, Methodology, Writing – review & editing. EM: Data curation, Investigation, Methodology, Writing – review & editing. MV-P: Conceptualization, Data curation, Formal analysis, Funding acquisition, Investigation, Methodology, Project administration, Resources, Software, Supervision, Validation, Visualization, Writing – original draft, Writing – review & editing.

Funding

The author(s) declare that financial support was received for the research and/or publication of this article. This research has received funding from La Caixa Foundation LCF/TR/CI22/52660002 and Spanish Research Agency grant CPP2021-008388D to VR-L; the Spanish Government under the PID2022 (PID2022-139840OA-I00-MYOFLUOGOLD) to MV-P; and the CNS2022 (CNS2022-135326-GOLDENEYE) and the RyC2021 (RYC2021-034218-I) programs to MV-P.

Conflict of interest

The authors declare that the research was conducted in the absence of any commercial or financial relationships that could be construed as a potential conflict of interest.

Generative AI statement

The authors declare that no Gen AI was used in the creation of this manuscript.

Publisher's note

References

1. Atchison DA, Woods RL, Bradley A. Predicting the Effects of Optical Defocus on Human Contrast Sensitivity. *J Opt Soc Am*. (1998) 15:2536–44. doi: 10.1364/josaa.15.002536

2. Radhakrishnan H, Pardhan S, Calver RI, O'Leary DJ. Effect of Positive and Negative Defocus on Contrast Sensitivity in Myopes and Non-Myopes. *Vis Res*. (2004) 44:1869–78. doi: 10.1016/j.visres.2004.03.007

3. Rucker FJ. The Role of Luminance and Chromatic Cues in Emmetropisation. *Ophthal Physiol Opt*. (2013) 33:196–214. doi: 10.1111/opo.12050

4. Baird PN, Saw S-M, Lanca C, Guggenheim JA, Smith EL, Iii XZ, et al. Myopia. *Nat Rev Dis Primers*. (2020) 6:99. doi: 10.1038/s41572-020-00231-4

5. McFadden SA, Tse DY, Bowrey HE, Leotta AJ, Lam CS, Wildsoet CF. Integration of Defocus by Dual Power Fresnel Lenses Inhibits Myopia in the Mammalian Eye. *Invest Ophthalmol Vis Sci*. (2014) 55:908–17. doi: 10.1167/iovs.13-11724

6. Nickla DL, Wildsoet CF. The Effect of the Nonspecific Nitric Oxide Synthase Inhibitor NG-Nitro-L-Arginine Methyl Ester on the Choroidal Compensatory Response to Myopic Defocus in Chickens. *Optom Vis Sci*. (2004) 81:111–8. doi: 10.1097/00006324-200402000-00009

7. Rosén R, Jaeken B, Petterson AL, Artal P, Unsbo P, Lundström L. Evaluating the Peripheral Optical Effect of Multifocal Contact Lenses. *Ophthal Physiol Opt*. (2012) 32:527–34. doi: 10.1111/j.1475-1313.2012.00937.x

8. Zheng H, Tse DY, Tang XChiho To, Lam TC. The Interactions Between Bright Light and Competing Defocus During Emmetropization in Chicks. *Invest Ophthalmol Vis Sci*. (2018) 59:2932–43. doi: 10.1167/iovs.17-22973

9. de Gracia P, Dorronsoro C, Gambra E, Marin G, Hernández M, Marcos S. Combining Coma with Astigmatism Can Improve Retinal Image over Astigmatism Alone. *Vis Res*. (2010) 50:2008–14. doi: 10.1016/j.visres.2010.07.014

10. McLellan JS, Marcos S, Prieto PM, Burns SA. Imperfect Optics May Be the Eye's Defence against Chromatic Blur. *Nature*. (2002) 417:174–6. doi: 10.1038/417174a

11. Vinas M, de Gracia P, Dorronsoro C, Sawides L, Marin G, Hernández M, et al. Astigmatism Impact on Visual Performance: Meridional and Adaptational Effects. *Optom Vis Sci*. (2013) 90:1430–42. doi: 10.1097/OPX.0000000000000063

12. Sabesan R, Yoon G. Visual Performance after Correcting Higher Order Aberrations in Keratoconic Eyes. *J Vis*. (2009) 9:6–610. doi: 10.1167/9.5.6

13. Vinas M, Sawides L, de Gracia P, Marcos S. Perceptual Adaptation to the Correction of Natural Astigmatism. *PLoS One*. (2012) 7:e46361. doi: 10.1371/journal.pone.0046361

14. Cufflin MP, Mankowska A, Mallen EAH. Effect of Blur Adaptation on Blur Sensitivity and Discrimination in Emmetropes and Myopes. *Investig Ophthalmol Vis Sci*. (2007) 48:2932–9. doi: 10.1167/iovs.06-0836

15. George S, Rosenfield M. Blur Adaptation and Myopia. *Optom Vis Sci*. (2004) 81:543–7. doi: 10.1097/00006324-200407000-00016

16. Summers JA, Schaeffel F, Marcos S, Hao W, Tkatchenko AV. Functional Integration of Eye Tissues and Refractive Eye Development: Mechanisms and Pathways. *Exp Eye Res*. (2021) 209:108693. doi: 10.1016/j.exer.2021.108693

17. Tkatchenko TV, Troilo D, Benavente-Perez A, Tkatchenko AV. Gene Expression in Response to Optical Defocus of Opposite Signs Reveals Bidirectional Mechanism of Visually Guided Eye Growth. *PLoS Biol*. (2018) 16:e2006021. doi: 10.1371/journal.pbio.2006021

18. Chakraborty R, Ostrin LA, Benavente-Perez A, Verkicharla PK. Optical Mechanisms Regulating Emmetropisation and Refractive Errors: Evidence from Animal Models. *Clin Exp Optom*. (2020) 103:55–67. doi: 10.1111/cxo.12991

19. Kruger S, Pola J. Stimuli for Accommodation: Blur, Chromatic Aberration and Size. *Vis Res*. (1986) 26:957–71. doi: 10.1016/0042-6989(86)90153-7

20. Phillips S, Stark L. Blur: A Sufficient Accommodative Stimulus. *Document Ophthalmol Adv Ophthalmol*. (1977) 43:65–89. doi: 10.1007/BF01569293

21. Tucker J, Charman WN. Reaction and Response Times for Accommodation. *Am J Optom Physiol Optic*. (1979) 56:490–503. doi: 10.1097/00006324-197908000-00003

22. Gambra E, Sawides L, Dorronsoro C, Marcos S. Accommodative Lag and Fluctuations When Optical Aberrations Are Manipulated. *J Vis*. (2009) 9:4–415. doi: 10.1167/9.6.4

23. Mutti DO, Lynn Mitchell G, Hayes JR, Jones LA, Moeschberger ML, Cotter SA, et al. Accommodative Lag before and after the Onset of Myopia. *Invest Ophthalmol Vis Sci*. (2006) 47:837–46. doi: 10.1167/iovs.05-0888

24. Liang J, Williams DR. Aberrations and Retinal Image Quality of the Normal Human Eye. *J Opt Soc Am A Opt Image Sci Vis*. (1997) 14:2873–83. doi: 10.1364/josaa.14.002873

25. Yoon G-Y, Williams DR. Visual Performance after Correcting the Monochromatic and Chromatic Aberrations of the Eye. *J Opt Soc Am A*. (2002) 19:266–75. doi: 10.1364/JOSAA.19.000266

26. Wilson BJ, Decker KE, Roorda A. Monochromatic Aberrations Provide an Odd-Error Cue to Focus Direction. *J Opt Soc Am A Opt Image Sci Vis*. (2002) 19:833–9. doi: 10.1364/josaa.19.000833

27. Buehren T, Collins MJ, Carney LG. Near Work Induced Wavefront Aberrations in Myopia. *Vis Res*. (2005) 45:1297–312. doi: 10.1016/j.visres.2004.10.026

28. He JC, Sun P, Held R, Thorn F, Sun X, Gwiazda JE. Wavefront Aberrations in Eyes of Emmetropic and Moderately Myopic School Children and Young Adults. *Vis Res*. (2002) 42:1063–70. doi: 10.1016/s0042-6989(02)00035-4

29. Paquin M-P, Hamam H, Simonet P. Objective Measurement of Optical Aberrations in Myopic Eyes. *Optom Vis Sci*. (2002) 79:285–91. doi: 10.1097/00006324-200205000-00007

30. Atchison DA, Schmid KL, Pritchard N. Neural and Optical Limits to Visual Performance in Myopia. *Vis Res*. (2006) 46:3707–22. doi: 10.1016/j.visres.2006.05.005

31. Carkeet A, Luo HD, Tong L, Saw SM, Tan DTH. Refractive Error and Monochromatic Aberrations in Singaporean Children. *Vis Res*. (2002) 42:1809–24. doi: 10.1016/s0042-6989(02)00114-1

32. Cheng XU, Arthur Bradley X, Hong I, Larry N. Relationship between Refractive Error and Monochromatic Aberrations of the Eye. *Optom Vis Sci*. (2003) 80:43–9. doi: 10.1097/00006324-200301000-00007

33. Porter J, Guirao A, Cox IG, Williams DR. Monochromatic Aberrations of the Human Eye in a Large Population. *J Opt Soc Am A*. (2001) 18:1793–803. doi: 10.1364/JOSAA.18.001793

34. Zadok D, Levy Y, Segal O, Barkana Y, Morad Y, Avni I. Ocular Higher-Order Aberrations in Myopia and Skiascopic Wavefront Repeatability. *J Cataract Refract Surg*. (2005) 31:1128–32. doi: 10.1016/j.jcrs.2004.10.075

35. Hashemi H, Khabazkhoob M, Jafarzadehpur E, Yekta A, Emamian MH, Shariati M, et al. Higher Order Aberrations in a Normal Adult Population. *J Curr Ophthalmol*. (2015) 27:115–24. doi: 10.1016/j.joco.2015.11.002

36. Marcos S, Diaz-Santana L, Llorente L, Dainty C. Ocular Aberrations with Ray Tracing and Shack–Hartmann Wave-Front Sensors: Does Polarization Play a Role? *J Opt Soc Am A*. (2002) 19:1063–72. doi: 10.1364/JOSAA.19.001063

37. Llorente L, Barbero S, Cano D, Dorronsoro C, Marcos S. Myopic versus Hyperopic Eyes: Axial Length, Corneal Shape and Optical Aberrations. *J Vis*. (2004) 4:288–98. doi: 10.1167/4.4.5

38. Bedford RE, Wyszecki G. Axial Chromatic Aberration of the Human Eye. *J Opt Soc Am*. (1957) 47:564. doi: 10.1364/JOSA.47.0564_1

39. Vinas M, Dorronsoro C, Cortes D, Pascual D, Marcos S. Longitudinal Chromatic Aberration of the Human Eye in the Visible and near Infrared from Wavefront Sensing, Double-Pass and Psychophysics. *Biomed Opt Express*. (2015) 6:948–22. doi: 10.1364/BOE.6.000948

40. Ware C. Human Axial Chromatic Aberration Found Not to Decline with Age. *Graefe's Arch Clin Exp Ophthalmol*. (1982) 218:39–41. doi: 10.1007/BF02134100

41. Aissati S, Vinas M, Benedi-Garcia C, Dorronsoro C, Marcos S. Testing the Effect of Ocular Aberrations in the Perceived Transverse Chromatic Aberration. *Biomed Opt Express*. (2020) 11:4052–68. doi: 10.1364/BOE.396469

42. Marcos S, Romero M, Benedí-García C, González-Ramos A, Vinas M, Alejandre N, et al. Interaction of Monochromatic and Chromatic Aberrations in Pseudophakic Patients. *J Refract Surg*. (2020) 36:230–8. doi: 10.3928/1081597X-20200303-01

43. Vinas M, Dorronsoro C, Garzón N, Poyales F, Marcos S. In Vivo Subjective and Objective Longitudinal Chromatic Aberration after Bilateral Implantation of the Same Design of Hydrophobic and Hydrophilic Intraocular Lenses. *J Cataract Refract Surg*. (2015) 41:2115–24. doi: 10.1016/j.jcrs.2015.11.009

44. Kruger SM, Aggarwala KR, Sanchez N. Chromatic Aberration and Ocular Focus: Fincham Revisited. *Vis Res*. (1993) 33:1397–411. doi: 10.1016/0042-6989(93)90046-Y

45. Seidemann A, Schaeffel F. Effects of Longitudinal Chromatic Aberration on Accommodation and Emmetropization. *Vis Res*. (2002) 42:2409–17. doi: 10.1016/S0042-6989(02)00262-6

46. Kruger PB, Aggarwala KR, Bean S, Mathews S. Accommodation to Stationary and Moving Targets. *Optom Vis Sci*. (1997) 74:505–10. doi: 10.1097/00006324-199707000-00018

47. Swiatczak B, Schaeffel F. Myopia: Why the Retina Stops Inhibiting Eye Growth. *Sci Rep*. (2022) 12:21704. doi: 10.1038/s41598-022-26323-7

48. Jiang X, Kuchenbecker JA, Touch P, Sabesan R. Measuring and Compensating for Ocular Longitudinal Chromatic Aberration. *Optica*. (2019) 6:981–90. doi: 10.1364/OPTICA.6.000981

49. Vinas M, Aissati S, Romero M, Benedi-Garcia C, Garzon N, Poyales F, et al. Pre-Operative Simulation of Post-Operative Multifocal Vision. *Biomed Opt Express*. (2019) 10:5801–17. doi: 10.1364/BOE.10.005801

50. Vinas M, Benedi-Garcia C, Aissati S, Pascual D, Akondi V, Dorronsoro C, et al. Visual Simulators Replicate Vision with Multifocal Lenses. *Sci Rep*. (2019) 9:1539. doi: 10.1038/s41598-019-38673-w

51. Howarth A, Bradley A. The Longitudinal Chromatic Aberration of the Human Eye, and Its Correction. *Vis Res Netherlands*. (1986) 26:361–6. doi: 10.1016/0042-6989(86)90034-9

52. Howarth PA, Zhang XX, Bradley A, Still DL, Thibos LN. Does the Chromatic Aberration of the Eye Vary with Age? *J Opt Soc Am A Opt Image Sci*. (1988) 5:2087–92. doi: 10.1364/josaa.5.002087

53. Marcos S, Burns SA, Moreno-Barriusop E, Navarro R. A New Approach to the Study of Ocular Chromatic Aberrations. *Vis Res*. (1999) 39:4309–23. doi: 10.1016/S0042-6989(99)00145-5

54. Schaeffel F, Swiatczak B. Mechanisms of Emmetropization and What Might Go Wrong in Myopia. *Vis Res*. (2024) 220:108402. doi: 10.1016/j.visres.2024.108402

55. Flitcroft DI, Harb EN, Wildsoet CF. The Spatial Frequency Content of Urban and Indoor Environments as a Potential Risk Factor for Myopia Development. *Invest Ophthalmol Vis Sci*. (2020) 61:42. doi: 10.1167/iovs.61.11.42

56. Thibos LN, Ye M, Zhang X, Bradley A. The Chromatic Eye: A New Reduced-Eye Model of Ocular Chromatic Aberration in Humans. *Appl Opt*. (1992) 31:3594–600. doi: 10.1364/AO.31.003594

57. Wildsoet CF, Atchison DA, Collins MJ. Longitudinal Chromatic Aberration as a Function of Refractive Error. *Clin Exp Optom*. (1993) 76:119–22. doi: 10.1111/j.1444-0938.1993.tb02956.x

Frontiers in Medicine

Translating medical research and innovation into improved patient care

A multidisciplinary journal which advances our medical knowledge. It supports the translation of scientific advances into new therapies and diagnostic tools that will improve patient care.

Discover the latest Research Topics

See more →

Frontiers

Avenue du Tribunal-Fédéral 34
1005 Lausanne, Switzerland
frontiersin.org

Contact us

+41 (0)21 510 17 00
frontiersin.org/about/contact